NHC PROJECT # 4454: SEISMICALLY RESILIENT PARTITION WALL DESIGN AND TESTING

Final Report

Principal Investigator (PI): Jitendra Bhatta, Postdoctoral Fellow, University of Canterbury, jitendra.bhatta@canterbury.ac.nz

Associate Investigator (AI): Stuart Oliver, Holmes ANZ, stuarto@holmesgroup.com

Key Researchers: Rajesh Dhakal, Alex Shegay, Timothy Sullivan

Industry Investigators: Mark Browne, Mike Inwood

PhD students: Mojtaba Hosseini, Rajesh Shrestha, Aasish Tiwari

Editor: Jitendra Bhatta

Submitted to: Natural Hazards Commission Toka Tū Ake

Submission date: 20/03/2026

ABSTRACT

This report details an experimental study on the seismic performance of three non-structural component systems. The study examines: (1) conventional New Zealand partition walls with No-Fix zones at junctions, (2) the same walls combined with a perimeter-restrained plasterboard ceiling, and (3) an innovative integrated assembly comprising rocking walls and a fully floating ceiling. The research aims to characterize and compare the damage progression and dynamic response of these configurations under seismic conditions, focusing particularly on wall-ceiling-piping interactions. The findings establish a foundation for assessing the efficacy of various design strategies for non-structural elements.

ACKNOWLEDGMENTS

This research was supported by funding from the New Zealand Natural Hazards Commission - Toka Tū Ake and QuakeCoRE. The dynamic test setup in the Structural Engineering Laboratory (SEL), developed by Liam Pledger during his PhD studies, was instrumental to this work; we gratefully acknowledge his contribution and his assistance with the Motion Capture system. We also extend our thanks to Rajesh Shrestha and Aasish Tiwari (University of Canterbury), and Mojtaba Hosseini (University of Auckland) for their invaluable help during testing and inspections. The authors gratefully acknowledge the input from Mark Browne and Mike Inwood from Holmes. We are grateful for the constructive discussions and feedback provided by Rajesh Dhakal and Timothy Sullivan (from University of Canterbury), Alex Shegay (also for allocating QuakeCoRE Fund; from University of Auckland), Andrew Baird (from Beca), Jan Stanway (from WSP). Finally, valuable assistance in the SEL lab is acknowledged from SEL staff Guillaume Roux, Alan Thirlwell, and Matthew Robinson.

TABLE OF CONTENTS

INTRODUCTION

In multi-unit residential buildings, non-structural components such as partition walls significantly influence post-earthquake occupancy, repair costs and safety. Similarly, in the design of essential facilities such as hospitals and schools, non-structural components, particularly partition walls, play a critical role in both life safety and the continued functionality of buildings following seismic events. Current industry practice, constrained by limited evidence regarding the seismic performance of resilient partition wall detailing, often results in the overly conservative design of very stiff structures. This approach increases construction costs and embodied carbon without necessarily delivering proportionate performance benefits.

The New Zealand building industry currently lacks sufficient empirical data on the performance of resilient gypsum board partition walls under seismic loading conditions, especially for displacements exceeding the 0.4 % inter-storey drift limit recommended in the New Zealand Seismic Code of Practice (AWCI, 2018). As a result, design teams face uncertainty when specifying these systems in buildings.

An immediate and cost-effective opportunity existed at the University of Canterbury to address this knowledge gap. The university's lab facilities, which are equipped for seismic testing, were available until the end of 2025. This provided a unique, time-sensitive window to conduct controlled seismic testing on full-scale partition wall systems. Utilising this facility our research team was able to gather critical performance data on existing practices for partition walls under seismic conditions for multi-unit residential buildings. Such data has the potential to inform code revisions, support more cost-effective and sustainable building designs, and reduce unnecessary material use in Low-Damage Seismic Design (LDSD) projects (MBIE & NHC, 2024).

This research aims to:

(1) **Evaluate the seismic performance of conventional detailed partition walls (Phase I).** This phase investigates the behaviour and seismic performance of partition walls with common New Zealand construction details, typical in multi-unit residential and essential buildings (e.g., hospitals), under simulated seismic demands of displacement and acceleration.

(2) **Evaluate the seismic performance and interaction of conventional partition walls with perimeter-restrained concealed plasterboard ceilings (Phase II).** This phase extends the investigation to include the coupled system of typical resilient walls ceilings, and mechanical pipes. It assesses their combined behaviour and interactive failures under seismic loading.

(3) **Evaluate the seismic performance and interaction of novel "rocking" partition walls with fully floating plasterboard ceilings (Phase III).** This phase assesses an innovative, decoupled partition wall and ceiling system (with mechanical pipes) designed for improved seismic resilience.

(4) **Translate research findings into industry best practice.** A core goal is to synthesize the experimental results into practical design guidance for engineers and architects. This will inform better decision-making for partition wall and ceiling systems, particularly in multi-unit residential construction.

BACKGROUND

Non-structural elements (NSEs), such as partition walls, suspended ceilings, mechanical and electrical systems, cladding, and windows, are essential to a building's functionality and operation. Although these components are secondary and are either attached to or

placed near structural members, they can interact with the structure or with one another during an earthquake, leading to significant damage (Baird et al., 2014; Dhakal, Rajesh et al., 2011; Dhakal, Rajesh P., 2010). Such damage often results in costly repairs, operational downtime, evacuations, and even full replacements(Bachman, 2004; FEMA, 1994; Filiatrault, 2002). Suspended ceilings, piping, and partition walls have been identified as major sources of economic loss following seismic events (FEMA, 1994; Filiatrault, 2002).

Partition walls

Lightweight internal partition walls are common in multi-story commercial buildings. Typically built with a steel or timber frame, comprising vertical studs, horizontal plates, and noggings, they are lined on both sides with gypsum plasterboard fastened with screws and/or adhesive. The walls are then finished by plastering joints, sanding, and painting.

Experimental research from various regions consistently shows that such walls begin to sustain seismic damage at very low drift levels. The serviceability limit, or onset of damage, typically occurs between 0.26% and 0.30% inter-story drift (Davies et al., 2011; Petrone et al., 2015; Tasligedik et al., 2015; Wang et al., 2021) with some studies reporting initial cracking as low as 0.05% (Restrepo & Bersofsky, 2011) or at 0.38% (Kim & Shin, 2021) underscoring their high vulnerability to even minor shaking.

The 2010–11 Canterbury Earthquake Sequence in New Zealand demonstrated this vulnerability, causing widespread partition wall damage such as screw failures, cracked or crushed plasterboard corners, and dislodged panels (AWCI, 2018; Baird et al., 2014; Dhakal, Rajesh P., 2010; Tasligedik, 2014).

Damage also recurred during aftershocks that exceeded serviceability limits (Arifin et al., 2021). Such early failures often lead to significant economic losses in minor

to moderate earthquakes, due to repair costs, replacements, and operational downtime (Bachman, 2004; Bradley et al., 2008; Whitman et al., 1973).

In response, seismic-resilient partition systems have been developed to improve performance. Innovations like seismic relief joints, flexible tracks, sliding connections, and specialized connectors allow walls to accommodate building drift without damage. For example, walls with 15–40 mm seismic gaps have remained intact up to 1.0%–2.0% drift in testing (Lee et al., 2007; Tasligedik et al., 2015). Flexible track systems that "bow" by detaching from structural junctions have also performed well (Davies et al., 2011; Mulligan et al., 2020). Similarly, a sliding/frictional connection developed by increased the drift at first damage from 0.10% to 2.13%, representing a more than twentyfold improvement over conventional designs (Araya-Letelier et al., 2019).

Suspended ceilings

Suspended ceilings are essential non-structural elements in modern buildings, concealing mechanical and electrical services while improving aesthetics and acoustics. Past earthquakes have caused extensive damage to these systems, resulting in major financial costs, operational disruptions, and even casualties (Bradley et al., 2008; Dhakal, Rajesh P. et al., 2016; Khakurel et al., 2020; Motosaka & Mitsuji, 2012). These ceilings generally fall into two categories: grid-and-tile systems and plasterboard systems. In grid-and-tile ceilings, lay-in tiles rest unattached within a metal grid of main and cross tees. Plasterboard ceilings, however, involve screwing plasterboards to concealed furring channels, leaving no exposed framework.

A standard grid-and-tile ceiling consists of a metal grid (main tees and cross tees), wall angles, lay-in tiles, and a suspension system of hanger wires. In New Zealand practice, two primary types are distinguished by how they transfer seismic forces to the

surrounding structure: perimeter-restrained ceilings and braced ceilings. In a perimeter-restrained ceiling, tees are riveted or screwed to wall angles on two adjacent sides, while the tees on the other two sides slide freely which may be within seismic clips. Axial forces in the tees are resisted by these fasteners and transferred via the wall angles into the building walls. In a braced ceiling, all perimeter tees are attached to wall angles, but the angles themselves are not connected to the walls. A gap is maintained to ensure the ceiling floats freely. Lateral forces are instead transferred upwards to the floor above through diagonal braces.

A third, innovative type is the fully floating ceiling (Pourali et al., 2017). While similar to a braced ceiling in its perimeter attachments, compressible isolation foam fills the gap between the wall angles and the surrounding walls. This foam prevents impact damage and allows controlled movement, using the foam itself to manage lateral forces rather than braces or restrained connections, creating a low-damage seismic solution.

REFERENCES

Araya-Letelier, G., Miranda, E., & Deierlein, G. (2019). Development and testing of a friction/sliding connection to improve the seismic performance of gypsum partition walls. *Earthquake Spectra, 35*(2), 653–677.

Arifin, F. A., Sullivan, T. J., MacRae, G., Kurata, M., & Takeda, T. (2021). Lessons for loss assessment from the Canterbury earthquakes: a 22-storey building. *Bulletin of Earthquake Engineering, 19*(5), 2081–2104.

AWCI. (2018). *Code of practice for the seismic design and installation of non-structural internal walls and partitions.* https://awci.org.nz/wp-content/uploads/COP-Internal-Walls-and-Partitions-coloured.pdf.

Bachman, R. E. (2004). The ATC-58 project plan for nonstructural components. Paper presented at the *Performance-Based Seismic Design: Concepts and Implementation, Proceedings of the International Workshop, Bled, Slovenia, 28 June–1 July 2004,*

Baird, A., Tasligedik, A. S., Palermo, A., & Pampanin, S. (2014). Seismic performance of vertical nonstructural components in the 22 February 2011 Christchurch earthquake. *Earthquake Spectra, 30*(1), 401–425.

Bradley, B., Dhakal, R., Cubrinovski, M., MacRae, G. A., & Lee, D. S. (2008). Seismic loss estimation for efficient decision making.

Davies, R. D., Retamales, R., Mosqueda, G., & Filiatrault, A. (2011). Experimental seismic evaluation, model parameterization, and effects of cold-formed steel-framed gypsum partition walls on the seismic performance of an essential facility.

Dhakal, R. P. (2010). Damage to non-structural components and contents in 2010 Darfield earthquake. *Bulletin of the New Zealand Society for Earthquake Engineering, 43*(4), 404–411.

Dhakal, R. P., MacRae, G. A., Pourali, A., & Paganotti, G. (2016). Seismic fragility of suspended ceiling systems used in NZ based on component tests. *Bulletin of the New Zealand Society for Earthquake Engineering, 49*(1), 45–63.

Dhakal, R., MacRae, G. A., & Hogg, K. (2011). Performance of ceilings in the February 2011 Christchurch earthquake.

FEMA. (1994). *FEMA 74: Reducing the Risks of Nonstructural Earthquake Damage.* Federal Emergency Management Agency. https://mitigation.eeri.org/files/fema-74.pdf

Filiatrault, A. (2002). *Guidelines, specifications, and seismic performance characterization of nonstructural building components and equipment*. Pacific Earthquake Engineering Research Center.

Khakurel, S., Dhakal, R. P., Yeow, T. Z., & Saha, S. K. (2020). Performance group weighting factors for rapid seismic loss estimation of buildings of different usage. *Earthquake Spectra, 36*(3), 1141–1165.

Kim, H., & Shin, D. (2021). Shake table test program of cold-formed steel in-plane partition walls. Paper presented at the *Structures, , 30* 503–517.

Lee, T., Kato, M., Matsumiya, T., Suita, K., & Nakashima, M. (2007). Seismic performance evaluation of non-structural components: drywall partitions. *Earthquake Engineering & Structural Dynamics, 36*(3), 367–382.

MBIE, & NHC. (2024). *Low Damage Seismic Design, Volume 1: benefits, options and getting started.* https://www.building.govt.nz/assets/Uploads/getting-started/seismic-work-programme/low-damage-seismic-design-for-buildings.pdf

Motosaka, M., & Mitsuji, K. (2012). Building damage during the 2011 off the Pacific coast of Tohoku Earthquake. *Soils and Foundations, 52*(5), 929–944.

Mulligan, J., Sullivan, T., & Dhakal, R. (2020). Experimental study of the seismic performance of plasterboard partition walls with seismic gaps. *Bulletin of the New Zealand Society for Earthquake Engineering, 53*(4), 175–188.

Petrone, C., Magliulo, G., Lopez, P., & Manfredi, G. (2015). Seismic fragility of plasterboard partitions via in-plane quasi-static tests. *Earthquake Engineering & Structural Dynamics, 44*(14), 2589–2606.

Pourali, A., Dhakal, R. P., MacRae, G., & Tasligedik, A. S. (2017). Fully floating suspended ceiling system: experimental evaluation of structural feasibility and challenges. *Earthquake Spectra, 33*(4), 1627–1654.

Restrepo, J. I., & Bersofsky, A. M. (2011). Performance characteristics of light gage steel stud partition walls. *Thin-Walled Structures, 49*(2), 317–324.

Tasligedik, A. S. (2014). Damage mitigation strategies for non-structural infill walls. https://ir.canterbury.ac.nz/bitstream/handle/10092/9462/thesis_fulltext.pdf?sequence=1&isAllowed=y

Tasligedik, A. S., Pampanin, S., & Palermo, A. (2015). Low damage seismic solutions for non-structural drywall partitions. *Bulletin of Earthquake Engineering, 13*(4), 1029–1050.

Wang, D., Zhi, X., Zhu, F., & Wang, Y. (2021). Seismic Fragility of Chinese Light-Gauge Steel Keel Gypsum Board Partition Walls. *Shock and Vibration, 2021*(1), 8875486.

Whitman, R., Hong, S., & Reed, J. (1973). Damage Statistic for High-Rise Buildings in the Vicinity of the San Fernando Earthquake. Optimum Seismic Protection and Building Damage Statistics.

PHASE I: SEISMIC PERFORMANCE OF FIRE-RATED TIMBER AND STEEL-FRAMED PARTITION WALLS WITH "NO-FIX ZONE" DETAILING FOLLOWING NEW ZEALAND INDUSTRY PRACTICE

ABSTRACT

This chapter details the results from Phase I of an experimental study on timber and steel-framed, fire-rated partition walls. The investigation evaluates the seismic performance of these walls incorporating a "No-Fix Zone" detailing system, constructed in accordance with typical New Zealand industry practice. Two full-scale, 3.55m high partition walls (one timber-framed and one steel-framed) were constructed to New Zealand industry standards with fire-rated plasterboard. They were tested between reinforced concrete slabs using motions simulating a six-storey building's response to earthquake records. The walls incorporated a deflection head track and intentionally offset "No-Fix zone" details to allow for in-plane drift and out-of-plane flexibility at junctions. Results showed that both wall systems, when configured with flexible detailing, sustained significantly greater lateral deformation while maintaining fire integrity compared to traditional designs. The steel-framed wall demonstrated superior performance, withstanding notably higher drift levels. The tests also confirmed the intended out-of-plane flexibility at wall junctions.

The findings demonstrate that flexible top-track detailing is an effective strategy for enhancing the seismic drift capacity of partition walls. However, the results also highlight potential deformation incompatibilities with adjacent non-structural elements, indicating a need for further research into system-level interactions to improve overall seismic resilience.

EXPERIMENTAL PROGRAMME AND METHODOLOGY

This research employs an experimental approach to assess the seismic performance of typical partition walls in multi-unit residential and essential facilities (such as hospitals), with a focus on improved detailing. The methodology consists of the following steps:

(1) Construction of two full-scale wall specimens (one timber-framed and one steel-framed) using current industry best practices.

(2) Laboratory testing under incrementally increasing seismic demands including displacements, velocities, and accelerations utilizing the University of Canterbury's structural testing facilities.

(3) Simulation of realistic building drift levels, both within and beyond current serviceability limits, to evaluate damage thresholds, failure modes, visual appearance, and approximate fire integrity.

(4) Comprehensive data collection through displacement and acceleration measurements, supplemented by photographic documentation of observed damage.

(5) Proposal of subsequent testing phases based on the outcomes of this experimental phase.

TEST SETUP

The 3D isometric view and side elevations of the test setup are shown in Figure 2.1, Figure 2.2 and Figure 2.3. The test setup comprises two 100 mm thick reinforced concrete slabs (3.5 m × 6 m) positioned at the top and bottom of steel columns (200 UC 46.2). The clear vertical spacing between the slabs is 3550 mm. The columns are hinged into the slabs, allowing free rotation during lateral movement in the X-direction. The bottom slab is elevated 500 mm above the laboratory floor using concrete blocks. The blocks are

mounted on a linear ball bearing and guideway assembly that permits sliding of the bottom slab in the X-direction. Lateral movement of the slabs is applied through 250 kN actuators with ±500 mm stroke capacity. Both actuators can be operated simultaneously, enabling coordinated movement of the slabs under the prescribed loading protocols. Stability in the Y-direction (perpendicular to loading) is provided by tension-only braces. In the X-direction (loading direction), these braces are removed during testing and reattached once the tests are complete.

Wall specimen design, configurations and details

Phase I – Walls with unrestrained ends (Unrestrained specimens)

Two wall specimens, one with timber framing and the other with steel framing, were constructed between the concrete slabs of the test setup.

(1) The walls are allowed to slide in-plane within the top deflection head track (DHT).
(2) Anchors connecting the wall DHTs to the top slab are prohibited within 1200 mm of the wall junction region, defined as the "No-Fix zones."
(3) Out-of-plane flexibility at the junction is provided by bending of the top timber plates in the timber wall and the DHT in the steel wall.
(4) At the junction, the DHT flanges are cut approximately 40 mm short to prevent premature interaction with adjacent DHTs or steel plates.
(5) The frames are lined with 13 mm GIB FYRELINE plasterboard following GIB EzyBrace® System specification GS2-N (GIB, 2016). However, the plasterboard is not fastened to the top DHTs.

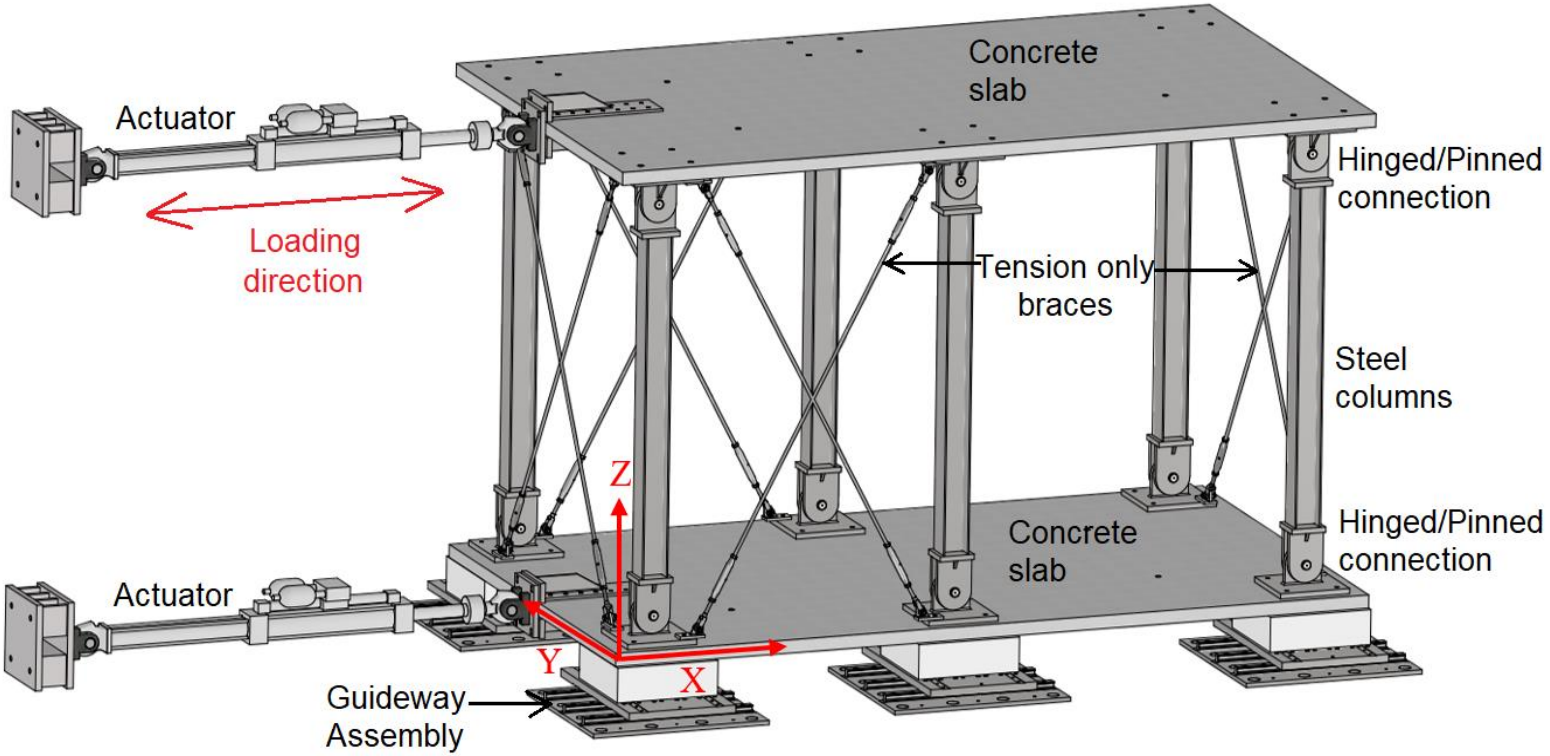

Figure 2.1. 3D Isometric view of the test setup showing main components (Pledger, 2026)

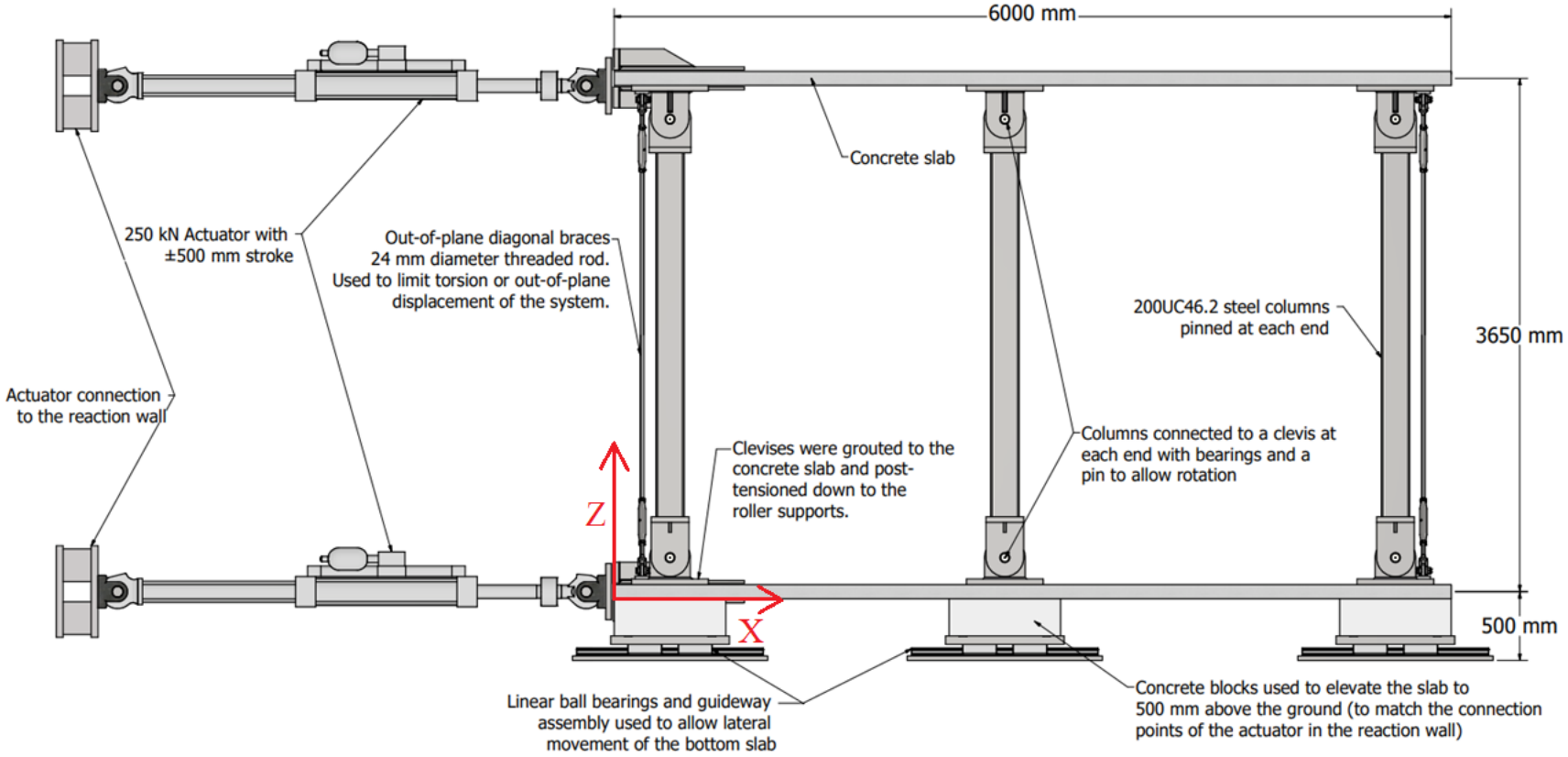

Figure 2.2. X-Z elevation of the test setup (Pledger, 2026)

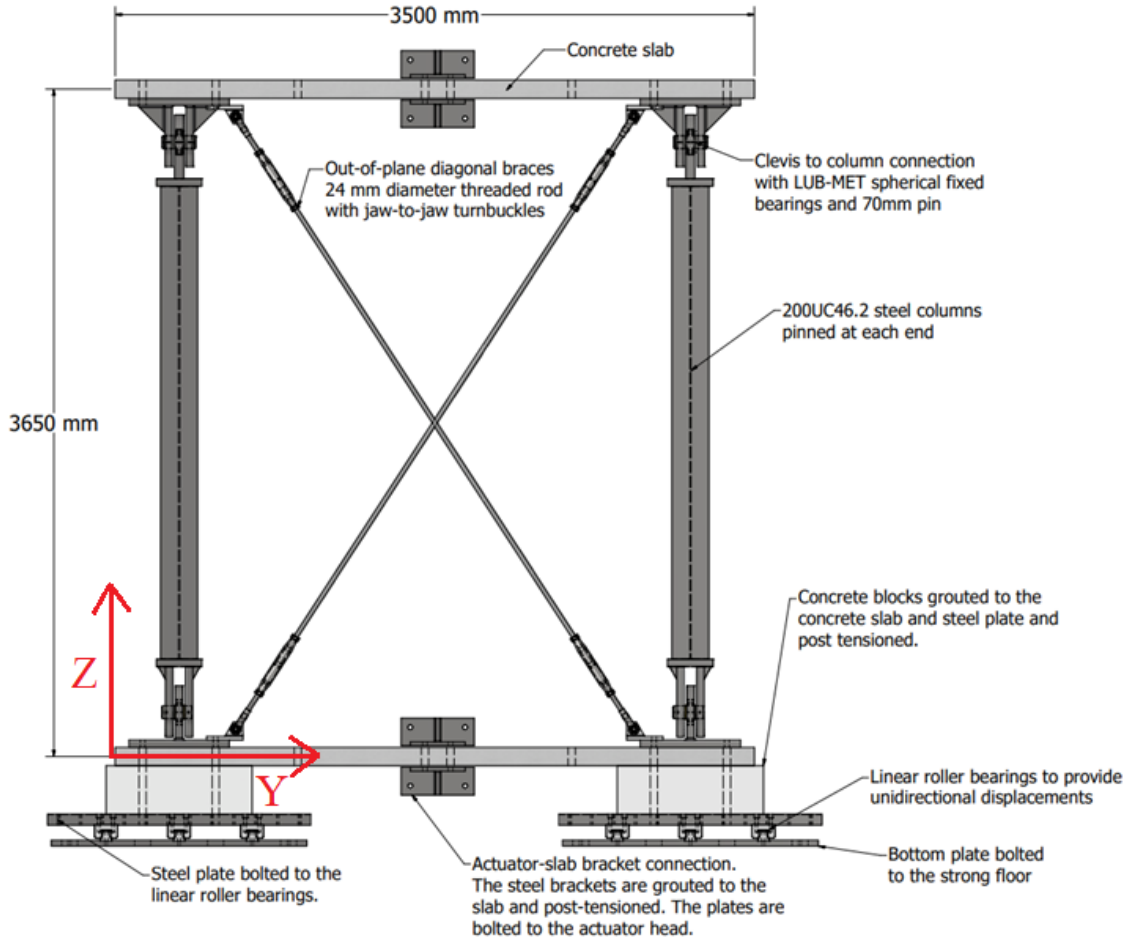

Figure 2.3. Y-Z elevation of the test setup (Pledger, 2026)

GIB EzyBrace® Systems specification GS2-N (slight adjustments for the specimens)

(1) **Fasteners:** Use 41 mm × 6 g GIB® Grabber® High Thread Screws, 32 mm × 7 g GIB® Grabber® Dual Thread Screws, or 30 mm GIB® Nails. If using the GIBFix® Angle, use only 32 mm × 7 g GIB® Grabber® Dual Thread Screws. Use 25mm × 6 g GIB® Grabber® High Thread Screws for steel frames.

(2) **Fastener centres:** Fasteners must be placed at 50, 100, 150, 225, and 300 mm maximum from each corner, and at 150 mm intervals thereafter around the perimeter of the bracing element. For vertically fixed sheets, place fasteners at maximum 300 mm centres along intermediate sheet joints. Apply daubs of GIBFix® adhesive at maximum 300 mm centres on intermediate studs. Fasteners must not be placed closer than 12 mm from paper-bound sheet edges or 18 mm from any sheet end or cut edge.

(3) **Jointing:** Joint strength is critical to bracing system performance. All fastener heads must be stopped, and all sheet joints reinforced with GIB® Joint Tape and stopped in accordance with the GIB® Site Guide.

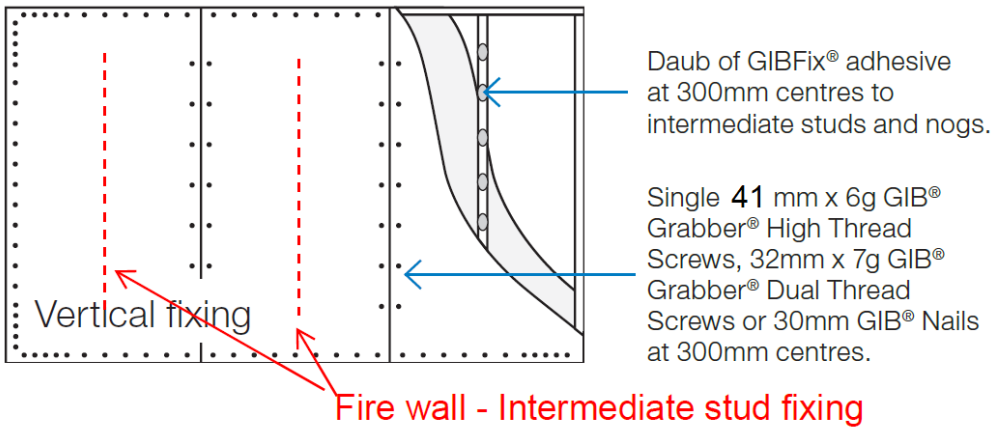

Figure 2.4. Plasterboard fixing details to timber framing (GIB, 2016)

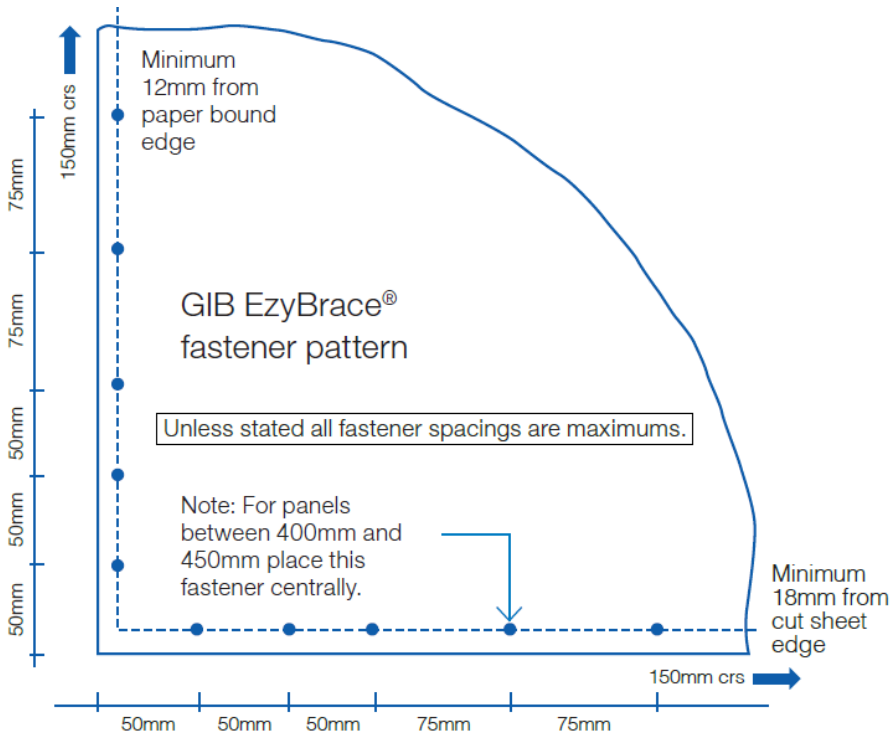

Figure 2.5. Fastener spacing on plasterboard lining (GIB, 2016)

The plans, elevations, and connection details are presented in Figure 2.6 to Figure 2.12.

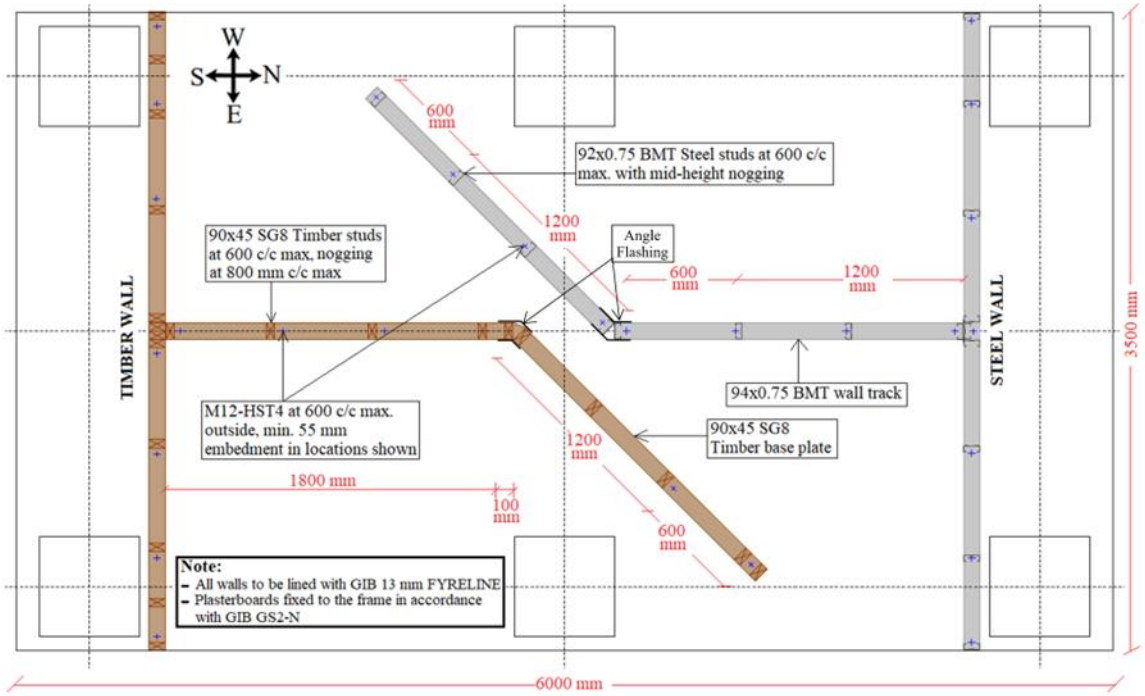

Figure 2.6. Timber and steel stud framing plan

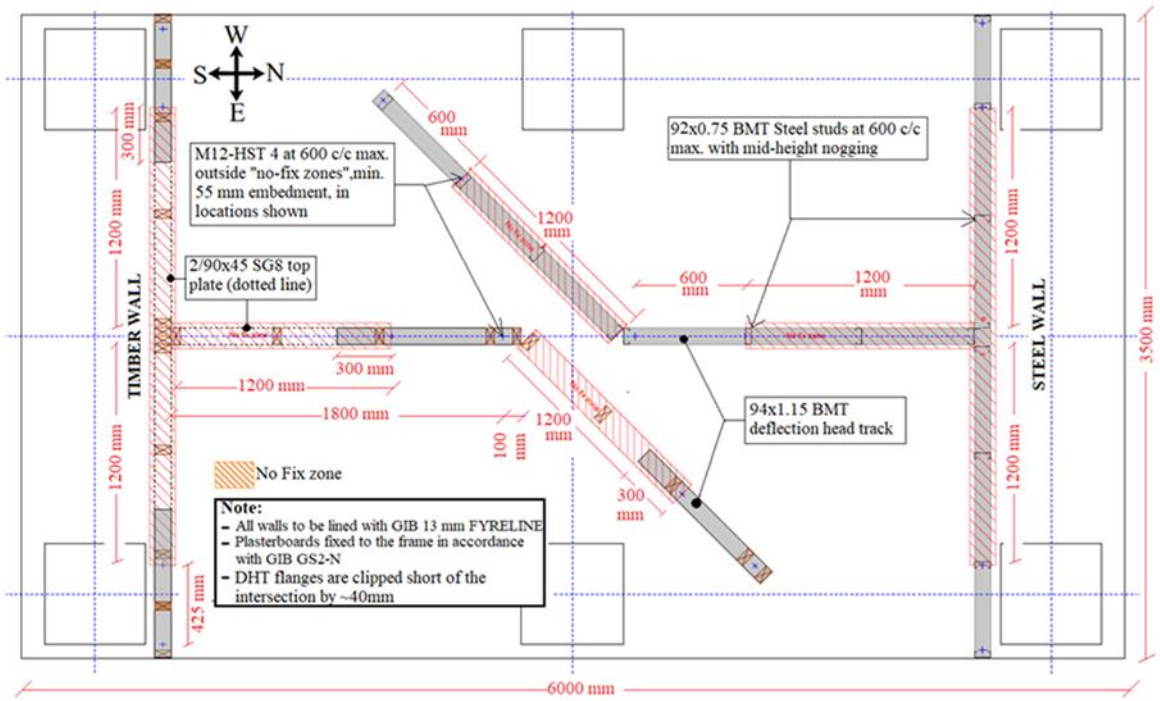

Figure 2.7. Timber and steel stud reflected ceiling plan

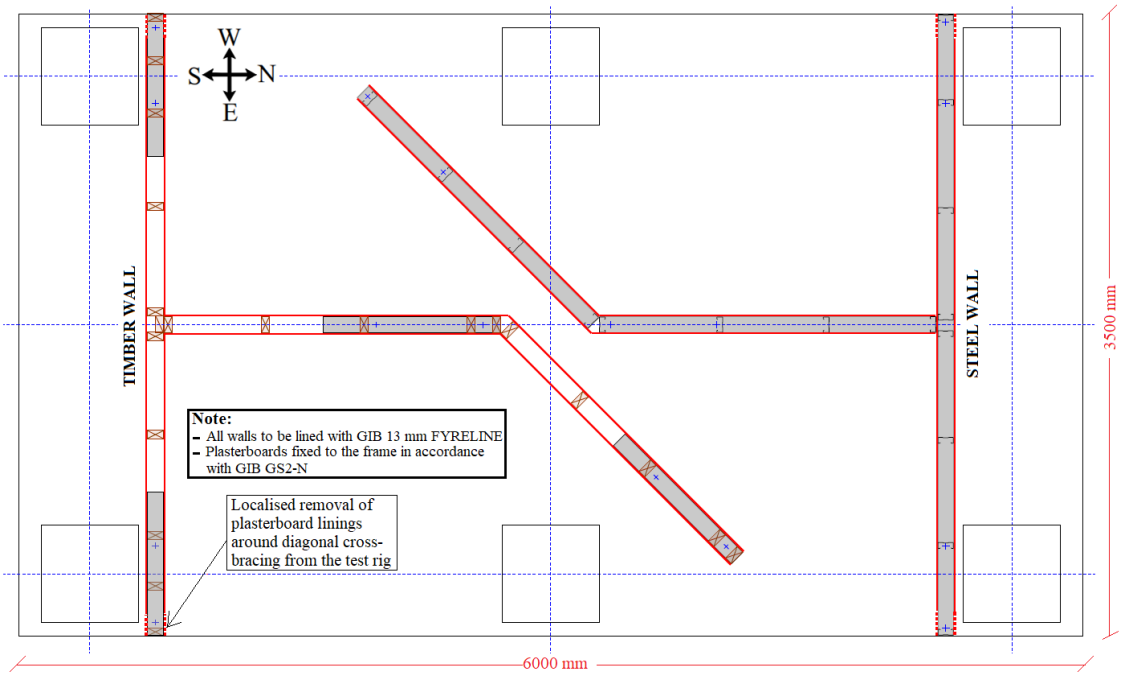

Figure 2.8. Timber and steel frame plasterboard lining plan

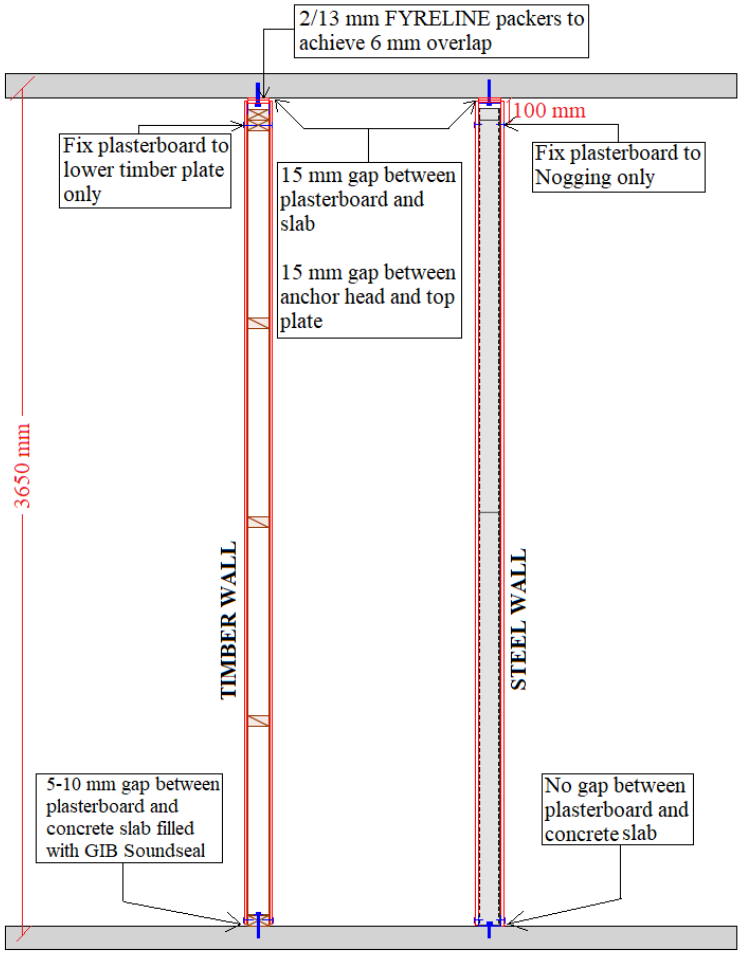

Figure 2.9. Typical wall section elevations

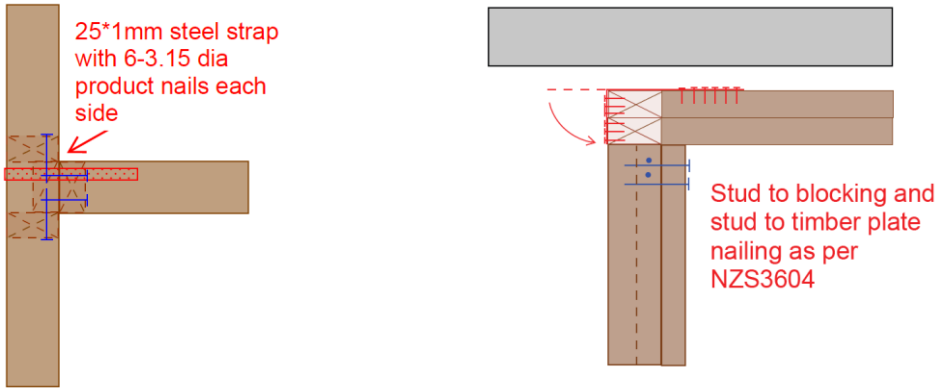

a) Plan view b) Side view

Figure 2.10. Return intersection details in timber wall

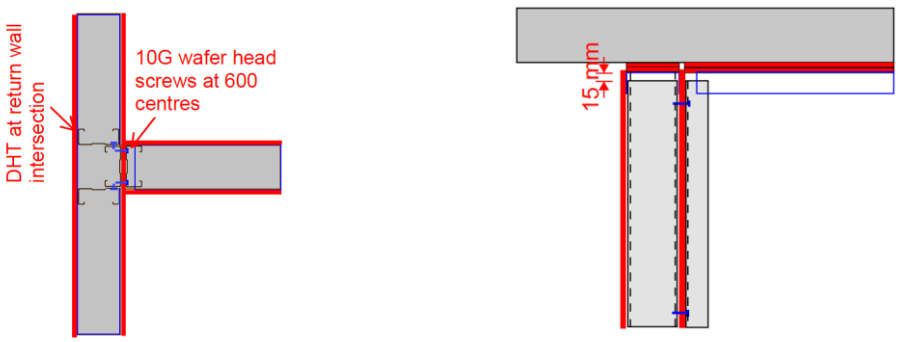

a) Plan view b) Side view

Figure 2.11. Return intersection details in steel wall

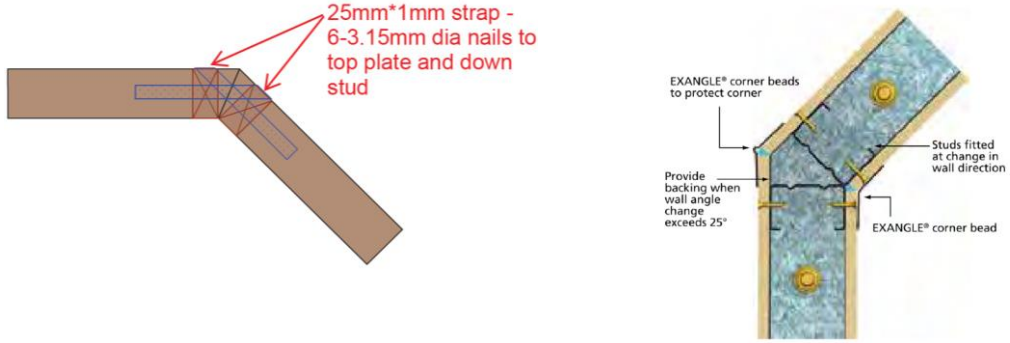

a) Timber wall (plan view) b) Steel wall (plan view)

Figure 2.12. Inclined wall intersection details

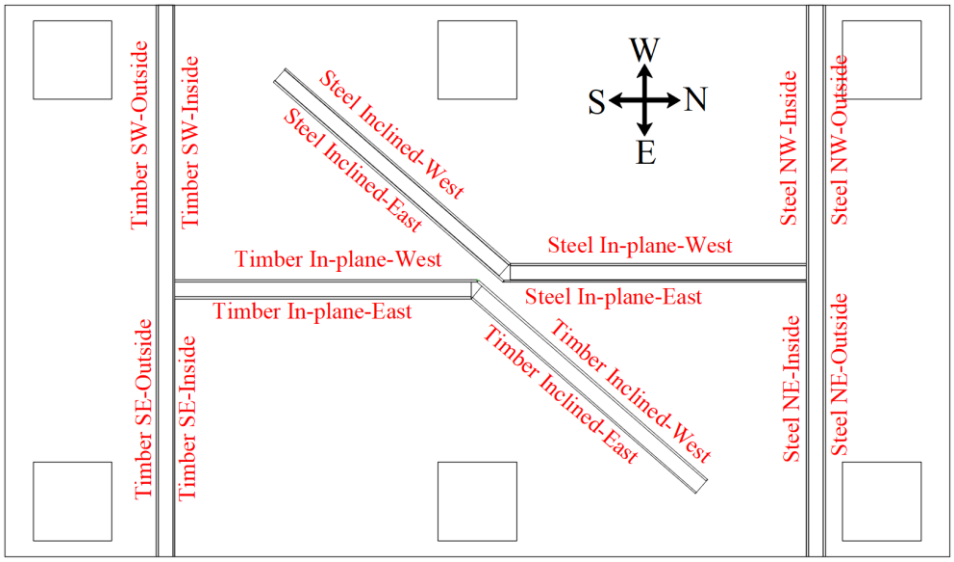

Figure 2.13. Wall nomenclature based on their wall frame and location on plan

Phase I – Walls with restrained ends (restrained specimens)

In the restrained wall specimens, the wall ends of the unrestrained wall specimens, were prevented from rotating, representing an approximately fixed boundary condition, by placing 2/45 × 90 timber elements tightly against the wall linings as shown in Figure 2.14. These timber elements were secured in position using threaded rods anchored into the top slab as shown in Figure 2.15.

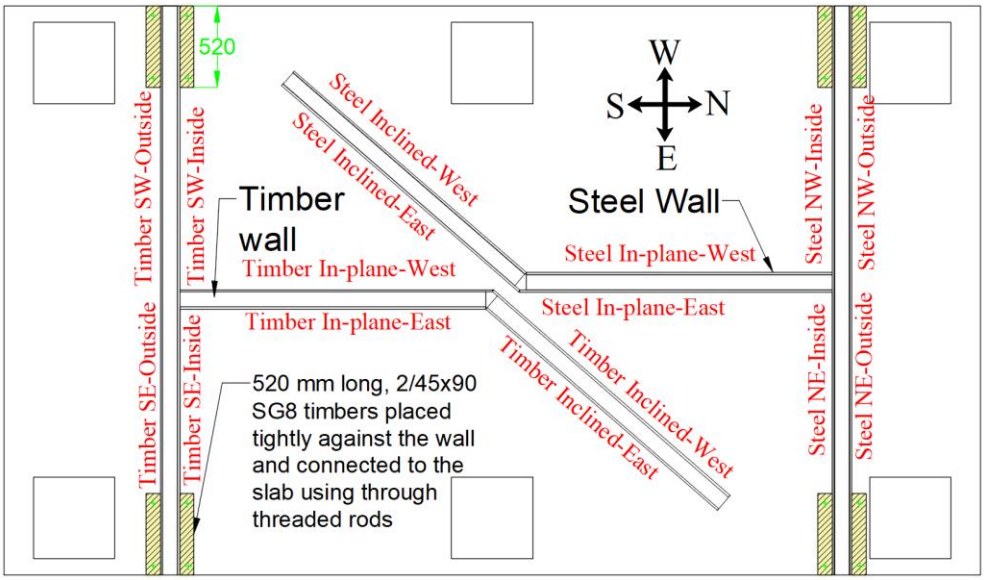

Figure 2.14. Wall specimens with restrained ends with timber members

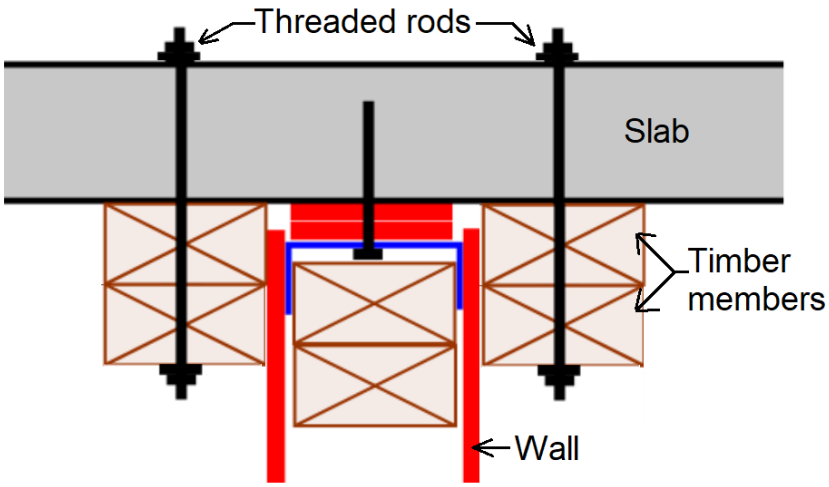

Figure 2.15. Side view of restrained ends of timber wall (steel wall similar)

As-built wall dimensions and photos of wall specimens

The as-built wall dimensions are shown in Figure 2.16 and photos are shown in Figure 2.17 to Figure 2.22.

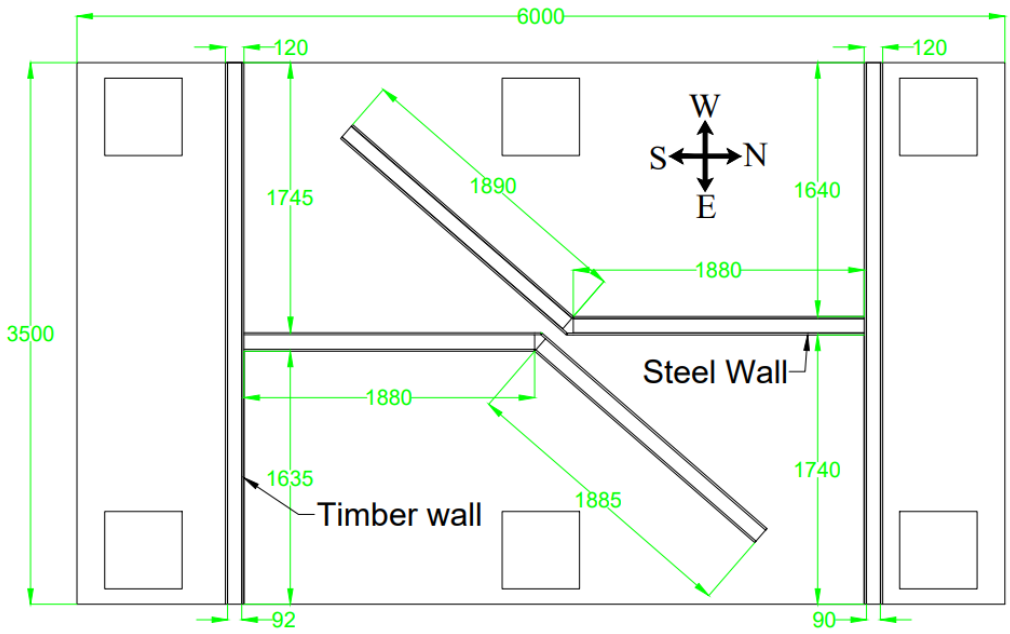

Figure 2.16. As-built wall dimensions shown in plan (dimensions in mm)

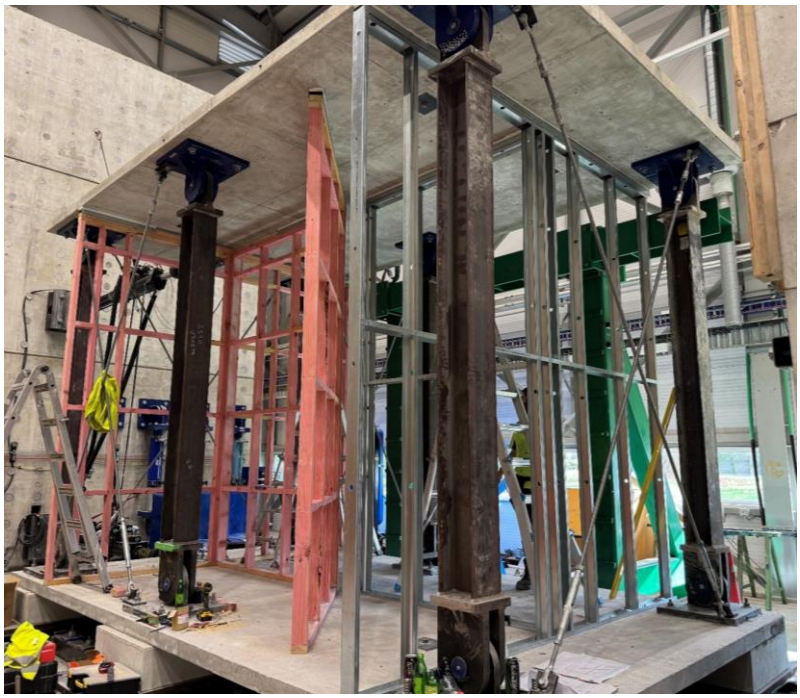

Figure 2.17. Photo of wall frames during construction (North-East view)

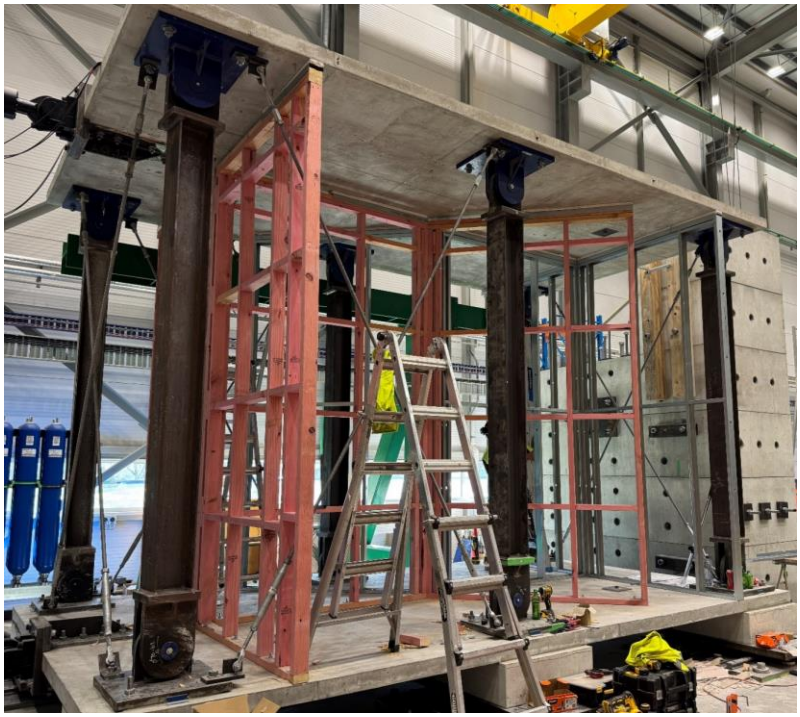

Figure 2.18. Photo of wall frames during construction (South-East view)

Phase I – Unrestrained specimens

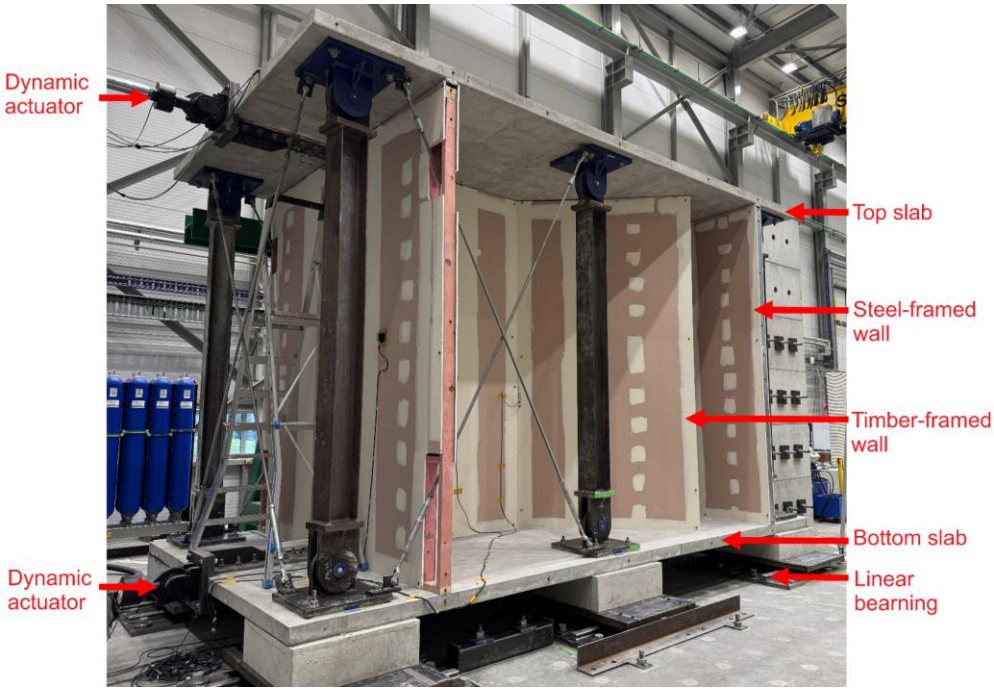

Figure 2.19. Photo of completed walls (South-East view)

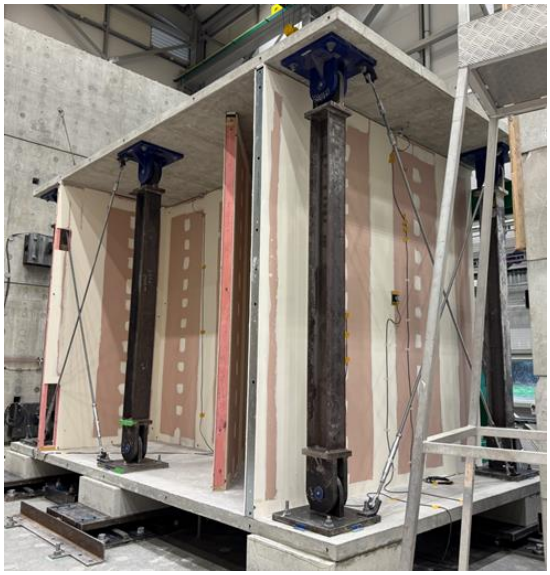

Figure 2.20. Photo of completed walls (North-East view)

a) 20 mm - at Steel NW-Outside Wall

b) 20 mm - at Steel NW-Inside Wall

c) 22 mm - at Timber SW-Inside Wall

d) 22 mm - at Timber SW-Outside Wall

Figure 2.21. Top vertical gap measurements between plasterboards and underneath of the top slab

Phase I – Restrained specimens

a) Steel North – East wall

b) Timber South-West wall

c) Timber South-West Outside wall

d) Timber South – East wall

Figure 2.22. Photos of restrained ends of the wall specimens

Loading protocols

Displacement time histories (referred to as "Motion") for the 2nd and 3rd floors were extracted from a numerical model of a five-storey reinforced concrete structure subjected to the peak ground velocities (PGVs) listed in Table 2.1 using the Imperial Valley earthquake record (El Centro, 1940, Array #9) (Pledger, 2026). The top and bottom slabs were then subjected to the scaled motions presented in Table 2.2, obtained by applying the scale factors given in Table 2.1 to the displacement time histories. This scaling was carried out to achieve the target inter-storey drifts listed in Table 2.1 and Table 2.2.

Spectral floor accelerations, velocities, and displacements for a selected PGVs are presented in Figure 2.24, Figure 2.25, and Figure 2.26, respectively. The input scaled displacement time histories for Motions 5, 10 and 16 are shown in Figure 2.27. It should be noted that the Phase I - unrestrained wall specimens were tested only up to Motion 10, corresponding to 1.0% inter-storey drift (Table 2.2), whereas the Phase I restrained wall specimens were subjected to all motions listed in Table 2.2

Instrumentation

Instrumentation of the structure

The test structure was instrumented with accelerometers placed on the top slab and beneath the bottom slab to record accelerations in the loading direction, i.e., the North - South (NS or X) axis. The accelerometer locations are illustrated in Figure 2.23 and Figure 2.28. The structure was further instrumented with Motion Capture (MoCap) target points (reflective markers) to measure deformations as shown in Figure 2.29. Five MoCap cameras, positioned facing the east elevation of the test setup, recorded the response during the applied motions.

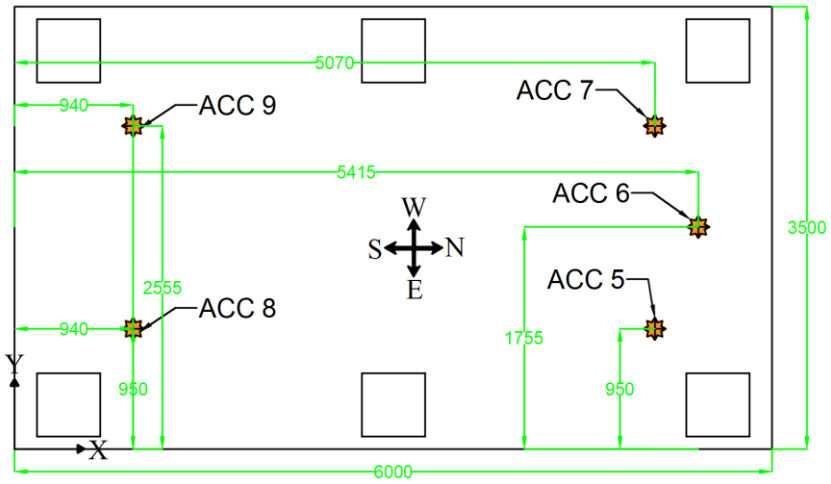

Figure 2.23. Location of accelerometers on top slab (dimensions in mm)

Table 2.1. Input absolute floor motion demands from the 1.0% Design Level structure and corresponding scale factors to achieve the target drift (Pledger, 2026)

Motion	PGV[1](cm/s)	PFA[2] Bottom slab (g)	PFV[3] Bottom slab (m/s)	PFD[4] Bottom slab (mm)	PFA Top slab (g)	PFV Top slab (m/s)	PFD Top slab (mm)	Target Inter- story drift (%)	Scale factor	Comments
0	10	0.11	0.11	27	0.15	0.15	34	0.26	0.1000	
1	10	0.11	0.11	27	0.15	0.15	34	0.26	0.3571	
2	10	0.11	0.11	27	0.15	0.15	34	0.26	0.7143	
3	10	0.11	0.11	27	0.15	0.15	34	0.26	1.0714	
4	20	0.23	0.22	53	0.31	0.3	67	0.52	0.6897	
5	20	0.23	0.22	53	0.31	0.3	67	0.52	0.8621	
6	20	0.23	0.22	53	0.31	0.3	67	0.52	1.0345	
7	30	0.34	0.33	68	0.39	0.45	88	0.87	0.8235	
8	30	0.34	0.33	68	0.39	0.45	88	0.87	0.9412	
9	30	0.34	0.33	68	0.39	0.45	88	0.87	1.0588	
10	40	0.42	0.42	88	0.5	0.56	113	1.11	0.8850	Final test for unrestrained wall specimens
11	50	0.51	0.49	114	0.63	0.63	130	1.3	0.9328	
12	70	0.73	0.62	158	0.88	0.76	163	1.5	0.9677	
13	90	0.94	0.8	193	1.13	0.86	196	1.73	0.9563	
14	110	1.19	0.96	233	1.37	0.97	247	2.04	0.9804	
15	30	0.34	0.33	68	0.39	0.45	88	2.41	0.9332	Bottom slab is locked
16	30	0.34	0.33	68	0.39	0.45	88	2.41	1.0369	Bottom slab is locked
17	30	0.34	0.33	68	0.39	0.45	88	2.41	1.1406	Bottom slab is locked
18	40	0.42	0.42	88	0.5	0.56	113	3.10	0.9690	Bottom slab is locked

[1] Peak Ground Velocity

[2] Peak Floor Acceleration

[3] Peak Floor Velocity

[4] Peak Floor Displacement

Table 2.2. Actual input motions to the test setup (scaled using scale factors from Table 2.1)

Motion	PGV[1] (cm/s)	PFA[2] Bottom slab (g)	PFV[3] Bottom slab (m/s)	PFD[4] Bottom slab (mm)	PFA Top slab (g)	PFV Top slab (m/s)	PFD Top slab (mm)	Target Inter-story drift (%)	Comments
0	1.00	0.01	0.01	2.70	0.02	0.02	3.40	0.03	
1	3.57	0.04	0.04	9.64	0.05	0.05	12.14	0.10	
2	7.14	0.08	0.08	19.29	0.11	0.11	24.29	0.20	
3	10.71	0.12	0.12	28.93	0.16	0.16	36.43	0.30	
4	13.79	0.16	0.15	36.55	0.21	0.21	46.21	0.40	
5	17.24	0.20	0.19	45.69	0.27	0.26	57.76	0.50	
6	20.69	0.24	0.23	54.83	0.32	0.31	69.31	0.60	
7	24.71	0.28	0.27	56.00	0.32	0.37	72.47	0.70	
8	28.24	0.32	0.31	64.00	0.37	0.42	82.82	0.80	
9	31.76	0.36	0.35	72.00	0.41	0.48	93.18	0.90	
10	35.40	0.37	0.37	77.88	0.44	0.50	100.00	1.00	Final test for unrestrained wall specimens
11	46.64	0.48	0.46	106.34	0.59	0.59	121.27	1.25	
12	67.74	0.71	0.60	152.90	0.85	0.74	157.74	1.50	
13	86.07	0.90	0.77	184.56	1.08	0.82	187.43	1.75	
14	107.84	1.17	0.94	228.43	1.34	0.95	242.16	2.00	
15	28.00	0	0	0	0.36	0.42	82.13	2.25	Bottom slab is locked
16	31.11	0	0	0	0.40	0.47	91.25	2.50	Bottom slab is locked
17	34.22	0	0	0	0.44	0.51	100.38	2.75	Bottom slab is locked
18	38.76	0	0	0	0.48	0.54	109.50	3.00	Bottom slab is locked

[1] Peak Ground Velocity [2] Peak Floor Acceleration [3] Peak Floor Velocity [4] Peak Floor Displacement

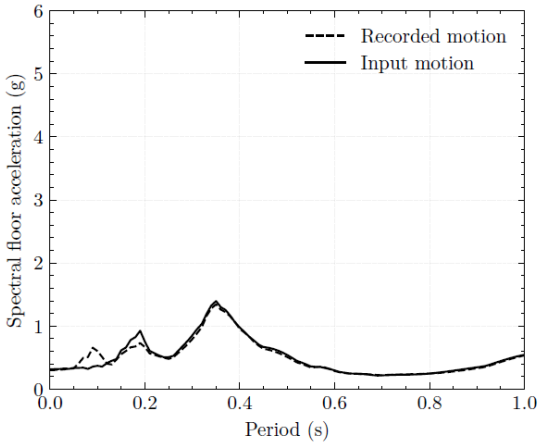

a) PGV = 20 cm/s

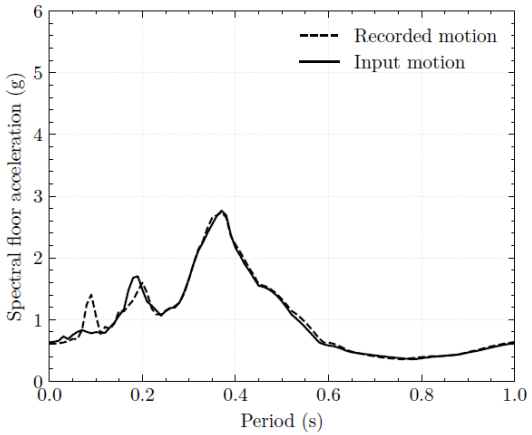

b) PGV = 50 cm/s

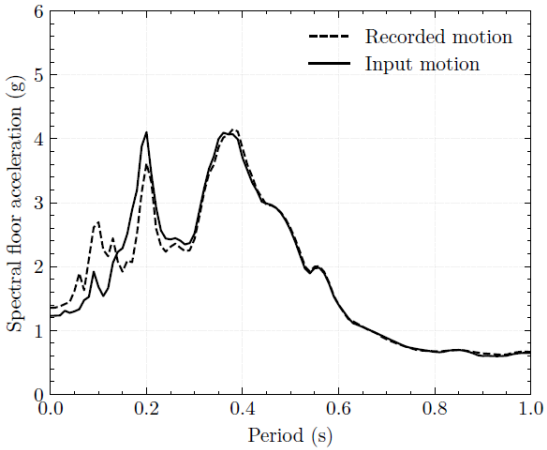

c) PGV = 100 cm/s

Figure 2.24. Spectral floor acceleration for 1.0 % design level structure at different peak ground velocities (PGVs) from Table 2.1 (Pledger, 2026)

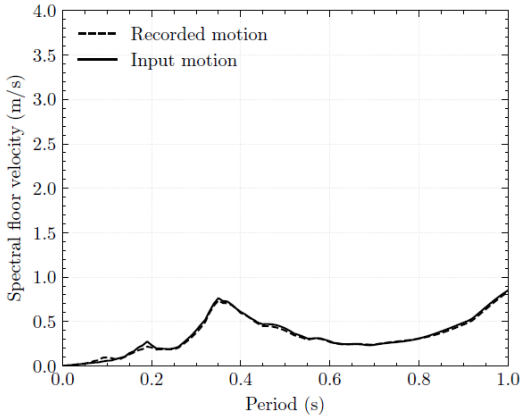

a) PGV = 20 cm/s

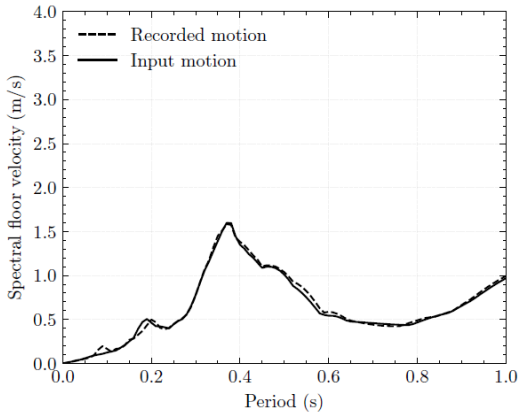

b) PGV = 50 cm/s

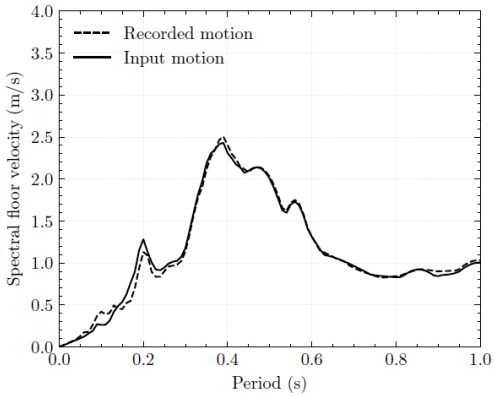

c) PGV = 100 cm/s

Figure 2.25. Spectral floor velocities for 1.0 % design level structure at different peak ground velocities (PGVs) from Table 2.1 (Pledger, 2026)

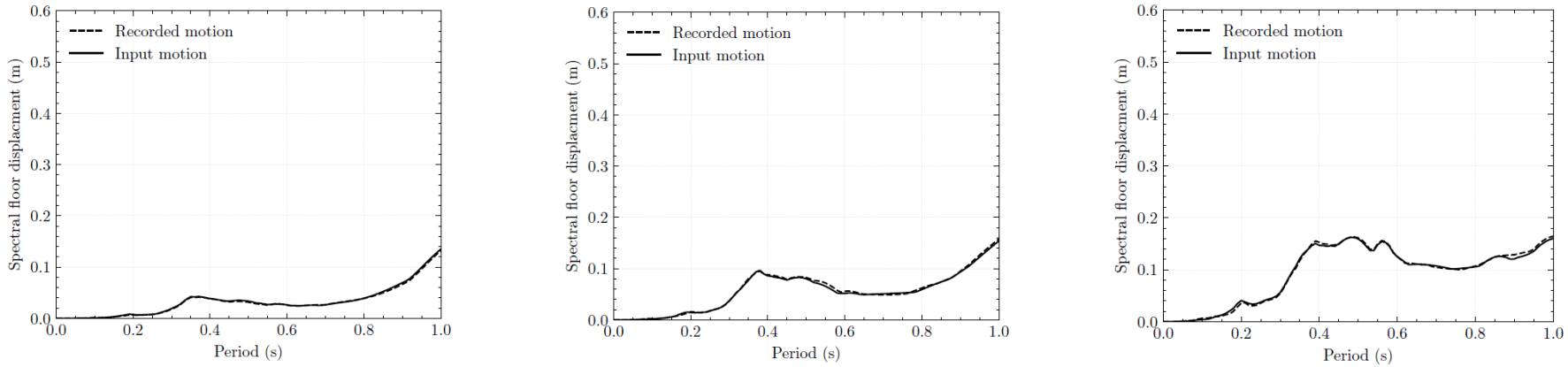

a) PGV = 20 cm/s b) PGV = 50 cm/s c) PGV = 100 cm/s

Figure 2.26. Spectral floor displacements for 1.0 % design level structure at different peak ground velocities (PGVs) from Table 2.1 (Pledger, 2026)

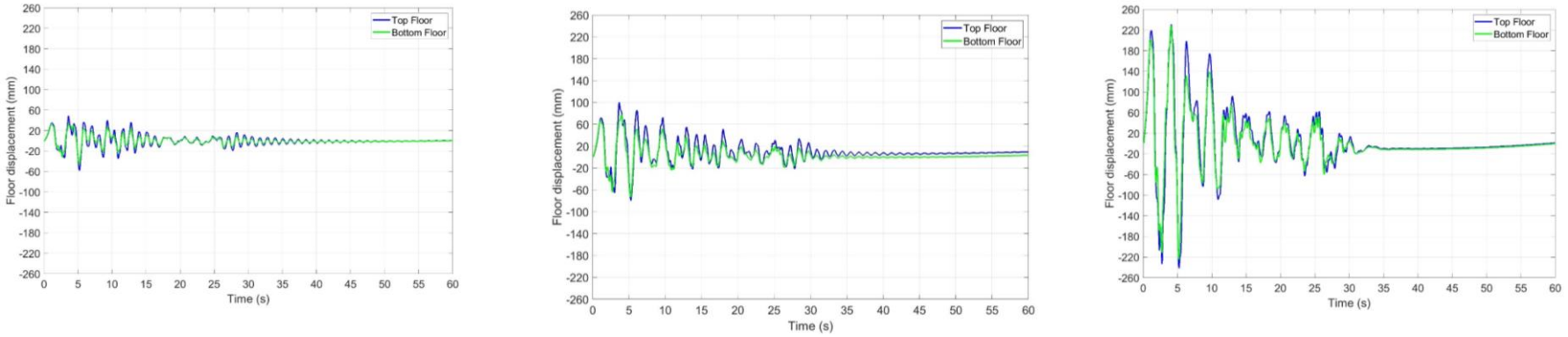

a) Motion 5 b) Motion 10 c) Motion 16

Figure 2.27. Floor displacement command time histories of top and bottom slabs during different scaled motions from Table 2.2

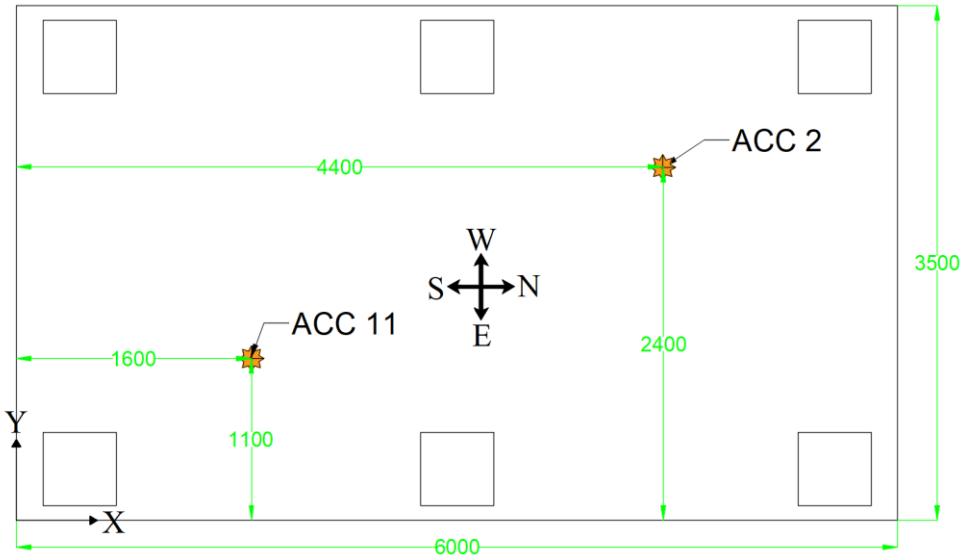

Figure 2.28. Location of accelerometers underneath the bottom slab (dimensions in mm)

Instrumentation of the wall specimens

The wall specimens were instrumented using displacement potentiometers, accelerometers and MoCap reflectors at key locations as illustrated in Figure 2.29 to Figure 2.33.

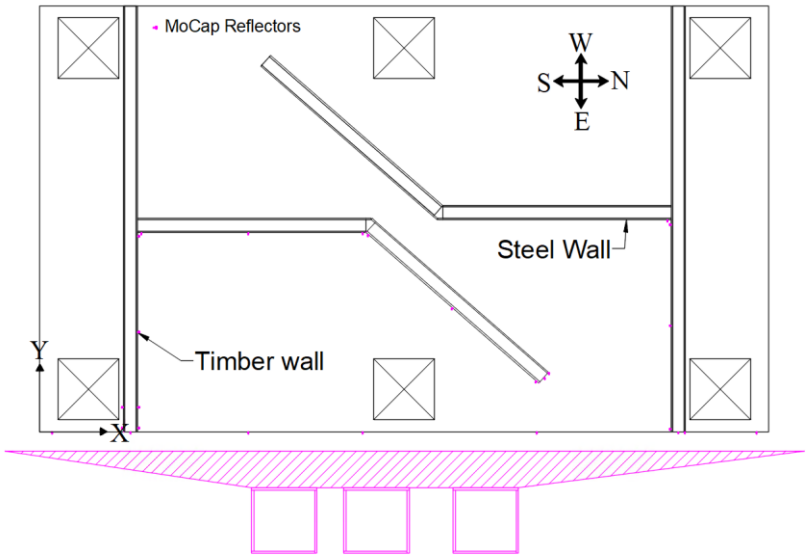

a) Plan view

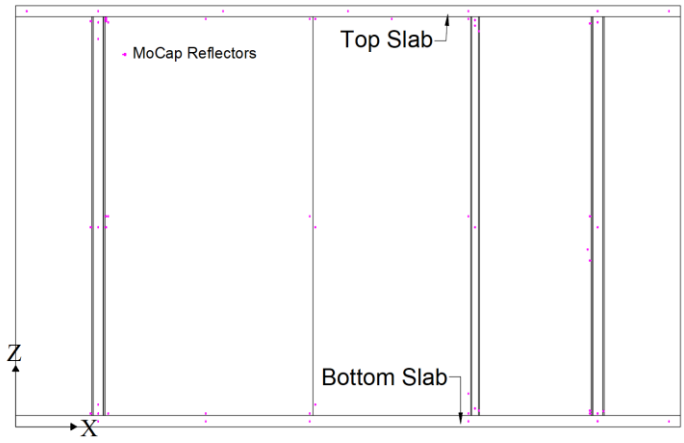

b) East elevation

Figure 2.29. Motion Capture (MoCap) target (reflector) points to record the deformation of the wall test structure and wall specimens

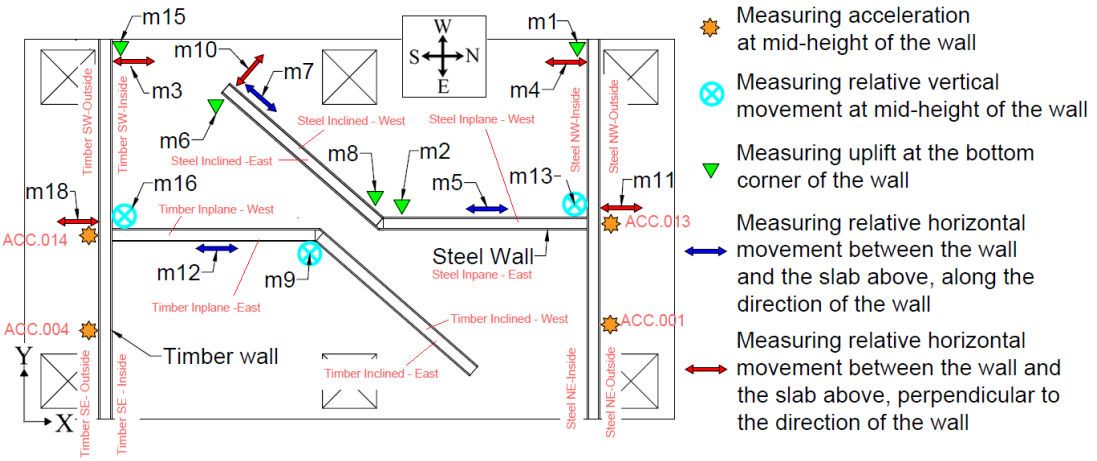

Figure 2.30. Phase I – unrestrained specimen instrumentation (Initial)

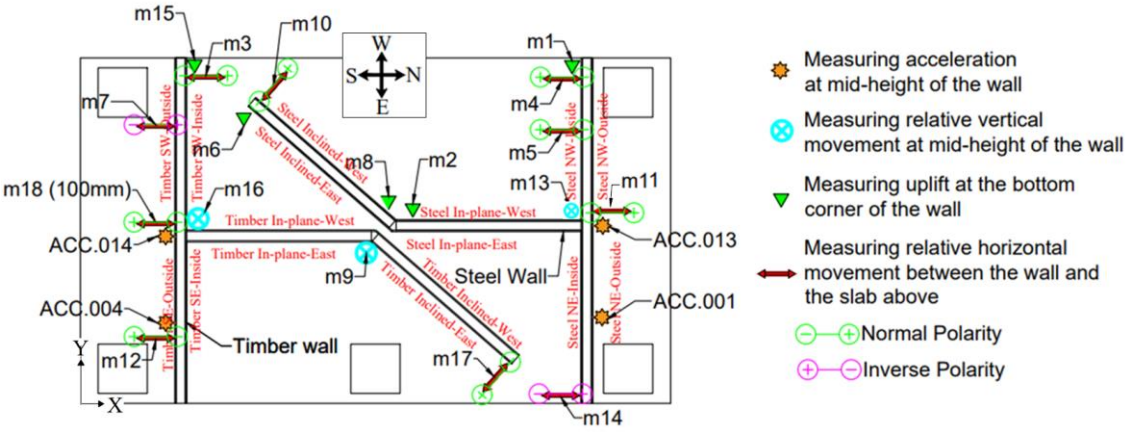

Figure 2.31. Phase I – unrestrained specimen instrumentation (revised)

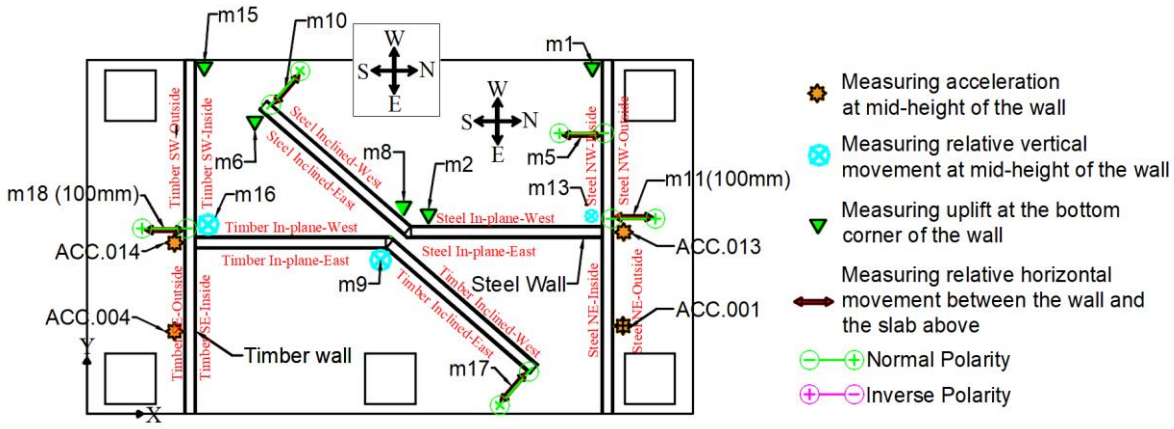

Figure 2.32. Phase I – Restrained specimen instrumentation

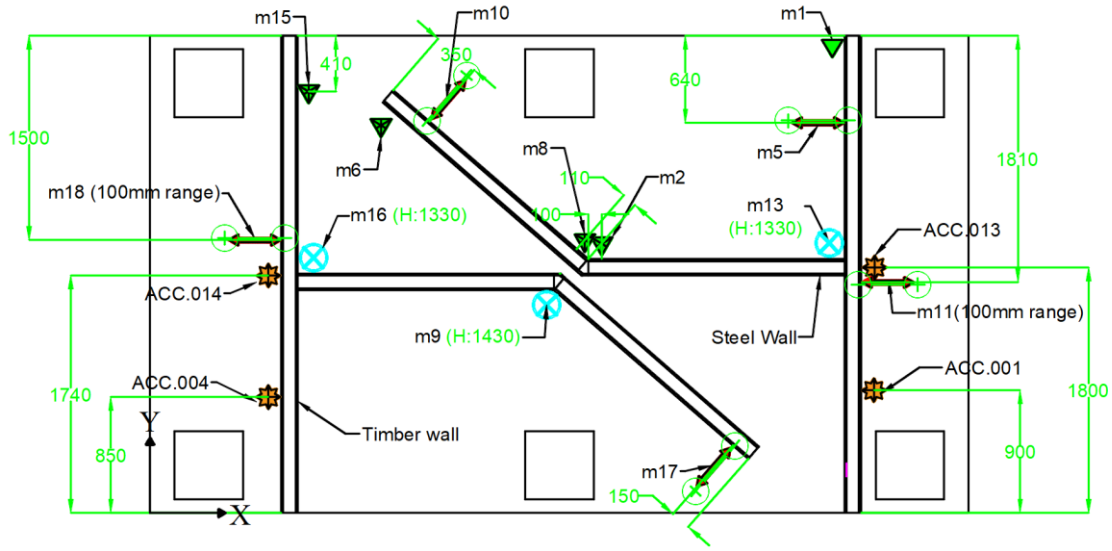

Figure 2.33. Phase I – Restrained specimen instrumentation locations on plan (dimensions in mm)

Data processing

The recorded acceleration data were filtered to remove noise. A 4th-order low-pass Butterworth filter (Butterworth, 1930; Parks & Burrus, 1987; Sorrentino, 2007) with a cutoff frequency of 50 Hz was applied, using a sampling frequency of 180 Hz. The 50 Hz cutoff was selected to capture local high-frequency responses of the specimens. Furthermore, to address instantaneous impulse peaks in the acceleration readings, a 4th order 1-dimensional median filter was employed for smoothing. This filter replaces each

point with the median value within a sliding window of size 4, thereby removing impulse noise while preserving signal edges, with zero-padding applied at the ends. The displacement data were used without postprocessing.

While analysing the data from the experimental sensors, the acceleration responses recorded during Motion 0 are disregarded for both structural and component-level analyses due to their negligible magnitude. Similarly, Motion 0 data is excluded from all structural drift calculations. For component displacement analysis, the data from Motion 0 is included in the plots for completeness but is omitted from discussion, as the measured displacements are considered insignificant.

DAMAGE STATE CLASSIFICATION SCHEME

Four damage states: Superficial, Minor Repair, Moderate Repair and Critical have been defined to classify the damage observed in the test. These discrete damage states are separated based on the repair requirements and impact on the functionality of the non-structural elements.

Superficial

The Superficial damage state includes damage that is primarily aesthetic, meaning it may not be immediately noticeable, and either does not require repair or only needs minor repair (not immediately). The damage does not impact the seismic performance and functionality of the non-structural element. Some examples include screw impressions, and hairline cracks on plasterboard linings.

Minor Repair

The Minor Repair damage state includes damage that does not immediately affect the seismic performance or functionality of the system but should be monitored and

addressed during future repairs or routine maintenance. This damage state does not substantially affect the load-bearing capacity, alter the system's alignment, or compromise the non-structural element's ability to remain in place under normal conditions. In some cases, temporary measures can be adopted to limit the spread of damage to other components damage before the actual repairs occur. Some examples include cracks and crushing of plasterboard linings which compromise the fire-rating (or acoustics) of the walls.

Moderate Repair

The Moderate Repair damage state includes damage that begins to affect its intended performance, but without creating an immediate safety hazard or causing complete loss of function. The system remains largely in place and attached to the structure, posing no immediate risk of falling or obstructing egress. However, the damage requires repair to restore full performance. For example, damage to few internal frame members while the wall remains standing and fully supported by the remaining framing, but the load path has been weakened and requires repair to restore full capacity.

Critical

The Critical damage state includes damage that impairs the seismic performance and/or functionality of the system, resulting in loss of function and demanding urgent repair (as soon as possible with high priority). Some examples include severe damage to the plasterboard linings, separation of walls at junctions and damage to frames of the walls.

Pre-test damage inspections

During pre-test inspections, the timber and steel wall specimens presented several types of damage. These included hairline shrinkage cracks in the plaster, incomplete plaster

coverage at junctions, and plasterboard cracks at corners and mid-height ends. Additional observations comprised minor damage to both the plasterboard and the bottom timber plate, as well as screw impressions at the base of the walls. Notably, in some areas no visible plaster shrinkage cracks were present. All damage is documented with photos and locations in **APPENDIX A.**

EXPERIMENTAL RESULTS

Response of the test structure

Inter-storey drifts

The measured peak inter-storey drifts between the two floors (to which the wall specimens were subjected to), derived from actuator data, are presented in

Figure 2.34.The unrestrained specimen was tested twice, each time reaching a peak drift of 0.98%, before the out-of-plane walls were restrained by timber blocks. Subsequently, the restrained wall specimen was tested up to an inter-storey drift of 3.08%. The recorded floor displacements from Tests 20 and 34 are shown as examples in Figure 2.35.

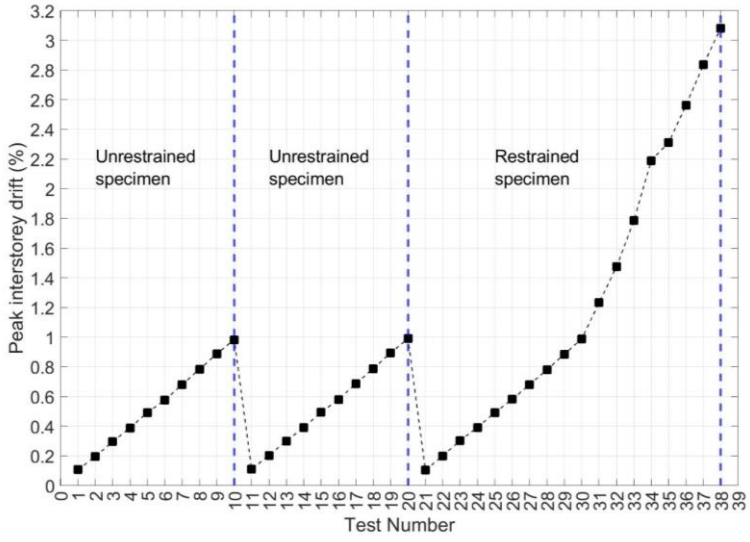

Figure 2.34 Recorded peak inter-storey drifts between floors

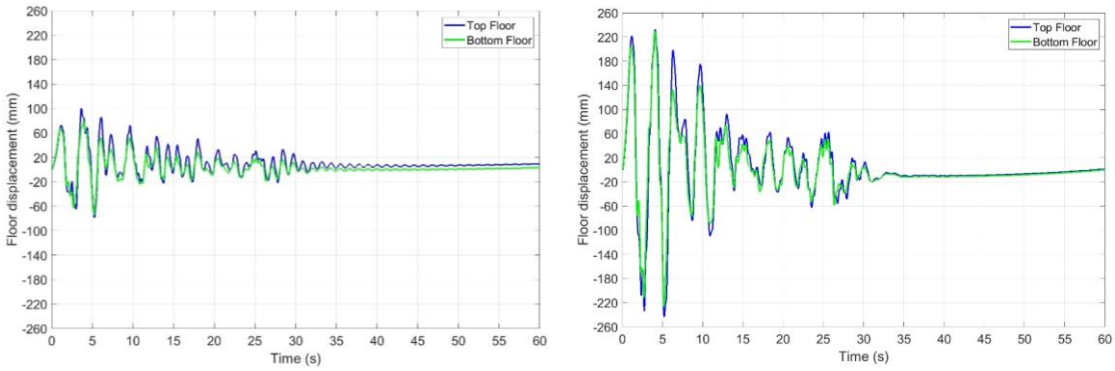

a) Test #20 b) Test #34

Figure 2.35 Recorded lateral floor displacement in the loading direction (X)

Floor accelerations

The recorded peak floor accelerations, calculated as the average of the maximum in-direction readings from all floors-mounted accelerometers after postprocessing, are presented in Figure 2.36. The top floor consistently exhibited higher maximum horizontal acceleration than the bottom floor. During Test #34, the peak horizontal accelerations reached 1.28 g on the top floor and 0.95 g on the bottom floor. The acceleration time histories in the X-direction, recorded by the floor-mounted accelerometers and after postprocessing during Test #34, are shown Figure 2.37.

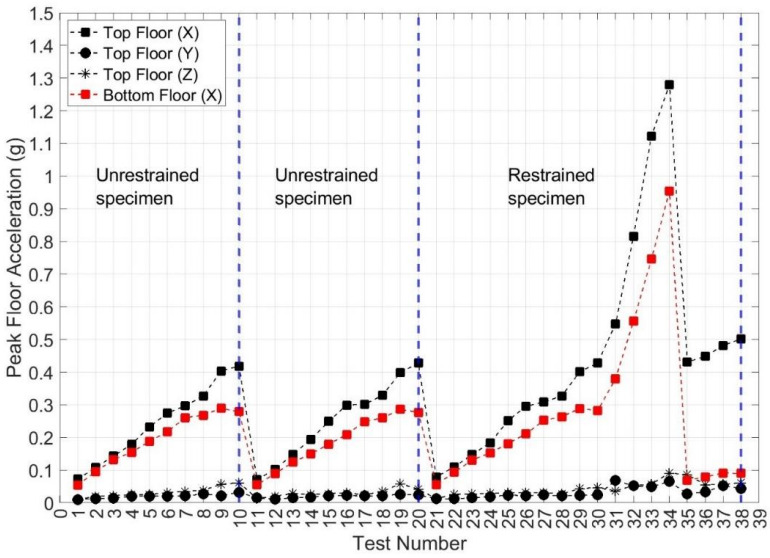

Figure 2.36 Recorded peak floor accelerations with direction shown inside brackets

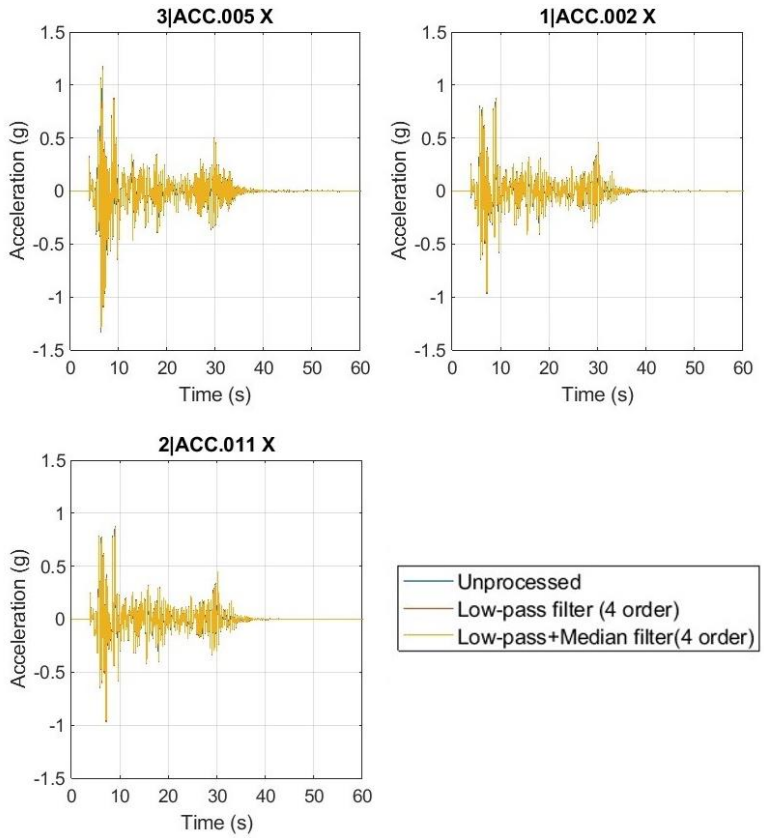

Figure 2.37 Recorded floor accelerations in X-direction (refer to Figure 2.23 and Figure 2.28 for locations of the accelerometers) during Test #34

Lateral forces

The measured peak lateral forces, recorded by the actuators connected to the floor slabs, are presented in Figure 2.38.

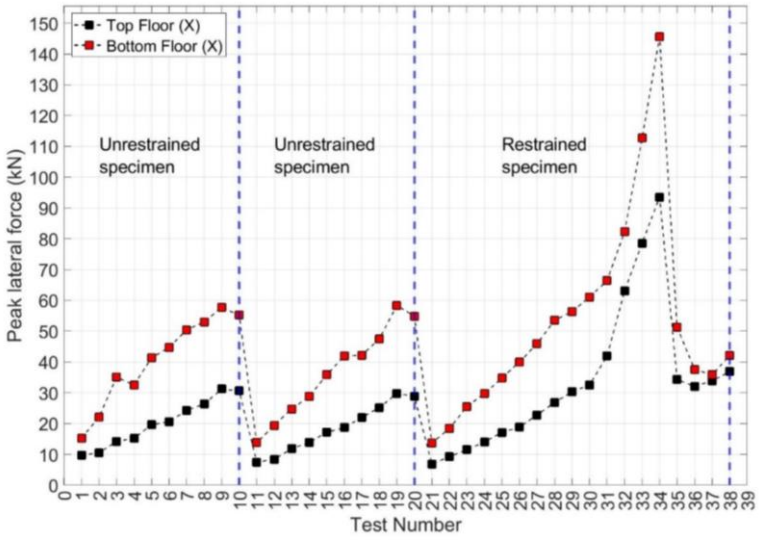

Figure 2.38 Recorded peak lateral forces on the floors

It can be observed that the lateral force on the bottom floor is higher than that on the top floor, which is attributed to the greater portion of the specimen's mass being transferred downward. The maximum lateral forces recorded on the bottom and top floors were 146 kN and 94 kN, respectively. The variations in the recorded forces correspond to the changes in acceleration shown in Figure 2.36.

Component response

Damage observation to specimens and their damage state classification

The progression of damage throughout the experimental program is analysed and discussed using the inter-storey drift as the primary engineering demand parameter.

Timber Specimens

Damage in the unrestrained timber specimen, which was tested up to 1.00 % drift demand, initiated at a very low inter-storey drift of 0.11% with the formation of hairline cracks at the wall junction. As drift increased, screw impressions became apparent at 0.39%, followed by minor cracking in the plasterboard at 0.78% drift. This progression indicates that the specimen experienced gradual damage, with cosmetic and minor issues emerging early in the loading protocol.

The restrained timber specimen, which was tested to a much higher drift of 3.0%, exhibited a different damage pattern influenced by prior testing. While hairline cracks in the plasterboard were noted at 0.30% drift, these were considered progressive from the earlier unrestrained test. More definitive new damage, in the form of a crack in the plasterboard that could adversely affect the fire seal, was observed at 0.58% drift. The first significant structural damage occurred at 0.99% drift, with the breaking of the top timber plates, a failure confirmed by loud sounds during testing and post-test inspection.

This shows that while restraint slightly delayed the onset of cosmetic damage, it caused the test specimen to sustain higher levels of damage at a drift level comparable to where the unrestrained test ended.

Steel Specimens

For the unrestrained steel specimen, tested up to 1.00 % drift demand, initial damage appeared simultaneously at 0.20% drift in the form of hairline cracks in the plasterboard and screw impressions (the latter attributed to a construction error). The damage remained minor, with only a small tear in the joint paper observed at 0.89% drift. The damage largely confined to finishes up to 1.00 % drift.

The restrained steel specimen, tested up to 3.08 % drift demand, demonstrated a significant delay in initial damage and a shift toward more severe failure modes. Screw impressions were not recorded until 0.99% drift, and a minor joint paper tear followed at 1.23% drift. Substantial damage began at 1.79% drift, with cracks in the plasterboard and tears in the plaster paper, both noted as potential compromises to the fire seal. Further cracking occurred at 2.19% drift. The defining failure event was the separation of the steel frames at the wall junctions, which occurred abruptly at 2.56% drift. This indicates that the restraint system suppressed early, minor damage but resulted in the accumulation of internal forces, leading to a sudden and brittle connection failure at high drift.

Photographic documentation and detailed descriptions of the damage observed in the wall specimens during testing, along with the corresponding inter-storey drift levels at which each damage occurred, are provided in Table 2.6 through Table 2.32 in **APPENDIX A.**

Table 2.3 documents the observed damage and its damage state classification for the wall specimens.

Table 2.3. Damage state of the tested specimen and corresponding inter-story drifts after which the damage was observed

Specimen	Damage State	Damage type	Inter-storey drift (%) (#Test number)	Comment/ Reference
Timber (Unrestrained) tested up to 1.0 % drift	Superficial	Hairline crack at wall junction	0.11 (#1)	Table 2.6
	Superficial	Screw Impressions	0.39 (#4)	Table 2.7
	Superficial	Minor crack in the plasterboard	0.78 (#8)	Table 2.9
Timber (Restrained) tested up to 3.0 % drift	Superficial	Hairline crack in plasterboard	0.30 (#23)	Although progressive damage from previous unrestrained specimen; Table 2.14
	Minor Repair	The crack in the plasterboard	0.58 (#26)	Although progressive damage; might adversely affect the fire seal. Table 2.16
	Moderate Repair	Damage to the top timber plates (break)	0.99 (#30)	Confirmed by loud sounds during tests and post-test frame inspection; Table 2.17
Steel (Unrestrained) tested up to 1.0 % drift	Superficial	Hairline crack in plasterboard	0.20 (#2)	Table 2.11
	Superficial	Screw impressions	0.20 (#2)	Construction error. Table 2.11
	Superficial	Minor tear in the joint paper	0.89 (#9)	Table 2.13
Steel (Restrained) tested up to 3.0 % drift	Superficial	Screw impressions	0.99 (#20)	Table 2.25
	Superficial	Minor tear in the joint paper	1.23 (#31)	Table 2.26
	Minor Repair	Crack in the plasterboard	1.79 (#33)	Might compromise the fire seal; Table 2.28
	Minor Repair	Tear in the plaster paper	1.79 (#33)	Might compromise the fire seal; Table 2.28
	Minor Repair	Crack in the plasterboard	2.19 (#34)	Might compromise the fire seal; Table 2.29
	Critical	Separation of walls at junctions	2.56 (#34)	Separation of connected steel frames at junctions; Table 2.31

Peak component accelerations and dynamic amplification factors

The peak component accelerations (PCA) recorded in the out-of-plane (X) direction at the wall junctions (ACC.014Z, ACC.013Z) and at mid-length of the overhang (ACC.001Z, ACC.004Z) are plotted against the average peak floor acceleration (PFA) of both floors for all 38 tests of the timber- and steel-framed walls in Figure 2.39. Accelerometer locations are shown in Figure 2.23 and Figure 2.28.

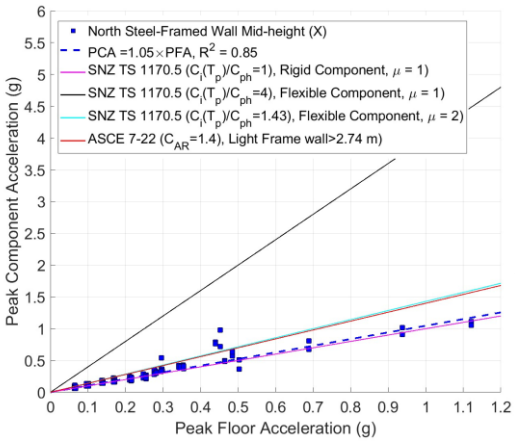

a) North Steel-framed wall

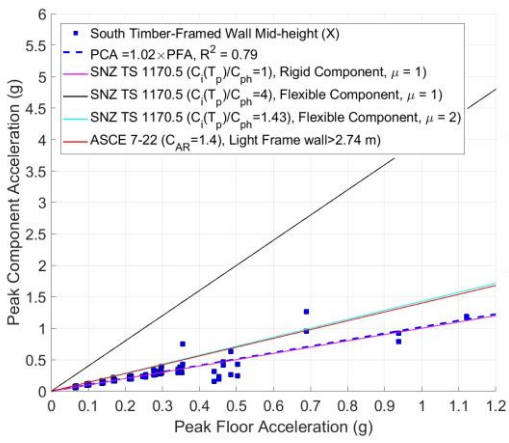

b) South Timber-framed wall

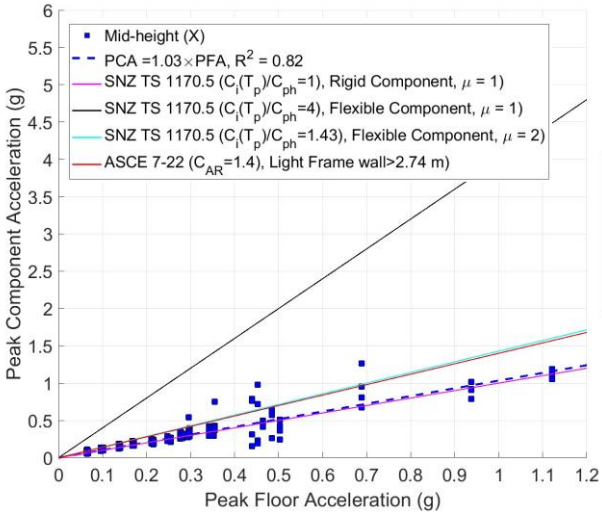

c) Both Steel and Timber – framed walls

Figure 2.39 Peak accelerations of wall specimens in out-of-plane direction (X) as a function of peak floor acceleration

Figure 2.39 also presents PCA values calculated by multiplying the average PFA from both top and bottom floors by: (1) the ratio $C_i(T_p)/C_{ph}$ for different ductility levels (μ), per SNZ TS 1170.5 (2025), and (2) the Component Resonance Ductility Factor (C_{AR}) from ASCE/SEI 7-22 (2022). $C_i(T_p)$ is the component spectral-shape coefficient and (C_{ph}) is the component horizontal-response factor. Additionally, a linear fit through the origin is plotted against the experimental data points.

Figure 2.39 (c) indicates that the PCA/PFA ratio (i.e., Dynamic Amplification Factors (DAF inclusive of part ductility (μ)) for the out-of-plane light-frame walls, as determined by the best-fit line through the origin, is approximately 1.03 with $R^2 = 0.82$. According to SNZ TS 1170.5 (2025), this experimental ratio corresponds to the design cases for a Rigid component ($\mu = 1$) or a Flexible component with high ductility ($\mu \geq 2.5$). The standard's provision for a Flexible component with $\mu = 2$ provides a conservative estimate, exceeding the measured ratio by a factor of 1.39. A similarly conservative estimate is given by ASCE/SEI 7-22 (2022), with a factor of 1.36.

Figure 2.40 plots the PCA/PFA ratio for the walls, calculated by dividing the PCA by the average PFA of both floors. The box plot in Figure 2.40 (c) shows a median PCA/PFA value of 1.05 for light-framed walls.

Component displacement analysis

Unrestrained wall specimens – initial test

Figure 2.42 presents the absolute maximum and residual displacements recorded at various locations on the timber wall specimen (refer Figure 2.30 and Figure 2.41 for measurement locations) during the initial test series .

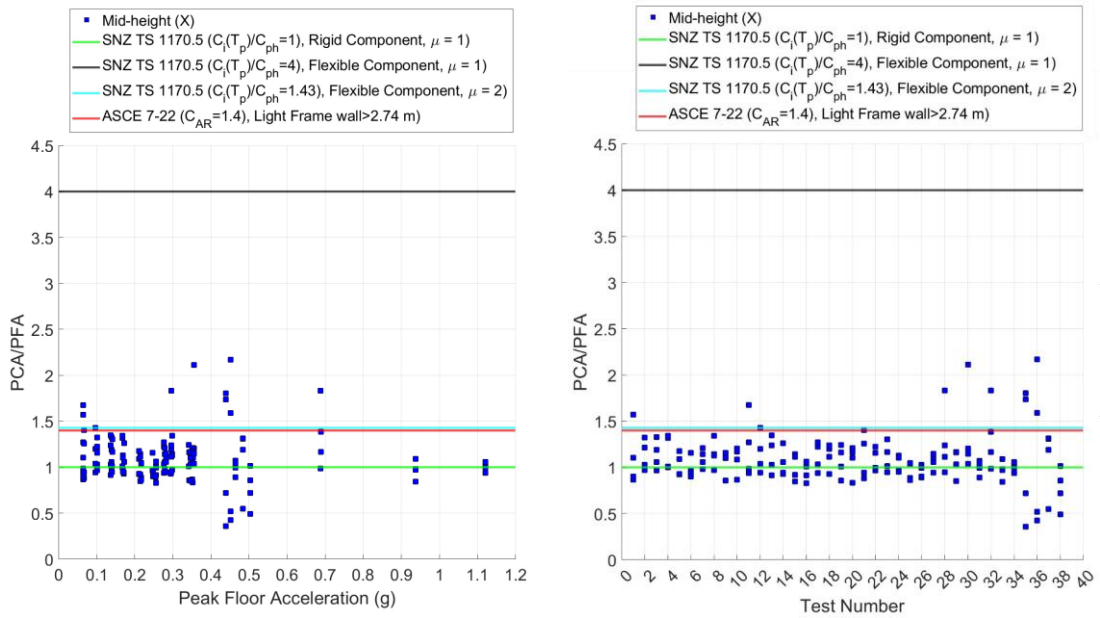

a) PCA/PFA as a function of PFA b) PCA/PFA as a function of Test number

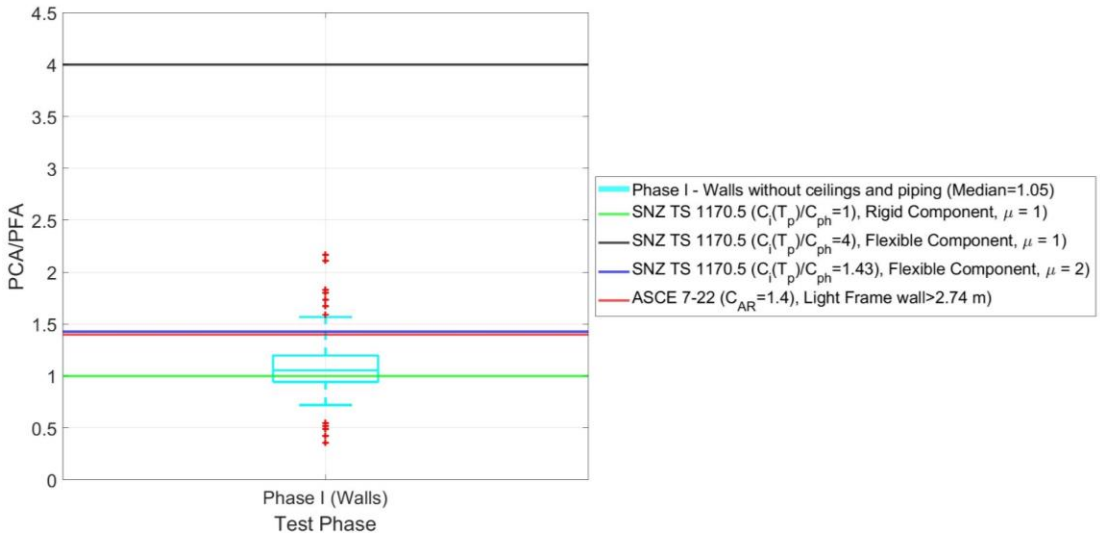

c) PCA/PFA box plot (Median = 1.05)

Figure 2.40 PCA/PFA in the out-of-plane direction (X) for light-framed walls

As shown in Figure 2.42 (a), the wall exhibited the anticipated in-plane sliding, with displacements aligning closely with the estimated values derived from the recorded drift ratio times the wall height (3550 mm). Concurrently, the West End of the out-of-plane wall remained largely stationary. This behaviour indicates that the out-of-plane wall curved at the junction, producing an out-of-plane displacement of approximately 21 mm at that point. Instruments m18 and m12 were removed from the dataset after exceeding

their measurement capacity at 0.68% drift. Figure 2.42 (b) indicates that residual displacements in the in-plane wall, including at the junction, initiated at a drift of 0.58% and accumulated to approximately 4 mm by 0.68% drift while there was no significant residual displacement at West End.

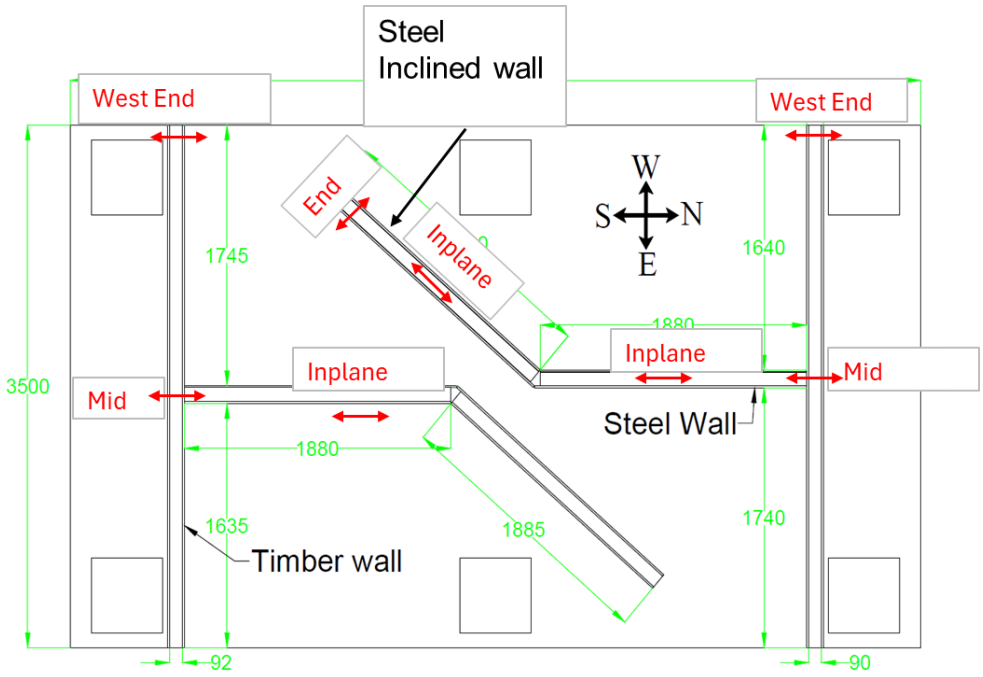

Figure 2.41 Indicative lateral displacement measurement locations for initial unrestrained wall specimens

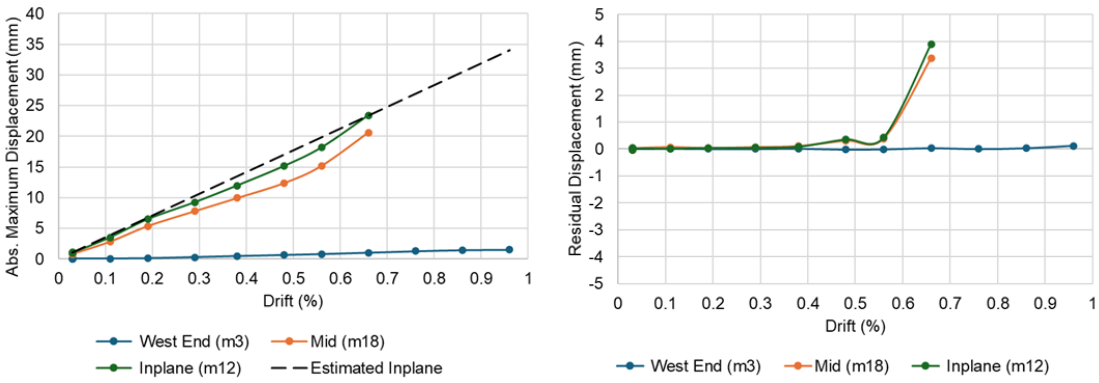

a) Absolute maximum displacements b) Residual displacements

Figure 2.42 Lateral displacements for the timber-framed wall specimen (approximate measurement locations shown and instrument numbers in brackets)

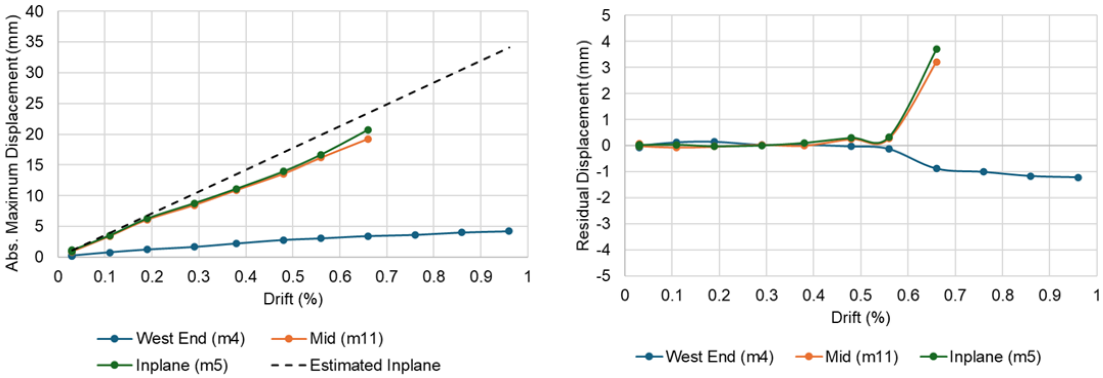

a) Absolute maximum displacements b) Residual displacements

Figure 2.43 Lateral displacement measurements for steel-framed wall specimen (approximate measurement locations shown and instrument numbers in brackets)

The steel-framed wall demonstrated in-plane behaviour analogous to its timber counterpart, as detailed in Figure 2.43 and Figure 2.44. During a drift of 0.98%, its West End displaced approximately 5 mm, retaining a residual displacement of about 3 mm. According to Figure 2.43(b), residual displacements in the steel in-plane wall began at 0.58% drift, reaching roughly 4 mm at 0.68% drift, while the West End retained a residual of 1.2 mm.

The response of the inclined steel-framed wall is shown in Figure 2.44. Figure 2.44 (a) illustrates the expected sliding of the in-plane wall relative to the top floor, with its End remaining largely stationary and exhibiting a maximum displacement of 3 mm; this plot also includes the estimated in-plane displacement for the inclined wall, derived by multiplying the inter-storey drift by the cosine of its angle (41°) relative to the primary in-plane wall. Figure 2.44 (b) shows that residual displacements in this wall initiated at 0.58% drift and grew to about 3 mm at 0.68% drift, with no significant residual at the West End by 0.98% drift.

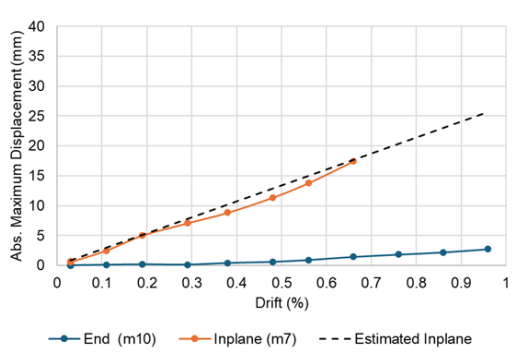

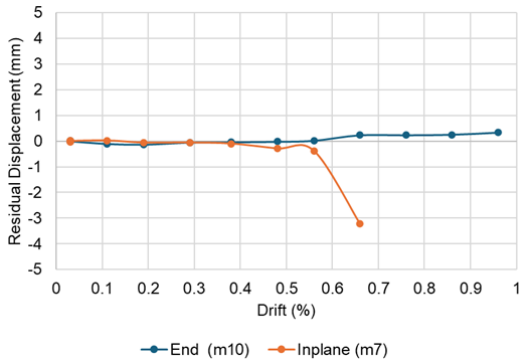

a) Absolute maximum displacements b) Residual displacements

Figure 2.44 Lateral displacement measurements for inclined steel-framed wall specimen (approximate measurement locations shown and instrument numbers in brackets)

Regarding vertical movement, Figure 2.45 indicates no substantial relative vertical displacement at the wall junctions for either specimen. The measurement locations are detailed in Figure 2.30. Uplift measurements showed the timber wall reached a maximum of 0.5 mm at 0.98% drift, whereas the steel wall exhibited greater uplift of 3 mm at its junction with the inclined wall, suggesting more pronounced racking at its West End than that of the timber wall.

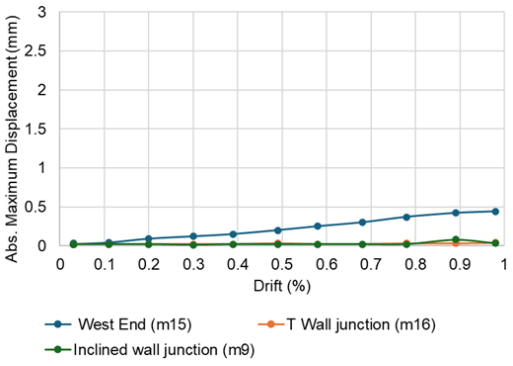

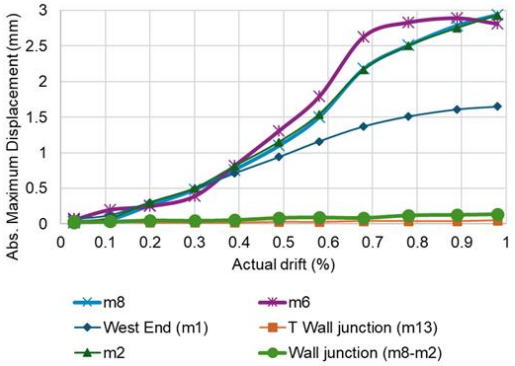

a) Timber wall b) Steel wall

Figure 2.45 Vertical displacement measurements for wall specimens (approximate measurement locations shown and instrument numbers in brackets)

Unrestrained wall specimens – repeated test

Figure 2.47 presents the absolute maximum and residual displacements recorded at various locations on the timber wall specimen (refer Figure 2.31 and Figure 2.46 for measurement locations) during the repeated test series .

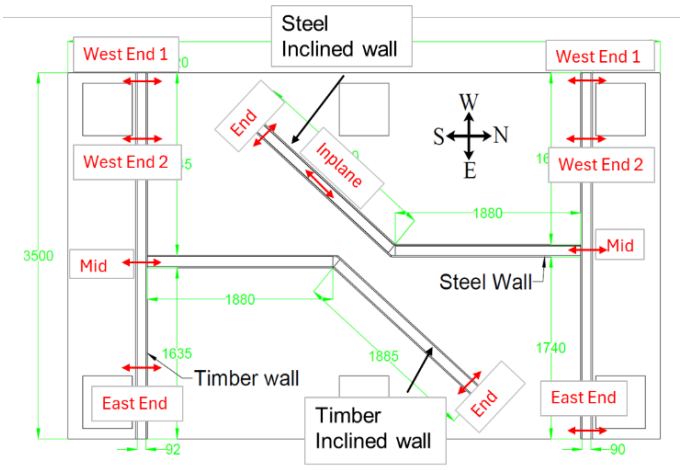

Figure 2.46 Indicative displacement measurement locations for repeated unrestrained wall specimens

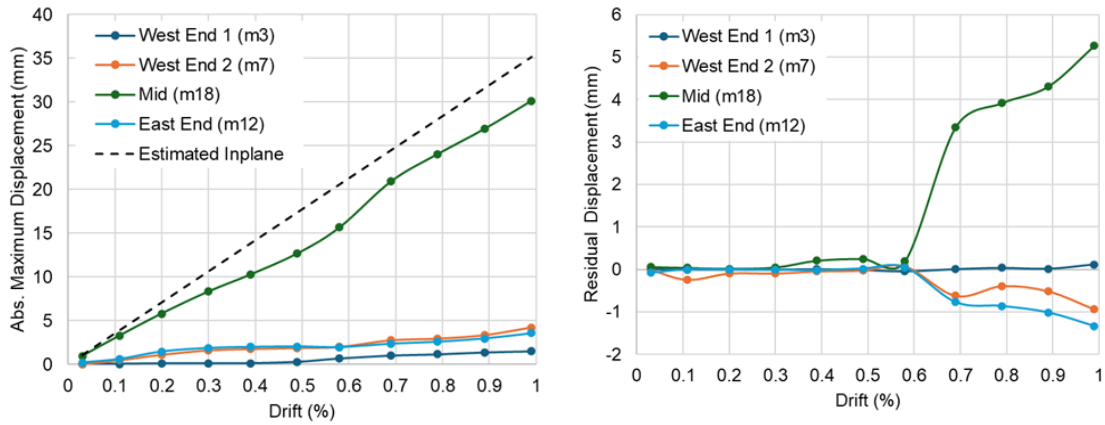

a) Absolute maximum displacements b) Residual displacements

Figure 2.47 Lateral displacement measurements for timber-framed wall specimen (approximate measurement locations shown and instrument numbers in brackets)

As depicted in Figure 2.47 (a), the timber wall demonstrated the expected in-plane sliding, with measured displacements closely matching the estimated values (calculated

as the recorded drift ratio multiplied by the 3550 mm wall height). Meanwhile, the West End 1 and East End of the out-of-plane wall remained predominantly fixed in place, while a maximum displacement of 5 mm was recorded at West End 2. This response pattern indicates that the out-of-plane wall curved at the junction, resulting in an approximate 30 mm out-of-plane displacement at that location under 0.99% drift.

Figure 2.47 (b) illustrates the residual displacements for the out-of-plane timber-framed wall. At 0.99% drift, West End 1 exhibited nearly no residual displacement, whereas the East End and West End 2 both showed residual displacements of about 1 mm. This distribution is anticipated, as West End 1 is positioned directly adjacent to the anchor connecting the wall's head track to the top floor, while the other measurement points are located slightly farther from anchor positions. The midpoint of the wall recorded a residual displacement of approximately 5.2 mm at the same drift level.

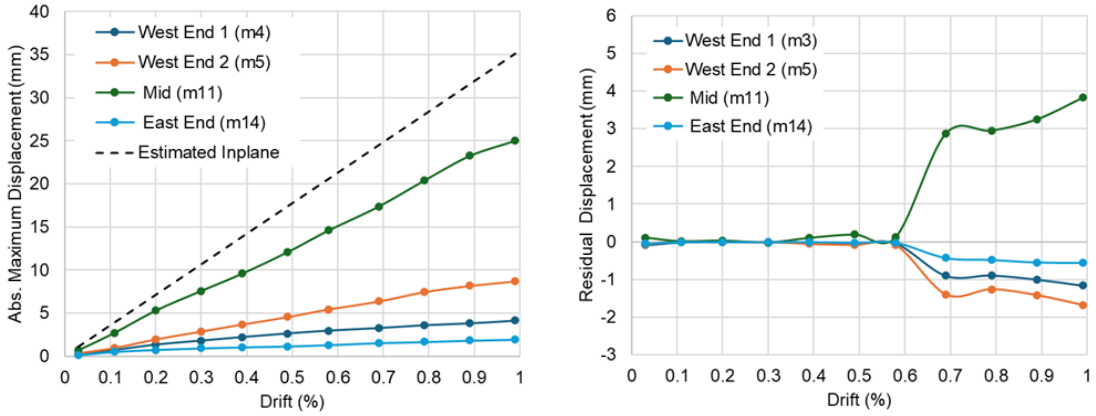

a) Absolute maximum displacements b) Residual displacements

Figure 2.48 Lateral displacement measurements for steel-framed wall specimen (approximate measurement locations shown and instrument numbers in brackets)

For the steel-framed wall specimen, Figure 2.48 (a) illustrates the in-plane wall sliding relative to the top slab, with a gradually increasing discrepancy between the estimated in-plane displacement and the measured displacement at the out-of-plane wall's midpoint. At 0.99% drift, the maximum displacements were approximately 4 mm at West

End 1, 2 mm at the East End, and about 9 mm at West End 2. Regarding residual displacements, shown in Figure 2.48 (b), the wall ends registered values below 2 mm, while the midpoint of the wall reached approximately 4 mm at 0.99% drift.

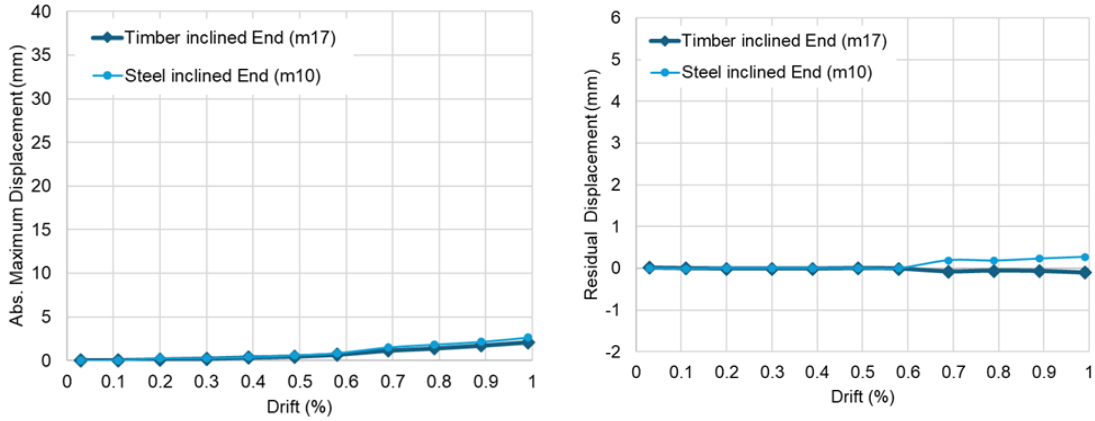

a) Absolute maximum displacements b) Residual displacements

Figure 2.49 Lateral displacement measurements for inclined wall specimen (approximate measurement locations shown and instrument numbers in brackets)

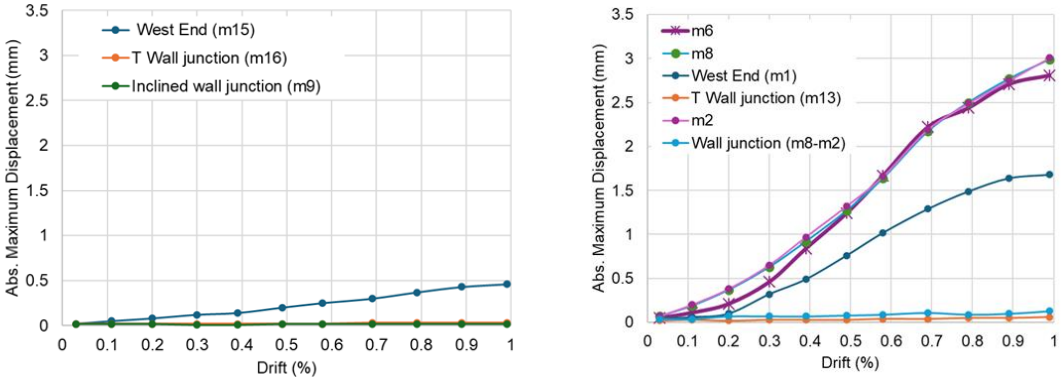

a) Timber wall b) Steel wall

Figure 2.50 Vertical displacement measurements for wall specimens (approximate measurement locations shown and instrument numbers in brackets)

Figure 2.49 shows that the inclined sections of both the timber and steel-framed wall specimens exhibited negligible out-of-plane and residual displacements. In terms of vertical movement, Figure 2.50 indicates no significant relative vertical displacement at

the wall junctions for either specimen, a behaviour consistent with the initially tested unrestrained wall specimens.

Restrained wall specimens

Figure 2.51 displays the absolute maximum and residual displacements measured at several locations on the timber wall specimen (see Figure 2.32 for locations) during the restrained wall test series.

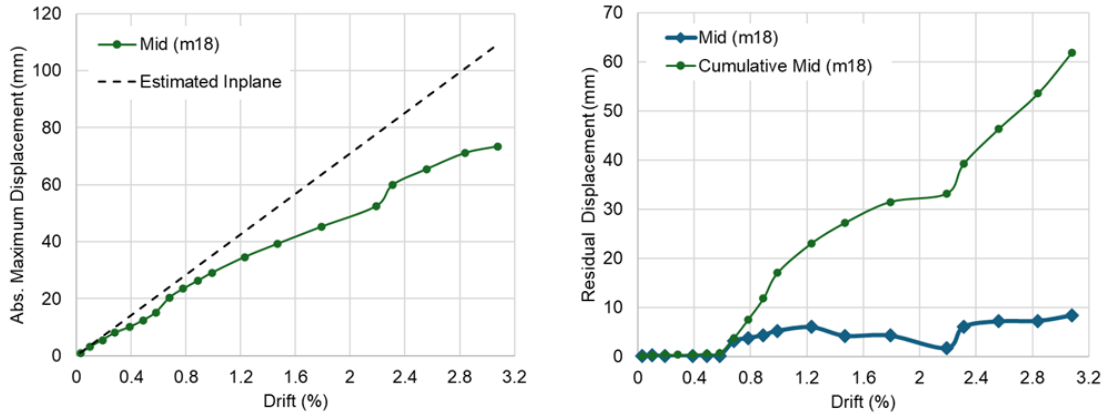

a) Absolute maximum displacements b) Residual displacements

Figure 2.51 Lateral displacement measurements for timber-framed wall specimen (approximate measurement locations shown and instrument numbers in brackets)

As shown in Figure 2.51 (a), the maximum displacements recorded at the junction (or near the middle of the out-of-plane wall) remain below the estimated in-plane displacements between the top slab and the wall's deflection head track. A gradually increasing discrepancy between the estimated maximum and measured displacements or a progressive decrease in the measured relative displacement between the out-of-plane wall and the top slab can be observed, likely resulting from accumulating damage in the specimen. Figure 2.51 (b) indicates that the residual displacement at the middle of the out-of-plane wall reaches a maximum of about 8.5 mm at 3.08% drift. However, when compared against the cumulative residual displacement at the same point, it is evident

that residual displacement begins accumulating from 0.58% drift, reaching approximately 17 mm at 0.99%, 33 mm at 2.19%, and 62 mm at 3.08% drift.

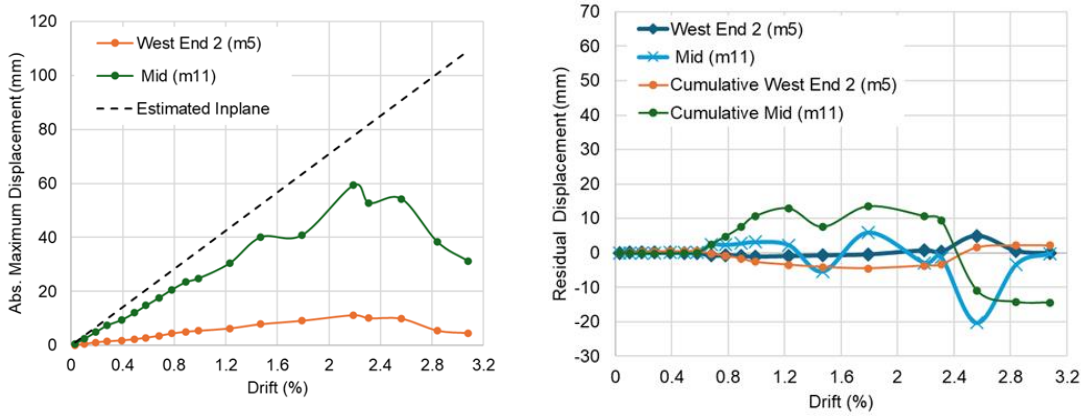

a) Absolute maximum displacements b) Residual displacements

Figure 2.52 Lateral displacement measurements for steel-framed wall specimen (approximate measurement locations shown and instrument numbers in brackets)

Figure 2.52 presents the absolute maximum and residual displacements recorded at various locations on the steel wall specimen (refer to Figure 2.32 for locations) during the restrained wall test series. As illustrated in Figure 2.52 (a), the maximum displacements at the junction (or near the middle of the out-of-plane wall) remain below the estimated in-plane displacements between the top slab and the wall's deflection head track. Beyond 2.56% drift, a sharp divergence emerges between the estimated and measured displacements, marked by a pronounced decrease in the measured relative displacement between the out-of-plane wall and the top slab. This shift is attributed to a separation between the in-plane and out-of-plane walls, allowing the out-of-plane wall to move with the top slab. Figure 2.52 (b) shows the residual displacement at the middle of the out-of-plane wall reaching a peak of approximately 20 mm at 2.56% drift. When viewed cumulatively, however, a significant reversal in the direction of the residual displacement occurs, signalling that major damage had taken place in the wall i.e., separation between the in-plane and out-of-plane walls.

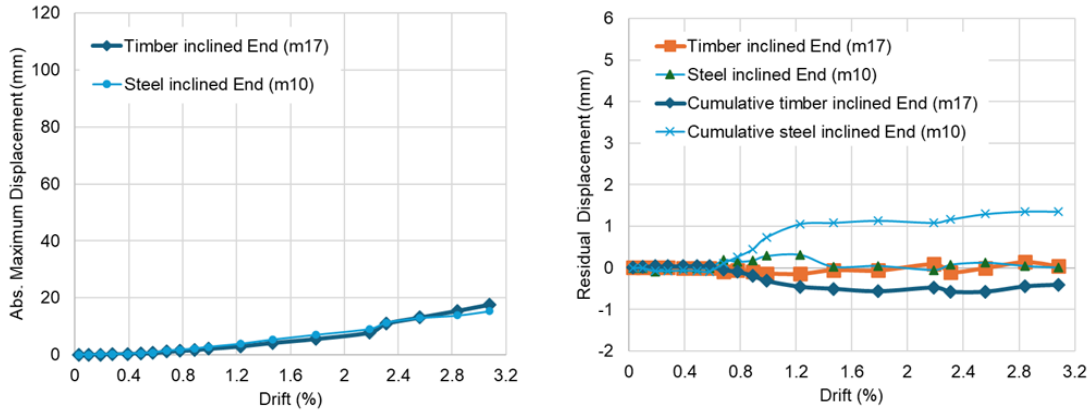

a) Absolute maximum displacements b) Residual displacements

Figure 2.53 Lateral displacement measurements for inclined wall specimen (approximate measurement locations shown and instrument numbers in brackets)

Figure 2.53 indicates that the inclined sections of both the timber and steel-framed wall specimens displayed comparable behaviour, with maximum out-of-plane displacements reaching approximately 18 mm at 3.08% drift while showing negligible residual displacements.

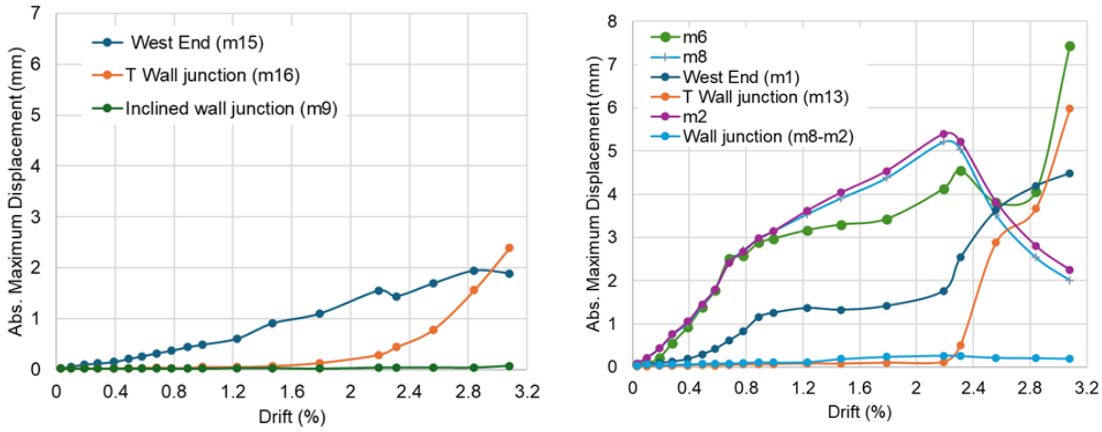

a) Timber wall b) Steel wall

Figure 2.54 Vertical displacement measurements for wall specimens (approximate measurement locations shown and instrument numbers in brackets)

Figure 2.54 (a) presents the vertical movement results for the timber wall specimen. The data shows no significant uplift at the West End, with a maximum displacement of only 2 mm at 3.08% drift. However, after reaching 1.79% drift, a gradual increase in relative vertical displacement occurs at the T-junction between the in-plane and return walls, reaching to approximately 2.4 mm by 3.09% drift. This progression suggests gradual damage accumulation. In contrast, the relative displacement at the inclined wall junction remains negligible, indicating no significant damage at that location.

For the steel-framed wall, Figure 2.54 (b) reveals that the wall ends experienced racking, with a maximum uplift of 7.50 mm at the end of the inclined wall at 3.08% drift. At the T-junction, no significant relative vertical displacement occurred up to 2.31% drift. A sharp increase to 2.88 mm then occurred at 2.56% drift, signalling separation at the junction. This displacement increased further, reaching 6 mm by 3.08% drift. Conversely, the vertical relative displacement at the inclined wall junction remained negligible, indicating the joint remained intact.

Comparison between unrestrained (retested) and restrained wall specimens

Figure 2.55 indicates that the relative displacement between the top floor and the midpoint of the out-of-plane walls at the T-junctions was similar for both the unrestrained and restrained wall specimens. A difference, however, is observed in the West End 2 displacement measurements between the unrestrained and restrained steel-framed walls, where the displacement is lower in the restrained specimen. This result is expected, as the timber blocks installed at the ends of the out-of-plane wall in the restrained configuration limit out-of-plane rotation and movement of the deflection head tracks (DHT). In contrast, the unrestrained DHTs possess more flexibility, as their movement is governed solely by

the anchor locations connecting them to the top slab.

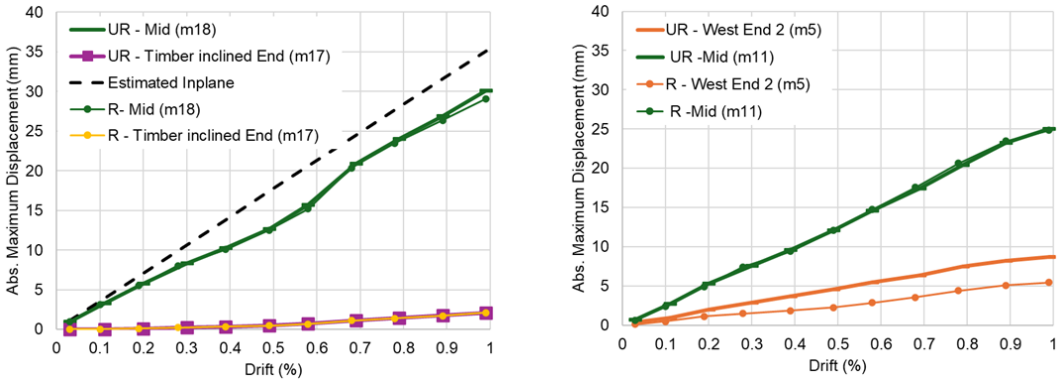

a) Timber-framed wall specimen b) Steel-framed wall specimen

Figure 2.55 Comparison of lateral displacement measurements between the restrained (R) and Unrestrained retested specimen (UR)

CONCLUSIONS AND FUTURE STEPS

This report presents the preliminary findings from partition wall tests on the wall designs currently adopted by the New Zealand construction industry. Two 3.55 m-high wall specimens, one with timber framing and the other with steel framing, were constructed with fire-rated plasterboard lining. Both walls were tested under dynamic loading conditions. Lateral sliding was enabled through a deflection head track (DHT) at the top, while out-of-plane flexibility at the wall junctions was provided by deformation of the timber top plates (in timber walls) and the DHTs (in steel walls). To facilitate this deformation, anchors at the junctions were set back 1.2 m from the wall ends, creating designated “No-Fix zones.”

The experimental results indicated that walls with (“unrestrained”/“pinned”) ends performed as intended and exhibited no damage that reduced fire rating when tested up to a maximum drift of 1.00 %, while the cosmetic damage in the form of hairline crack at wall junctions occurred between 0.11 % (in timber wall) and 0.20 % drift (in steel wall). When the wall ends were rotationally “restrained”, effectively converting them to “fixed”

ends, plasterboard crack damage reducing the fire-rating was observed at 0.60 % drift in the timber wall and at 1.80 % drift in the steel wall. Damage requiring moderate repair was deemed to occur at 1.00 % drift in the timber wall due to cracking of the top plate. In the steel wall, at 2.50 % drift, separation at the junctions occurred which likely compromises the fire rating and occupancy. It should be noted that damage progression in the "restrained" walls is influenced by prior "unrestrained" testing, meaning the drift values at which damage appears are likely lower-bound estimates.

The preliminary results indicated that walls with "pinned" ends deformed as intended and exhibited no damage which reduced the fire-ratings when tested up to a maximum drift of 1.00 %. When the wall ends were restrained, effectively converting them to "fixed" ends, damage was observed at 0.60% drift in the timber wall and at 1.80 % drift in the steel wall. Damage requiring immediate repair was deemed to occur at 1.00 % drift in the timber wall due to cracking of the top plate, and at 2.50 % drift in the steel wall due to separation at the junctions. Moreover, the median dynamic amplification factor was for the tested wall specimens was found to be about 1.05, which corresponds to the design cases for a Rigid component ($\mu=1$) or a Flexible component with high ductility ($\mu\geq2.5$) as per (SNZ TS 1170.5, 2025). The SNZ TS 1170.5 (2025) provision for a Flexible component with $\mu=2$ and ASCE/SEI 7-22 (2022) provides a conservative estimate, exceeding the measured ratio by a factor of 1.30. The specimens were tested upto about 1.12 g peak floor acceleration.

The displacement potentiometer recordings of the walls demonstrated significant out-of-plane flexibility around the junction regions (No-Fix zones). As a result, potential deformation incompatibilities are anticipated with attached or adjacent elements such as suspended ceilings, façades, doors, windows, service penetrations, and nearby structural members (e.g., columns or structural walls). Further investigation is needed to develop

drift-compatible detailing, and Phase II tests are being planned to examine wall details, layouts and interactions with other non-structural components. A detailed dynamic characterization and displacement analysis of wall deformations will be carried out using Motion Capture Camera recordings in future publications.

An important direction for future research is to evaluate the post-earthquake fire performance of partition walls that have already sustained seismic damage. Although this study defined damage states based on observed failure modes and drift ratios, the implications of such damage for fire resistance have not yet been assessed. Experimental fire testing of seismically damaged wall assemblies would quantify the extent to which earthquake-induced damage compromises their fire-rating performance. The findings could provide the empirical basis needed to confirm or refine current code-prescribed drift limits. If damaged walls are shown to maintain their required fire resistance, higher allowable drift limits in seismic design may be justified, potentially delivering greater economic efficiency and design flexibility without reducing post-earthquake life safety.

REFERENCES

ASCE/SEI 7-22. (2022). *Minimum design loads and associated criteria for buildings and other structures*. Reston, VA: American Society of Civil Engineers (ASCE). doi: https:/doi.org/10.1061/9780784415788

Butterworth, S. (1930). On the theory of filter amplifiers. *Wireless Engineer, 7*(6), 536–541.

GIB. (2016). *GIB-EzyBrace-system-sheet-GS2-N* GIB. Retrieved from https://www.gib.co.nz/assets/Uploads/GIB-EzyBrace-System-sheet-GS2-N.pdf

Parks, T. W., & Burrus, C. S. (1987). *Digital filter design* Wiley-Interscience.

Pledger, L. (2026). The effects of reducing design drift limits for structures. (PhD, University of Canterbury).

SNZ TS 1170.5, &. (2025). *Structural design actions – part 5: Earthquake actions – New Zealand*. Wellington, New Zealand:

Sorrentino, R. (2007). *Electronic filter simulation & design* McGraw-Hill Professional

APPENDIX A

PRE-TEST DAMAGE INSPECTIONS

Timber wall specimen (Phase I - unrestrained)

Table 2.4. Photos of damage observed in the Timber Wall specimen during pre-test inspections

Location	Observation	Photo
Timber SE inside and Timber in-plane East Junction 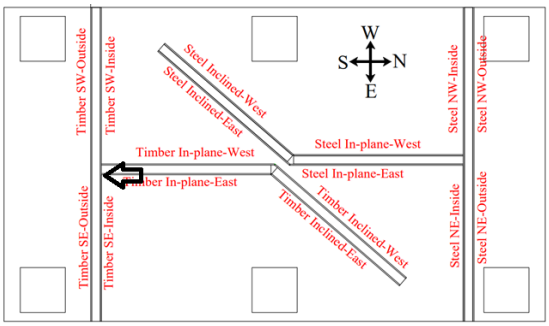	Hairline shrinkage cracks of plaster	
Timber In plane East and Timber inclined East 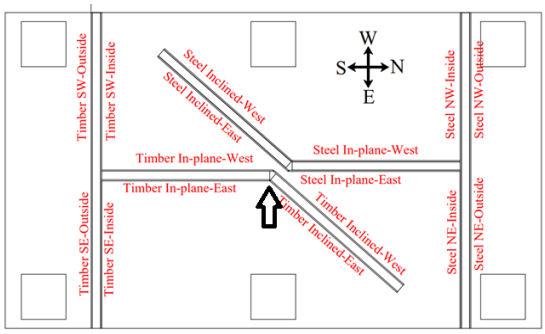	The plaster not completely on the junction line	
Timber In-plane West and Timber SW Inside junction 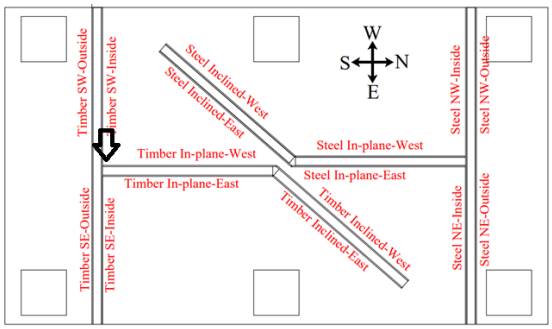	No visible shrinkage plaster cracks	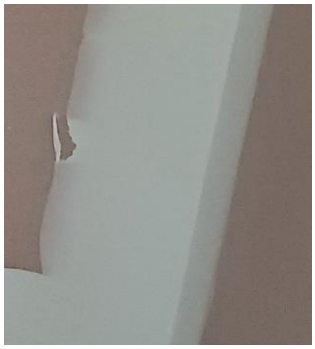

Timber SW outside 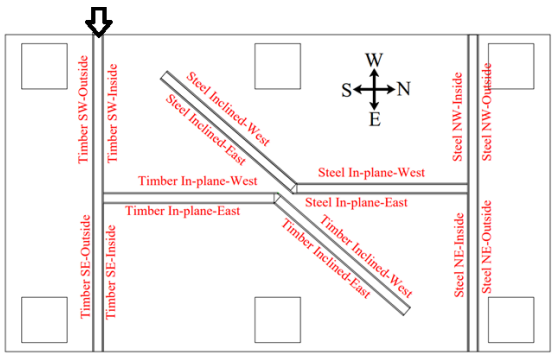	Plasterboard cracks at plasterboard corner and mid-height of the ends	 
Timber SW outside, Top corner, next to the top plate near the joint of stud and top plate 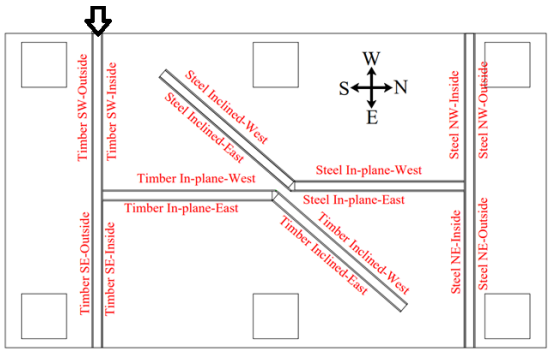	Damage to plasterboard	
Timber SE Outside, bottom corner 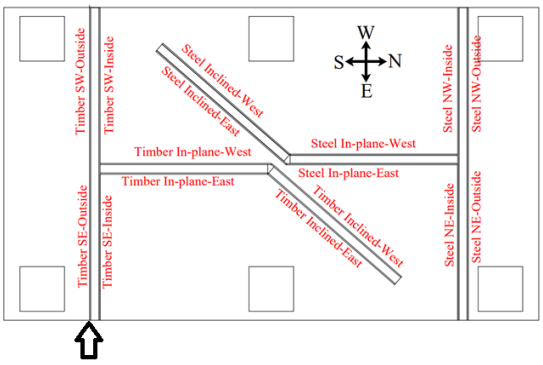	Damage to plasterboard and bottom timber plate	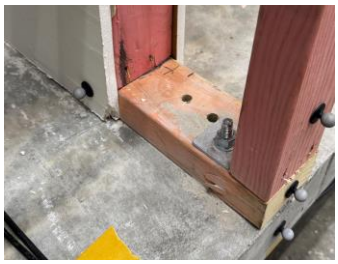

Timber SE outside near top corner 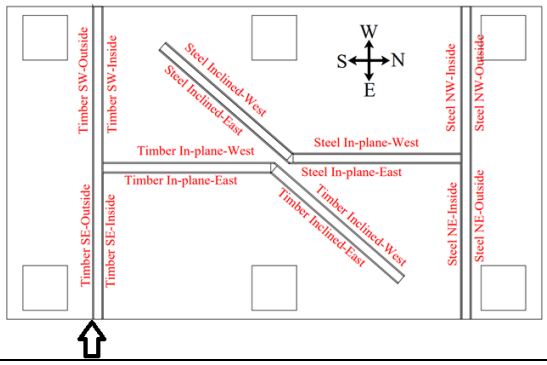	Slight crack in plasterboard	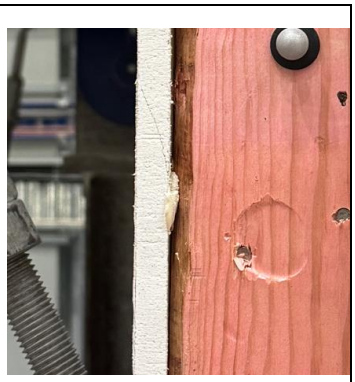
Timber Inclined West wall 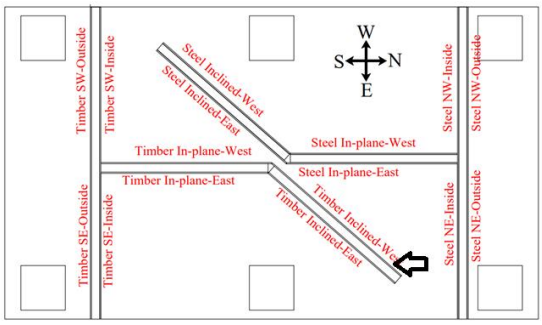	Screw impressions at the bottom	

Steel wall specimen (Phase I - unrestrained)

Table 2.5. Photos of damage observed in the Steel Wall specimen during pre-test inspections

Location	Observation	Photo
Steel NE outside 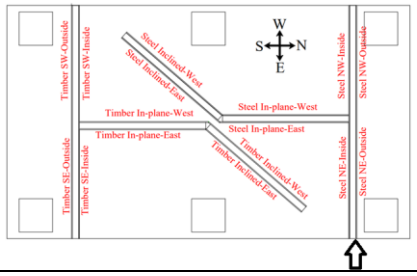	Crack on plasterboard corner	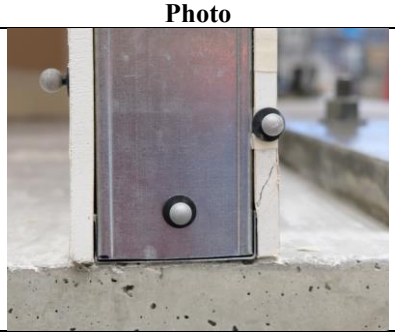
Steel NW outside 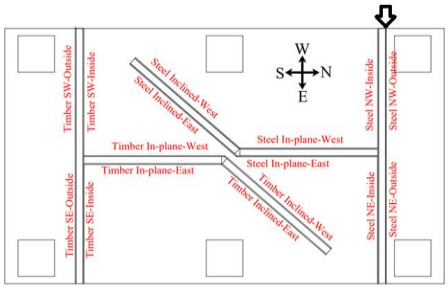	Crack on plasterboard corner	

Steel NW outside 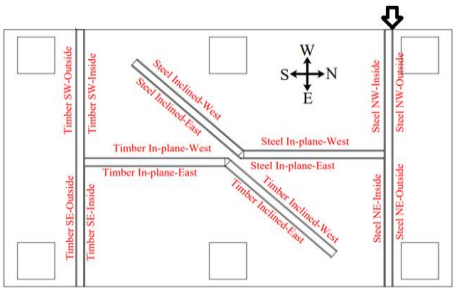	Crack on plasterboard edge around mid-height	
Steel NW inside and Steel In-plane west junction 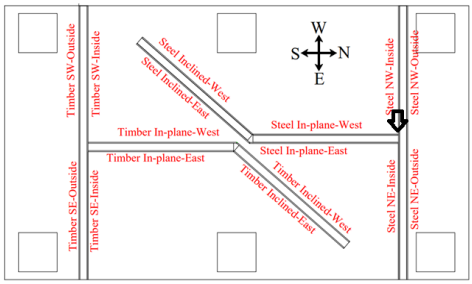	Minor hairline shrinkage cracks	
Steel In-plane West and Inclined West junction 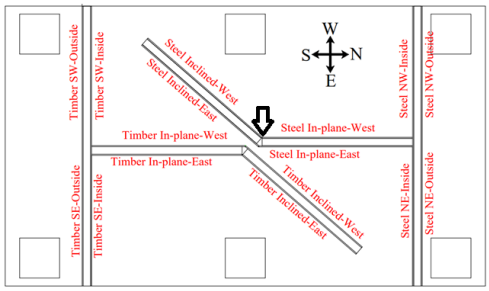	Either the plaster not throughout the junction line or visible hairline plaster shrinkage cracks	

Observed damage during tests

Timber Wall specimen (Phase I - unrestrained)

Table 2.6. Motion 1, 0.11 % inter-story drift

Location	Observation	Photo
Near the bottom of Timber SW and Timber In-plane West junction 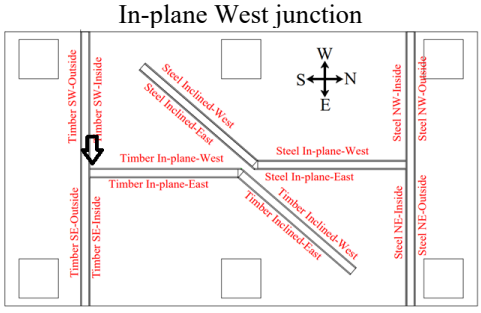	Hairline crack at wall junction	

Table 2.7. Motion 4, 0.39 % inter-story drift

Location	Observation	Photo
Near mid-length at the top of Timber SW Outside wall 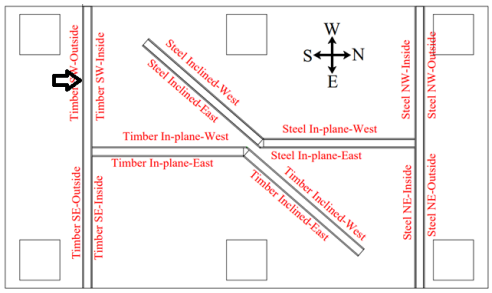	Screw impressions	

Table 2.8. Motion 5, 0.49 % inter-story drift

Location	Observation	Photo
Near mid-length at the top of Timber SW/SE outside wall 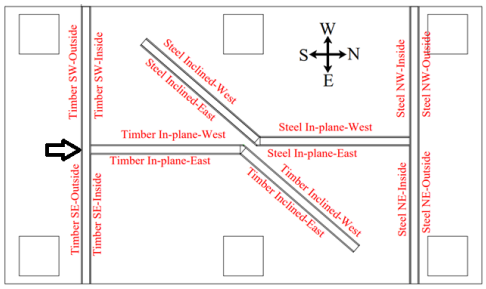	Screw impressions	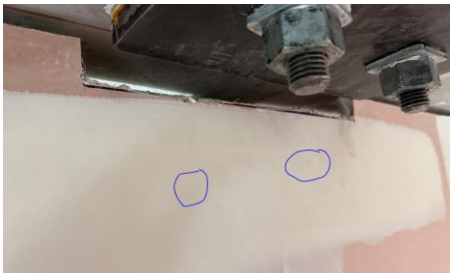
Near mid-length at the top of Timber SW inside wall 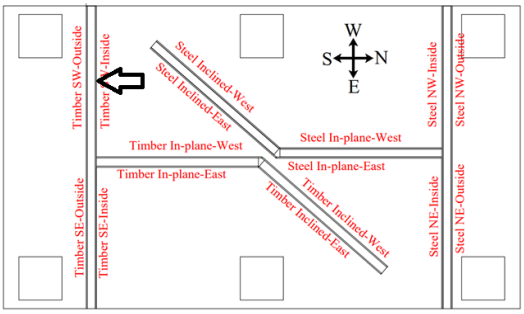	Screw impressions	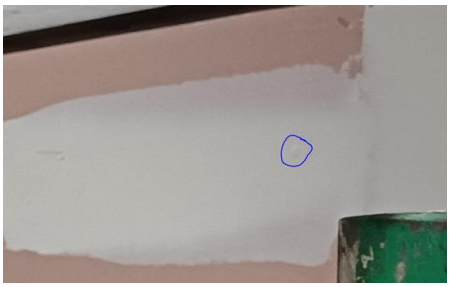

Table 2.9. Motion 8, 0.79 % inter-story drift

Location	Observation	Photo
Top of Timber inclined east wall 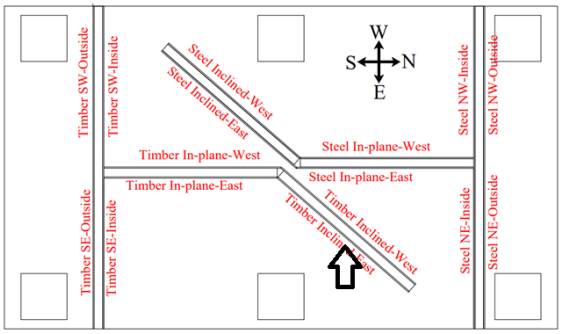	Screw impressions	

At the end of the DHT in Timber wall SW Inside 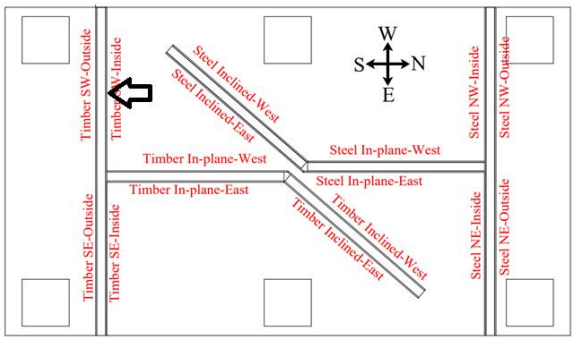	Minor crack in the plasterboard	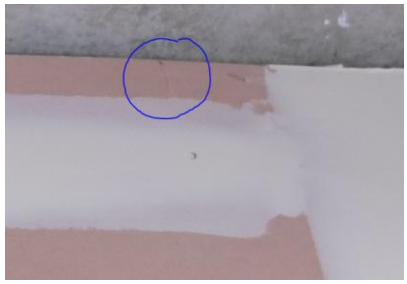
At the end of the DHT in Timber wall SE Inside 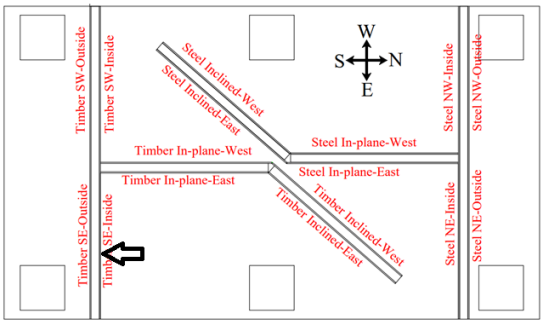	Minor crack in the plasterboard	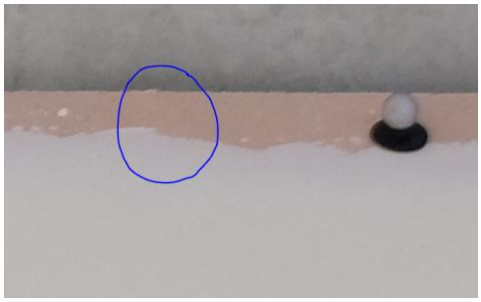

Table 2.10. Motion 10, 0.99 % inter-story drift

Location	Observation	Photo
Top of Timber SW Inside wall 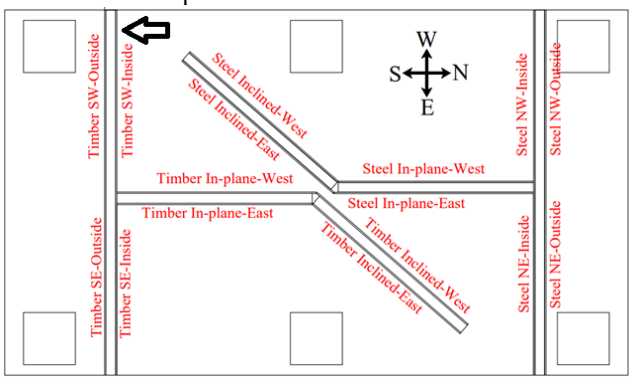	Screw impressions	
Near top of Timber SW outside wall (around mid-length) 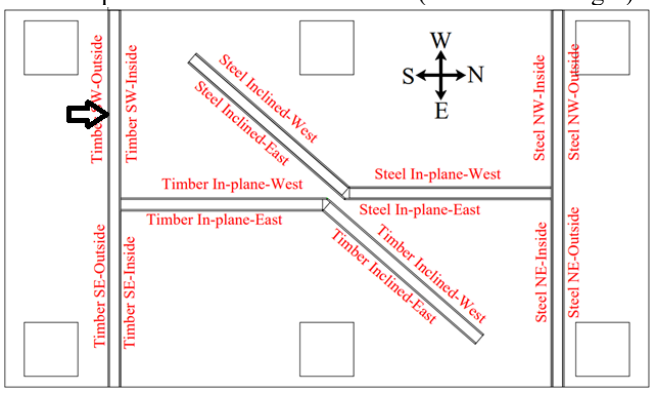	Hairline crack in the plasterboard	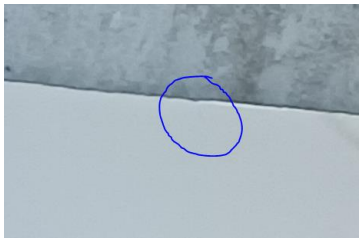

Steel Wall specimen (Phase I - unrestrained)

Table 2.11. Motion 2, 0.20 % inter-story drift

Location	Observation	Photo
Top Corner of Steel Inclined West wall 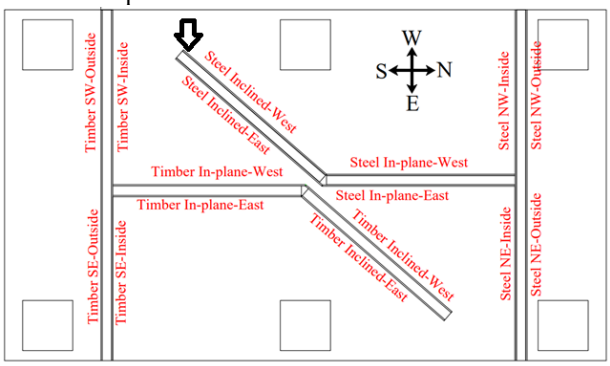	Screw impressions; The screw is likely to be driven into the head track (not in the nearest nogging)	
At the bottom of Steel NE inside and In-plane East wall junction 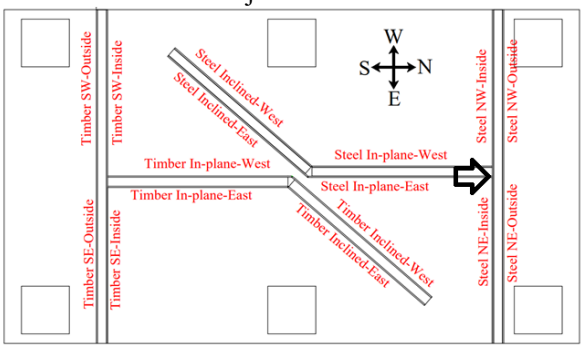	Hairline crack in the plasterboard	

Table 2.12. Motion 3, 0.30 % inter-story drift

Location	Observation	Photo
at bottom of the steel NW and In-plane West wall junction 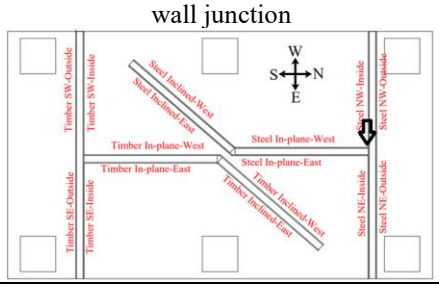	Hairline crack	
Top Corner of Steel Inclined West wall 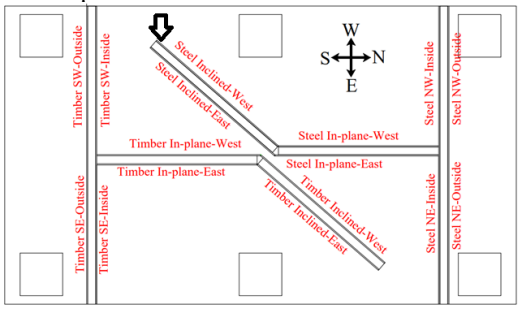	Progressive damage - screw popping out	

Table 2.13. Motion 9, 0.89 % inter-story drift

Location	Observation	Photo
At the top of the Steel NW and Steel In-plane West wall 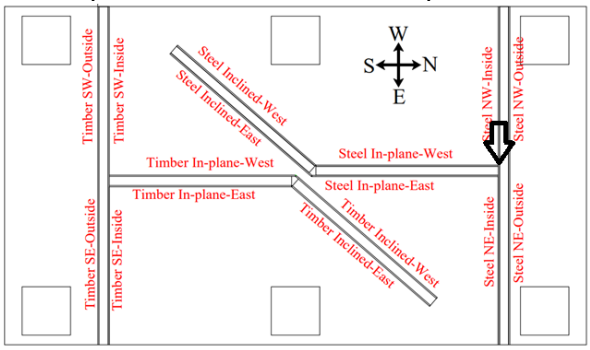	Tearing of joint paper tape	

Timber Wall specimen (Phase I - Restrained)

Table 2.14. Motion 3, 0.30 % inter-story drift

Location	Observation	Photo
At the end of the DHT in Timber wall SE Inside 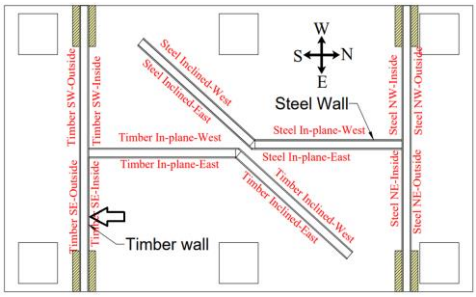	Progressive damage: Crack in the plasterboard (Observed earlier in the unrestrained specimen at 0.8 % drift)	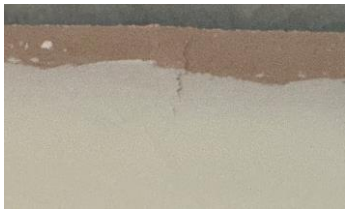

Table 2.15.Motion 5, 0.49 % inter-story drift

Location	Observation	Photo
At the end of the DHT in Timber wall SE Inside 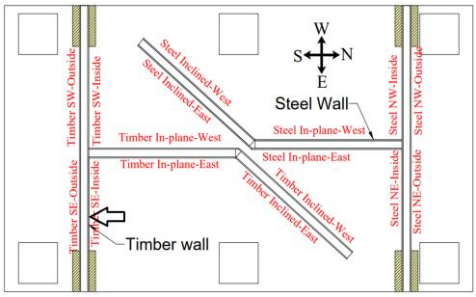	Progressive damage: Crack in the plasterboard	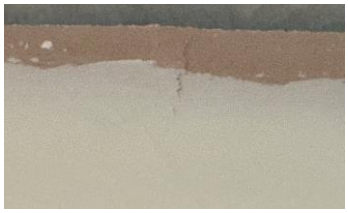

Table 2.16.Motion 6, 0.58 % inter-story drift

Location	Observation	Photo
At the end of the DHT in Timber wall SE Inside 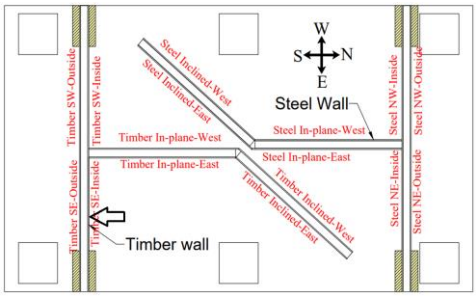	Progressive damage: Crack in the plasterboard Perhaps the crack is severe enough to compromise the fire seal.	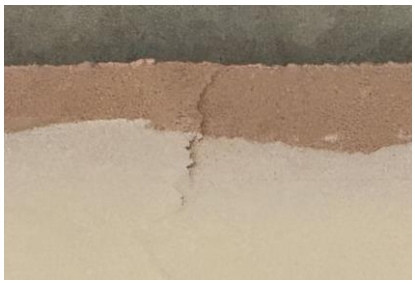

Table 2.17.Motion 10, 0.99 % inter-story drift

Location	Observation	Photo
Timber wall SW/SE and Timber in-plane wall junctions and where there were nails securing the strap 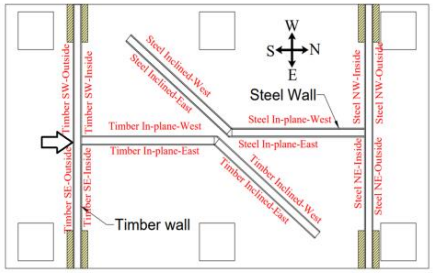  	One loud “popping” sound of brittle damage – damage to crack in the top plates	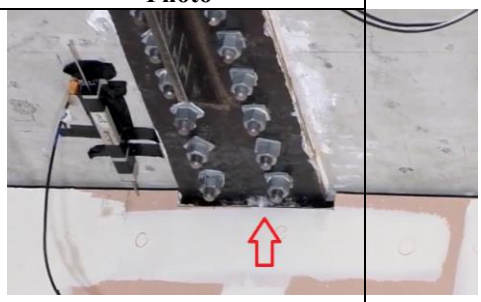 Video link [DSCF0059.MOV] [DSCF4003.MOV]
		
At the top of Timber SW outside wall near end of DHT 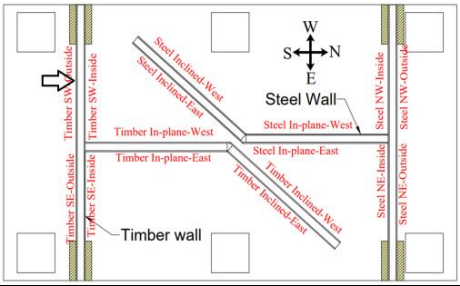	Hairline crack	

Table 2.18.Motion 11, 1.23 % inter-story drift

Location	Observation	Photo
Timber wall SW/SE and Timber in-plane wall junctions and where there were nails securing the strap 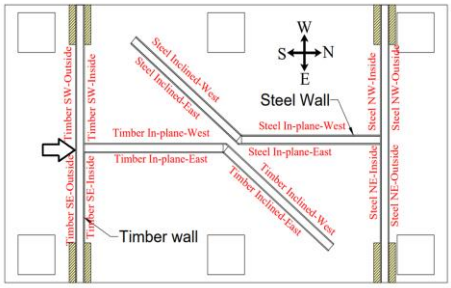	Three loud “popping” sounds of brittle damage – damage to crack in the top plates	Video link: DSCF0060.MOV DSCF4004.MOV

Table 2.19.Motion 12, 1.47 % inter-story drift

Location	Observation	Photo
Timber wall SW/SE and Timber in-plane wall junctions and where there were nails securing the strap 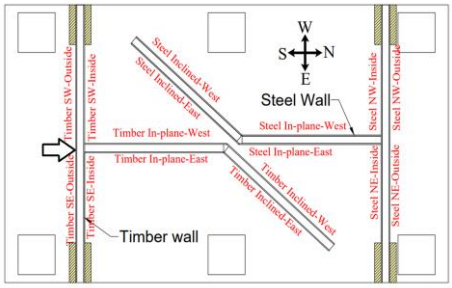	More loud “popping” sounds of brittle damage – damage to crack in the top plates Video link: DSCF0061.MOV DSCF4005.MOV	
At the top Timber wall SW/SE outside at mid-length 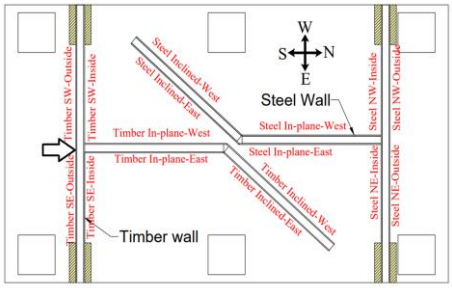	Crack in the plasterboard	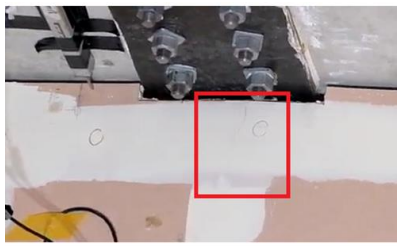

Table 2.20.Motion 13, 1.79 % inter-story drift

Location	Observation	Photo
At the Timber SE Inside wall at the top of the junction with Timber In-plane East wall 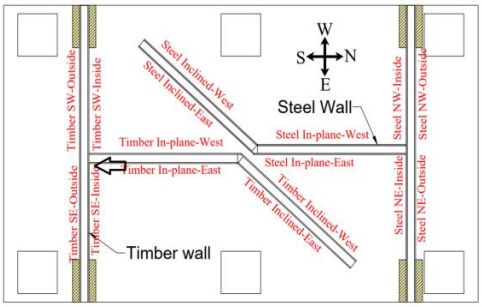	Hairline crack in the plasterboard	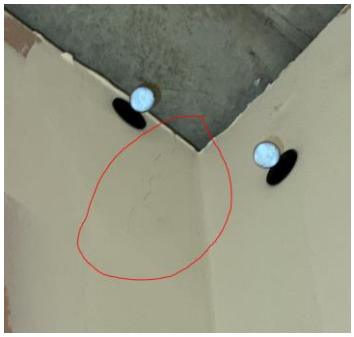

At the top of the Timber inclined west wall at the Timber in-plane West junction 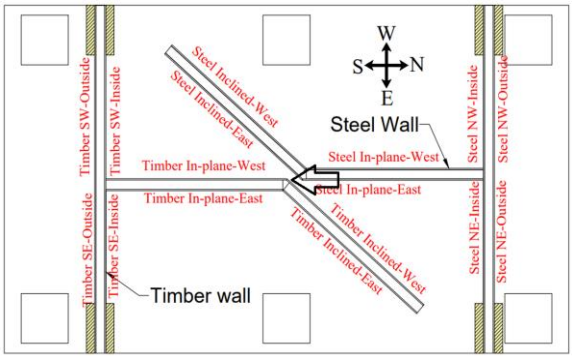	Crack in the plasterboard	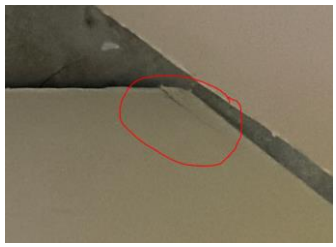
At mid-length of Timber wall SW outside 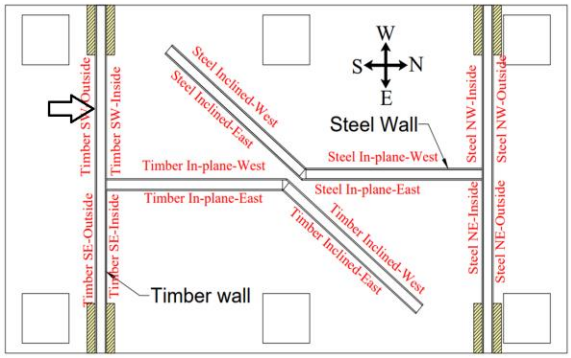	Crack throughout the height of the plasterboard Video link: DSCF0062.MOV	
At the end of the DHT in Timber wall SE Inside 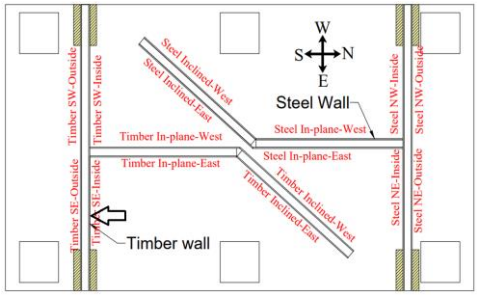	Progressive damage: Crack in the plasterboard	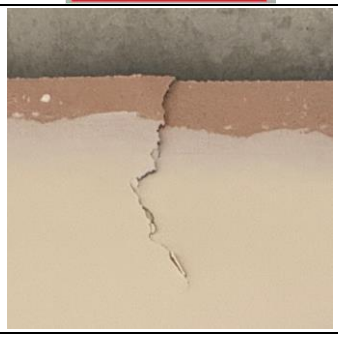

Table 2.21.Motion 14, 2.19 % inter-story drift

Location	Observation	Photo
At the Timber SE Inside wall at the top of the junction with Timber In-plane East wall 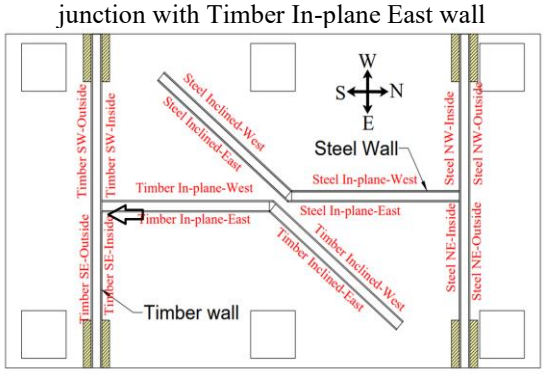	Progressive damage: Break in the plasterboard	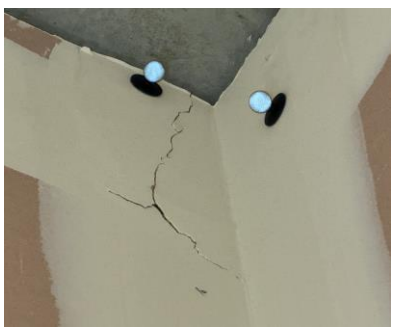

Timber SW inside and Timber in-plane west wall junction 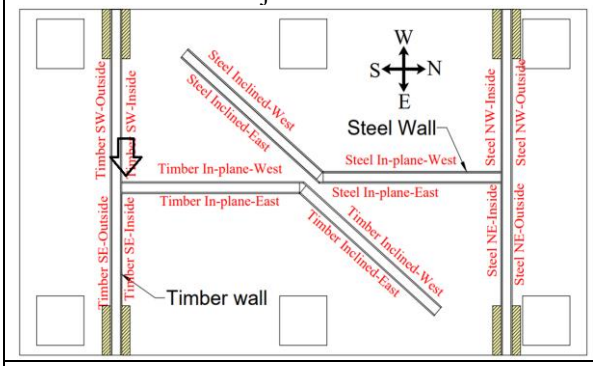	Cracks slightly wider than hairline along the height	
Timber SE inside and Timber in-plane East wall junction 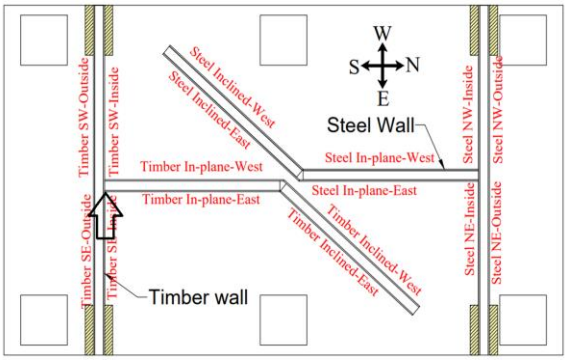	Cracks slightly wider than hairline along the height	
At the top of the Timber inclined west wall at the Timber in-plane West junction 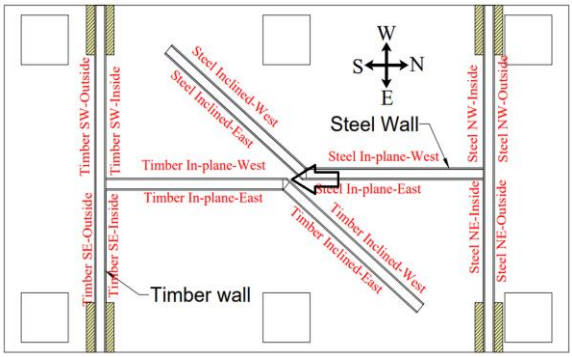	Progressive damage: Crack in the plasterboard	
At the top of the Timber in-plane east and Timber inclined east junction 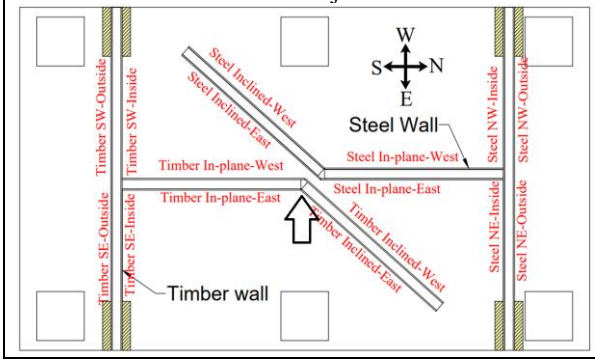	Break in the plasterboard	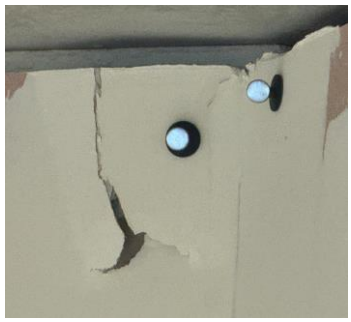

At the top of the Timber inclined east wall near mid-length 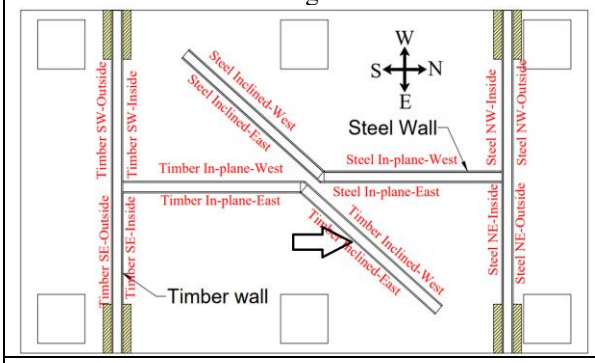	Crack in the plasterboard	
At mid-length of Timber wall SW outside 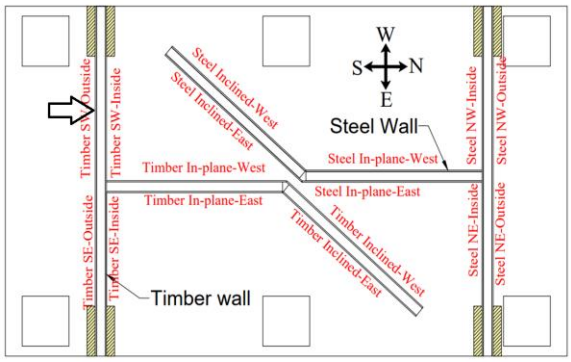	Progressive damage: Crack throughout the height of the plasterboard	 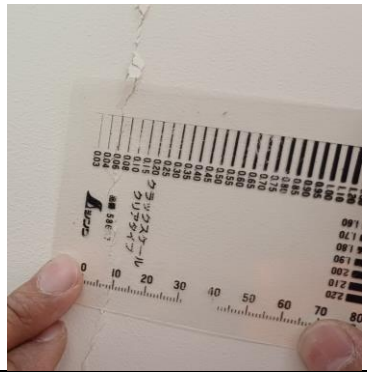

Table 2.22.Motion 16, 2.56 % inter-story drift

Progressive damage to the damage observed in previous motions.

Location	Observation	Photo
At the end of the DHT in Timber wall SW Inside Top 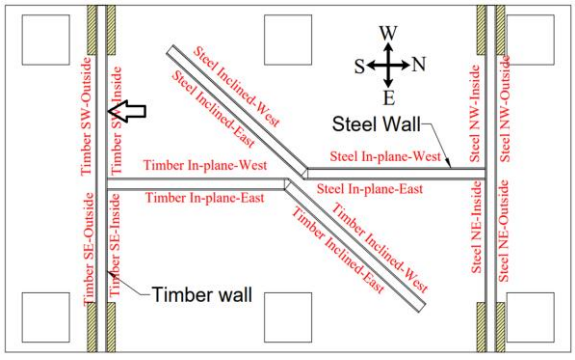	Progressive damage: Break in the plasterboard	

At the top of the Timber inclined west wall at the Timber in-plane West junction 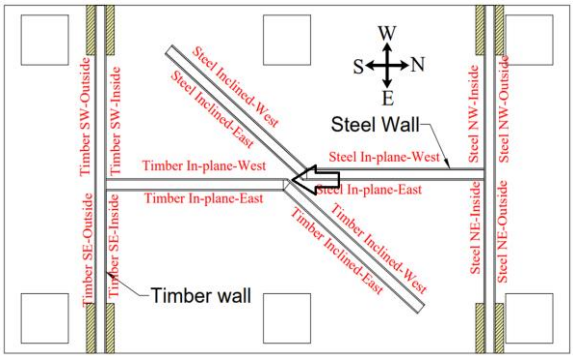	Progressive damage: Damage to the plasterboard	

Table 2.23.Motion 17, 2.84 % inter-story drift

Location	Observation	Photo
Near the end of DHT of the Timber inclined West wall 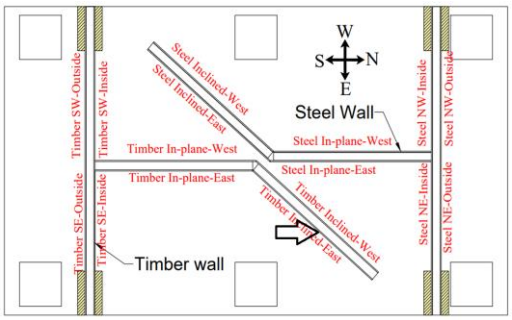	Crack in the plasterboard	
At the end of the DHT in Timber SW Outside wall 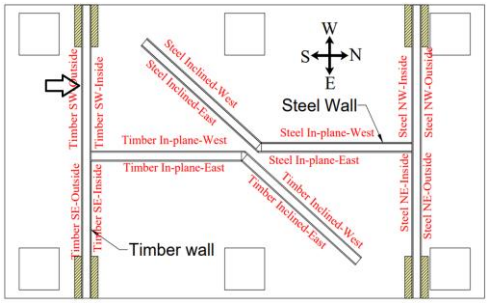	Progressive damage: Break in the plasterboard	

Table 2.24.Motion 18, 3.08 % inter-story drift

Location	Observation	Photo
At the top corner of the Timber SE Inside wall 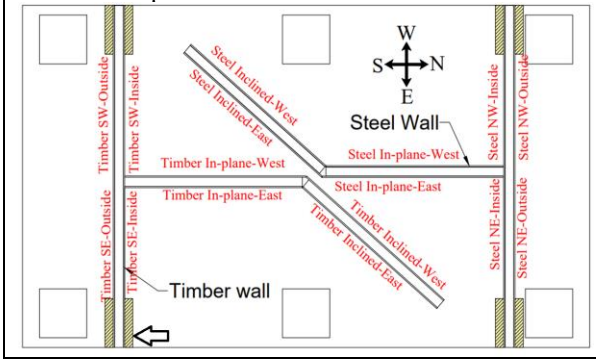	Screw impression	

At the top of the plasterboard at Timber wall SE inside near the end of the DHT 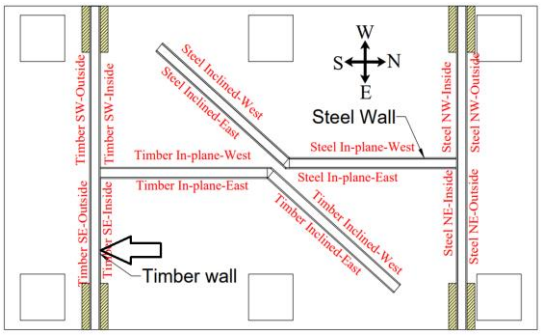	Progressive damage – crack at the top of the plasterboard	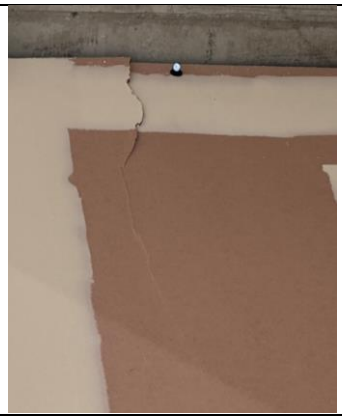

Steel Wall specimen (Phase I - Restrained)

Table 2.25.Motion 10, 0.99 % inter-story drift

Location	Observation	Photo
Top of Steel NW inside wall at the junction with steel in-plane wall West 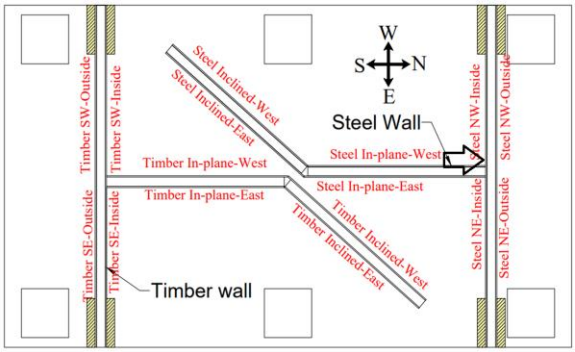	Screw impression	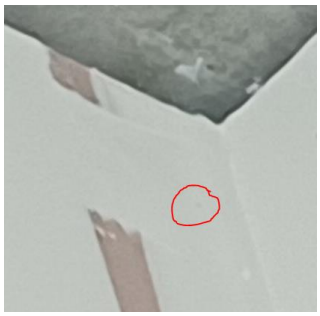

Table 2.26. Motion 11, 1.23 % inter-story drift

Location	Observation	Photo
At the top of the Steel NE inside and Steel in-plane East wall junction 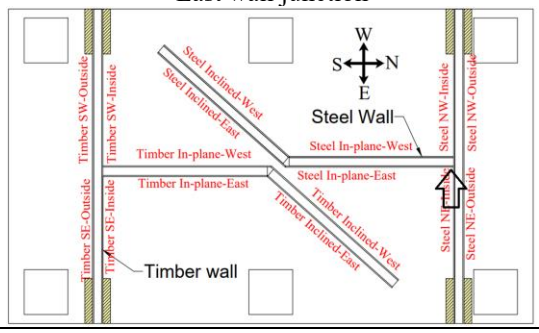	Tear in the plaster paper	

At the top of the Steel NW inside and Steel in-plane West wall junction 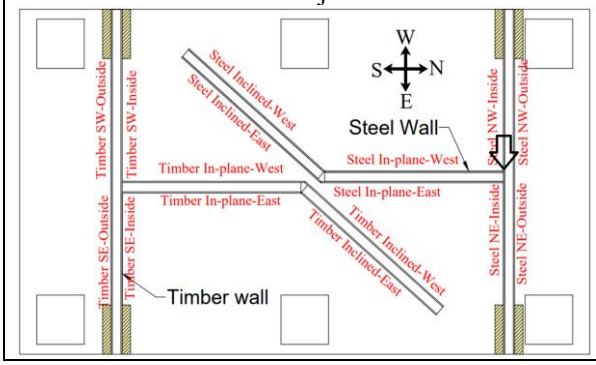	Tear in the plaster paper	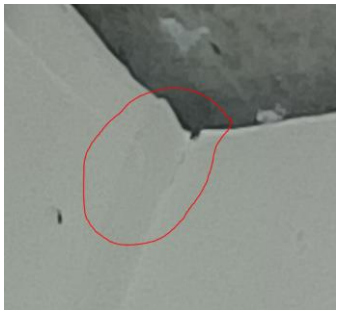

Table 2.27.Motion 12, 1.47 % inter-story drift

Location	Observation	Photo
At the top of the Steel NW inside and Steel in-plane West wall junction 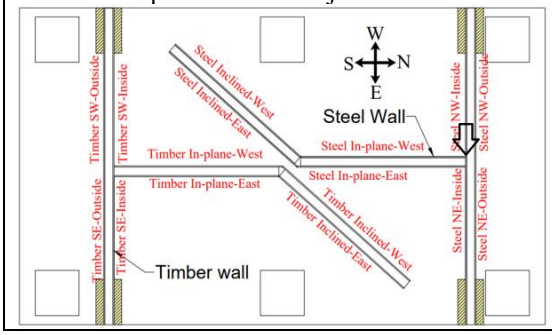	Progressive damage: Tear in the plaster paper	

Table 2.28.Motion 13, 1.79 % inter-story drift

Location	Observation	Photo
At the top Steel wall NW/NE outside at mid-length 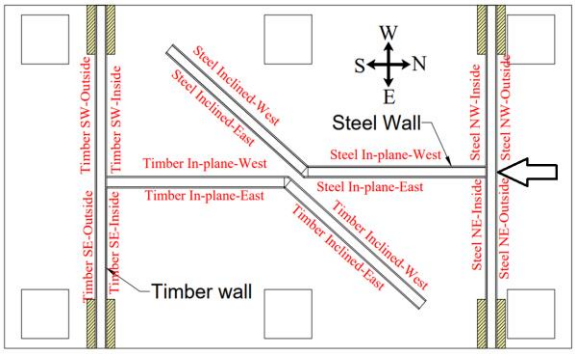	Crack in the plasterboard	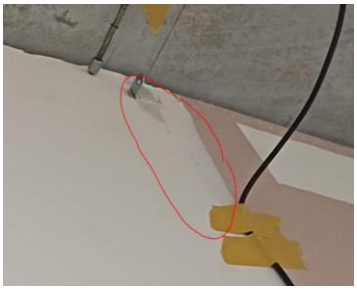
At the top of the Steel NE inside and Steel in-plane East wall junction 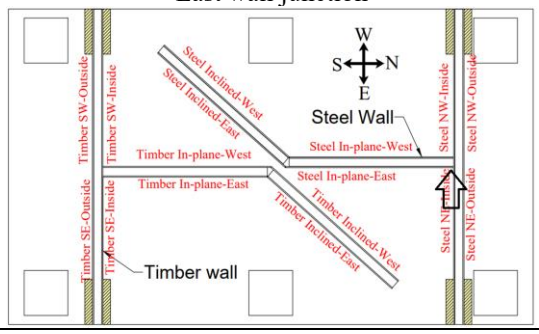	Progressive damage: Tear in the plaster paper	

Table 2.29.Motion 14, 2.19 % inter-story drift

Location	Observation	Photo
Steel wall NW/NE outside at mid-length 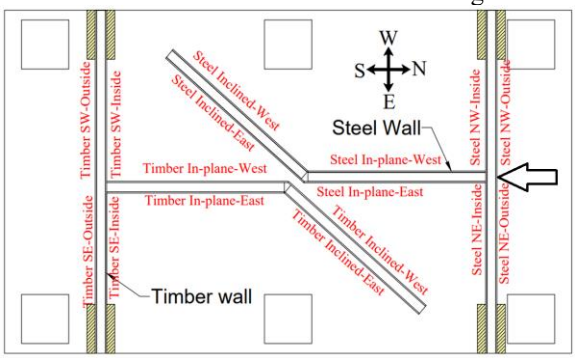	Progressive damage: Crack throughout the 1/3rd height of the plasterboard from the top	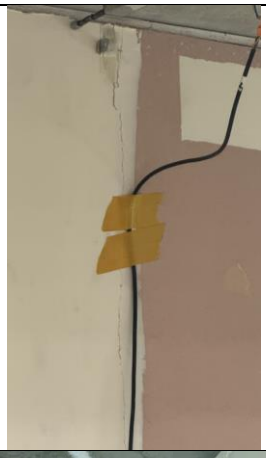
At the top of the Steel NE inside and Steel in-plane East wall junction 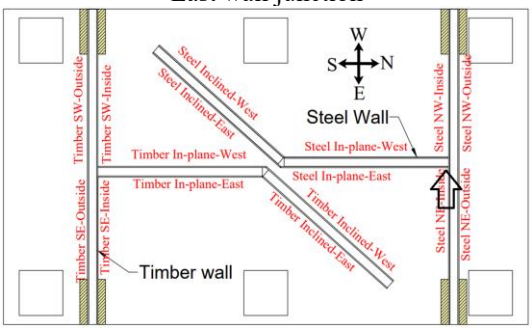	Progressive damage: Tear in the plaster paper	
Near the top Steel NE inside and Steel in-plane East wall junction 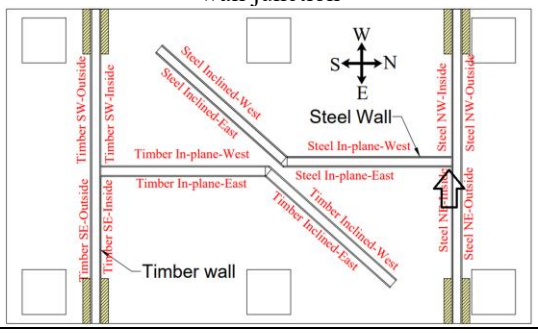	Cracks are slightly wider than hairline	
At the top of the Steel inclined east wall at the Steel in-plane East junction 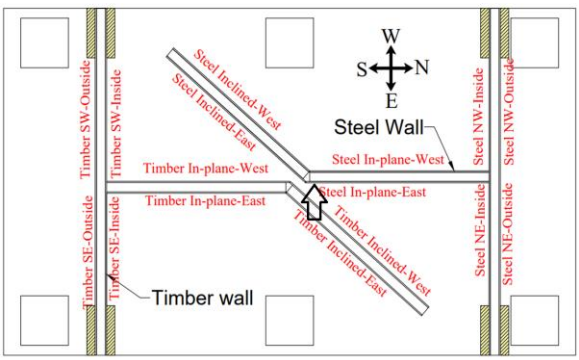	Crack in the plasterboard	

Table 2.30.Motion 15, 2.31 % inter-story drift

Location	Observation	Photo
At the top of the Steel NE inside and Steel in-plane East wall junction 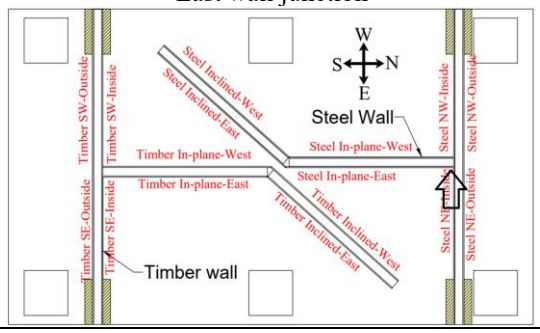	Progressive damage: Tear in the plaster paper	
At the top of the Steel inclined east wall at the Steel in-plane East junction 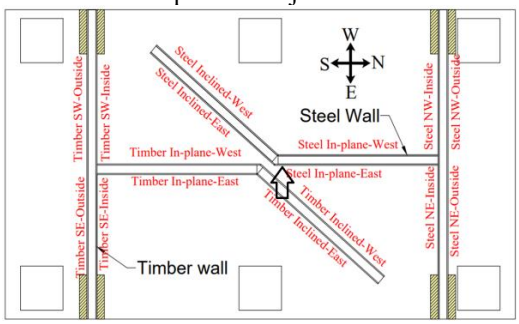	Progressive damage: Crack in the plasterboard	
At the top of the Steel NW inside and Steel in-plane West wall junction 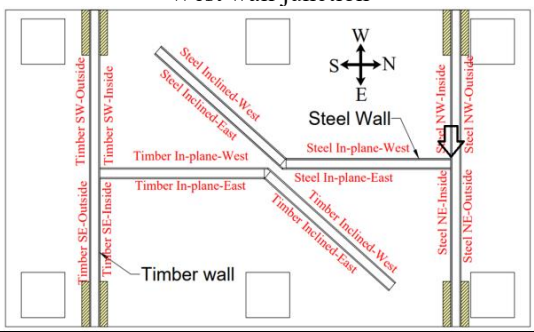	Progressive damage: Tear in the plaster paper	

Table 2.31.Motion 16, 2.56 % inter-story drift

Location	Observation	Photo
At junction Steel NE Inside wall from the Steel in-plane East Wall 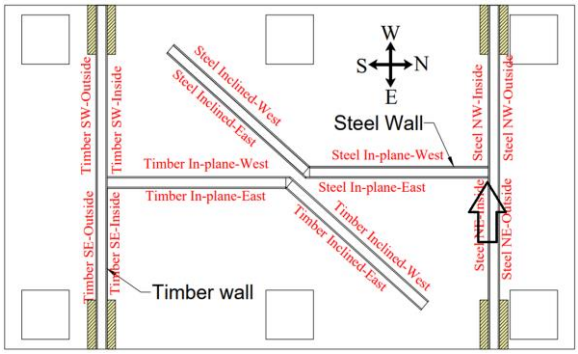	Separation of the walls at the junction	

At junction Steel NW Inside wall from the Steel in-plane West Wall 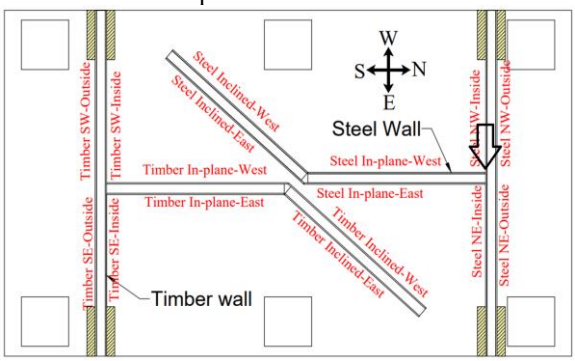	Separation of the walls at the junction	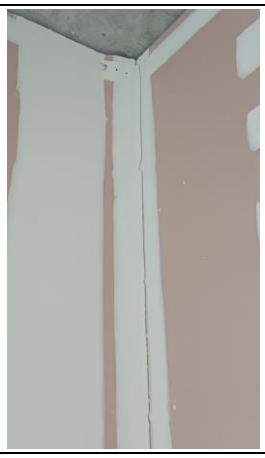

Table 2.32.Motion 17, 2.84 % inter-story drift

Location	Observation	Photo
At the top of the Steel in-plane West at junction with Steel inclined west wall 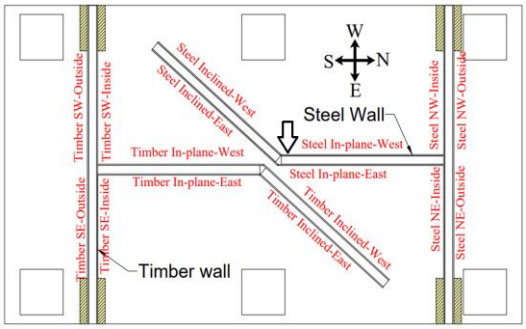	Crack in plaster	
At the top corner of the steel inclined east wall at the steel in-plane east junction 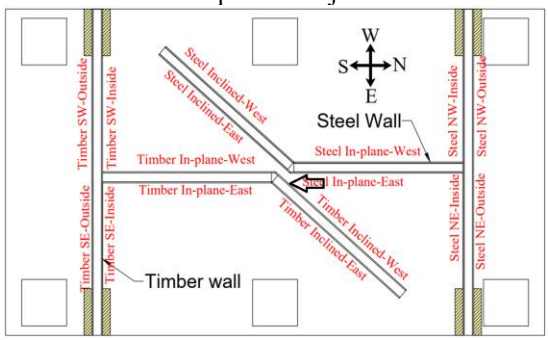	Crack in the plasterboard	
Along the length at top of the Steel NE/NW outside Wall 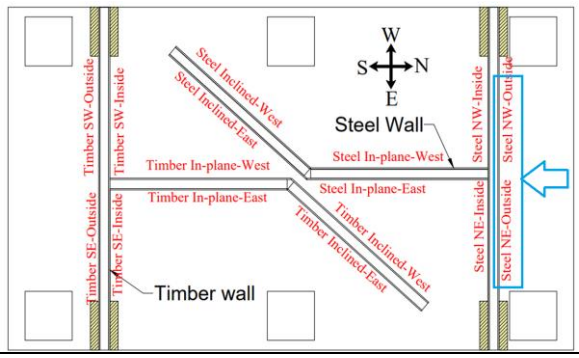	Screw impressions	

Photos of restrained wall specimens after Motion 18, 3 % inter-storey drift

Figure 2.56. Wall specimen after motion 18 - 3 % inter-storey drift (North-East elevation)

Figure 2.57. Steel NE Outside wall after motion 18 - 3 % inter-storey drift

Figure 2.58. Steel wall west return junction after motion 18 - 3 % inter-storey drift

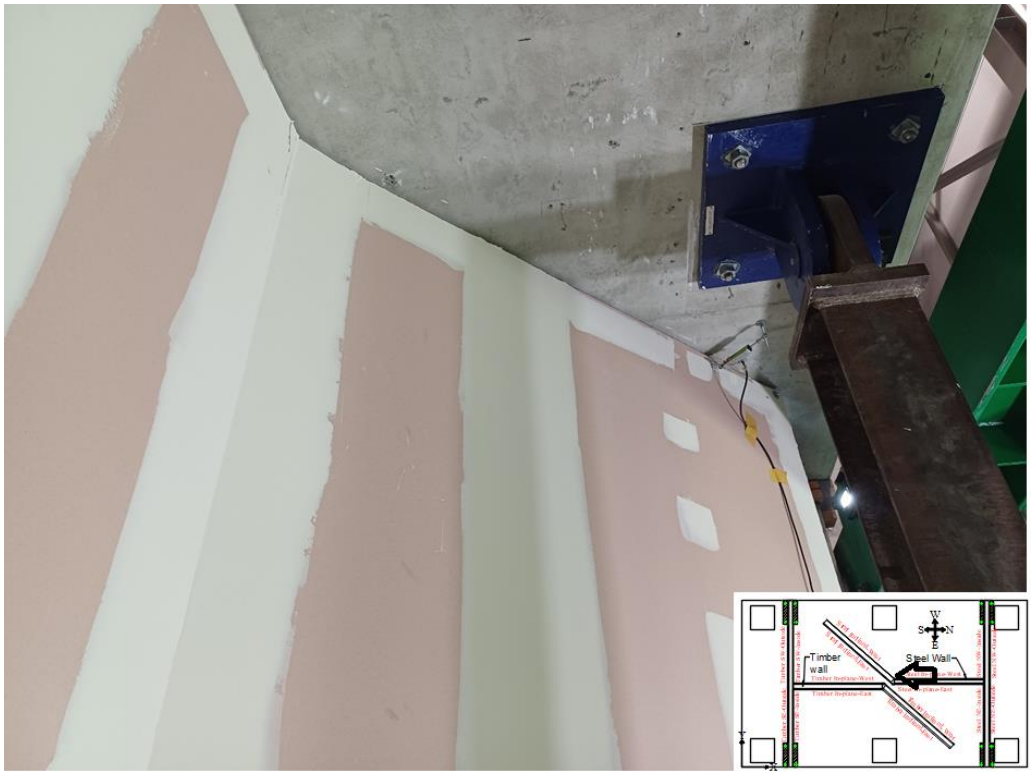

Figure 2.59. Steel wall West inclined junction after motion 18 - 3 % inter-storey drift

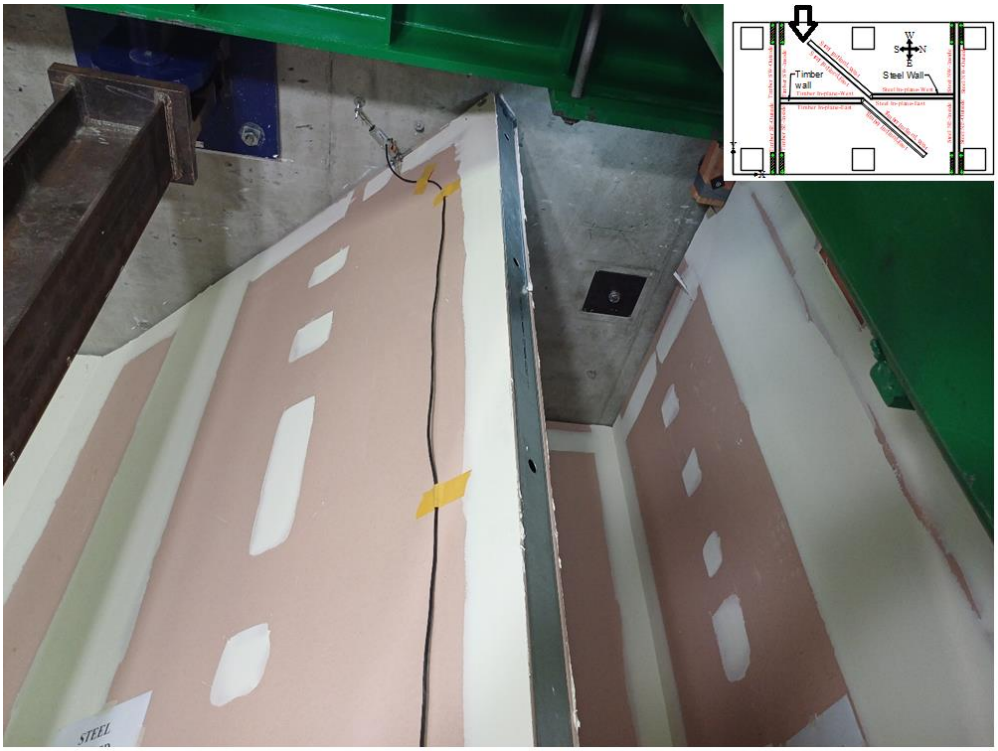

Figure 2.60. Steel wall West inclined junction after motion 18 - 3 % inter-storey drift

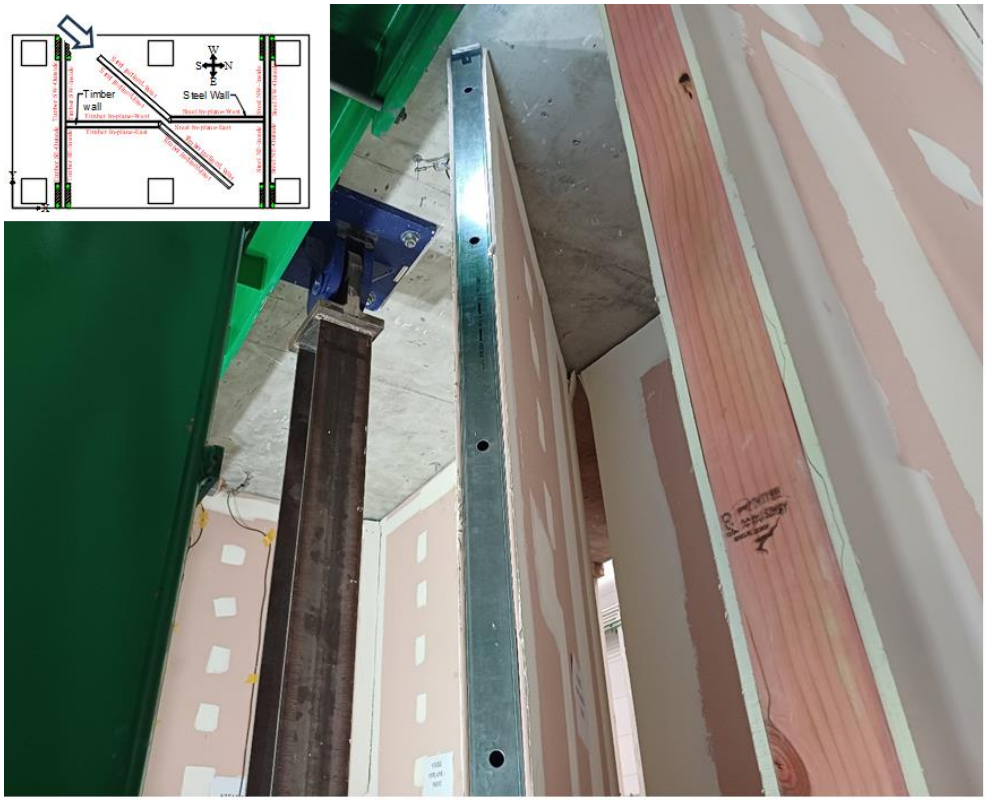

Figure 2.61.Walls elevation from South-West direction after motion 18 - 3 % inter-storey drift

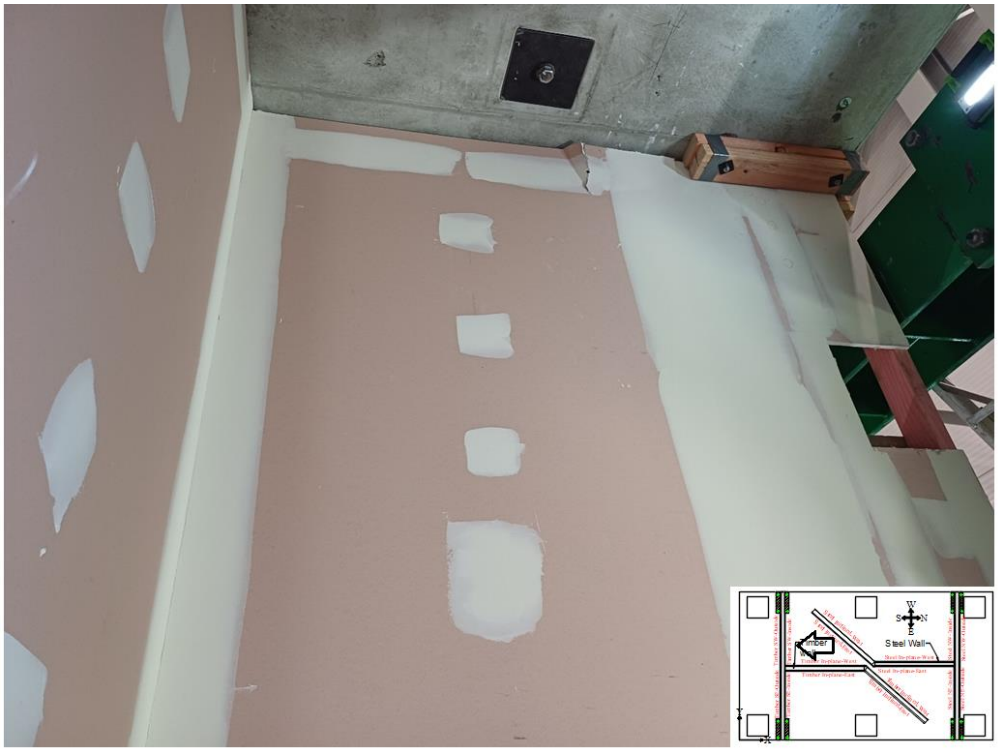

Figure 2.62. Timber South-West Inside wall after motion 18 - 3 % inter-storey drift

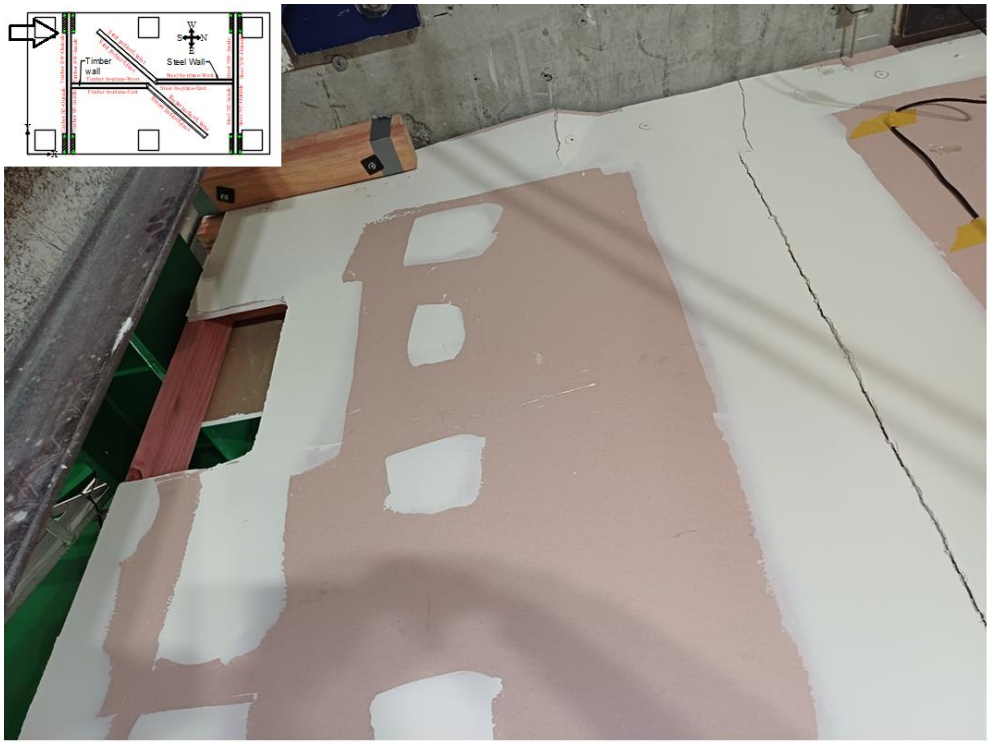

Figure 2.63. Timber South-West Outside wall after motion 18 - 3 % inter-storey drift

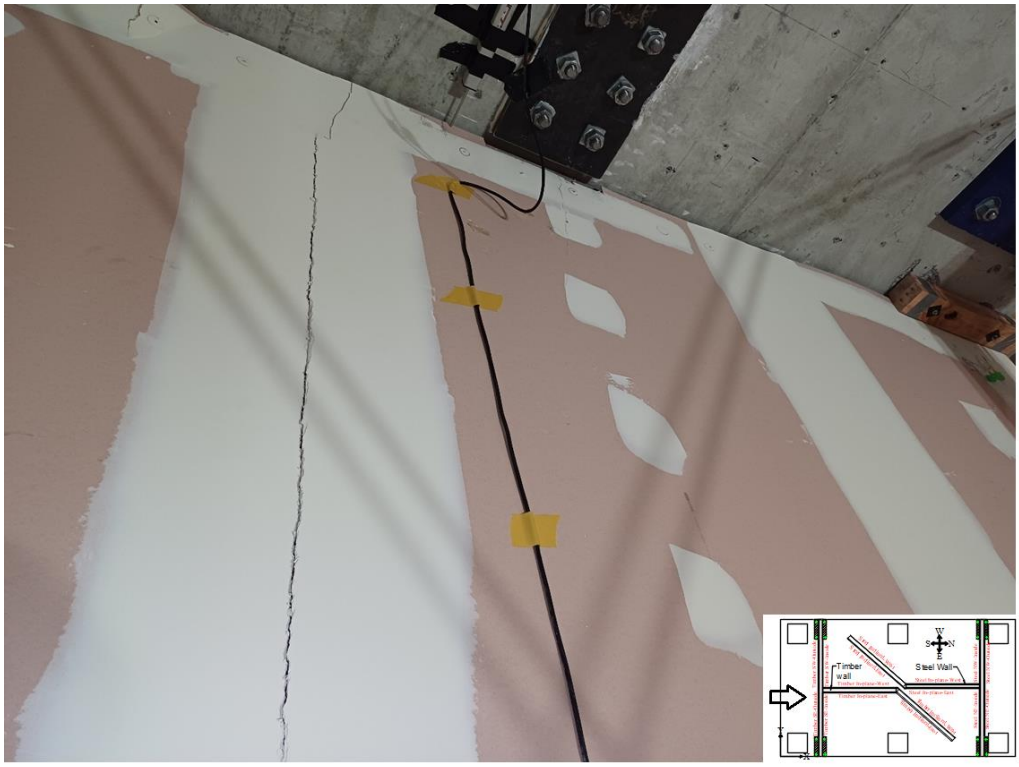

Figure 2.64. Timber South Outside wall after motion 18 - 3 % inter-storey drift

Figure 2.65. Timber Southeast Outside wall after motion 18 - 3 % inter-storey drift

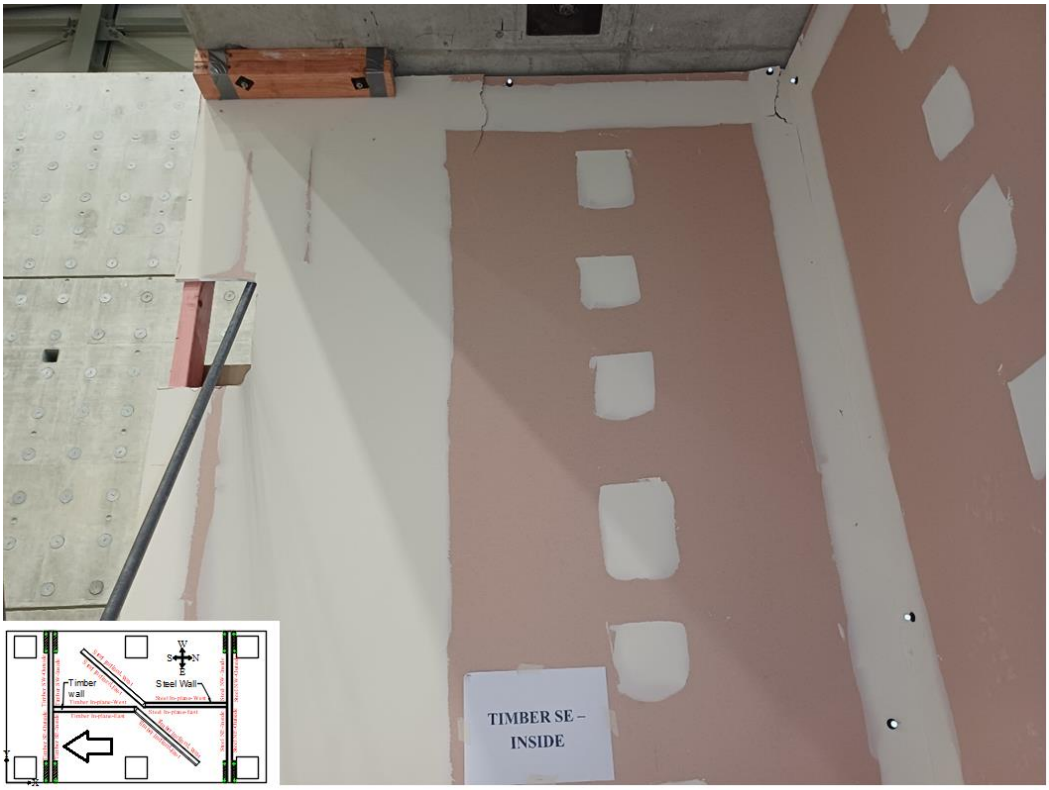

Figure 2.66. Timber Southeast Inside wall after motion 18 - 3 % inter-storey drift

Figure 2.67. Timber East Inclined wall junction after motion 18 - 3 % inter-storey drift

Figure 2.68. Walls from East direction after motion 18 - 3 % inter-storey drift

Figure 2.69. Walls from North-East direction after motion 18 - 3 % inter-storey drift

Figure 2.70. Timber wall inclined junction West and Steel wall inclined junction East after motion 18 - 3 % inter-storey drift

Post-test Frame damage inspections (after 3.0 % inter-story drift)

Table 2.33. Post-test frame damage inspection of restrained timber wall specimen

Location	Observation	Photo
Timber SE wall 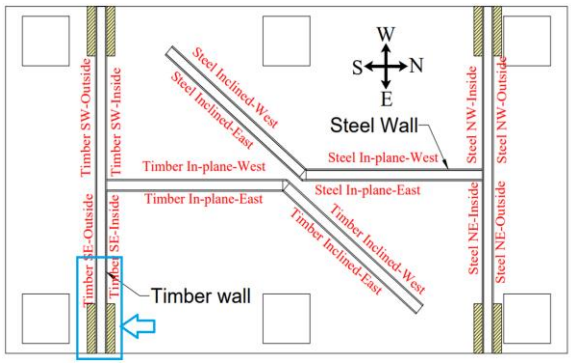	Bending of DHT flanges	 

Timber SW wall 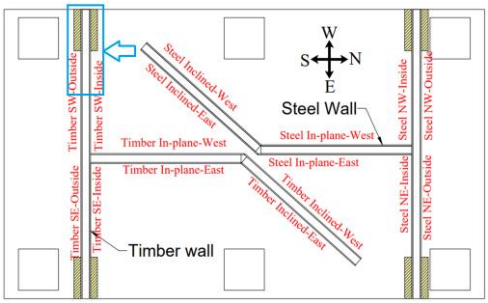 	Bending of DHT flanges	 
Timber Inclined wall 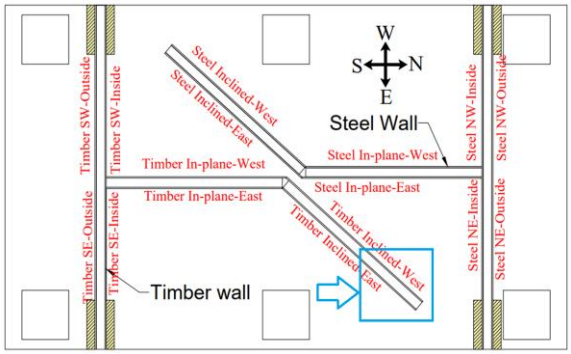 	Bending of DHT flanges	
At junction of Timber in-plane east and Timber inclined East wall 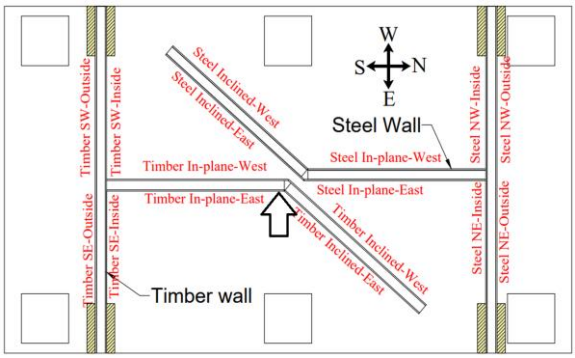 	Damage to steel plate due to the interaction with DHT	 
At the timber inclined West wall junction	Damage to top timber plate, break in the steel strap, and DHT damage	

<table>
<tr>
<td> 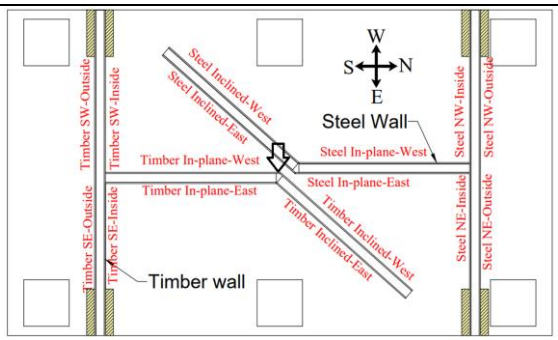

 </td>
<td></td>
<td>  </td>
</tr>
<tr>
<td>Timber wall SW/SE and Timber in-plane wall junctions and where there were nails securing the strap
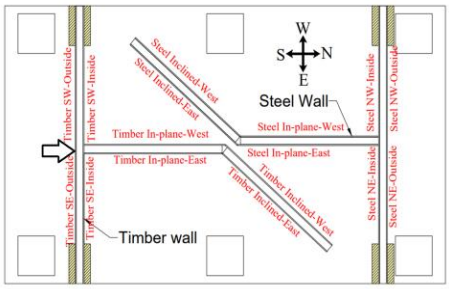

 </td>
<td>Crack in the top plate</td>
<td> 

 </td>
</tr>
</table>

Table 2.34.Post-test frame damage inspection of restrained steel wall specimen

Location	Observation	Photo
NW/NE wall and the Steel in-plane wall frames due to yielding of the DHT 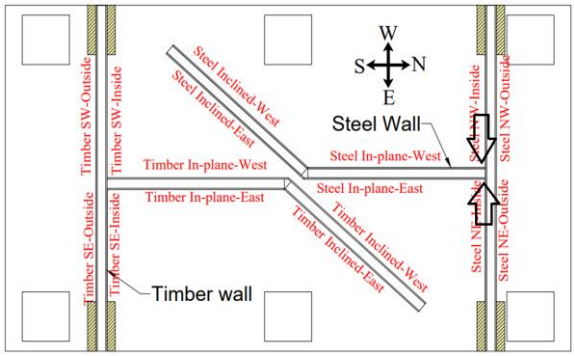	Separation of the connected steel Frames (studs)	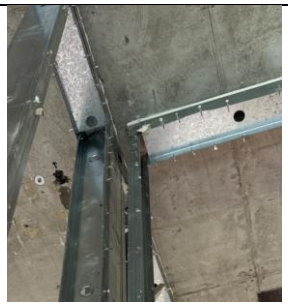 
In steel inclined wall West and Steel in-plane west junction 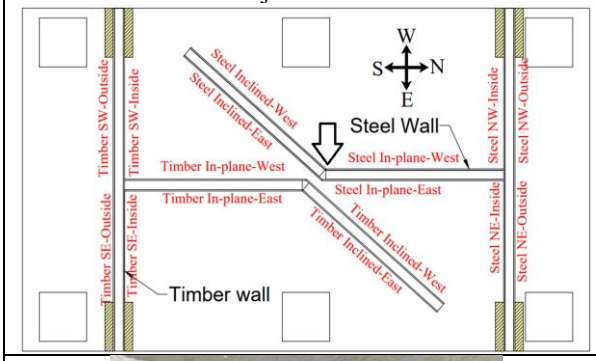  	Damage to DHT and studs due to interaction with steel angle plate	  

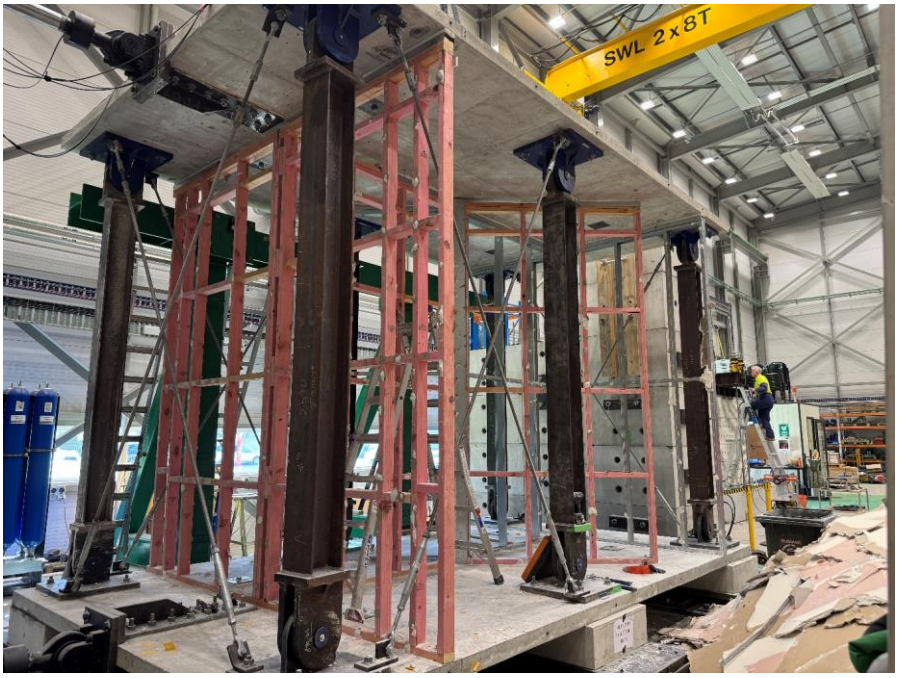

Figure 2.71. Photo of wall frames after motion 18 - 3 % inter-storey drift (Southeast elevation)

Figure 2.72. Photo of wall frames after motion 18 - 3 % inter-storey drift (East elevation)

PHASE II: SEISMIC PERFORMANCE OF FIRE-RATED TIMBER PARTITION WALLS WITH "NO-FIX ZONE" DETAILING INTERACTING WITH PERIMETER-RESTRAINED CONCEALED PLASTERBOARD CEILING

ABSTRACT

This chapter details the Phase II experimental investigation into the seismic interaction between a timber-framed partition wall and two connected non-structural systems: a perimeter-restrained plasterboard ceiling and an unbraced mechanical pipe. Building upon the successful performance of the steel-framed wall established in Phase I, this phase focuses exclusively on timber construction.

The primary aim was to observe the combined system behaviour and evaluate dynamic effects, specifically examining how deformation and acceleration demands are transferred between the deforming wall and the adjacent non-structural elements. The study documents sequential damage progression, revealing that drift-induced deformations of the primary test structure were a more significant damage driver for integrated assemblies than pure inertial forces.

A key finding indicates a dynamic interaction between the ceiling and its supporting wall, suggesting ceiling accelerations are influenced by wall response, not just floor motion. The results validate certain code-prescribed factors while identifying areas for refinement. This work underscores the critical need for future research to directly quantify these interactions through advanced instrumentation, paving the way for more resilient integrated system design.

EXPERIMENTAL PROGRAMME AND METHODOLOGY

Test Setup

The test setup for this phase remained consistent with that established in Phase I. For a comprehensive description of the test-setup configuration, please refer to the relevant section in the Phase I.

Specimen design, configurations and details

Partition walls

A timber framed 'H' shaped wall specimen were constructed between the concrete slabs of the test setup. The major details are as follows:

(1) The walls are allowed to slide in-plane within the top deflection head track (DHT).
(2) Anchors connecting the wall (DHTs) to the top slab are prohibited within 1200 mm of the wall junction region, defined as the "No-Fix zones."
(3) Out-of-plane flexibility at the junction is provided by bending of the top timber plates.
(4) The frames are lined with 13 mm GIB FYRELINE plasterboard following GIB EzyBrace® System specification GS2-N (GIB, 2016). However, the plasterboard is not fastened to the top DHTs.

The out-of-plane wall ends are restrained with timber blocks, consistent with the method used for the restrained specimens in Phase I.

Figure 3.1 and Figure 3.2 show the layout of the partition walls constructed between two slabs, with their elevation provided in Figure 3.3. The wall oriented in the North-South direction, referred to here as the "in-plane" wall, connects to the northern and southern walls oriented in the East-West direction (referred as "out-of-plane walls)

via T-junctions, detailed in Figure 3.4. An 800 mm wide by 2000 mm high door opening was incorporated into the southern out-of-plane wall. The elevation detail of the door lintel is shown in Figure 3.5

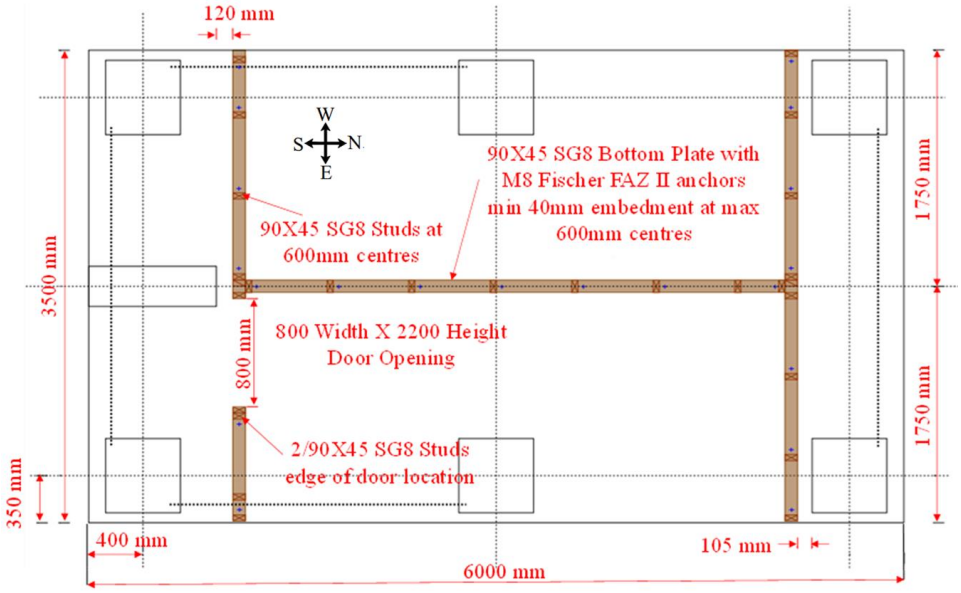

Figure 3.1. Timber and steel stud framing plan

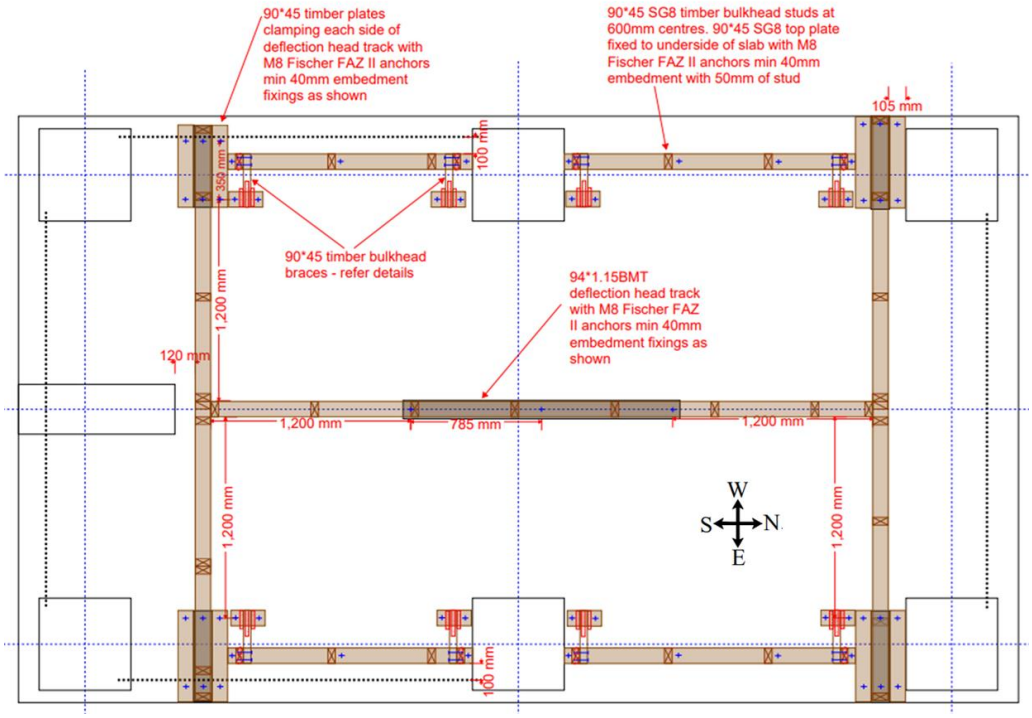

Figure 3.2. Timber and steel stud reflected ceiling plan

As shown in Figure 3.2, the anchors for the deflection head track (DHT) were installed at approximately 1200 mm from the T-junctions on all connecting walls. Accordingly, the DHT sections on the out-of-plane walls were sized only to span between the two anchors at their ends, rather than running the full wall length. The same principle was applied to the in-plane wall, where DHT anchors were positioned at least 1200 mm from the northern and southern T-junctions. The DHT section for this wall was similarly cut to a length that spans just the three installed anchors.

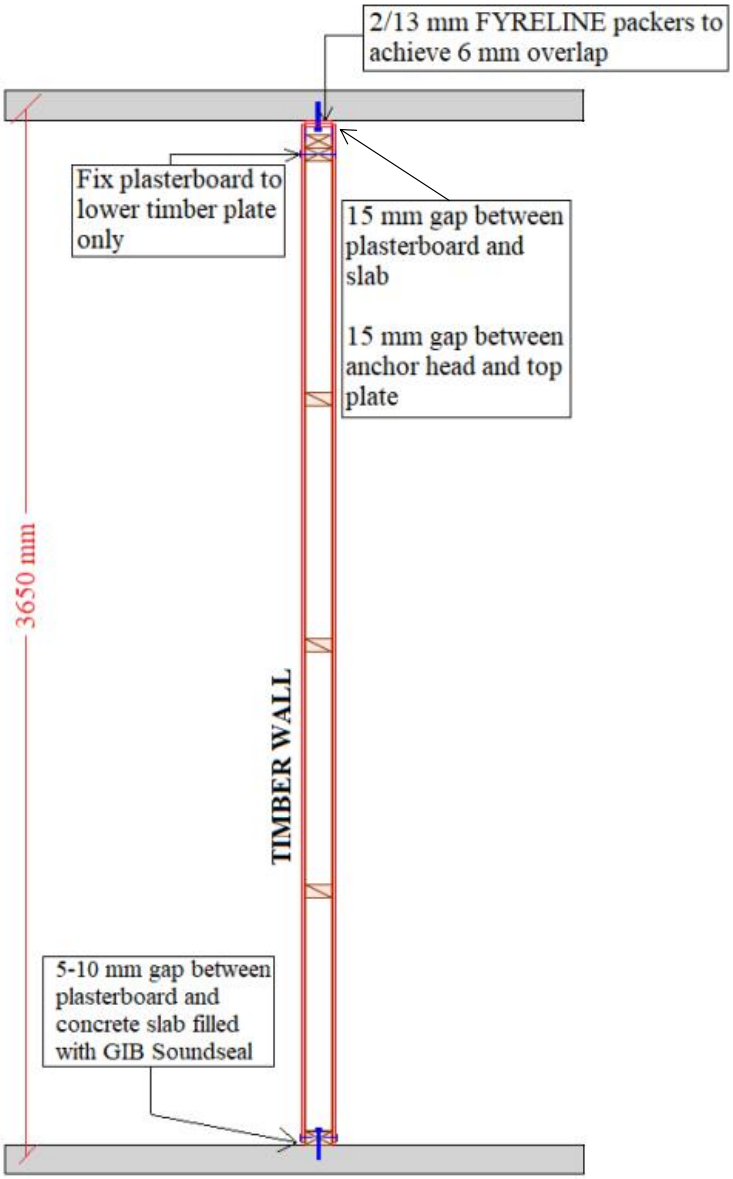

Figure 3.3. Typical wall section elevations

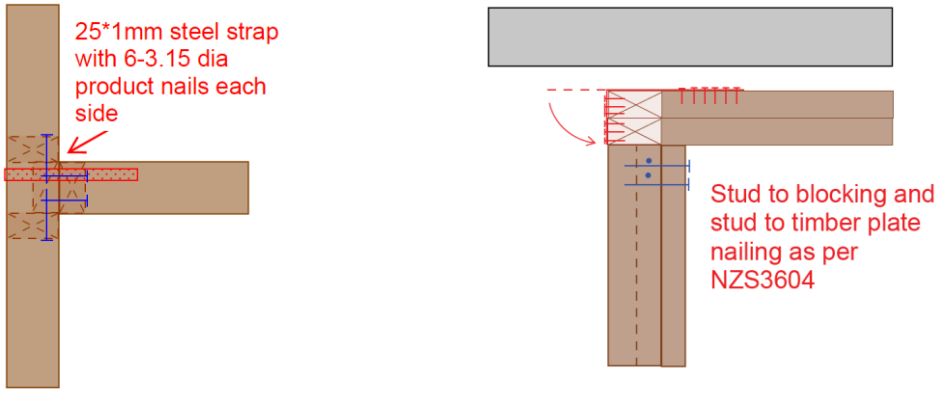

a) Plan view b) Side view

Figure 3.4. Return intersection details in timber wall

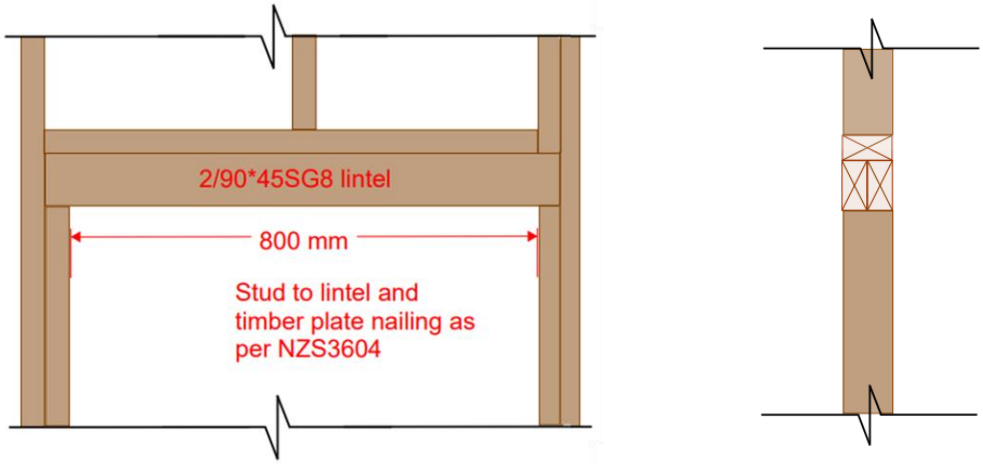

a) Front view b) side view

Figure 3.5. Door lintel elevation detail

The placement of bulkheads (to support plasterboard ceilings), restraining timber blocks at the ends of the out-of-plane walls, and deflection head tracks for walls are illustrated in Figure 3.2. Two bulkheads were installed on the east and west edges of the top slab to support the ceilings, with their detailed construction shown in Figure 3.6.

Restraining timber blocks were installed at the upper ends of the out-of-plane walls on both sides to better simulate real-world boundary conditions, in which connecting elements typically restrict movement at the wall ends. To represent an approximately fixed boundary and prevent rotation, 45 mm × 90 mm timber elements

were tightly fitted against the wall linings, as shown in Figure 3.2 and Figure 3.6. These timber blocks were fastened in place using threaded rods anchored into the top slab.

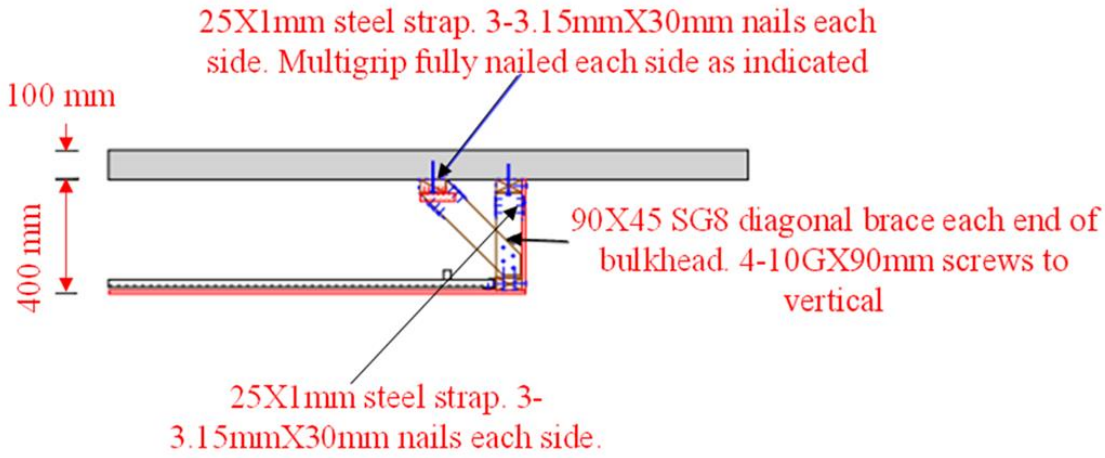

Figure 3.6. Bulkhead details (side view)

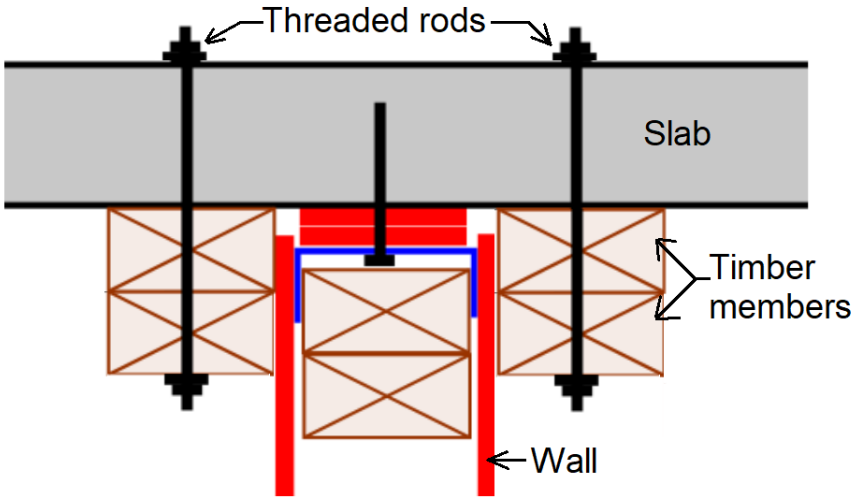

Figure 3.7. Side view of restrained ends of timber wall

Suspended Ceilings

The concealed plasterboard ceiling, intended to be perimeter-restrained, was installed within the space defined by the bulkheads and walls shown in Figure 3.10. Square inspection holes were placed at four locations to assess damage to the ceiling components.

However, due to construction deviations, the as-built ceiling details differ, as illustrated in Figure 3.9.

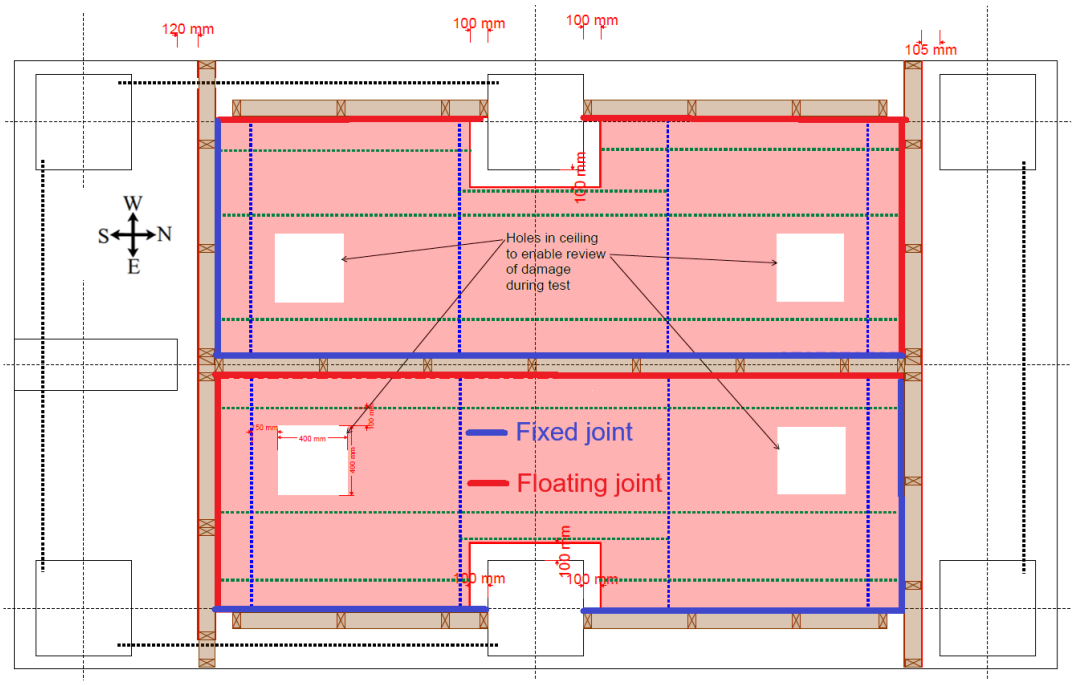

Figure 3.8.Area of ceiling installation with intended perimeter joint details (plan)

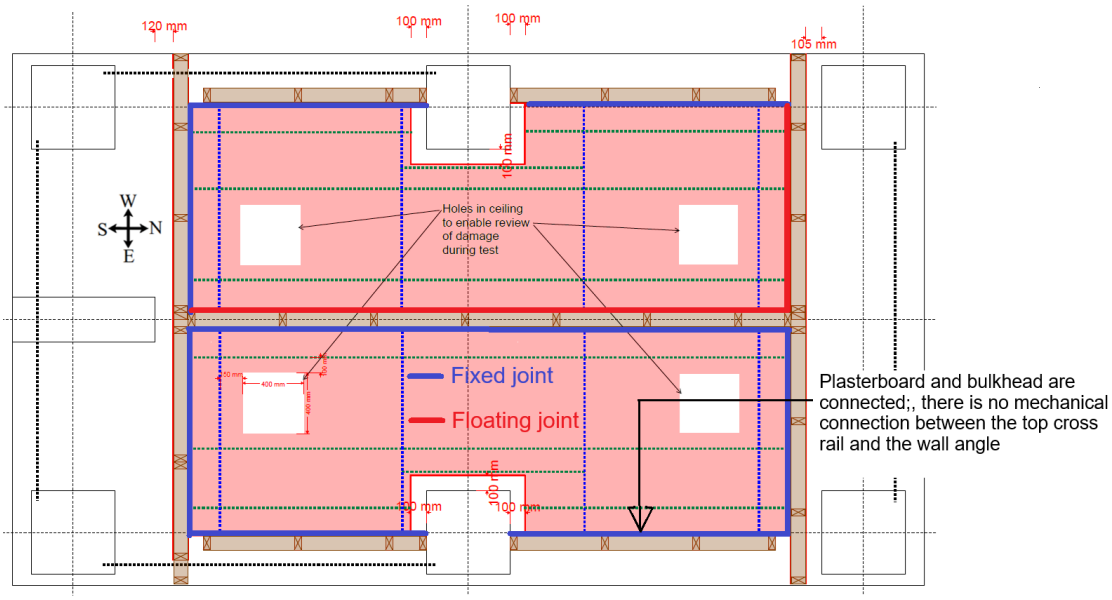

Figure 3.9.Area of ceiling installation with as-built perimeter joint details (plan)

The primary variation involved a change in the locations of the fixed and floating perimeter joints. The ceiling on the east side maintained the typical configuration with fixed and floating edges on adjacent sides, allowing for the evaluation of standard construction. In contrast, the ceiling on the west side was fixed on nearly all sides. At the bulkhead, the connection consisted only of the plasterboard attached to its underside, with no mechanical fasteners between the top cross rails and the wall angle. This configuration provided a useful comparison between a ceiling with all sides fixed and the typical perimeter-restrained design

The suspended ceiling framing plan, detailing the layout of top-cross rails (TCR), furring channels (FC), and sleeve anchors for the supporting wires, is shown in Figure 3.10. The TCRs are spaced at 1200 mm centres with furring channels installed at 600 mm centres. Standard details for the fixed and floating edge connections of the concealed plasterboard ceiling are provided in Figure 3.11 through Figure 3.14. The ceiling was lined with 13 mm GIB Standard plasterboard, which was fixed to the furring channels in compliance with GIB specifications, resulting in plenum height of 400 mm.

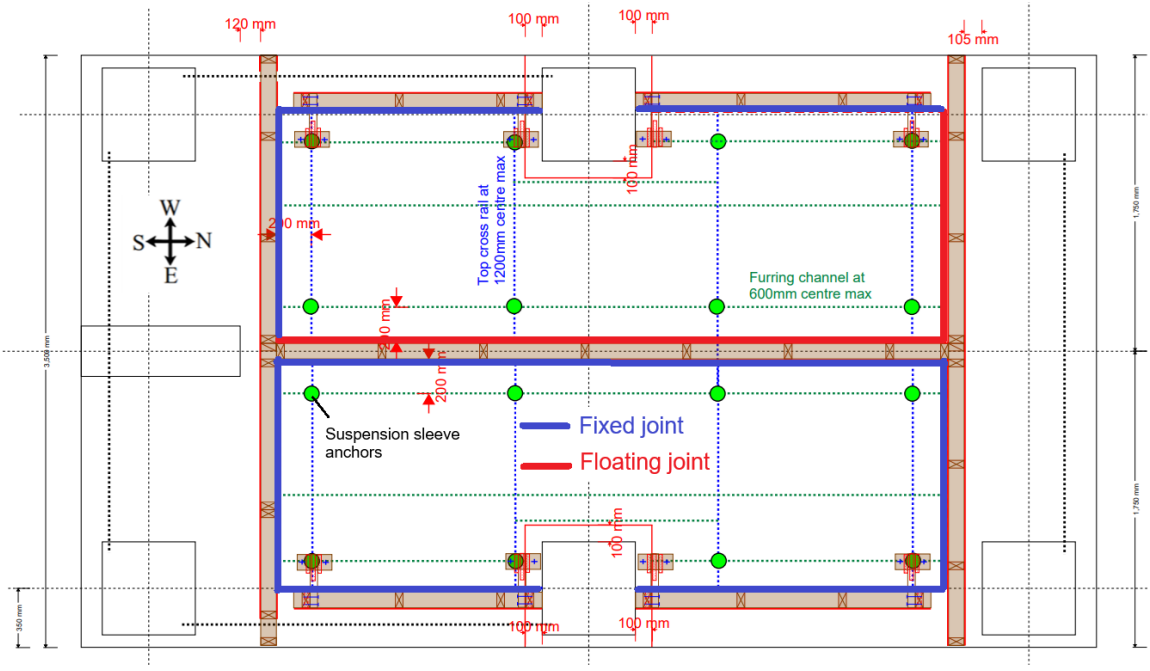

Figure 3.10.Suspended ceiling framing (plan)

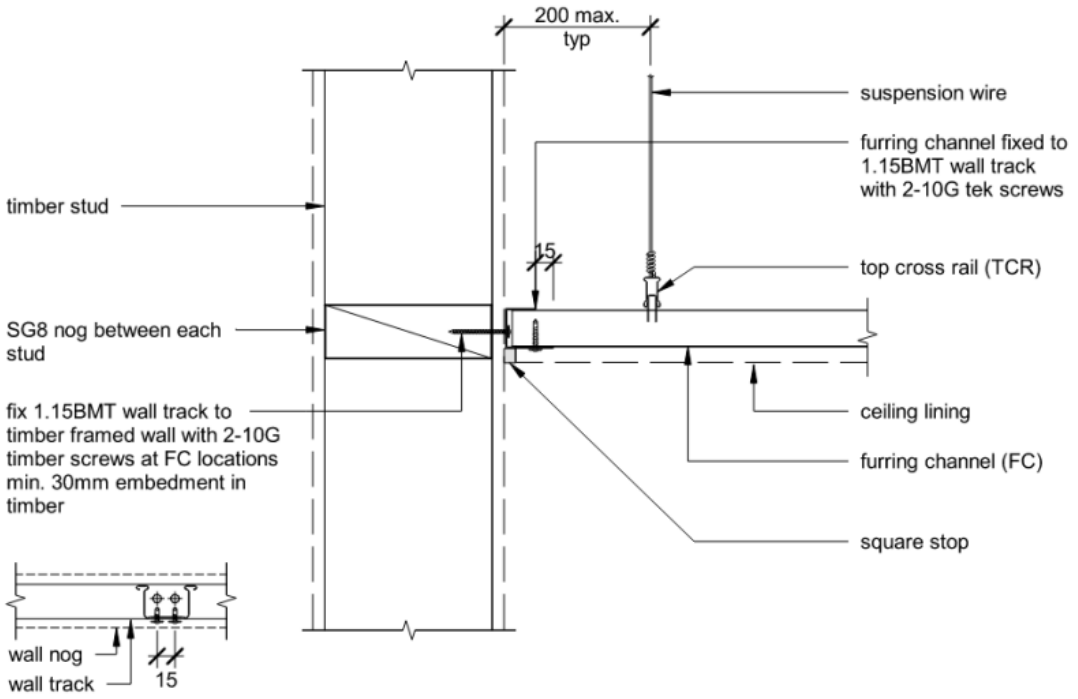

Figure 3.11. Furring channel fixed edge connection detail

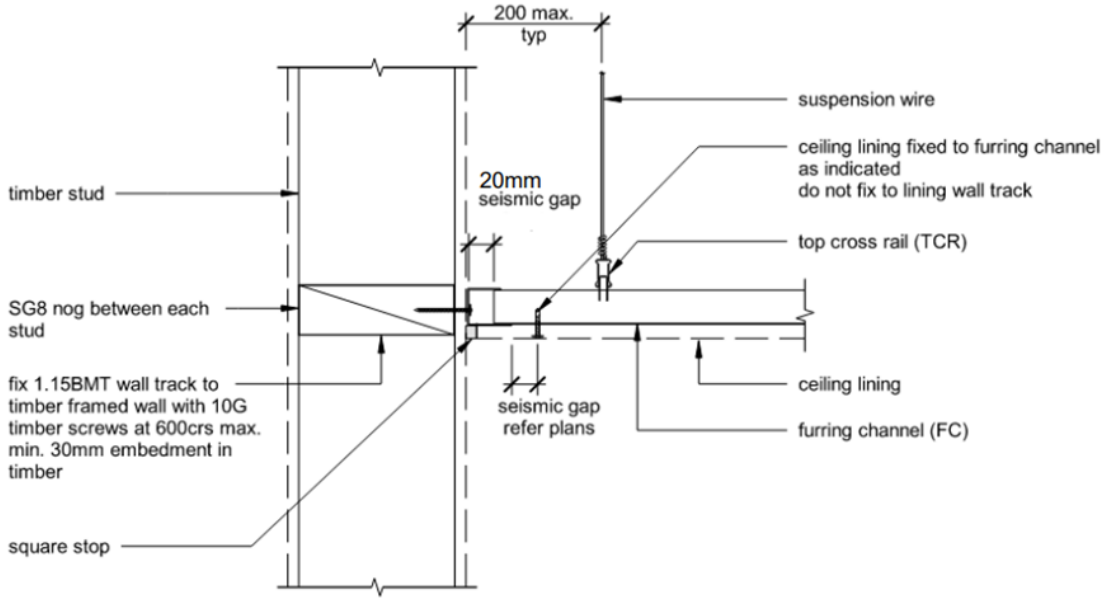

Figure 3.12. Furring channel floating edge connection detail

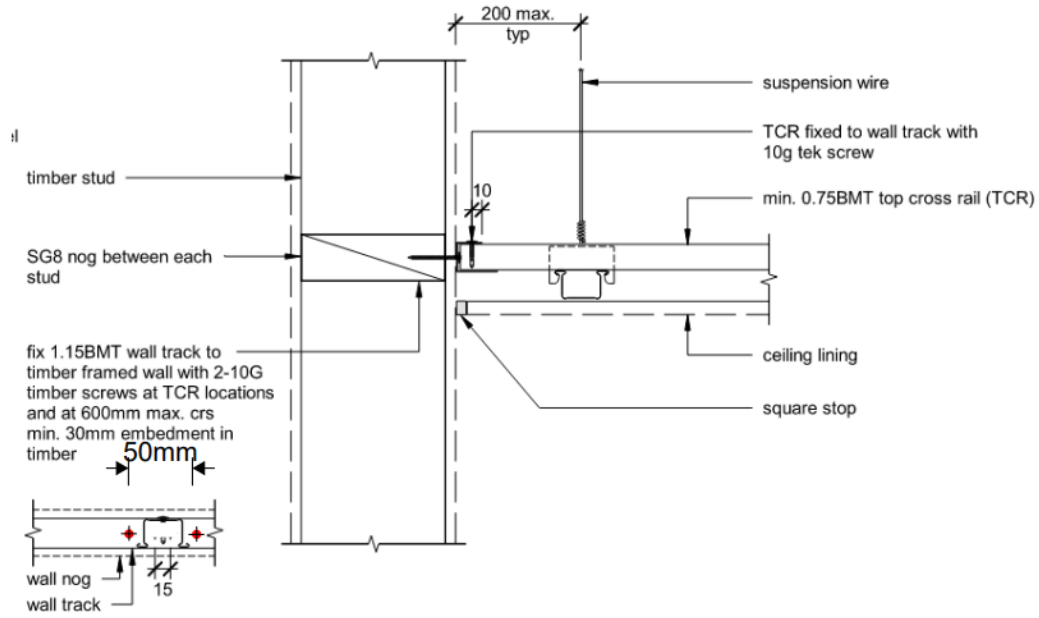

Figure 3.13. Top cross rail fixed edge connection detail

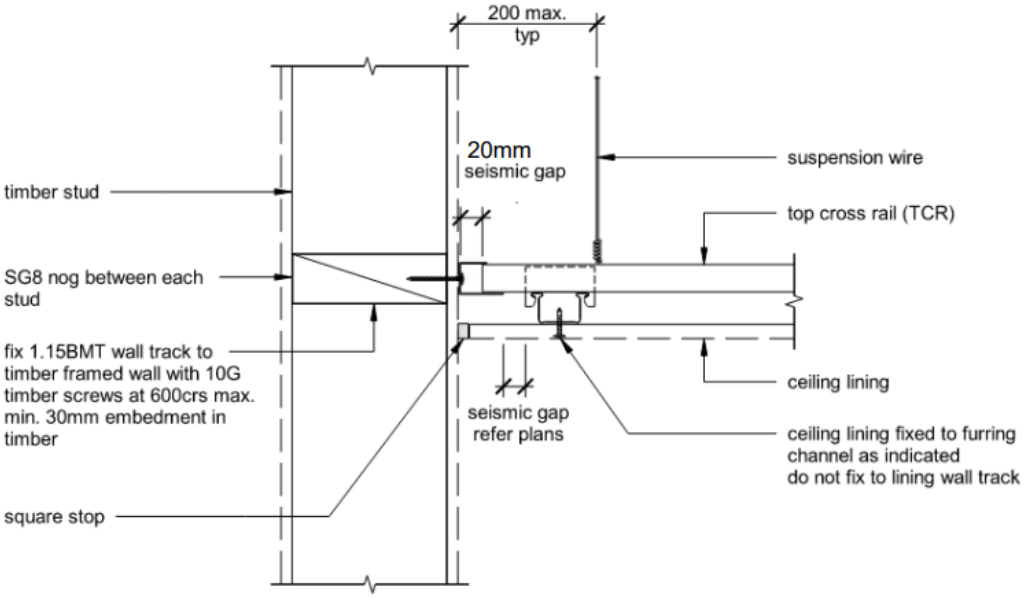

Figure 3.14. Top cross rail floating edge connection detail

Mechanical pipes

Two 50 mm diameter mechanical pipes (Pipe 1 and Pipe 2), each approximately 2600 mm long, were installed within the ceiling plenum, passing through the in-plane wall as

shown in Figure 3.15 To increase their mass, additional steel sections were welded onto the pipe ends. An 80 mm clearance hole was created in the wall for each pipe. The pipes supported by M10 threaded rods (as shown in Figure 3.16 (a)) positioned 1 m from the in-plane wall, with their centreline located 240 mm below the top slab. The gap between the pipes and the wall openings was filled with HILTI CP606 sealant, as shown in Figure 3.16 (b). However, the sealant was not smoothed flush, as would be typical in actual construction. It is anticipated that this application where sealant is merely smeared or piled across the opening will not perform adequately in a fire scenario.

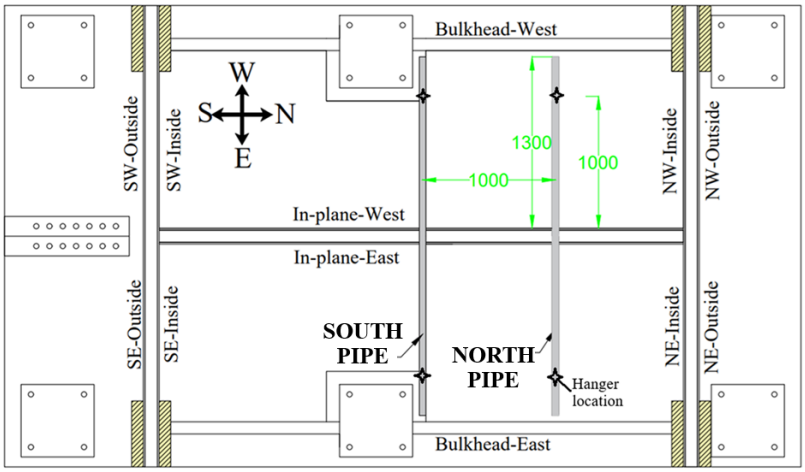

Figure 3.15. Location of mechanical pipes (plan)

a) Pipe supported by M10 hanger

b) Pipe penetrating through wall with fire-sealant applied

Figure 3.16.Mechanical pipe details

Photos of the constructed specimen

The photos of the constructed specimen are shown in Figure 3.17 through Figure 3.20.

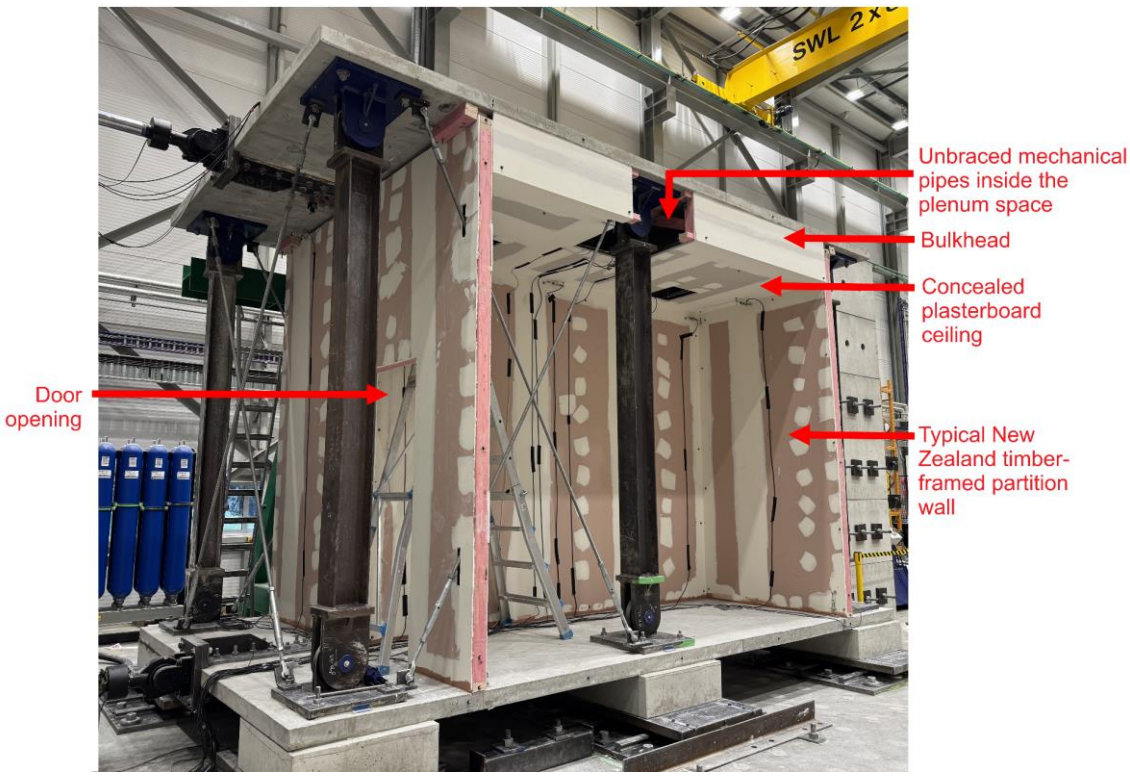

Figure 3.17. Photo of constructed specimen (Southeast elevation)

Figure 3.18. Photo of constructed specimen (Northeast elevation)

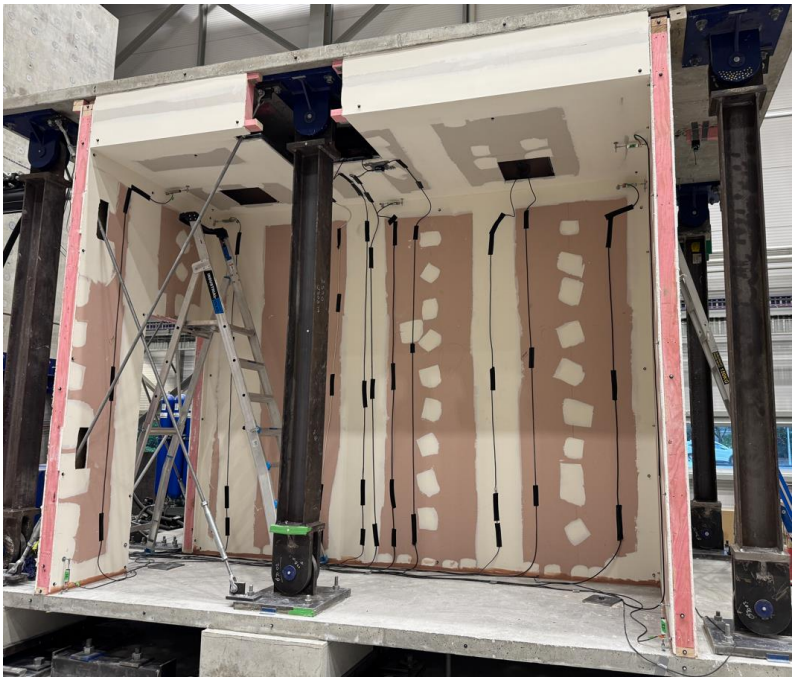

Figure 3.19. Photo of constructed specimen (East elevation)

Figure 3.20. Photo of constructed specimen inside the ceiling plenum

The construction quality for Phase II was observed to deviate from the standards achieved in Phase I, with three primary issues identified.

(1) First, the top plate of the in-plane wall required reconstruction, as its initial assembly with the DHT and top slab inadvertently restrained the intended sliding mechanism between the wall and the top floor.

(2) Second, the fire-rated sealant application at the mechanical pipe penetration was inconsistent; it was smeared and not properly tooled, rendering the resulting performance data on sealant integrity non-representative of typical construction.

(3) Finally, the perimeter-restrained ceiling on the East side (room) was inadvertently constructed with all edges effectively fixed to the boundary wall and bulkhead, resulting in an "all-fixed" configuration rather than the intended "fixed-float" detail. While non-conforming, this variation provided a beneficial opportunity for direct comparison between the two connection types.

Loading protocols

For Phase II testing, the same displacement time histories from Phase I were applied. To summarize, these "Motion" histories for the 2nd and 3rd floors were derived from a numerical model of a five-storey reinforced concrete structure subjected to the Imperial Valley earthquake record (El Centro, 1940, Array #9) at the peak ground velocities (PGVs) listed in Table 3.1. Refer to (Pledger, 2026) for details. The top and bottom slabs were subjected to the scaled motions presented in Table 3.2. These were generated by applying the scale factors from Table 3.1 to the original displacement histories, a process designed to achieve the target inter-storey drifts specified in Table 3.1

The resulting spectral floor accelerations, velocities, and displacements for a selected PGV are presented in Figure 3.21, Figure 3.22, and Figure 3.23. Examples of the input scaled displacement time histories for Motions 5, 10, and 14 are shown in Figure 3.24. It is noted that Phase II specimens were tested only up to Motion 16, which corresponds to a target inter-storey drift of 2.50% (Table 3.2).

Table 3.1. Input absolute floor motion demands from the 1.0% Design Level structure and corresponding scale factors to achieve the target drift (Pledger, 2026)

Motion	PGV[1] (cm/s)	PFA[2] Bottom slab (g)	PFV[3] Bottom slab (m/s)	PFD[4] Bottom slab (mm)	PFA Top slab (g)	PFV Top slab (m/s)	PFD Top slab (mm)	Target Inter- story drift (%)	Scale factor	Comments
0	10	0.11	0.11	27	0.15	0.15	34	0.26	0.1000	
1	10	0.11	0.11	27	0.15	0.15	34	0.26	0.3571	
2	10	0.11	0.11	27	0.15	0.15	34	0.26	0.7143	
3	10	0.11	0.11	27	0.15	0.15	34	0.26	1.0714	
4	20	0.23	0.22	53	0.31	0.3	67	0.52	0.6897	
5	20	0.23	0.22	53	0.31	0.3	67	0.52	0.8621	
6	20	0.23	0.22	53	0.31	0.3	67	0.52	1.0345	
7	30	0.34	0.33	68	0.39	0.45	88	0.87	0.8235	
8	30	0.34	0.33	68	0.39	0.45	88	0.87	0.9412	
9	30	0.34	0.33	68	0.39	0.45	88	0.87	1.0588	
10	40	0.42	0.42	88	0.5	0.56	113	1.11	0.8850	
11	50	0.51	0.49	114	0.63	0.63	130	1.30	0.9328	Test run two times
12	70	0.73	0.62	158	0.88	0.76	163	1.50	0.9677	
13	90	0.94	0.80	193	1.13	0.86	196	1.73	0.9563	
14	110	1.19	0.96	233	1.37	0.97	247	2.04	0.9804	
15	110	1.19	0.96	233	1.37	0.97	247	2.04	1.1029	Test not run
16	130	1.46	1.13	276	1.60	1.17	300	2.67	0.9363	Final Test
17	130	1.46	1.13	276	1.60	1.17	300	2.67	1.0300	Test not run
18	140	1.51	1.23	298	1.62	1.24	327	3.03	0.9901	Test not run

1Peak Ground Velocity, 2 Peak Floor Acceleration, 3 Peak Floor Velocity, 4 Peak Floor Displacement

Table 3.2. Actual input motions to the test setup (scaled using scale factors from Table 3.1)

Motion	PGV[1] (cm/s)	PFA[2] Bottom slab (g)	PFV[3] Bottom slab (m/s)	PFD[4] Bottom slab (mm)	PFA Top slab (g)	PFV Top slab (m/s)	PFD Top slab (mm)	Target Inter-story drift (%)	Comments
0	1.00	0.02	0.02	3.00	0.02	0.02	4.00	0.03	
1	3.58	0.04	0.04	10.00	0.06	0.06	13.00	0.10	
2	7.15	0.08	0.08	20.00	0.11	0.11	25.00	0.20	
3	10.72	0.12	0.12	29.00	0.17	0.17	37.00	0.30	
4	13.80	0.16	0.16	37.00	0.22	0.21	47.00	0.40	
5	17.25	0.2	0.19	46.00	0.27	0.26	58.00	0.50	
6	20.69	0.24	0.23	55.00	0.33	0.32	70.00	0.60	
7	24.71	0.28	0.28	56.00	0.33	0.38	73.00	0.70	
8	28.24	0.32	0.32	64.00	0.37	0.43	83.00	0.80	
9	31.77	0.36	0.35	72.00	0.42	0.48	94.00	0.90	
10	35.40	0.38	0.38	78.00	0.45	0.50	100.00	1.00	
11	46.65	0.48	0.46	107.00	0.59	0.59	122.00	1.25	Test run two times
12	67.75	0.71	0.6	153.00	0.86	0.74	158.00	1.50	
13	86.07	0.9	0.77	185.00	1.09	0.83	188.00	1.75	
14	107.85	1.17	0.95	228.44	1.35	0.96	242.16	2.00	
15	121.33	1.32	1.06	256.99	1.52	1.07	272.43	2.25	Test not run
16	130.00	1.46	1.13	258.43	1.60	1.17	280.90	2.50	Final Test
17	130.00	1.46	1.13	284.27	1.60	1.17	308.99	2.75	Test not run
18	140.00	1.51	1.23	295.05	1.62	1.24	323.77	3.00	Test not run

[1] Peak Ground Velocity [2] Peak Floor Acceleration [3] Peak Floor Velocity [4] Peak Floor Displacement

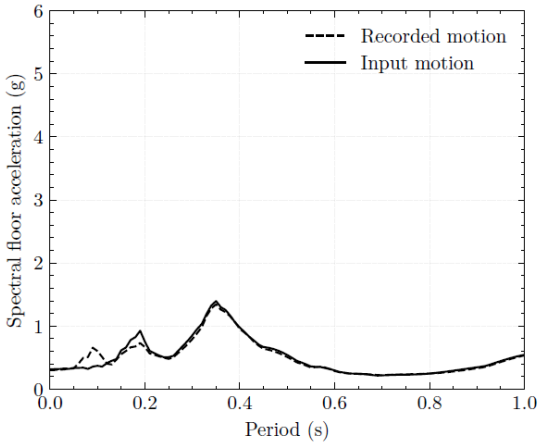

a) PGV = 20 cm/s

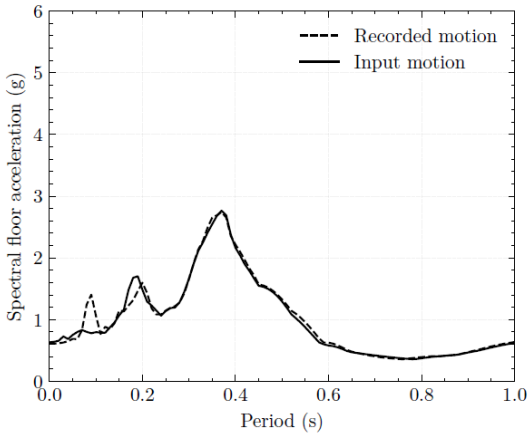

b) PGV = 50 cm/s

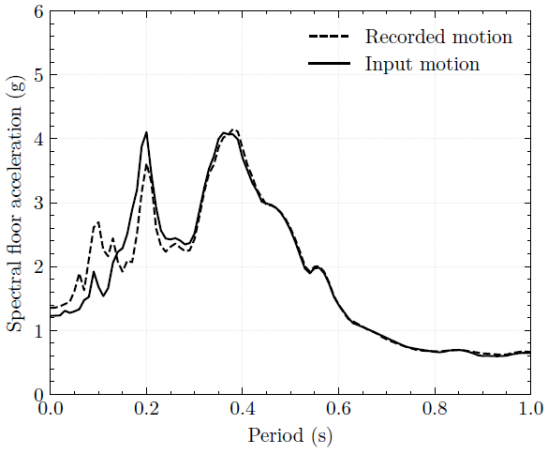

c) PGV = 100 cm/s

Figure 3.21. Spectral floor acceleration for 1.0 % design level structure at different peak ground velocities (PGVs) from Table 3.1 (Pledger, 2026)

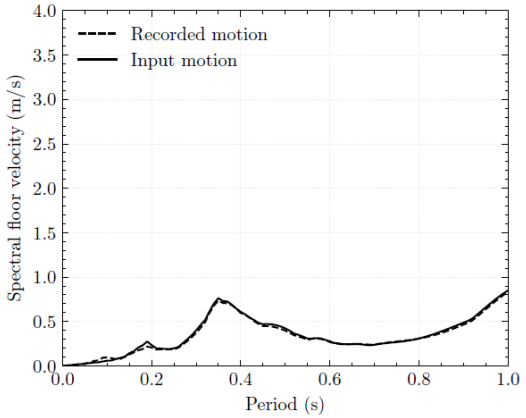

a) PGV = 20 cm/s

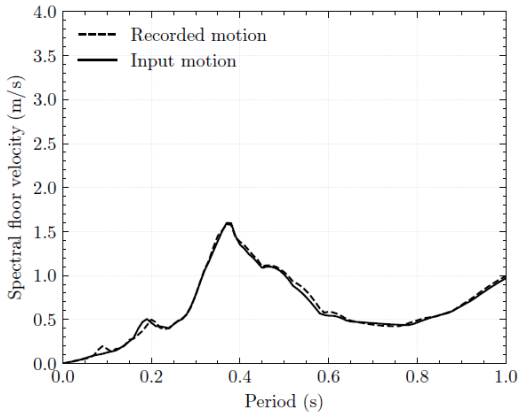

b) PGV = 50 cm/s

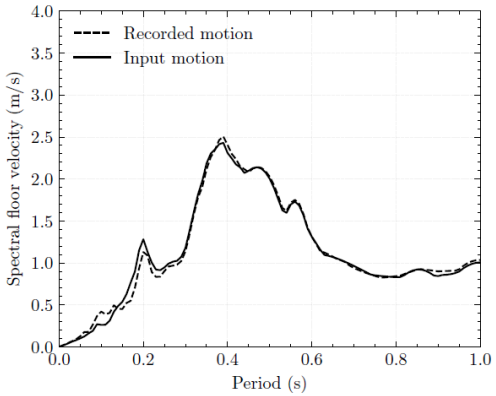

c) PGV = 100 cm/s

Figure 3.22. Spectral floor velocities for 1.0 % design level structure at different peak ground velocities (PGVs) from Table 3.1 (Pledger, 2026)

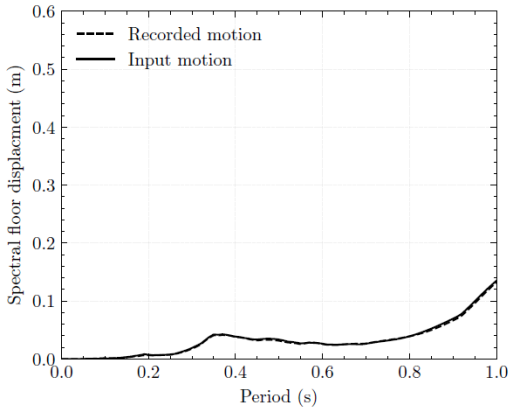

a) PGV = 20 cm/s

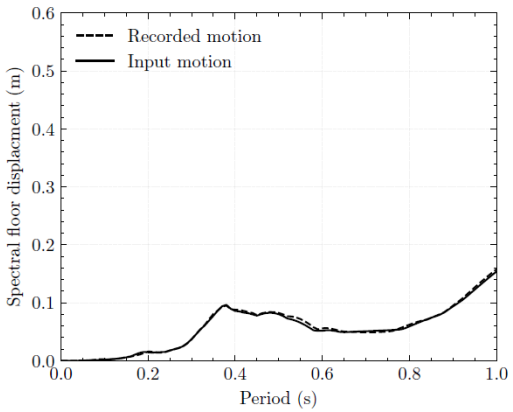

b) PGV = 50 cm/s

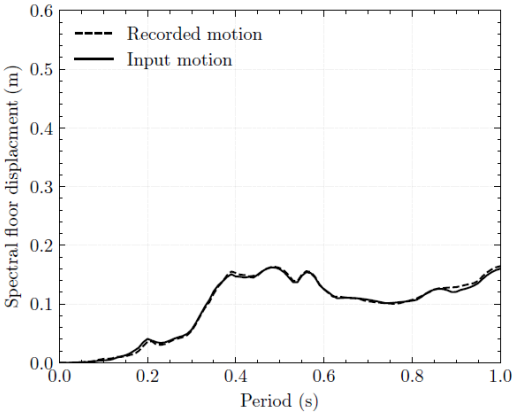

c) PGV = 100 cm/s

Figure 3.23. Spectral floor displacements for 1.0 % design level structure at different peak ground velocities (PGVs) from Table 3.1 (Pledger, 2026)

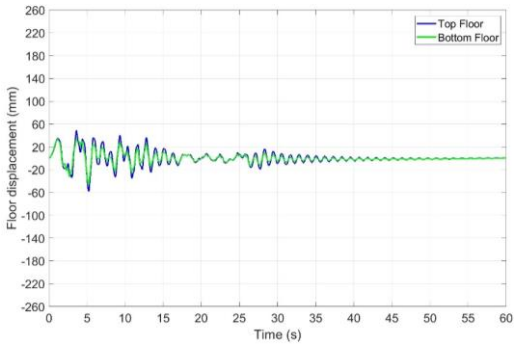

a) Motion 5

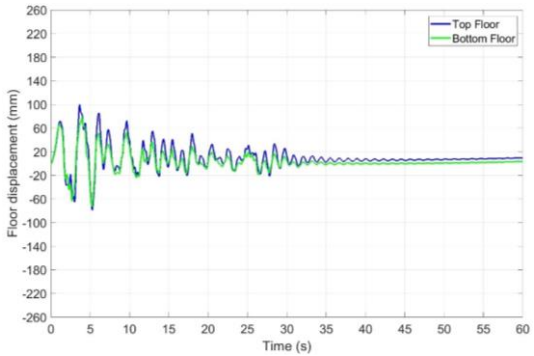

b) Motion 10

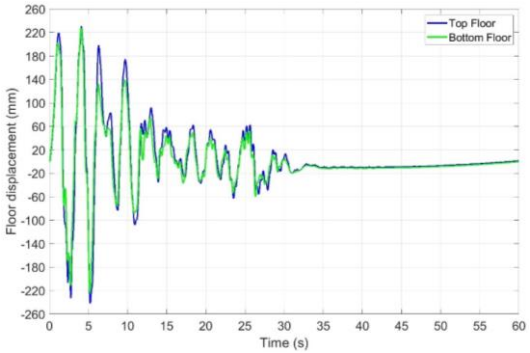

c) Motion 14

Figure 3.24. Floor displacement command time histories of top and bottom slabs during different scaled motions from Table 3.1

Instrumentation

Instrumentation of the structure

The test structure was instrumented with accelerometers placed on the top slab and beneath the bottom slab to record accelerations in the loading direction, i.e., the North–South (NS or X) axis. The accelerometer locations are illustrated in Figure 3.25 and Figure 3.26. The structure was further instrumented with Motion Capture (MoCap) target points (reflective markers) to measure deformations. Five MoCap cameras, positioned facing the east elevation of the test setup, recorded the response during the applied motions.

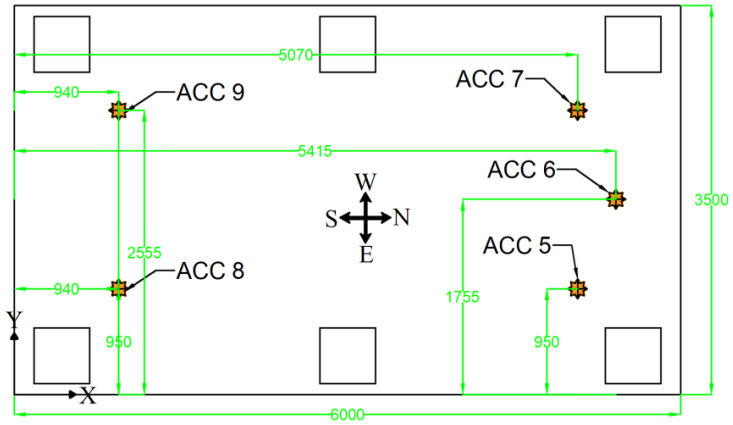

Figure 3.25. Location of accelerometers on top slab (dimensions in mm)

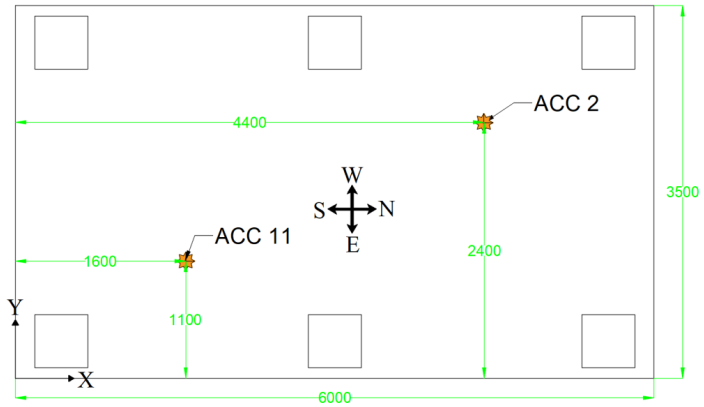

Figure 3.26. Location of accelerometers underneath the bottom slab (dimensions in mm)

Instrumentation of the specimens

The specimens were instrumented using displacement potentiometers, accelerometers and Motion Capture Camera reflectors at key locations as illustrated in Figure 3.27 through Figure 3.31. Go-Pro cameras were also installed in the ceiling plenum.

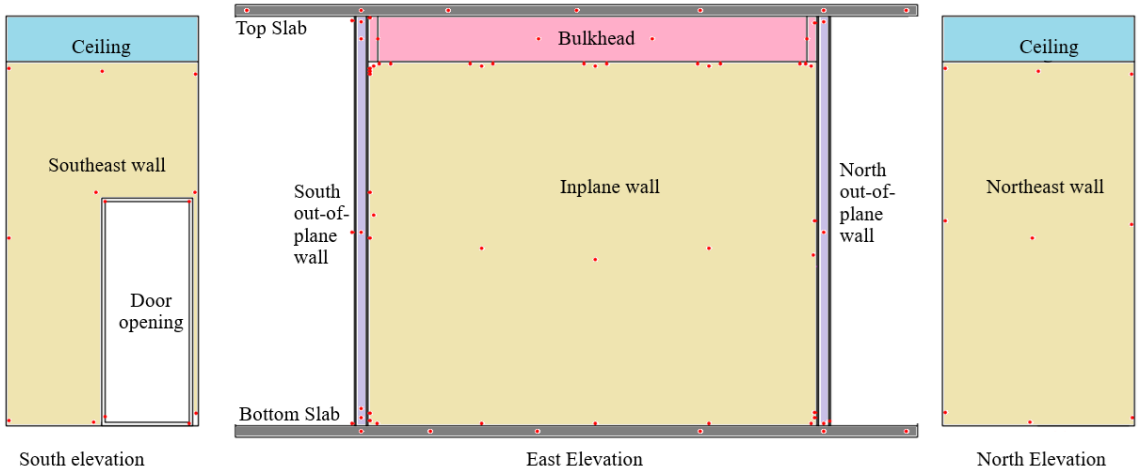

Figure 3.27. Motion Capture (MoCap) target (reflector) points to record the deformation of the test structure and wall and ceiling specimens

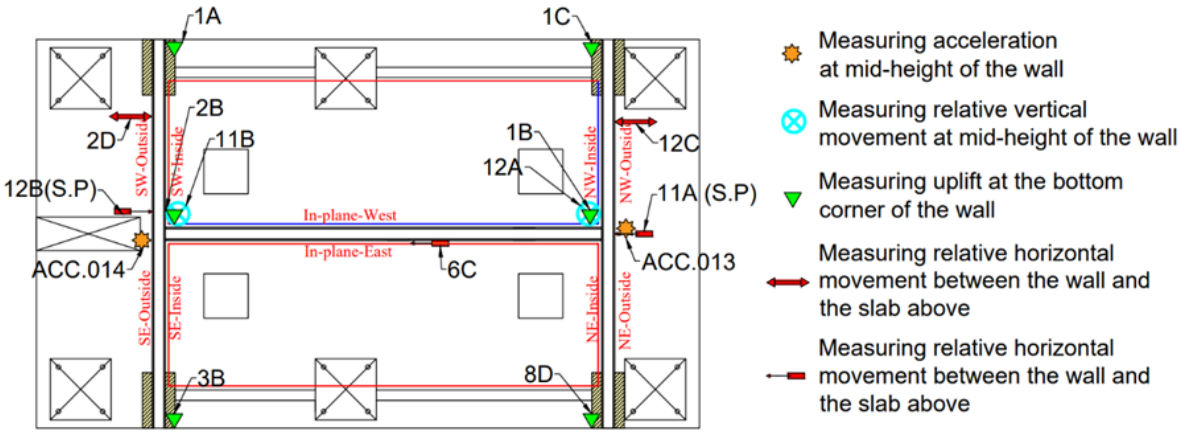

Figure 3.28. Instrumentation plan for walls (Part 1)

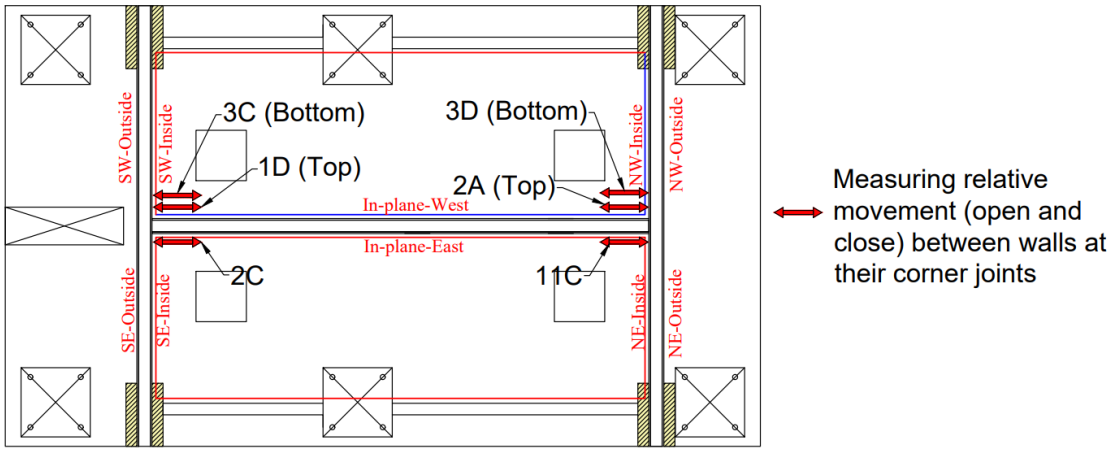

Figure 3.29. Instrumentation plan for walls (Part 2)

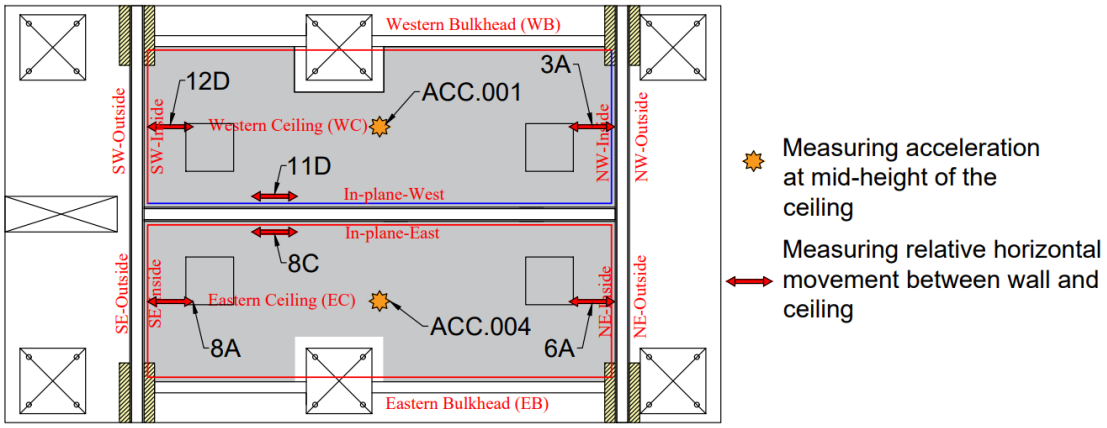

Figure 3.30. Instrumentation plan for ceilings

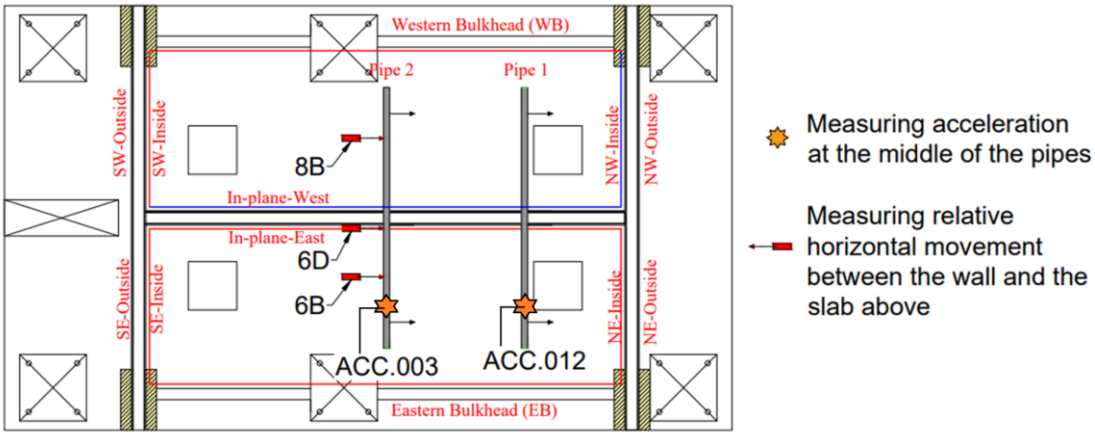

Figure 3.31. Instrumentation plan for pipes

Data processing

The recorded acceleration data were filtered to remove noise. A 4th-order low-pass Butterworth filter (Butterworth, 1930; Parks & Burrus, 1987; Sorrentino, 2007) with a cutoff frequency of 50 Hz was applied, using a sampling frequency of 180 Hz. The 50 Hz cutoff was selected to capture local high-frequency responses of the specimens. Furthermore, to address instantaneous impulse peaks in the acceleration readings, a 4th-order 1-dimensional median filter was employed for smoothing. This filter replaces each point with the median value within a sliding window of size 4, thereby removing impulse noise while preserving signal edges, with zero-padding applied at the ends. The displacement data were used without postprocessing.

While analysing the data from the experimental sensors, the acceleration responses recorded during Motion 0 are disregarded for both structural and component-level analyses due to their negligible magnitude. Similarly, Motion 0 data is excluded from all structural drift calculations. For component displacement analysis, the data from Motion 0 is included in the plots for completeness but is omitted from discussion, as the measured displacements are considered insignificant.

DAMAGE STATE CLASSIFICATION SCHEME

Four damage states: Superficial, Minor Repair, Moderate Repair and Critical have been defined to classify the damage observed in the test. These discrete damage states are separated based on the repair requirements and impact on the functionality of the non-structural elements.

Superficial

The Superficial damage state includes damage that is primarily aesthetic, meaning it may

not be immediately noticeable, and either does not require repair or only needs minor repair (not immediately). The damage does not impact the seismic performance and functionality of the non-structural element. Some examples include screw impressions, and hairline cracks on plasterboard linings.

Minor Repair

The Minor Repair damage state includes damage that does not immediately affect the seismic performance or functionality of the system but should be monitored and addressed during future repairs or routine maintenance. This damage state does not substantially affect the load-bearing capacity, alter the system's alignment, or compromise the non-structural element's ability to remain in place under normal conditions. In some cases, temporary measures can be adopted to limit the spread of damage to other components damage before the actual repairs occur. Some examples include cracks and crushing of plasterboard linings which compromise the fire-rating (or acoustics) of the walls.

Moderate Repair

The Moderate Repair damage state includes damage that begins to affect its intended performance, but without creating an immediate safety hazard or causing complete loss of function. The system remains largely in place and attached to the structure, posing no immediate risk of falling or obstructing egress. However, the damage requires repair to restore full performance. For example, damage to few internal frame members while the wall remains standing and fully supported by the remaining framing, but the load path has been weakened and requires repair to restore full capacity.

Critical

The Critical damage state includes damage that impairs the seismic performance and/or functionality of the system, resulting in loss of function and demanding urgent repair. Some examples include severe damage to the plasterboard linings, separation of walls at junctions and damage to frames of the walls.

EXPERIMENTAL RESULTS

Response of the test structure

Inter-storey drifts

The measured peak inter-storey drifts between the two floors, to which the wall specimens were subjected, are presented in Figure 3.32. These values were derived from actuator data. Testing continued up to a peak inter-storey drift of 2.75%, which was achieved in Test #16. Recorded floor displacement time histories from Tests #11 and #15 are provided as examples in Figure 3.33.

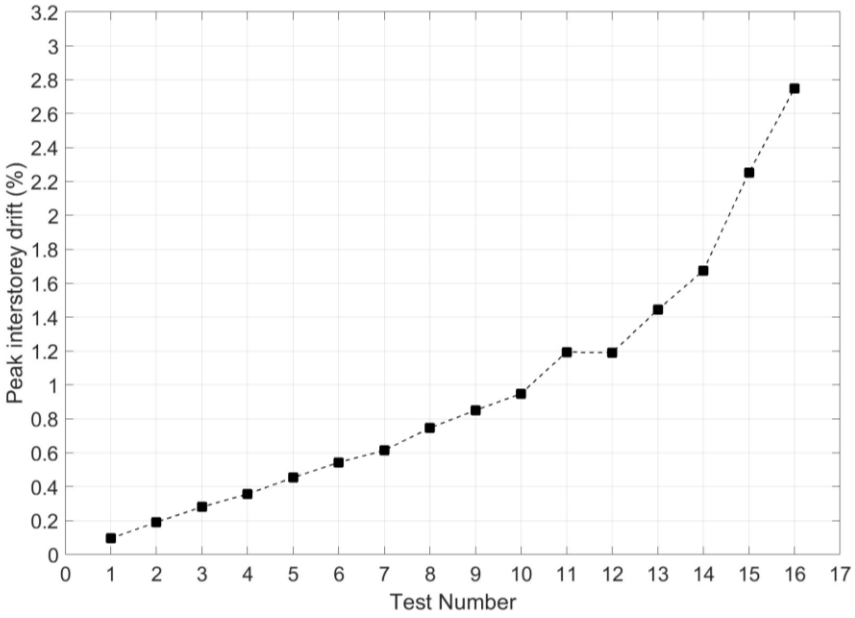

Figure 3.32 Recorded peak inter-storey drifts between floors

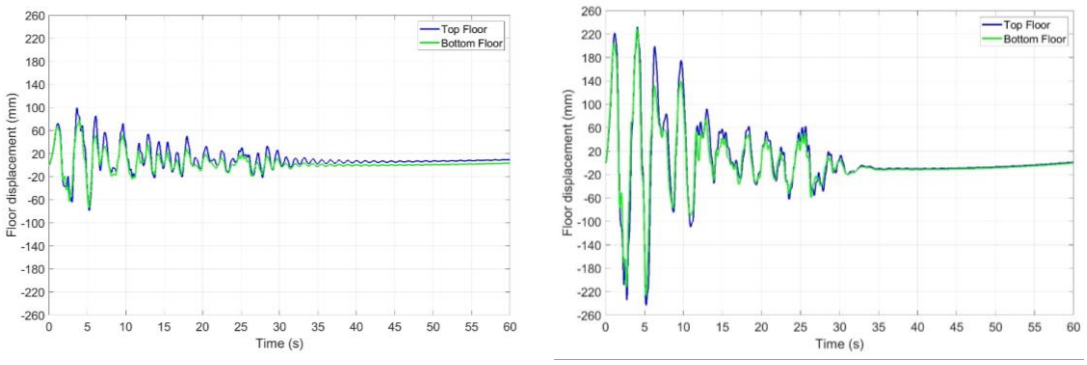

a) Test #11 b) Test #15

Figure 3.33 Recorded lateral floor displacement in the loading direction (X)

Floor accelerations

The recorded peak floor accelerations, calculated as the average of the maximum in-direction readings from all floors-mounted accelerometers after postprocessing, are presented in Figure 3.34.

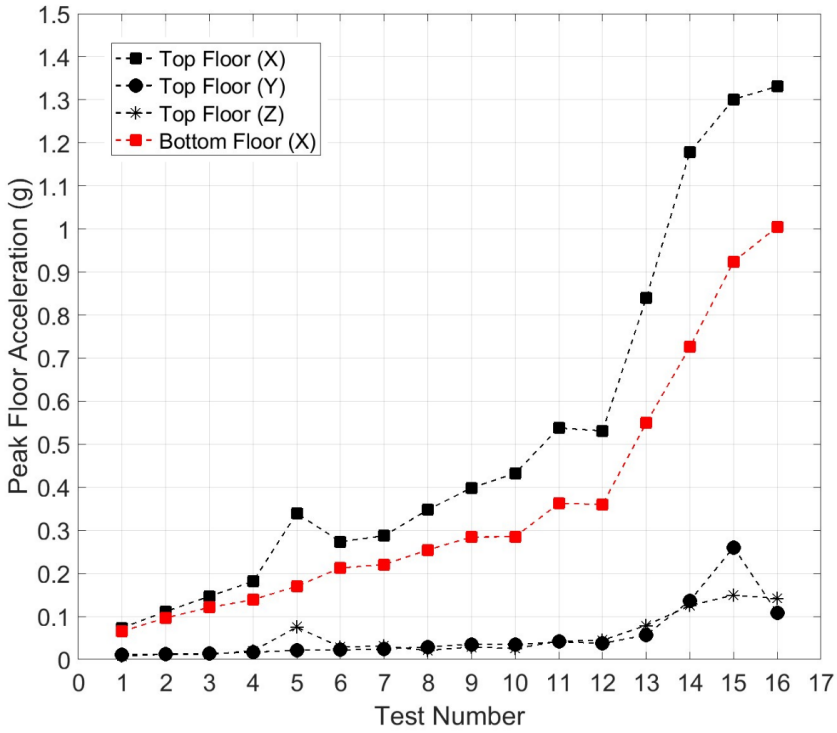

Figure 3.34 Recorded peak floor accelerations with direction shown inside brackets

The top floor consistently exhibited higher maximum horizontal acceleration than the bottom floor in the X direction (loading direction). During Test #16, the peak horizontal accelerations reached 1.33 g on the top floor and 1.00 g on the bottom floor. The acceleration time histories in the X-direction, recorded by the floor-mounted accelerometers and after postprocessing during Test #34, are shown Figure 3.35.

Lateral forces

The measured peak lateral forces, recorded by the actuators connected to the floor slabs, are presented in Figure 3.36. It can be observed that the lateral force on the bottom floor is higher than that on the top floor, which is attributed to the greater portion of the specimen's mass being transferred downward. The maximum lateral forces recorded on the bottom and top floors were 142 kN and 104 kN, respectively. The variations in the recorded forces correspond to the changes in acceleration shown in Figure 3.34.

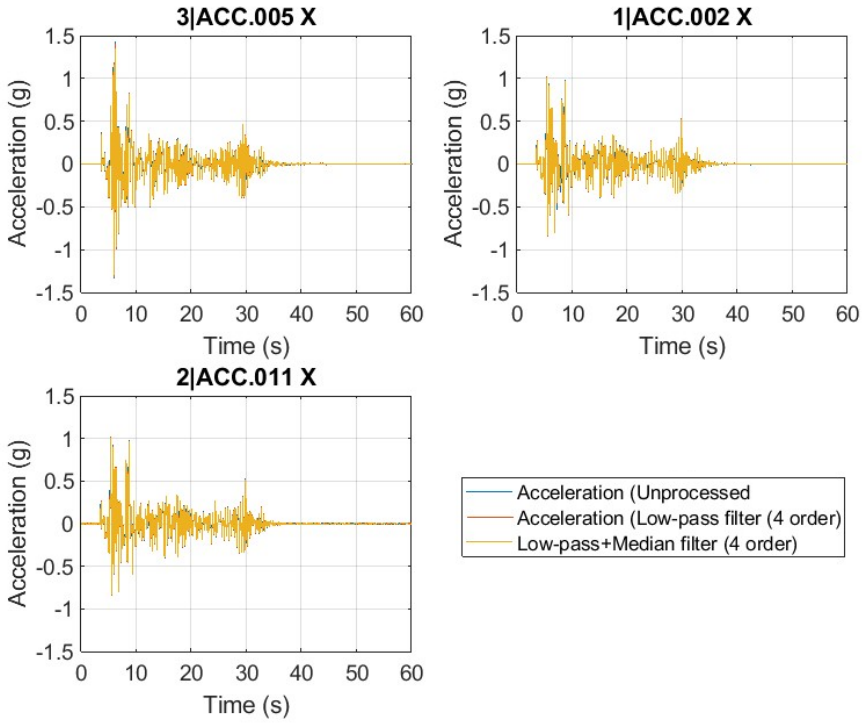

Figure 3.35 Recorded floor accelerations in X-direction (refer to Figure 3.25 and Figure 3.26 for locations of the accelerometers) during Test #16

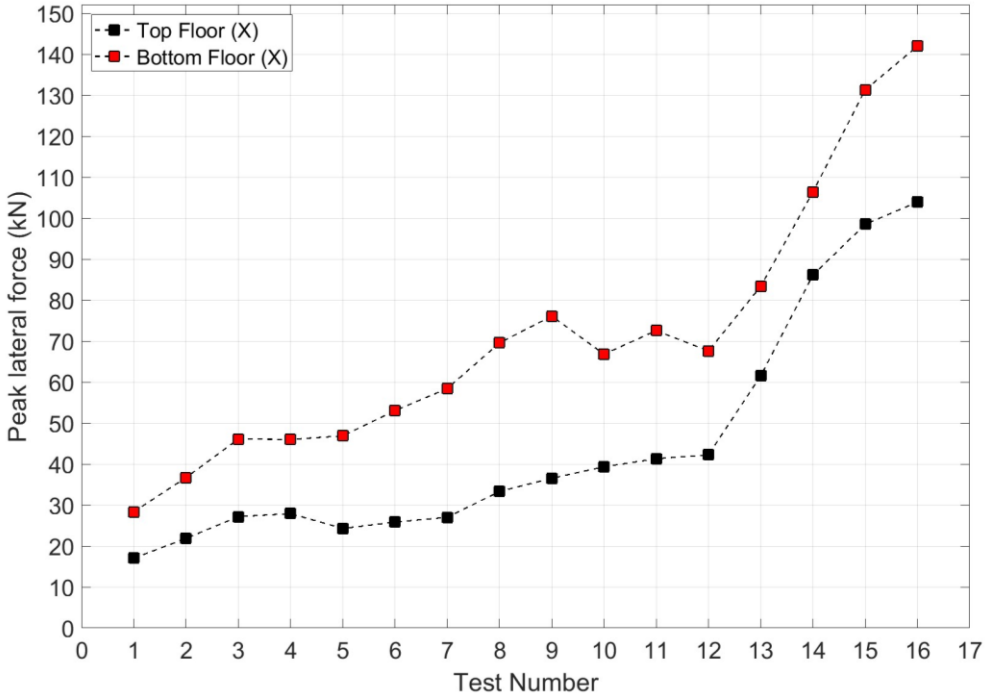

Figure 3.36 Recorded peak lateral forces on the floors

Component response

Damage observation to specimens and their damage state classification

The progression of damage throughout the experimental program is analysed and discussed using the inter-storey drift as the primary engineering demand parameter while peak floor accelerations are provided where relevant. Photographic documentation and detailed descriptions of the damage observed in the specimens during testing, along with the corresponding inter-storey drift and peak floor acceleration levels at which each damage occurred, are provided in Table 3.4 through Table 3.14 in **APPENDIX** B**.** Table 3.3 documents the observed damage and its damage state classification for the tested specimens.

Table 3.3. Damage state of the tested specimen and corresponding inter-story drifts after which the damage was observed

Specimen	Damage State	Damage Type	Inter-story drift (%)	Peak Floor Accelerations (g)	Comment/Reference
Timber-framed partition wall	Superficial	Hairline crack in the plasterboard at wall junctions	NA	NA	The presence of abundant pre-existing hairline cracks at the wall junctions made it challenging to determine the specific demand at which such cracking initially occurred during the tests.
	Minor Repair	Crack in the plasterboard (likely to reduce the fire rating)	1.19	Top: 0.54 g Bottom: 0.36 g	Table 3.10
	Moderate Repair	Separation of the steel multi-grip strap connecting the timber plates in the in-plane and out-of-plane walls.	1.44	Top: 0.84 g Bottom: 0.55 g	Table 3.11
	Critical	Separation of walls at wall junctions	1.67	Top: 1.18 g Bottom: 0.72 g	Table 3.12
Concealed Plasterboard Ceiling	Superficial	Crack and flacking of the paper tape at the interface of wall to ceiling	0.54	Top: 0.27 g	Table 3.5
		Crack and Screw impressions on the plasterboard lining of the ceiling	0.95	Top: 0.43 g	Table 3.5
	Minor Repair	Partial Detachment in the wall track	1.19	Top: 0.54 g	Table 3.10
		Separation between ceiling and wall	1.19	Top: 0.54 g	Table 3.10
	Moderate Repair	Crumpling at the end of the furring channel	1.44	Top: 0.84 g	Table 3.11
		Detachment in the wall track	1.44	Top: 0.84 g	Table 3.11
Mechanical Pipes (without bracing) *	Superficial	Minor separation between sealant and pipe (unlikely to compromise fire-rating performance)	0.95	Top: 0.43 g	Table 3.9
	Minor Repair	Moderate Separation (Likely reduced Fire-Rating)	1.44	Top: 0.84 g	Table 3.11
	Moderate repair	Major Separation	1.67	Top: 1.18 g	Table 3.12
* Due to the poor quality of the initial sealant application at the pipe penetration location through the in-plane wall, the observed damage progression may not be representative of a properly installed system in practice.					

Timber-framed walls

The damage progression in the timber-framed walls, quantified by inter-storey drift, followed a sequence of increasing severity. Initial hairline cracks at the wall junctions were abundantly present before testing began, making it impossible to attribute their initiation to a specific drift demand. The first identifiable new damage, a crack in the plasterboard likely to compromise fire rating, occurred at a drift of 1.19%. The damage then advanced with the separation of the steel multi-grip strap connecting the timber plates of the in-plane and out-of-plane walls at 1.44% drift. This was followed by a major plasterboard joint separation at the junction at 1.67% drift. Finally, at a drift of 2.75%, a significant increase in the width of the wall joint separations was observed, marking the most severe visible damage.

Concealed Plasterboard Ceiling

The ceiling system exhibited a clear progression of damage with increasing inter-story drift. The first observed damage was the cracking and flaking of the paper tape at the wall-to-ceiling interface, occurring at a drift of 0.54% under a peak floor acceleration (PFA) of 0.27 g at the top level. At 0.95% drift (PFA: 0.43 g), cracks and screw impressions appeared on the plasterboard. A significant increase in damage occurred at 1.19% drift (PFA: 0.54 g), marked by partial detachment of the wall track and a visible separation between the ceiling and the wall. The damage intensified further at 1.44% drift (PFA: 0.84 g), with observations of crumpling at the ends of the furring channels and detachment of the wall track.

Although the screw connections to the wall angles are designed to resist forces from the ceiling's mass and acceleration, the progression of damage appears to be governed more by the deformations occurring in the supporting walls. In the ceiling with

typical construction, damage to ceiling components was more concentrated and severe near the wall junction (where fixed and floating edges meet, and where two floating edges meet) compared to damage at the restrained wall ends. In contrast, damage in the all-fixed ceiling was more uniformly distributed across the system.

Mechanical Pipe

Due to the poor quality of the initial sealant application at the pipe penetration location through the in-plane wall, the observed damage progression may not be representative of a properly installed system in practice. Nevertheless, the results are briefly summarized. The pipe penetration seals showed a clear degradation pattern. A minor separation between the sealant and the pipe, unlikely to compromise fire-rating performance, was first observed at 0.95% inter-story drift under a peak floor acceleration of 0.43 g at the top level. This progressed to a moderate separation, which likely compromised the fire-rating, at 1.44% drift (PFA: 0.84 g). Finally, a major separation between the sealant and pipe occurred at 1.67% drift (PFA: 1.18 g).

Peak component accelerations and dynamic amplification factors

The recorded peak component accelerations (PCAs) for the tested wall, ceiling, and pipe specimens are briefly discussed in the following analysis. These PCA values are compared with the peak floor accelerations (PFA) at the corresponding attachment levels. From this comparison, the PCA/PFA ratios, or dynamic amplification factors, are derived from the experimental data and subsequently evaluated against the provisions of SNZ TS 1170.5, 2025) and ASCE/SEI 7-22 (2022).

It is important to note that while the accelerations were recorded on specific components, these elements interacted dynamically during testing. Consequently, the

measured PCA values, although attributed to a particular specimen, were likely influenced by the behaviour of adjacent and connected elements. The authors contend that this interaction realistically represents conditions in an actual building, where various non-structural elements do not respond in isolation but as part of a coupled system (unless absolutely detached).

Timber-framed wall specimen

The peak component accelerations (PCA) recorded in the out-of-plane (X) direction at the mid-height of the wall junctions (ACC.014, ACC.013) are plotted against the average of the peak floor accelerations of both floors (PFA) for all 16 tests in Figure 3.37. Accelerometer locations are shown in Figure 3.25, Figure 3.26, Figure 3.28, and Figure 3.29.

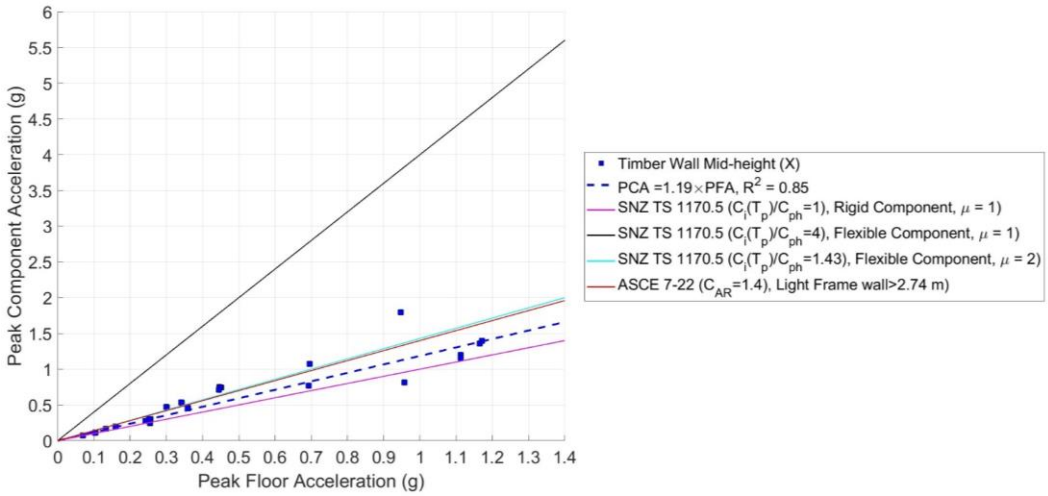

Figure 3.37 Peak accelerations of wall specimens in out-of-plane direction (X) as a function of peak floor acceleration

Figure 3.37 also presents PCA values calculated by multiplying the average PFA from both top and bottom floors by: (1) the ratio $C_i(T_p)/C_{ph}$ for different ductility levels (μ), per SNZ TS 1170.5 (2025), and (2) the Component Resonance Ductility Factor (C_{AR})

from ASCE/SEI 7-22 (2022). $C_i(T_p)$ is the component spectral-shape coefficient and (C_{ph}) is the component horizontal-response factor. Additionally, a linear fit through the origin is plotted against the experimental data points.

Figure 3.37 indicates that the PCA/PFA ratio (i.e., Dynamic Amplification Factors (DAF) inclusive of part ductility (μ)) for the timber-framed walls, as determined by the best-fit line through the origin, is approximately 1.19 with $R^2 = 0.85$. According to SNZ TS 1170.5 (2025), this experimental ratio corresponds to the design cases for a Flexible component with ductility ($2 < \mu < 2.5$). The standard's provision for a Flexible component with $\mu = 2$ provides a conservative estimate, exceeding the measured ratio by a factor of 1.20. A similarly conservative estimate is given by ASCE/SEI 7-22 (2022), with a factor of 1.18.

Figure 3.38 plots the PCA/PFA ratio for the walls, calculated by dividing the PCA by the average PFA of both floors. The box plot in Figure 3.38 (c) shows a median PCA/PFA value of 1.22 for timber-framed walls which is conservatively estimated by the by SNZ TS 1170.5 (2025) for Flexible component with $\mu = 2$ (1.43) and ASCE/SEI 7-22 (2022) (1.40).

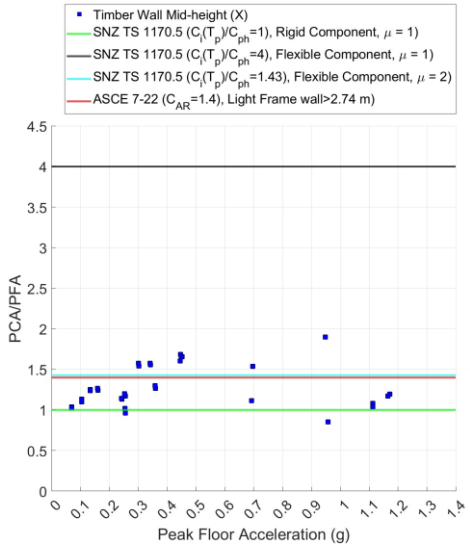

a) PCA/PFA as a function of PFA

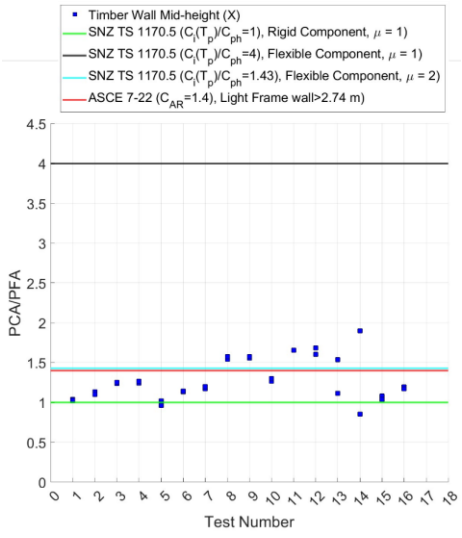

b) PCA/PFA as a function of Test number

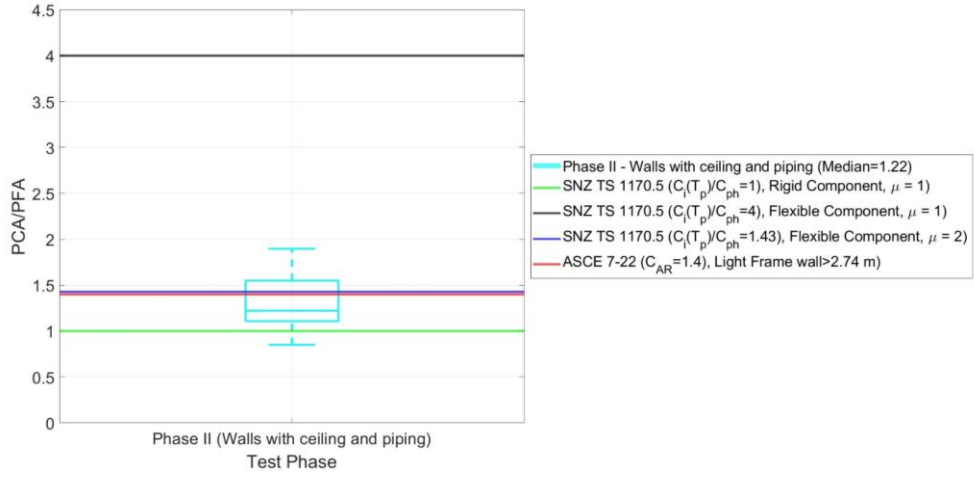

c) PCA/PFA box plot (Median = 1.22)

Figure 3.38 PCA/PFA in the out-of-plane direction (X) for timber-framed walls

Perimeter-restrained concealed plasterboard ceiling

The peak component accelerations (PCA) recorded in the loading (X) direction located approximately at the geometric centre of the ceilings (attached to the plasterboard) (ACC.001, ACC.004) are plotted against the peak floor acceleration of top floor (PFA) to which the ceiling is connected to for all 16 tests in Figure 3.39. Accelerometer locations are shown in Figure 3.25 and Figure 3.30.

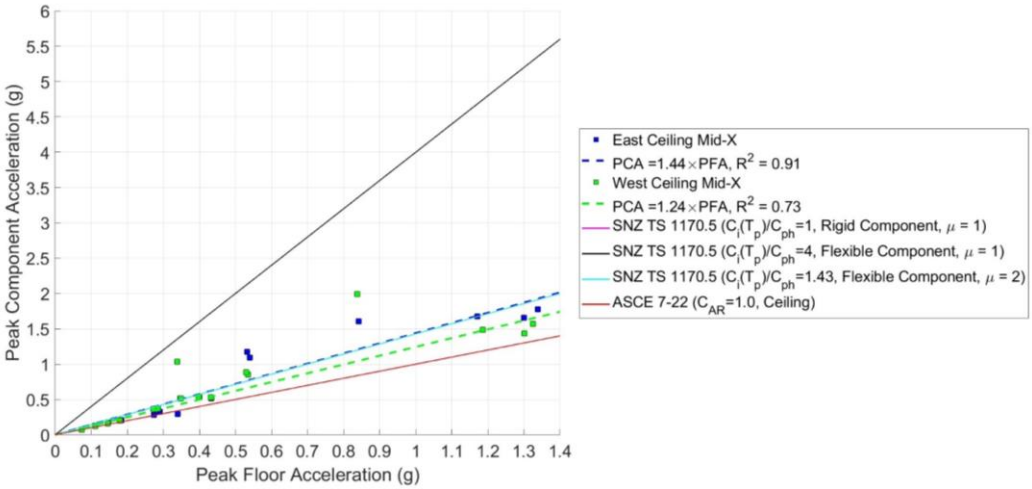

Figure 3.39 Peak accelerations of perimeter restrained concealed plasterboard ceiling specimens in loading direction (X) as a function of peak floor acceleration

Figure 3.39 also presents PCA values calculated by multiplying the PFA from the top floor by: (1) the ratio $C_i(T_p)/C_{ph}$ for different ductility levels (μ), per SNZ TS 1170.5 (2025), and (2) the Component Resonance Ductility Factor (C_{AR}) from ASCE/SEI 7-22 (2022). $C_i(T_p)$ is the component spectral-shape coefficient and (C_{ph}) is the component horizontal-response factor. Additionally, a linear fit through the origin is plotted against the experimental data points.

The experimental data plots of PCA as a function of PFA for both the East and West ceiling specimens were merged to derive a single, representative linear fit for PCA as a function of PFA as shown in Figure 3.40.

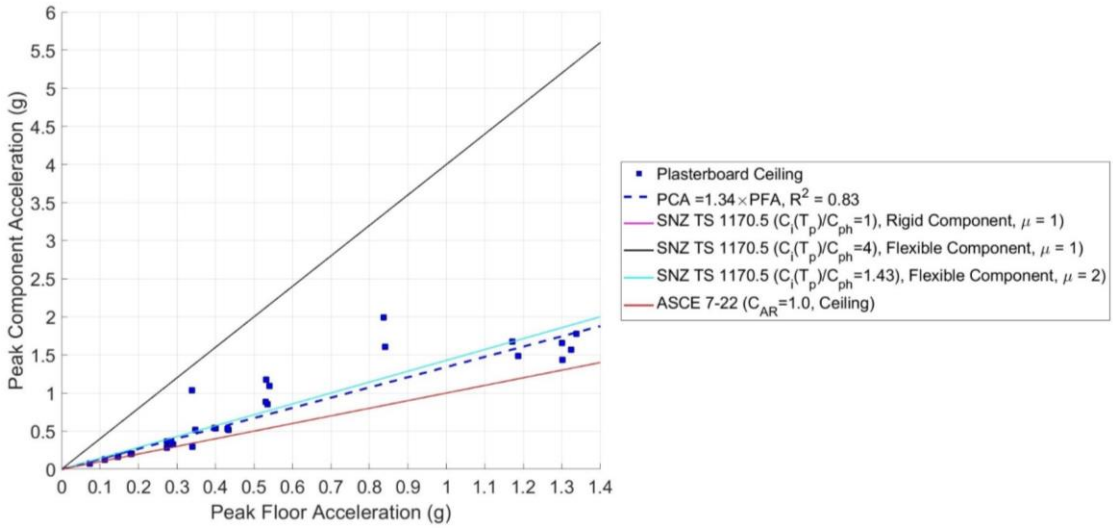

Figure 3.40 Peak accelerations of perimeter restrained concealed plasterboard ceiling specimen in loading direction (X) as a function of peak floor acceleration

Figure 3.40 indicates that the PCA/PFA ratio (i.e., Dynamic Amplification Factors (DAF) inclusive of part ductility (μ)) for the concealed plasterboard, as determined by the best-fit line through the origin, is approximately 1.34 with $R^2 = 0.83$. According to SNZ TS 1170.5 (2025), this experimental ratio corresponds to the design cases for a Flexible component with ductility ($2 < \mu < 2.5$). The standard's provision for a Flexible component with $\mu = 2$ provides a conservative estimate, exceeding the

measured ratio by a factor of 1.07. However, ASCE/SEI 7-22 (2022) recommends a factor of 1.0 for ceilings which is unconservative as compared to the experimental value of 1.34.

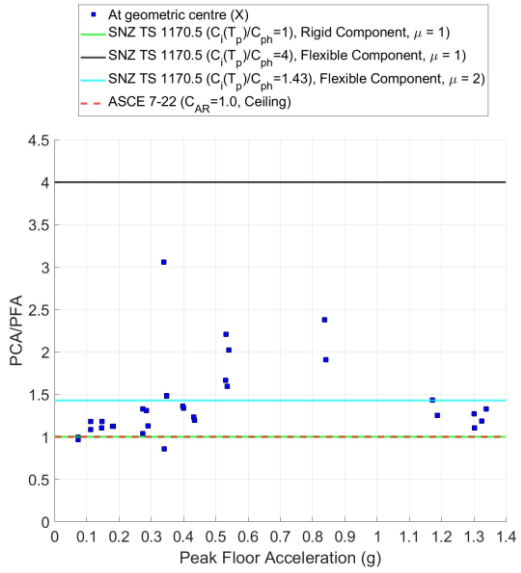

a) PCA/PFA as a function of PFA

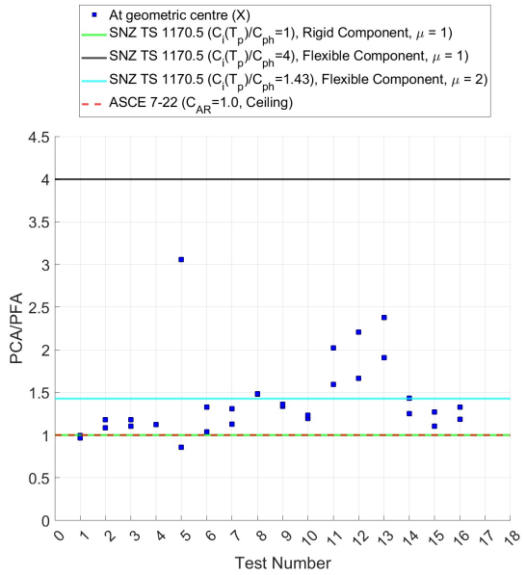

b) PCA/PFA as a function of Test number

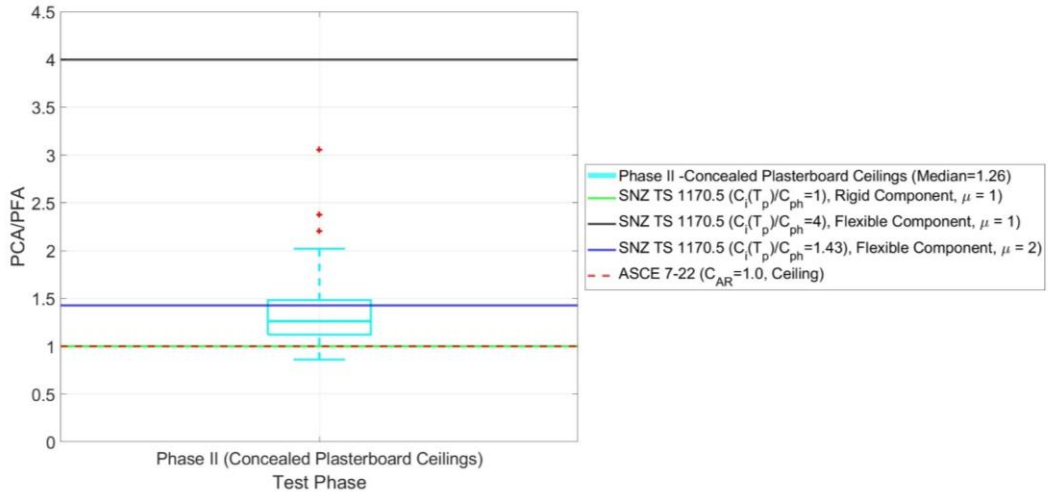

c) PCA/PFA box plot (Median = 1.26)

Figure 3.41 PCA/PFA in the loading direction (X) for perimeter restrained concealed plasterboard ceilings

Figure 3.41 plots the PCA/PFA ratio for the concealed plasterboard ceilings, calculated by dividing the PCA by the PFA of the top floor. The box plot in Figure 3.41 (c) shows a median PCA/PFA value of 1.26 for perimeter restrained concealed

plasterboard ceilings. The SNZ TS 1170.5 (2025), provision for a Flexible component with μ=2 provides a conservative estimate, exceeding the measured ratio by a factor of 1.13. However, ASCE/SEI 7-22 (2022) recommends a factor of 1.0 for ceilings which is unconservative as compared to the experimental median value of 1.26.

The experimental median PCA/PFA ratio for the ceilings (1.26) is comparable to that of the walls (1.22). This similarity suggests that, when ceilings are connected to walls, their accelerations during seismic shaking can be significantly influenced by the dynamic response of the walls to which they are attached.

Mechanical Pipes

The peak component accelerations (PCA) recorded in the transverse direction of the pipe's orientation (X) direction located approximately at the hanger location (attached to the pipes) (ACC.003, ACC.012) are plotted against the peak floor acceleration of top floor (PFA) to which the ceiling is connected to for all 16 tests in Figure 3.42. Accelerometer locations are shown in Figure 3.25 and Figure 3.31.

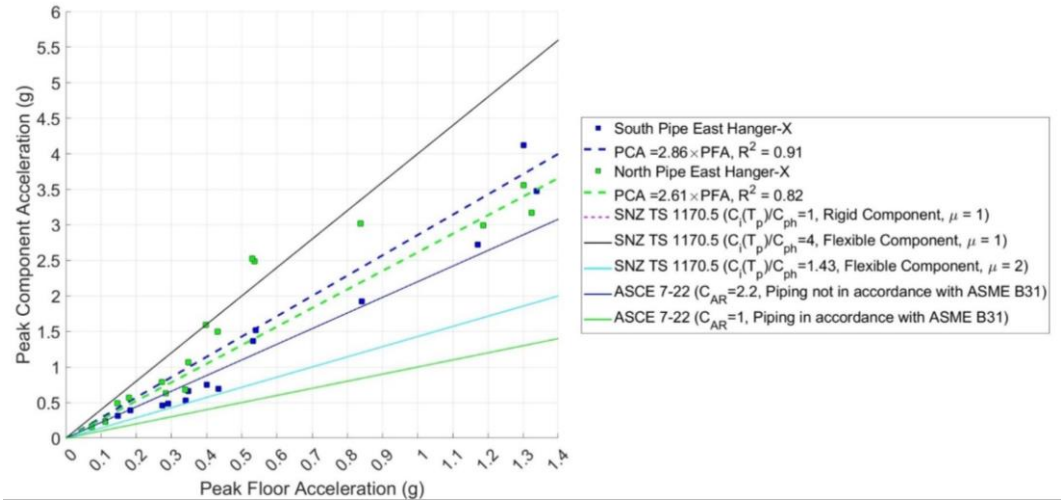

Figure 3.42 Peak accelerations of unbraced mechanical pipes specimens in the transverse direction of the pipe's orientation (X) as a function of peak floor acceleration

Figure 3.42 also presents PCA values calculated by multiplying the PFA from the top floor by: (1) the ratio $C_i(T_p)/C_{ph}$ for different ductility levels (μ), per SNZ TS 1170.5 (2025), and (2) the Component Resonance Ductility Factor (C_{AR}) from ASCE/SEI 7-22 (2022). $C_i(T_p)$ is the component spectral-shape coefficient and (C_{ph}) is the component horizontal-response factor. Additionally, a linear fit through the origin is plotted against the experimental data points.

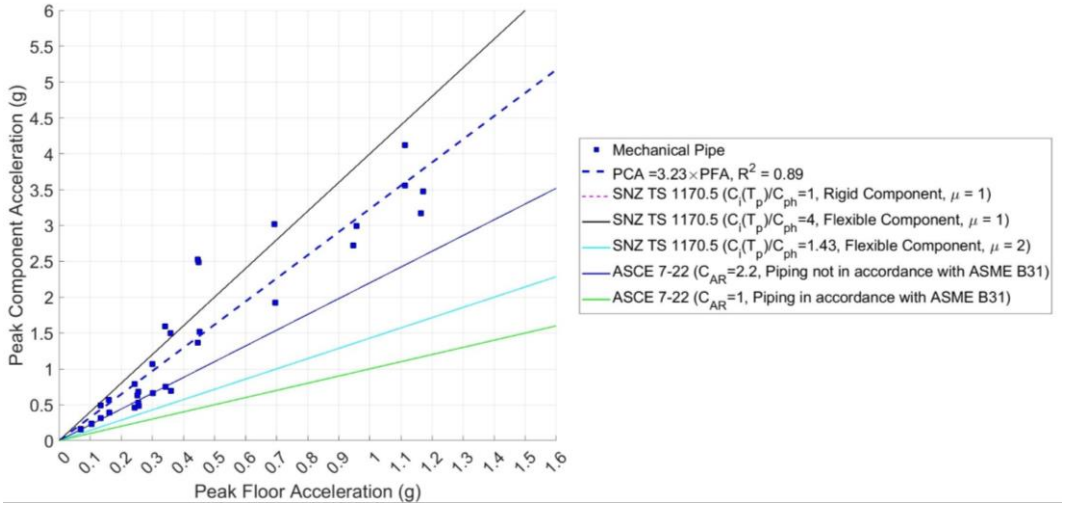

Figure 3.43 Peak accelerations of unbraced mechanical pipes specimens in the transverse direction of the pipe's orientation (X) as a function of peak floor acceleration

Figure 3.43 indicates that the PCA/PFA ratio (i.e., Dynamic Amplification Factors (DAF) inclusive of part ductility (μ)) for the unbraced mechanical pipes, as determined by the best-fit line through the origin, is approximately 3.23 with $R^2 = 0.89$. According to SNZ TS 1170.5 (2025), this experimental ratio corresponds to the design cases for a Flexible component with ductility ($1 < \mu < 2$). The standard's provision for a Flexible component with $\mu = 1$ provides a conservative estimate, exceeding the measured ratio by a factor of 1.24. However, ASCE/SEI 7-22 (2022) recommends a factor of 2.20 for pipes which is unconservative as compared to the experimental value of 3.23.

Figure 3.44 plots the PCA/PFA ratio for the unbraced mechanical pipes, calculated by dividing the PCA by the PFA of the top floor. The box plot Figure 3.44 (c)

shows a median PCA/PFA value of 2.36 for unbraced mechanical pipes. The SNZ TS 1170.5 (2025), provision for a Flexible component with μ=1.25 (not shown in Figure 3.44) provides a conservative estimate, exceeding the measured ratio by a factor of 1.21. However, ASCE/SEI 7-22 (2022) recommends a factor of 2.20 for mechanical pipes which is comparable to the experimental median value of 2.36.

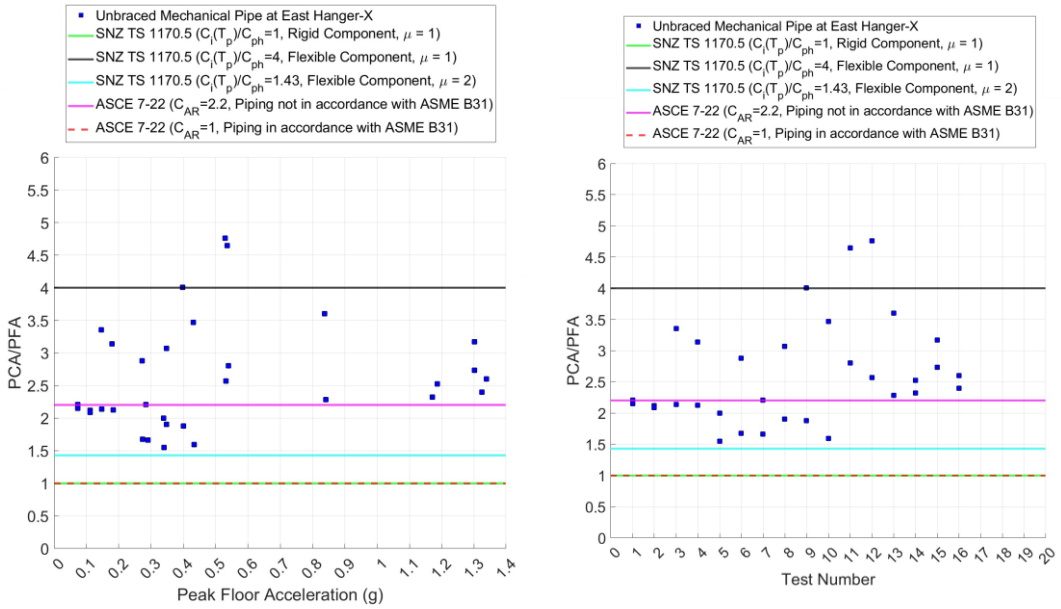

a) PCA/PFA as a function of PFA

b) PCA/PFA as a function of Test number

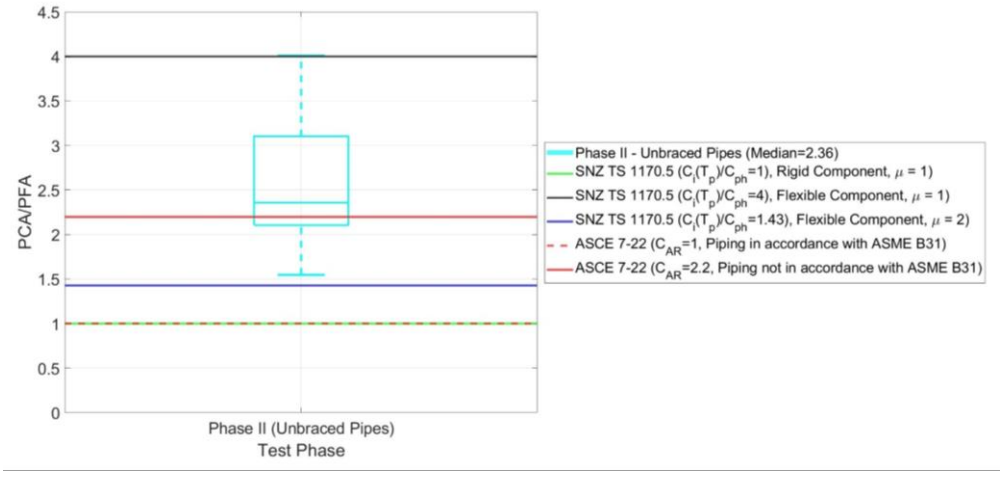

c) PCA/PFA box plot (Median = 2.36)

Figure 3.44 PCA/PFA for unbraced mechanical pipes specimens in the transverse direction of the pipe's orientation (X)

Displacement analysis

Timber-framed Walls

As illustrated in Figure 3.45 (a), the wall displayed the expected in-plane sliding, with measured displacements closely matching the estimated values (calculated as the drift ratio multiplied by the 3550 mm wall height) up to a drift of 1.67%.

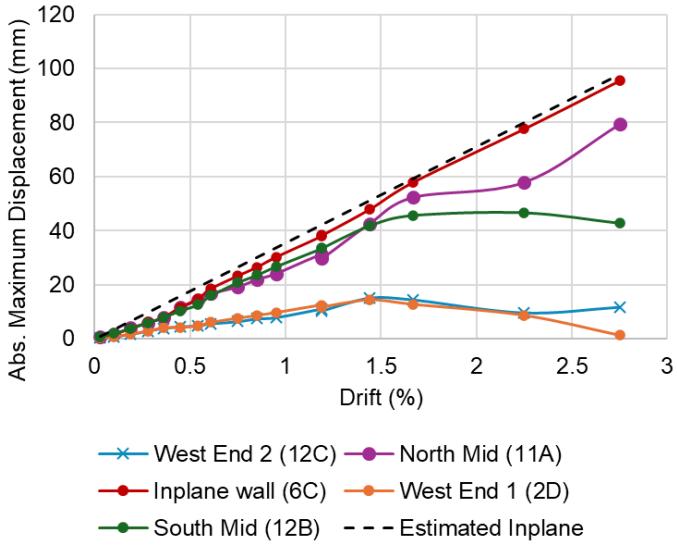

a) Absolute maximum displacements

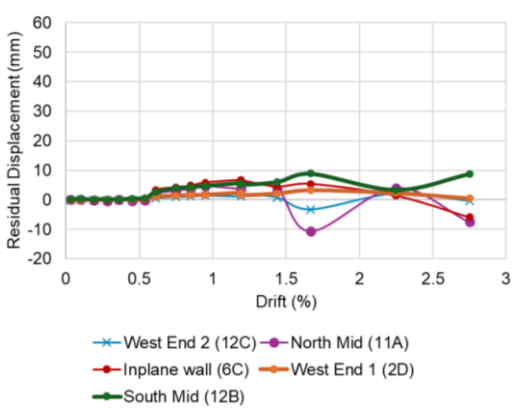

b) Residual displacements

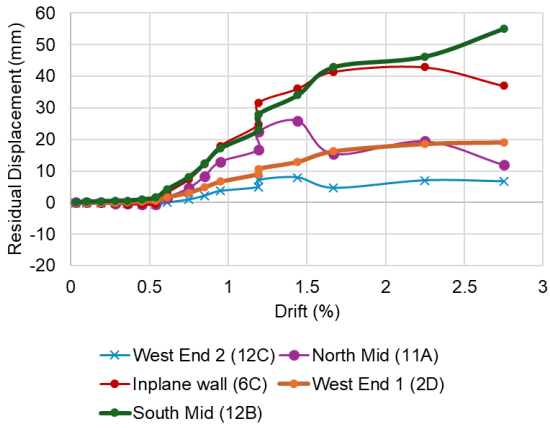

c) Cumulative residual displacements

Figure 3.45 Lateral displacement measurements for timber-framed wall specimen (approximate measurement locations shown and instrument numbers in brackets)

Throughout this phase, the West Ends of the out-of-plane walls remained largely fixed in place because of the timber restraints. This response indicates that the out-of-plane wall curved at its junction, generating an out-of-plane displacement of approximately 60 mm at that location at 1.67 % drift. Notably, the maximum displacement measurements at these junctions (in the out-of-plane direction) begin to deviate from the expected in-plane displacement relative to the top slab, signalling the onset of differential movement between the in-plane and out-of-plane walls at their connections at junctions.

Figure 3.45 (b) shows that residual displacements in the walls initiated at 0.54% drift, with the maximum residual reaching about 10 mm at 1.67% drift. The progression of cumulative damage is captured in Figure 3.45(c), which plots the cumulative residual displacements. This measure reached roughly 20 mm in both the out-of-plane walls at the junction and the in-plane wall by 1.19% drift and increased significantly to approximately 55 mm by 2.75% drift.

The opening and closing behaviour of the wall junctions during testing is presented in Figure 3.46. Figure 3.46 (a) shows that the top of the junctions between the in-plane and out-of-plane walls began opening at approximately 0.45% drift, while the bottom of the junctions remained largely intact until about 2.25% drift. It should be noted that some instruments reached their measurement capacity and were removed during the tests. As shown in Figure 3.46 (b), the residual displacement at the junction openings was below 2.50 mm for each test at 1.44% drift. However, the cumulative residual displacement at these openings reached approximately 6 mm by the same drift level as shown in Figure 3.46 (c).

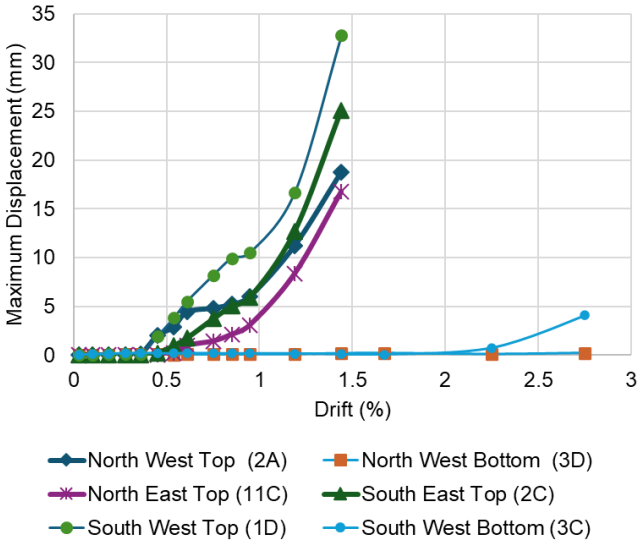

a) Maximum joint opening displacements

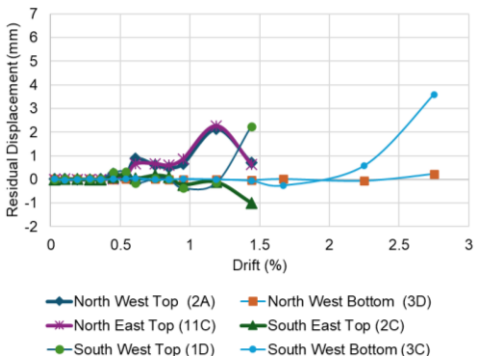

b) Residual displacements

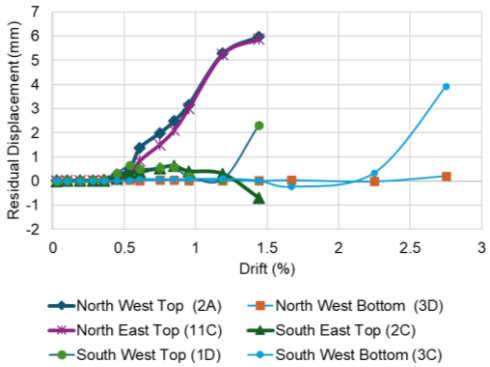

c) Cumulative residual displacements

Figure 3.46 Opening and closing measurements of wall junctions of timber-framed wall specimen (approximate measurement locations shown and instrument numbers in brackets)

Figure 3.47 (a) details the vertical movement observed during the tests. It indicates no significant wall uplifts at the wall ends, with a maximum uplift of only about 3 mm recorded at 2.75% drift. In contrast, a notable relative vertical displacement occurred at the wall junctions, initiating at 1.19% drift and increasing to approximately 7.5 mm by 2.75% drift. The corresponding residual displacements from this vertical movement remained minimal, as shown in Figure 3.47 (b) and (c).

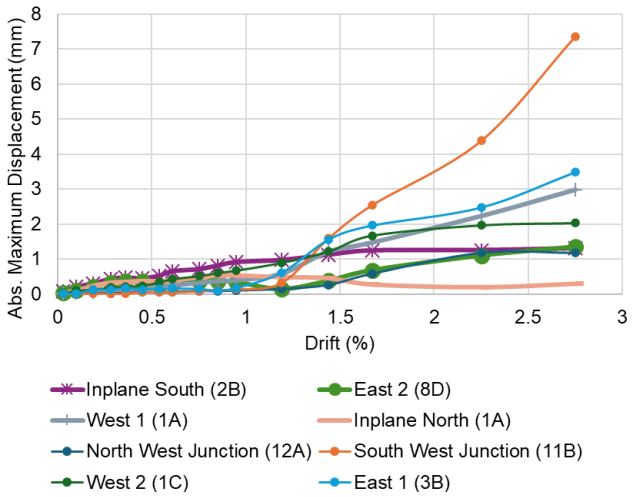

a) Absolute maximum uplift displacements

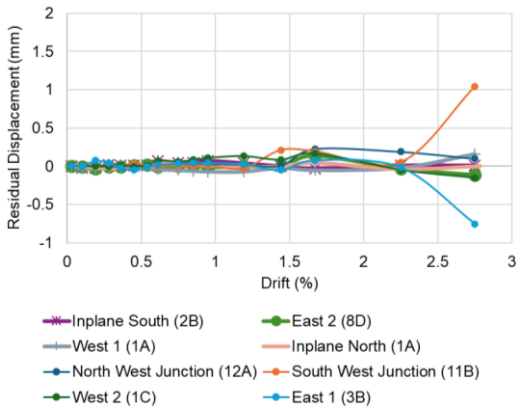

b) Residual displacements

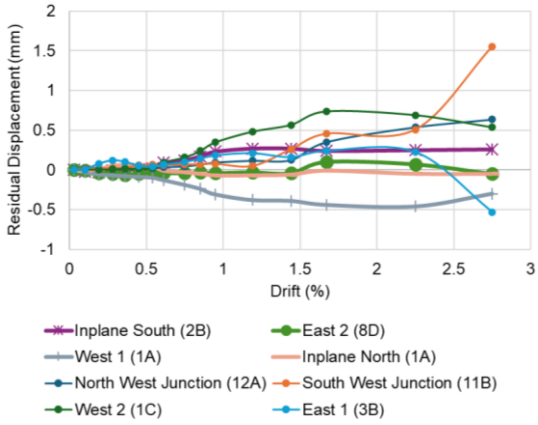

c) Cumulative residual displacements

Figure 3.47 Vertical displacement measurements for wall specimens with indicative measurement location and measuring instrument number shown in brackets.

Perimeter-restrained ceilings

As discussed in the specimen description above, the West ceiling represents a typical perimeter-restrained configuration, with fixed joints on two adjacent edges and floating joints on the other two edges where it connects to walls and bulkheads. The East ceiling, in contrast, has all its edges essentially fixed to the surrounding walls and bulkheads.

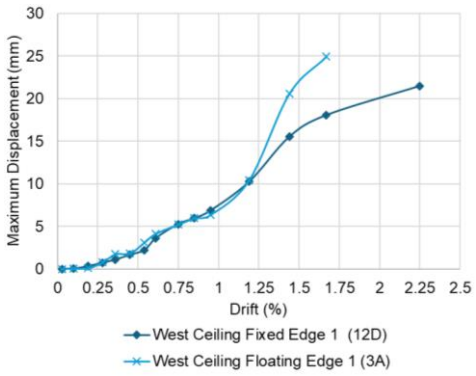

a) Maximum opening displacements of West Ceiling

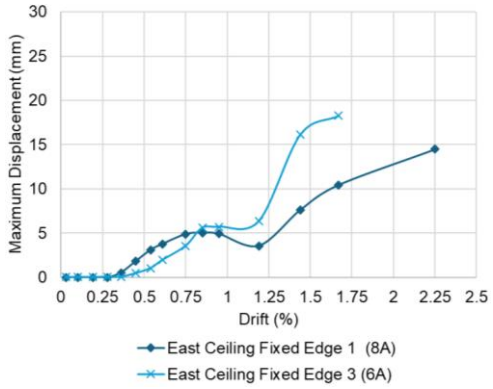

b) Maximum opening displacements of East Ceiling

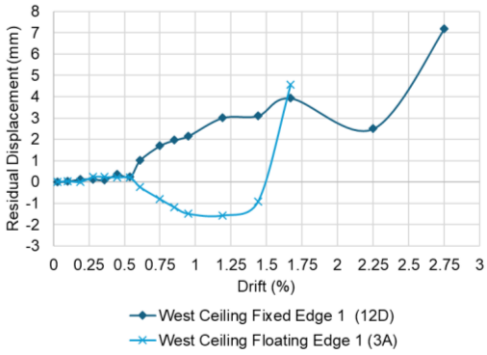

c) Residual displacements of West Ceiling

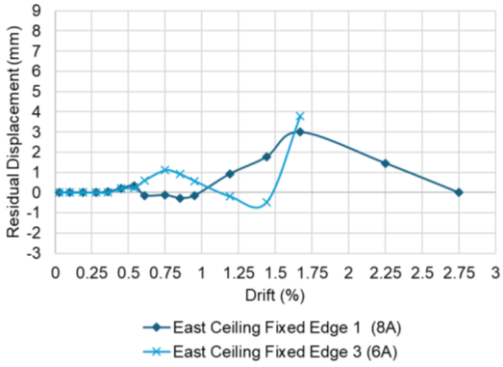

d) Residual displacements of East Ceiling

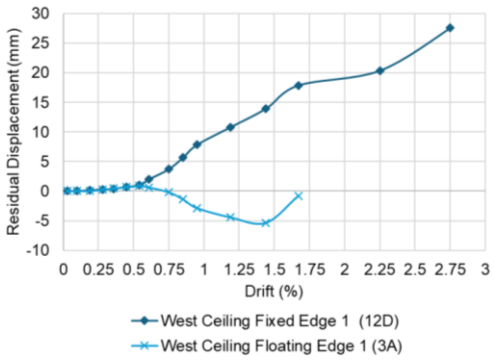

e) Cumulative residual displacements of West Ceiling

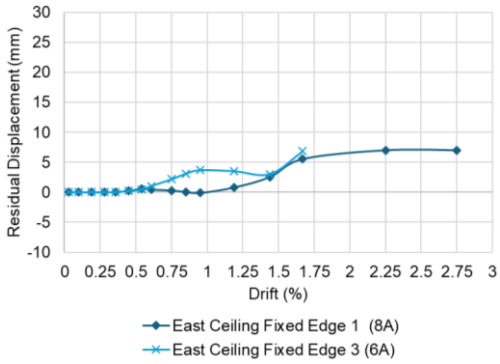

f) Cumulative residual displacements of East Ceiling

Figure 3.48 Opening and closing of ceiling to wall square-stop joints with indicative measurement location and measuring instrument number shown in brackets

Figure 3.48 (a) and (b) show that both ceiling systems began experiencing joint opening at approximately 0.28% drift (PFA: 0.15 g) at both fixed and floating edges. Contrary to expectations, the fixed edges did not exhibit negligible movement. This initial opening

occurred when the PFA and the acceleration at the mid-height of the supporting out-of-plane walls were relatively low (~0.15 g). It was This early joint movement can likely be attributed to the gradual withdrawal of the screws fastening the ceiling's wall angle to the wall.

The onset of residual joint openings and closings is shown in Figure 3.48 (c) and (d), beginning at 0.54% drift (PFA: 0.27 g, which also corresponded to a similar acceleration level at the supporting walls). While the residual opening magnitude was comparable between the West and East ceilings, the cumulative displacement behaviour differed significantly. As illustrated in Figure 3.48 (e) and (f), the fixed edge of the West ceiling accumulated substantially more displacement, reaching about 15 mm by 1.44 % drift. In contrast, the cumulative displacement for the East ceiling at the same drift level was only around 3 mm.

Figure 3.49 presents the shear displacements at the ceiling-to-wall joints. As shown in Figure 3.49 (a), shear displacement began earlier at the floating edge of the West ceiling than at the fixed edge of the East ceiling, which is an expected result. This also indicates that damage to square-stops can occur sooner at floating edges due to shear displacement, a phenomenon observed in these tests. Residual shear displacements at the floating joint of the West ceiling initiated at 0.54% drift (PFA: ~0.27 g; peak out-of-plane wall acceleration: ~0.27 g). For the fixed joint of the East ceiling, residual shear displacements began later at 1.19% drift (PFA: ~0.54 g; peak out-of-plane wall acceleration: ~0.80 g).

Both the residual and cumulative shear displacements at the fixed edge of the East ceiling, illustrated in Figure 3.49 (b) and (c), were substantially lower than those for the West ceiling. By 1.19% drift, the cumulative displacement reached about 26 mm for the West ceiling, compared to only around 3 mm for the East ceiling. This performance of the East ceiling can be attributed to two factors: the loosening of screws in the

plasterboard lining at the bulkhead end, which allowed some shear movement, and the pulling out of the wall angle at the fixed edge connection to the out-of-plane wall (as recorded by instrument 6A). This progressive degradation effectively transformed the East ceiling's boundary condition from fully fixed to a hybrid state; fixed on two adjacent sides and floating on the other two.

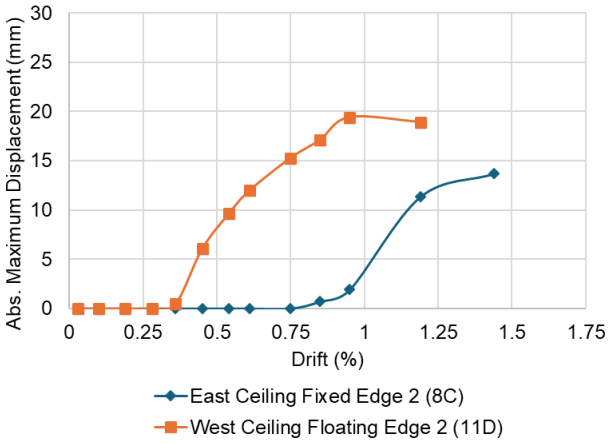

a) Absolute maximum displacements of ceilings

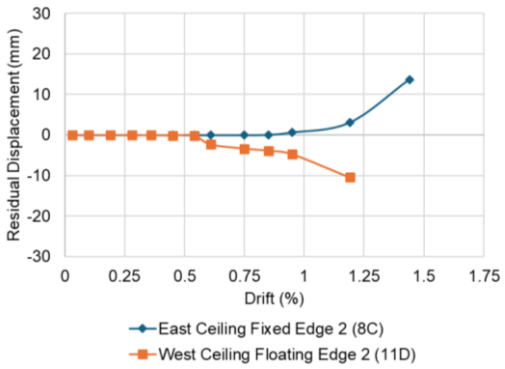

b) Residual displacements of ceilings

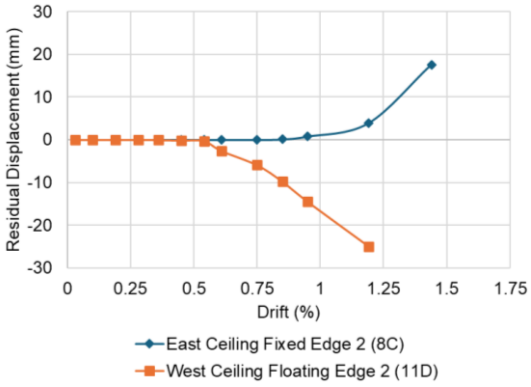

c) Cumulative residual displacements of ceilings

Figure 3.49 Shearing of ceiling to wall square-stop joints with indicative measurement location and measuring instrument number shown in brackets

Mechanical pipes

Figure 3.50 plots the lateral displacement measurements for the unbraced mechanical pipe specimen.

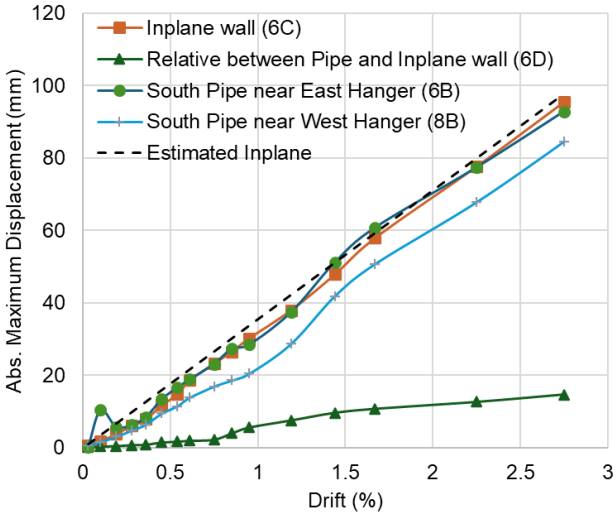

a) Absolute maximum displacements

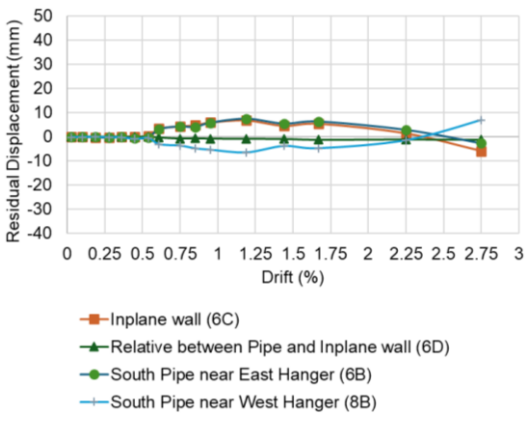

b) Residual displacements

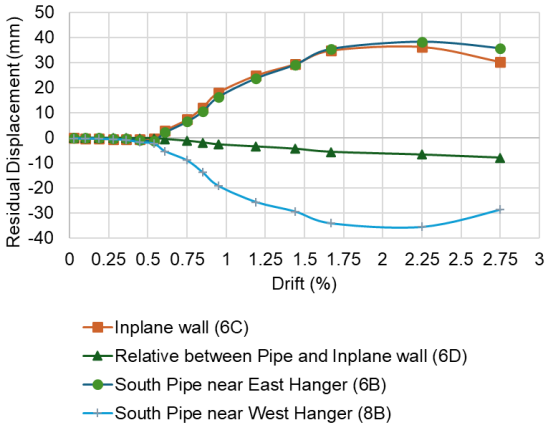

c) Cumulative residual displacements

Figure 3.50 Lateral displacement measurements for unbraced mechanical pipes specimen with indicative measurement location and measuring instrument number shown in brackets

In Figure 3.50 (a), it can be observed that the relative displacement between the pipe and the top slab is consistent with the displacement of the in-plane wall up to 0.95% drift (PFA: 0.43 g), after which a sudden deviation occurs. This deviation indicates the engagement of the in-plane wall with the pipe, which happened when the initial gap (approximately 10 mm) between them closed. Following this engagement, the displacement trend of the pipe continues to align with that of the in-plane wall. This suggests the pipe moved together with the wall while the hanger rods bent to accommodate the resulting relative displacement between the pipe and the top slab.

Consequently, as shown in Figure 3.50 (b) and (c), the residual displacements of the pipe are consistent with those of the in-plane wall.

CONCLUSIONS AND FUTURE STEPS

The Phase II experimental program investigated a full-scale timber-framed wall with typical construction details interacting with two key non-structural components: a perimeter-restrained concealed plasterboard ceiling and an unbraced mechanical pipe passing through the wall.

The testing documented a clear, sequential progression of damage for both the timber walls and the ceiling. Identifiable damage states were triggered at specific inter-storey drift levels, such as 0.54%, 1.19%, 1.44%, and 1.67%. The experimental program generated valuable data on component amplification factors (PCA/PFA ratios), which are critical for force-based seismic design. For the timber-framed walls, the median experimental PCA/PFA ratio of 1.22 conservatively estimated by code-prescribed values for flexible components, such as 1.40 in ASCE/SEI 7-22 (2022) and 1.43 in SNZ TS 1170.5 (for a part ductility, μ, of 2), thereby validating current code approaches for these elements.

In contrast, the median experimental ratio of 1.26 for the perimeter-restrained concealed plasterboard ceiling presents a significant finding. This value challenges the ASCE/SEI 7-22 (2022) factor of 1.0 as potentially unconservative, while indicating that the SNZ TS 1170.5 factor of approximately 1.43 (for μ=2) is slightly conservative. Importantly, the similarity between the ceiling ratio (1.26) and the wall ratio (1.22) strongly suggests that ceiling accelerations are dynamically coupled to, and amplified by, the response of the supporting walls, rather than being driven solely by floor motion. For the unbraced mechanical pipe, the high median PCA/PFA ratio of 2.36 confirms its

dynamic flexibility and significant inertial amplification which occurred due to interaction with the wall. This value is comparable to the ASCE/SEI 7-22 (2022) factor of 2.20, supporting its use, whereas the corresponding provision in SNZ TS 1170.5 for part ductility of 2 is unconservative.

The observed damage highlighted the interplay of two distinct mechanisms: drift-sensitive and acceleration-sensitive damage. Drift-sensitive damage, dominant in components like ceilings and pipe penetrations that are attached at multiple points, manifested as cracking, tearing, and separation at boundaries due to relative deformations. Acceleration-sensitive damage, related to inertial forces on a component's own mass, may also be present but requires further scrutiny in future work. The results suggest that for ceilings integrated with walls, drift-induced deformations of the supporting system were perhaps a more significant damage driver than pure inertial loading from the floor. Notably, the damage progression in these walls was delayed compared to the isolated timber wall specimen tested in Phase I.

The influence of construction detailing was clear. A comparison between the “typical” ceiling (with fixed and floating edges) and an “all-fixed” ceiling variant showed a distinct difference in damage distribution. Damage in the typical ceiling was concentrated at wall junctions, whereas it was more uniform in the all-fixed system. This underscores the critical role of perimeter connection details and boundary conditions on seismic performance.

A critical next step is to quantify the wall-ceiling dynamic interaction. Given the evidence that ceiling response is influenced by wall dynamics, future tests need to be conducted with accelerometers instrumented directly on ceiling components, such as furring channels and plasterboard, as well as on the adjacent wall studs and linings at the same elevation. Subsequent system identification and transfer function analysis are

required to quantify the amplification between the floor, the wall, and the ceiling element. This will clarify whether the ceiling's peak component acceleration is better correlated with wall acceleration than with floor acceleration. Furthermore, the analysis of dynamic characteristics and recorded Motion Capture Camera data is pending and is expected to provide a better understanding of the displacement behaviour of the tested non-structural components.

REFERENCES

ASCE/SEI 7-22,. (2022). Minimum design loads and associated criteria for buildings and other structures. Reston, VA: American Society of Civil Engineers (ASCE). doi:https:/doi.org/10.1061/9780784415788

Butterworth, S. (1930). On the theory of filter amplifiers. Wireless Engineer, 7(6), 536–541.

GIB. (2016). GIB-EzyBrace-system-sheet-GS2-N GIB. Retrieved from https://www.gib.co.nz/assets/Uploads/GIB-EzyBrace-System-sheet-GS2-N.pdf

Parks, T. W., & Burrus, C. S. (1987). Digital filter design Wiley-Interscience.

Pledger, L. (2026). The effects of reducing design drift limits for structures. (PhD, University of Canterbury).

SNZ TS 1170.5, &. (2025). Structural design actions – part 5: Earthquake actions – New Zealand. Wellington, New Zealand:

Sorrentino, R. (2007). Electronic filter simulation & design McGraw-Hill Professional.

APPENDIX B

OBSERVED DAMAGE DURING TESTS

Table 3.4. Test 4, 0.36 % drift (PFA Top: 0.18 g)

Location	Observation	Photo
Southern part of the Eastern Bulkhead 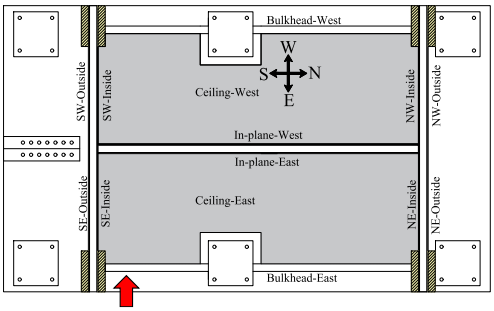	Minor Screw Impressions	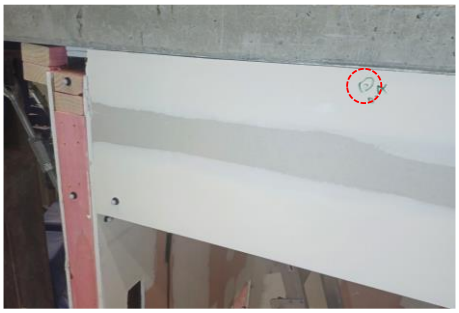
Pipe 1-Back Side 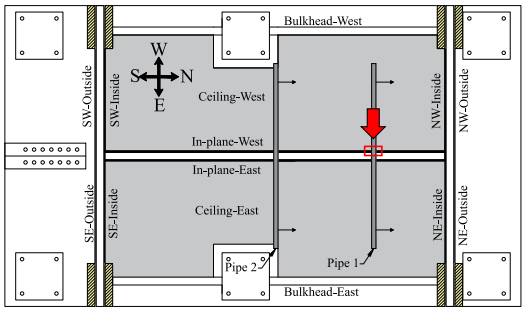	Minor wear and tear	

Table 3.5. Test #6, 0.54 % drift (PFA Top: 0.27g)

Location	Observation	Photo
Corner joint interface between the In-plane-west wall and the west ceiling 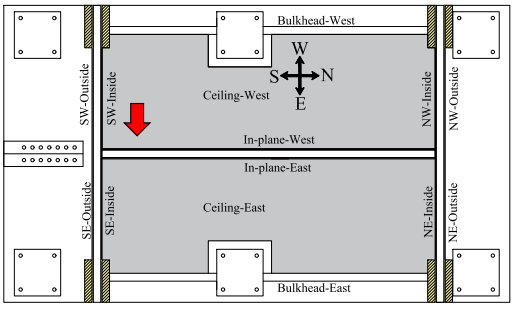	Minor flaking of the paper tape	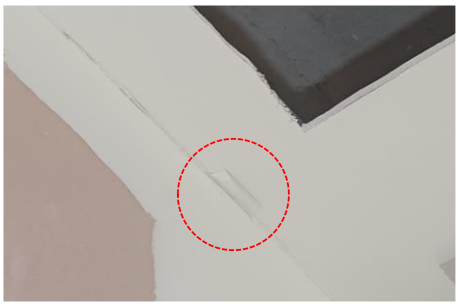

Corner joint interface between the in-plane west wall, the NW inside wall, and the west ceiling 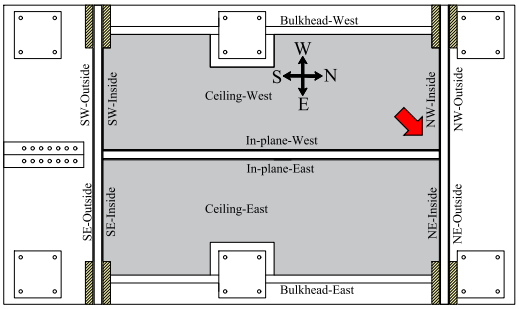	Hairline crack on the plaster	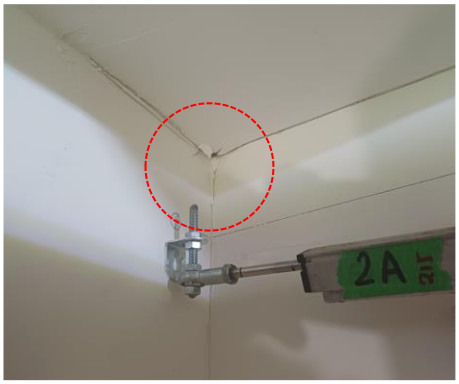

Table 3.6. Test 7, 0.61 % drift (PFA Top: 0.29 g)

Location	Observation	Photo
Corner joint interface between the SE-Inside wall and the East ceiling 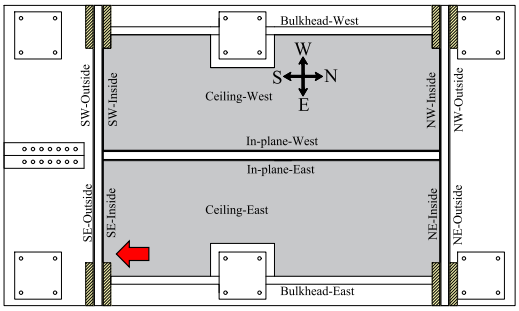	Minor flaking of the paper tape	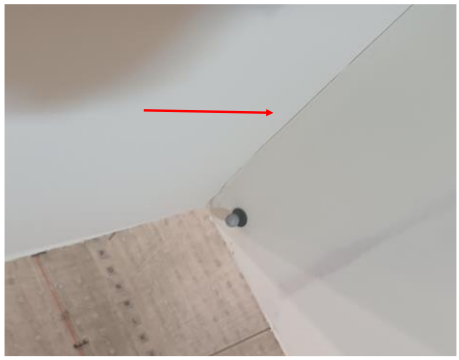
Corner joint interface between the NE-Inside wall and the East ceiling 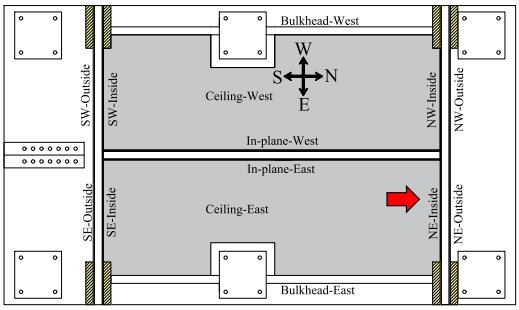	Minor Crack and Flaking of the Paper Tape.	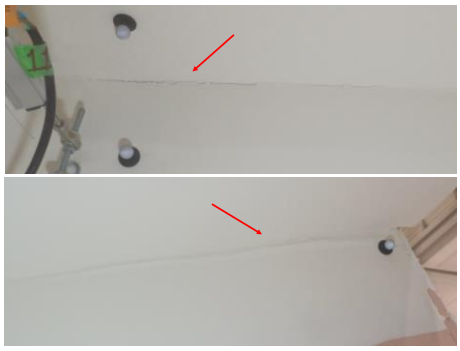
Inside the plenum — joint between the SW-inside wall and the west ceiling 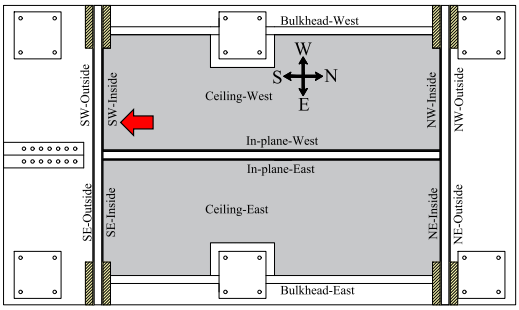	Screw Pulling in the Wall Track	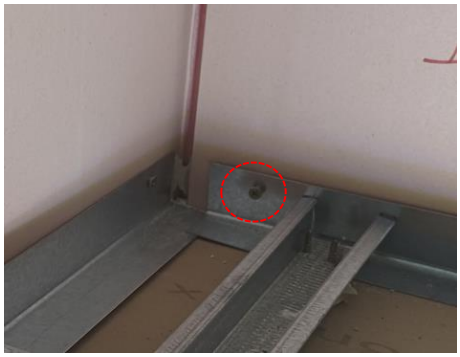

Corner joint interface between the SW-Inside wall and the West ceiling 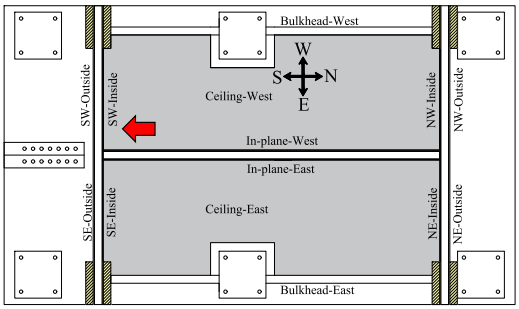	Flaking of the paper tape	

Table 3.7. *Test #8*, 0.75 % *drift (PFA Top: 0.35 g)*

Location	Observation	Photo
Corner joint interface between the NE-Inside wall and the East ceiling 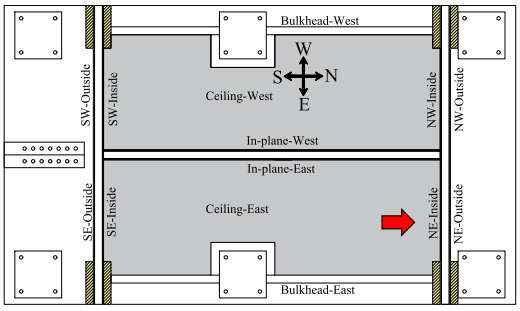	Flaking of the paper tape	
Corner joint interface between the NW-Inside wall and the west ceiling 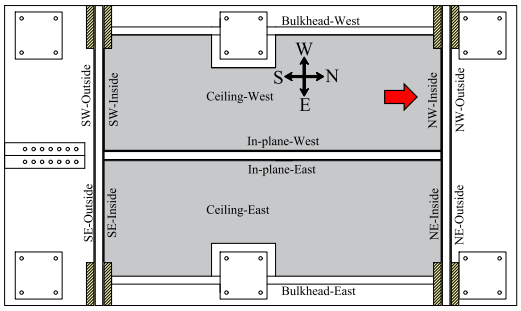	Flaking of the paper tape	
Corner joint interface between the In-plane west wall and the west ceiling 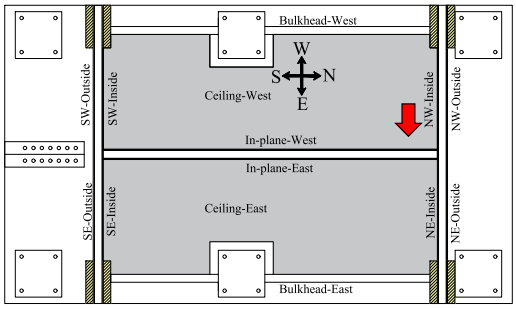	Flaking of the paper tape	

Corner joint interface between the SW-Inside wall and the west ceiling 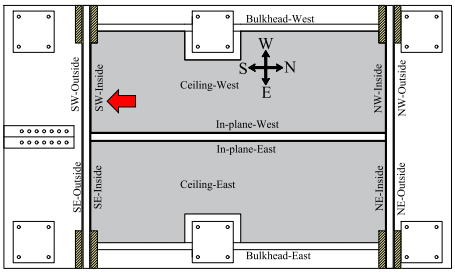	Flaking of the paper tape	
Pipe 1-Back side 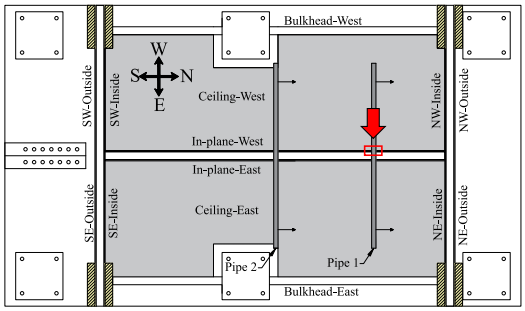	Minor wear and tear	

Table 3.8. *Test #9*, 0.85 % drift (PFA Top: 0.40 g)

Location	Observation	Photo
Corner joint interface between the NE-Inside wall and the east ceiling 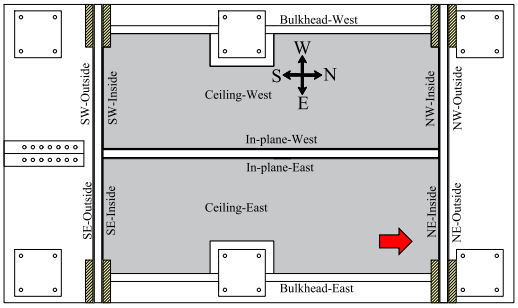	Flaking of the paper tape	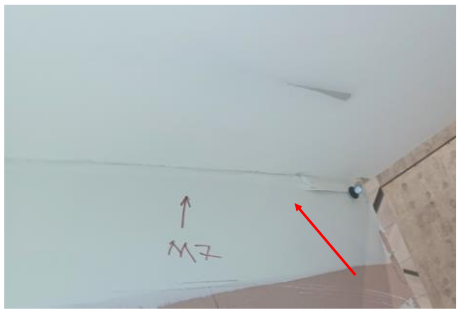
Corner joint interface between the NW-Inside wall and the west ceiling 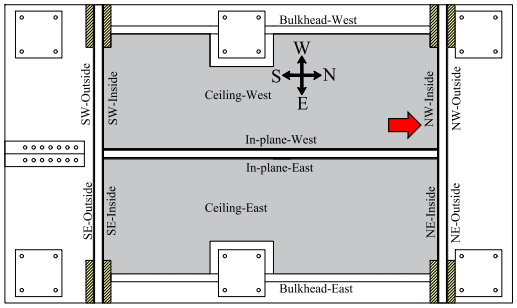	Separation of the Corner Joint Paper Tape	

Table 3.9. *Test* #10, 0.95 % drift (PFA Top: 0.43 g)

Location	Observation	Photo
Corner joint interface between the NE-Inside wall and the east ceiling 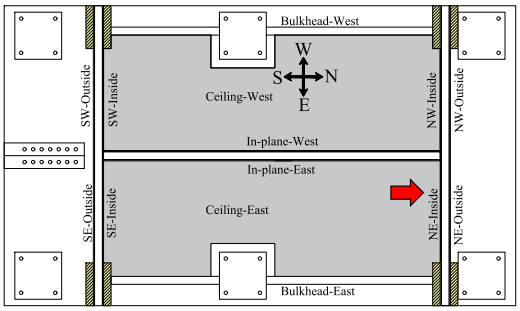	Separation of the Corner Joint Paper Tape	
Middle of the East Ceiling 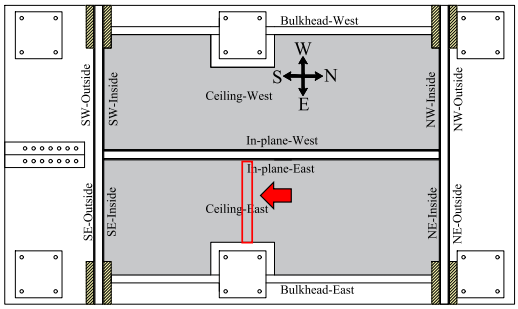	Cracks on the Plaster and Screw Impressions	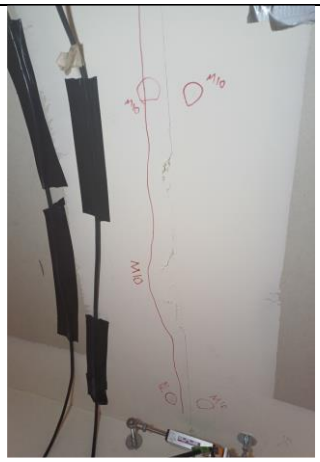
Corner joint interface between the SE-Inside wall and the east ceiling 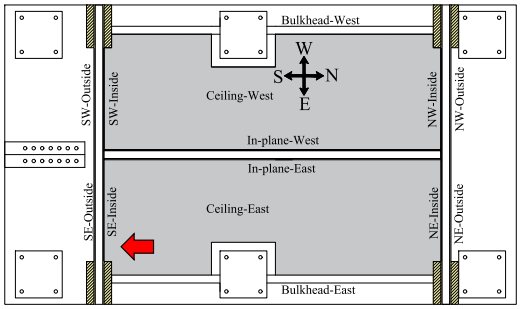	Cracks on the Plaster and Flaking of the paper tape	
Corner joint interface between the SW-Inside wall and the west ceiling 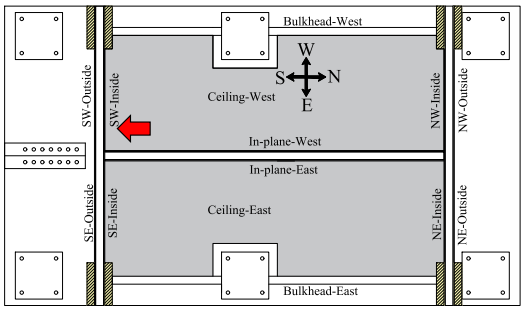	Separation of the Corner Joint Paper Tape	

Corner joint interface between the NW-Inside wall and the west ceiling 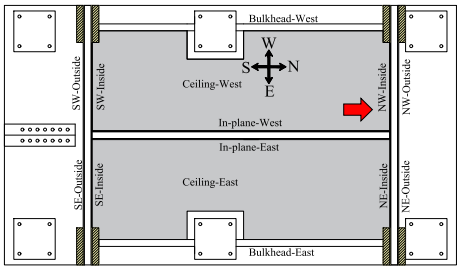	Separation of the Corner Joint Paper Tape	
Corner joint interface between the In-plane west wall and the west ceiling 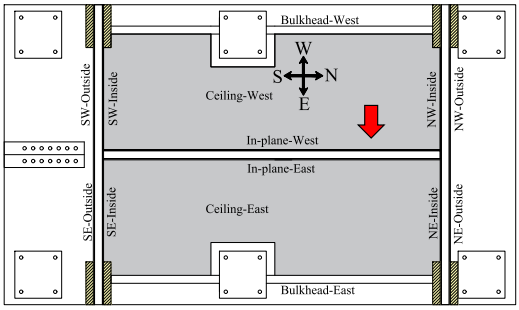	Crack in the Plaster	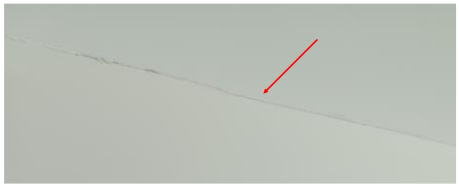
Pipe1-Back Side 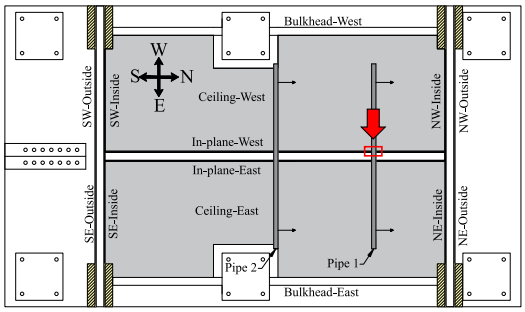	Minor separation (unlikely to compromise fire-rating performance)	

Table 3.10. Tests 11 and 12, 1.19 % drift (PFA Top: 0.54 g)

Location	Observation	Photo
Corner joint interface between the NE-Inside wall and the east ceiling 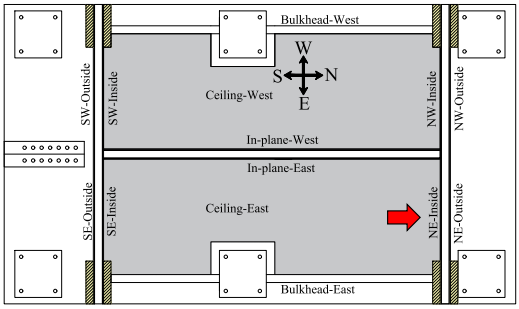	Separation of the Corner Joint Paper Tape	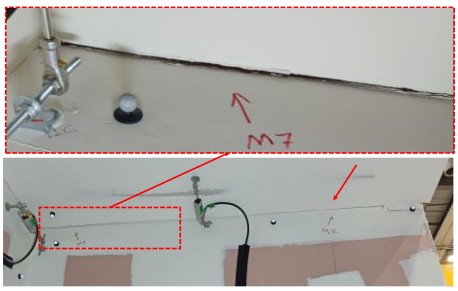

Corner joint interface between the NW-Inside wall and the west ceiling 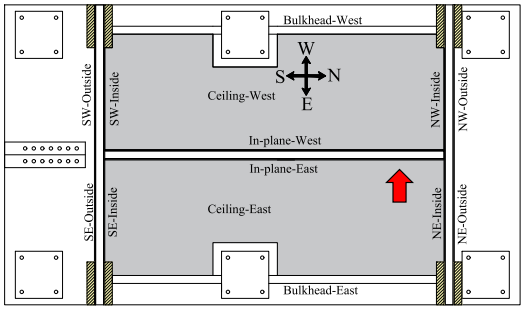	Crack on the plaster and corner joint paper tape	
Inside the plenum — junction between the in-plane east wall and the east ceiling 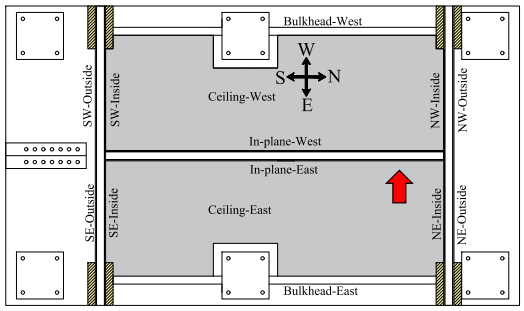	Screw Pulling in the wall track	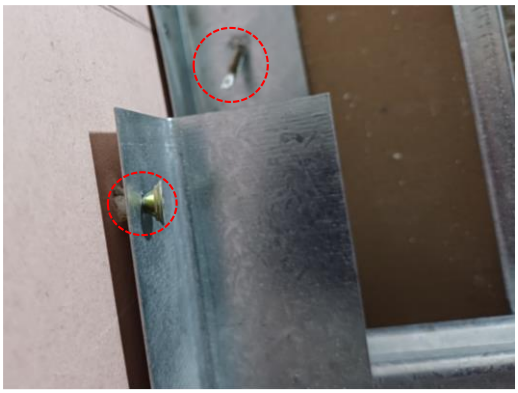
Middle of the East Ceiling 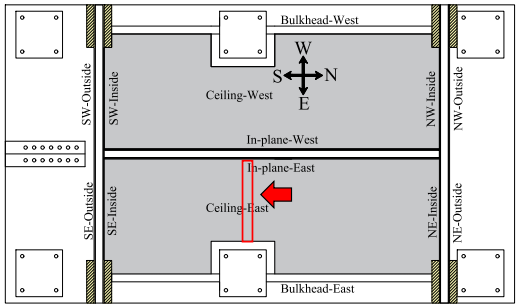	Cracks on the Plaster and Screw Impressions	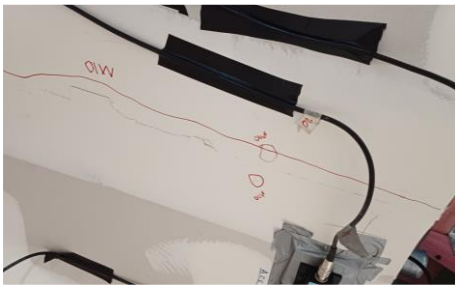
Top corner of the SE inside wall near its corner joint with the in-plane east wall and the east ceiling 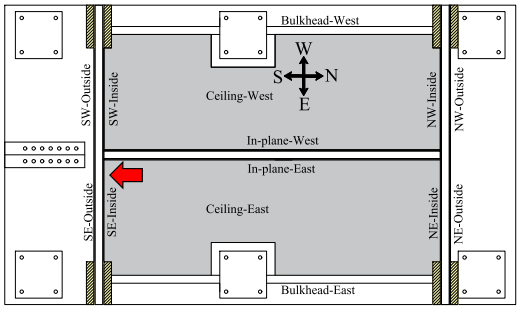	Crack in the plasterboard	

Top corner of the NW inside wall near its corner joint with the in-plane west wall and the west ceiling 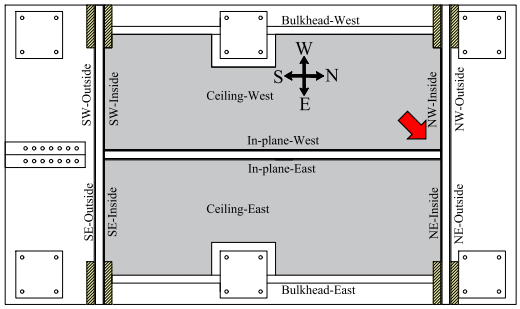	Crack in the plasterboard	
Top corner of the NW inside wall near its corner joint with the west bulkhead and the west ceiling 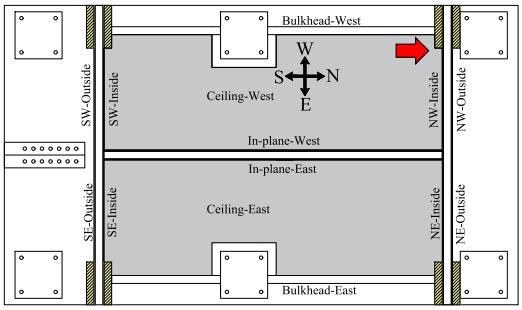	Crack in the plasterboard	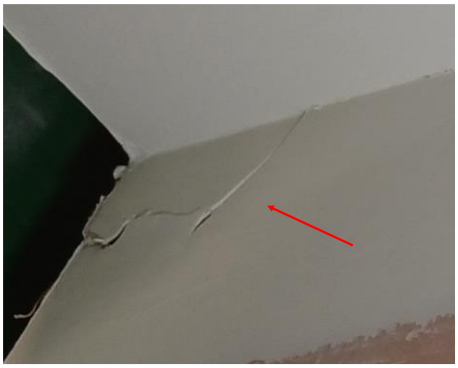
Corner joint interface between the In-plane west wall and the west ceiling 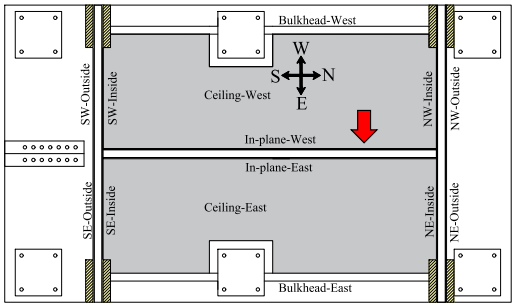	Split in the corner joint paper tape	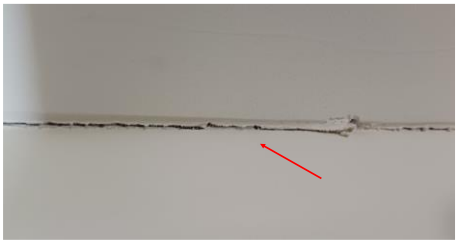
Top corner of the SW-Inside wall near its corner joint with the in-plane west wall and the west ceiling 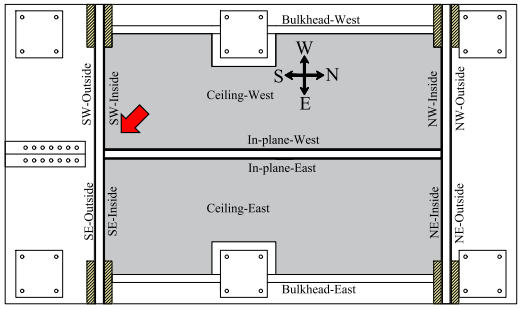	Crack in the plasterboard	

Inside the plenum — joint between the SW-inside wall and the west ceiling 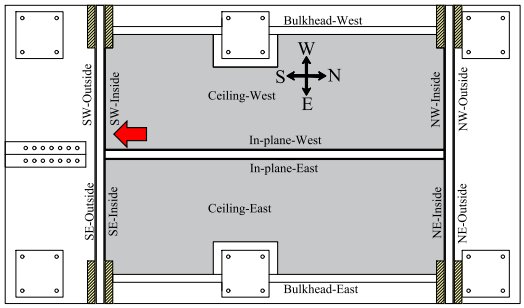	Screw pulling and detachment of the end part of wall track	
Inside the plenum — joint between the SW-inside wall and the west ceiling 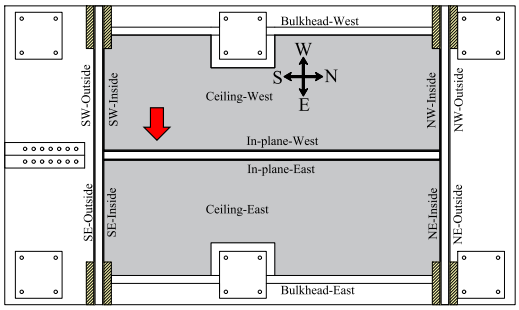	Screws pulled from the wall track	
Pipe1-Back Side 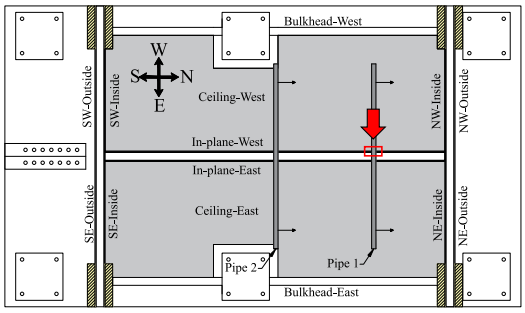	Moderate Separation (Fire-Rating Impact Uncertain)	

Table 3.11. *Test* #13, 1.44 % drift (PFA Top: 0.84 g)

Location	Observation	Photo
Corner joint interface between the NE-Inside wall and the east ceiling 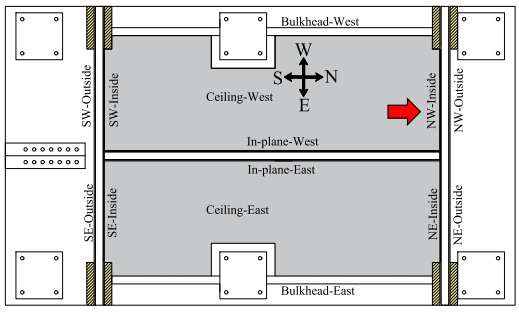	Separation at the corner joint between the ceiling and wall	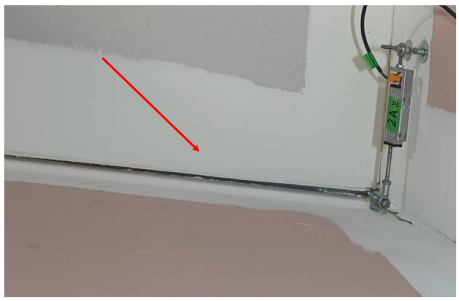

Corner joint interface between the In-plane west wall and the west ceiling 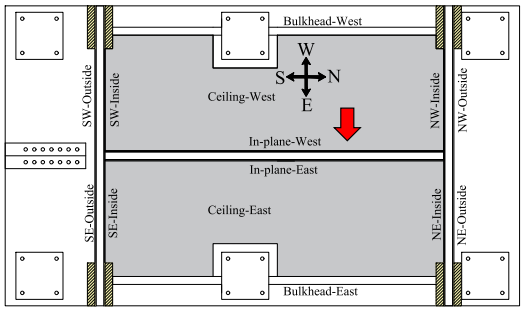	Split in the corner joint paper tape	
Top corner of the NW inside wall near its corner joint with the in-plane west wall 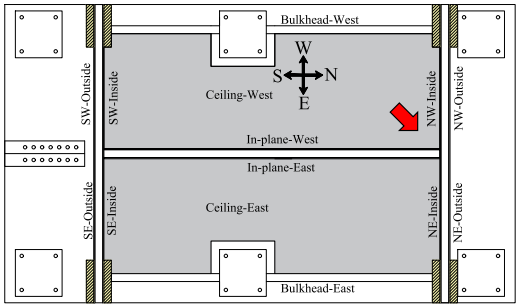	Crack in the plasterboard	
Top corner of the NW inside wall near its corner joint with the west bulkhead and the west ceiling 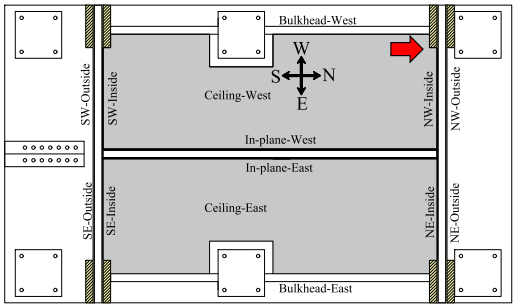	Crack in the plasterboard	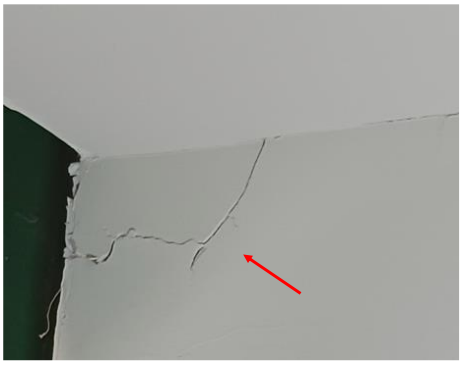
Inside the plenum — joint between the NW-inside wall and the west ceiling 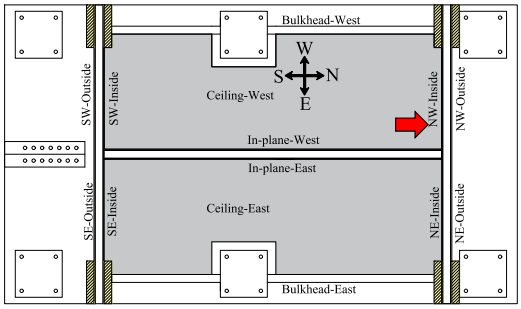	Crumpling at the end of the furring channel (due to inappropriate connection to the wall track)	

Top corner of the SW-Inside wall near its corner joint with the in-plane west wall and the west ceiling 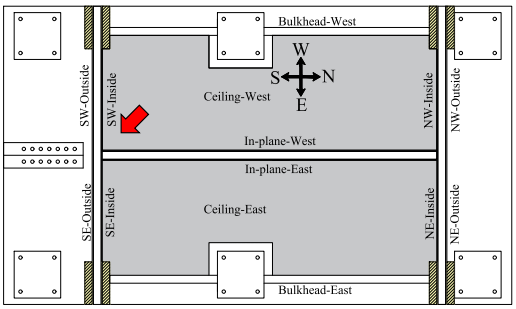	Crack in the plasterboard	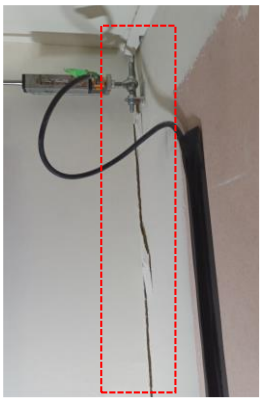
Corner joint interface between the SW-Inside wall and the west ceiling 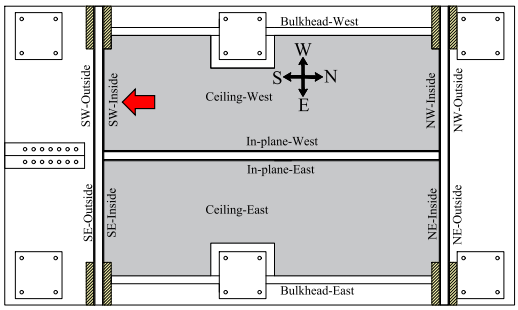	Separation in the Corner Joint Paper Tape	
Inside the plenum — joint between the SW-inside wall and the west ceiling 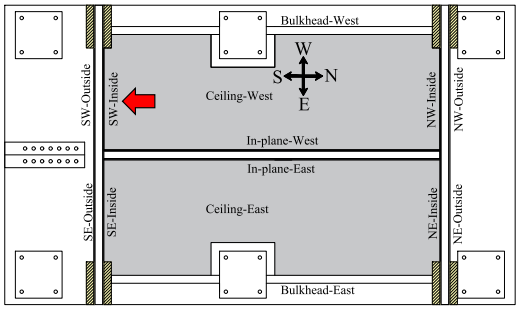	Screw pulling and detachment of the wall track in some parts	
Top of the T-junction between the in-plane wall and the southern wall 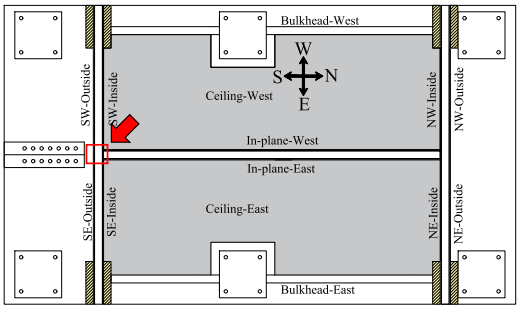	Detachment of the tie strap connecting two walls to each other at the T-junction	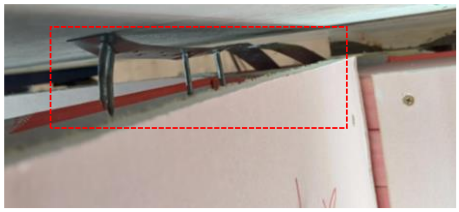

Top corner of the SW inside wall near the restraining timbers 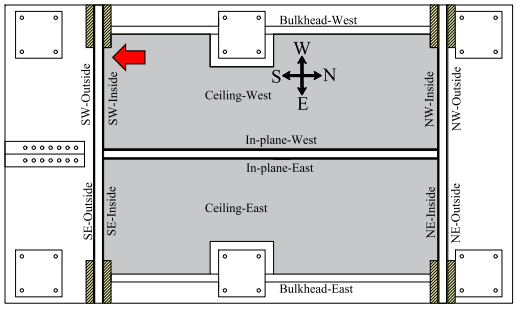	Crack in the plasterboard	
Top and middle of SE-Inside wall close to its corner joint with the in-plane east wall 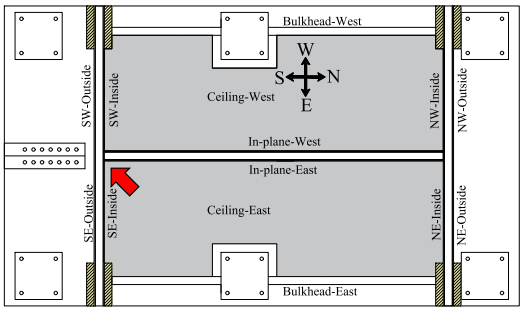	Major Crack in the plasterboard	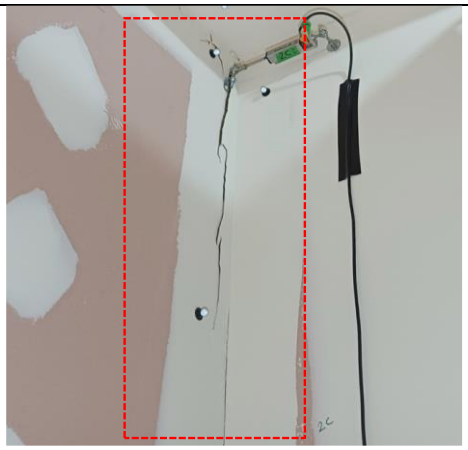
Corner joint interface between the NE-Inside wall and the east ceiling 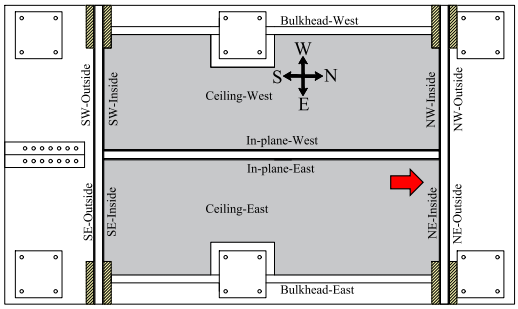	Separation at the corner joint between the ceiling and wall	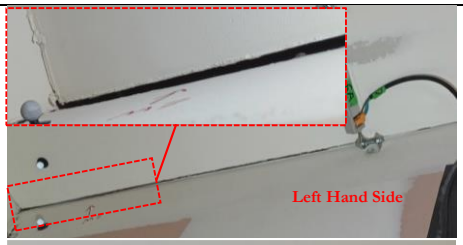 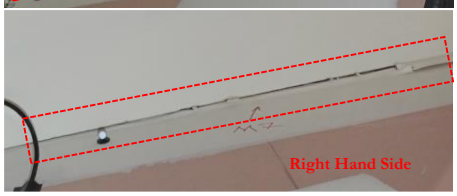
Top corner of the NE inside wall near its corner joint with the in-plane west wall and the east ceiling 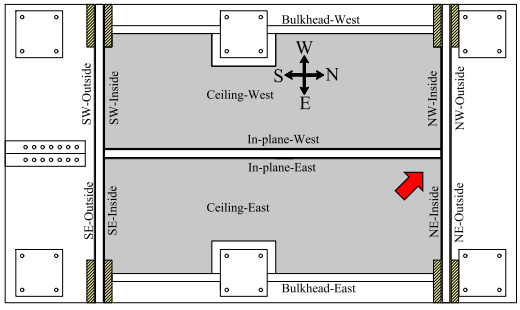	Crack in the plasterboard	

Middle of the East Ceiling 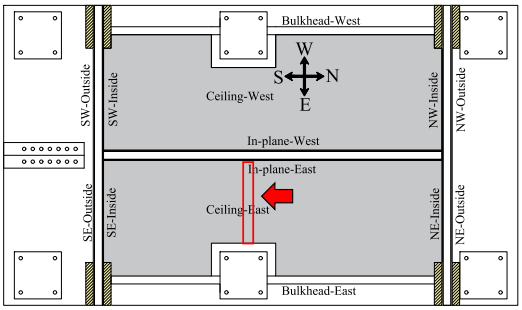	Cracks on the Plaster and Screw Impressions	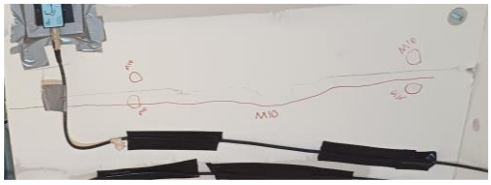
Corner joint interface between the SE-Inside wall and the east ceiling 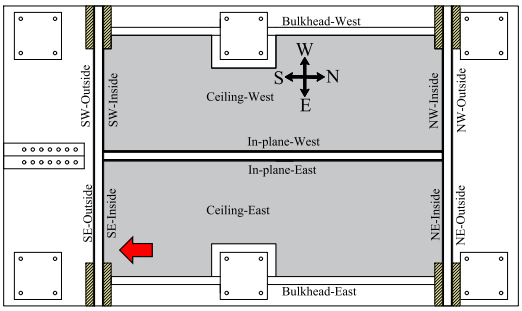	Flacking of the corner joint paper tape	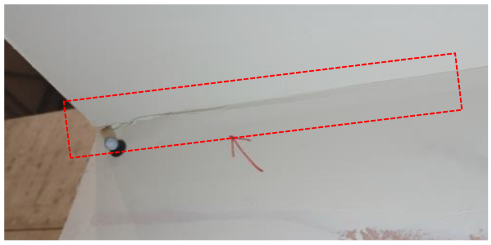
Corner joint interface between the In-plane east wall and the east ceiling 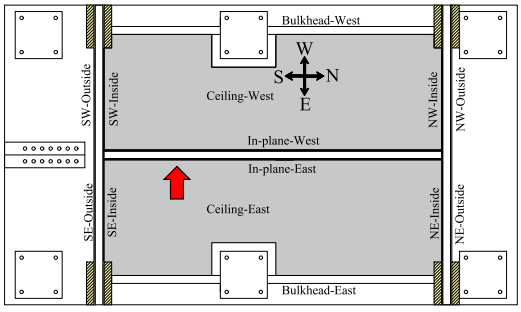	Split in the corner joint paper tape	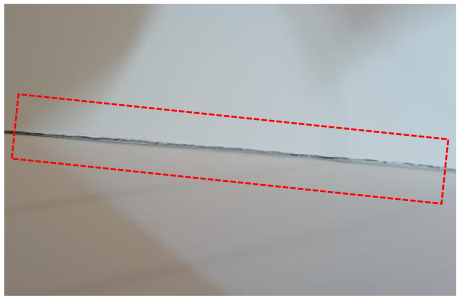
Top of the T-junction between the in-plane wall and the Northern wall 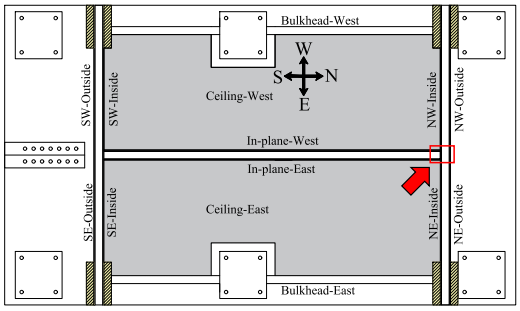	Partial detachment of the tie strap connecting two walls to each other at the T-junction due to pulled nails	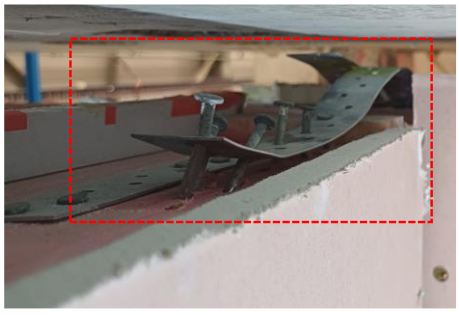

Pipe1-Back Side 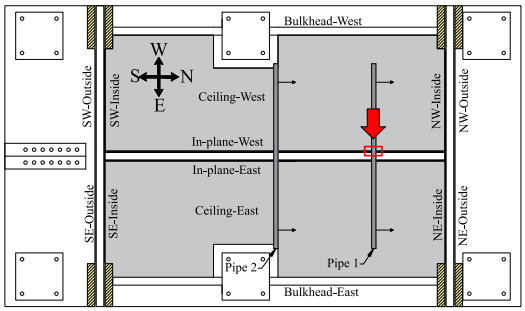	Visible Separation (Likely to Compromise Fire-Rating Performance)	

Table 3.12. *Test* #14, 1.67 % drift (PFA Top: 1.18 g)

Location	Observation	Photo
Top corner of the NE-inside wall near its corner joint with the in-plane East wall 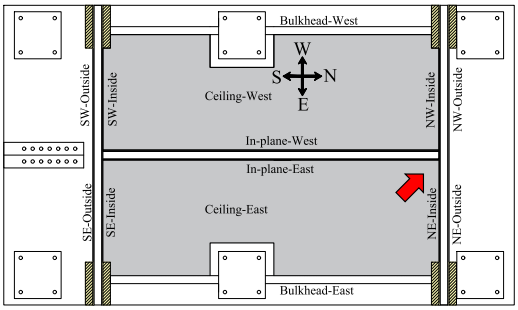	Major Crack in the plasterboard	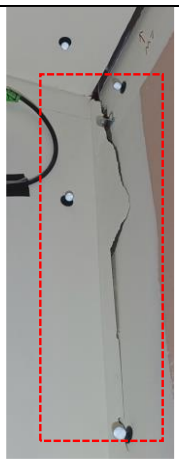
Corner joint interface between the NW-Inside wall and the west ceiling 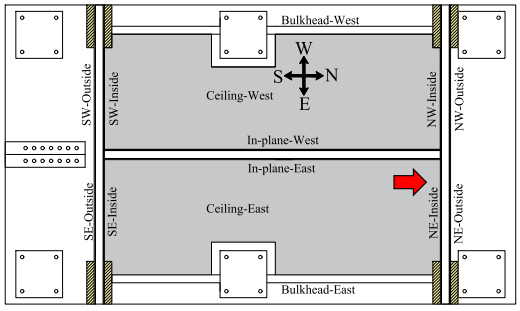	Separation at the corner joint between the ceiling and wall	 
Corner joint interface between the In-plane east wall and the east ceiling 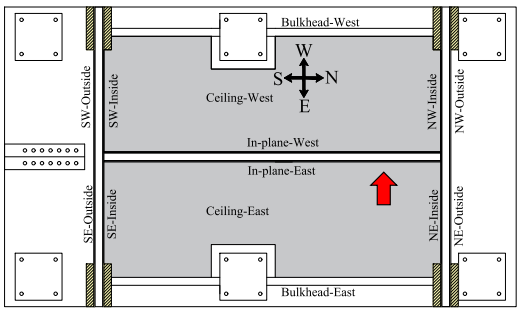	Split in the corner joint paper tape	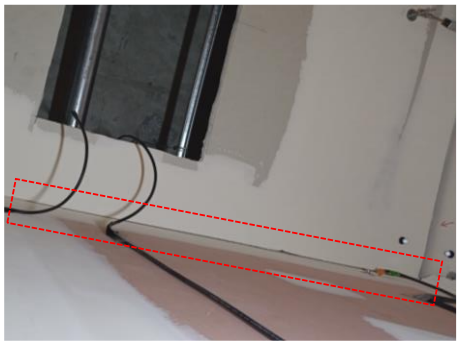

Top corner of the SE-Inside wall near its corner joint with the in-plane East wall 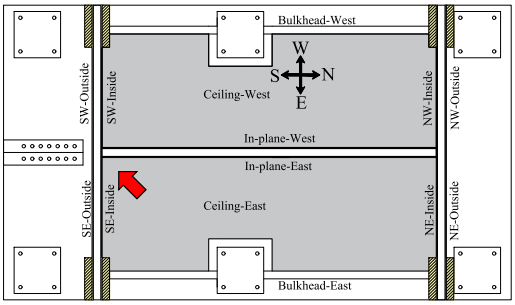	Major Crack in the plasterboard	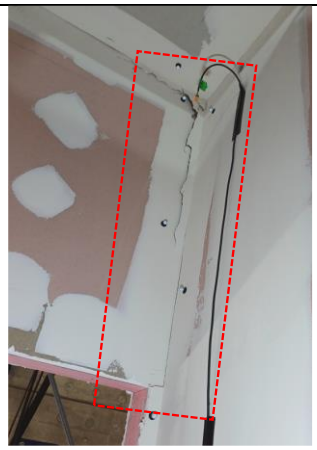
Inside the plenum — junction between the in-plane east wall and the east ceiling 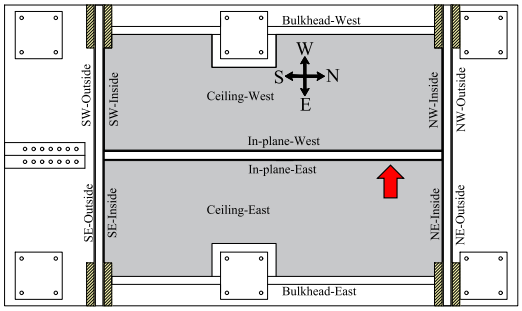	Screw pull-out and damage to the wall track and ceiling plasterboard	 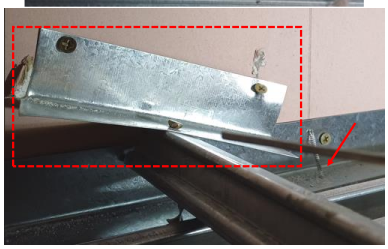
Top of the T-junction between the in-plane wall and the Northern wall 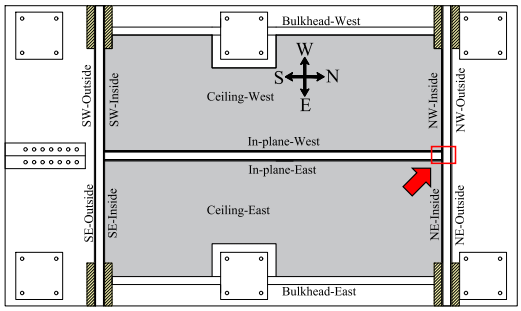	Detachment of the tie strap connecting two walls to each other at the T-junction	
Inside the plenum — joint between the NE-inside wall and the east ceiling 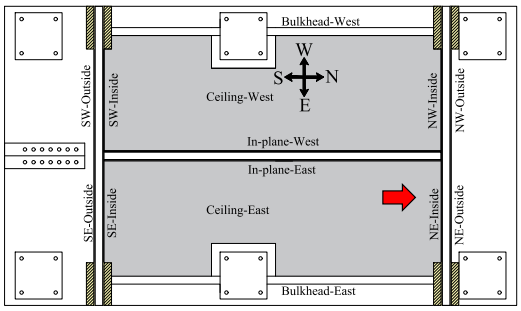	Screw pull-out and detachment of the wall track from the wall plasterboard	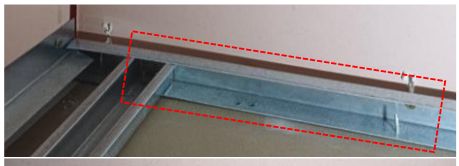 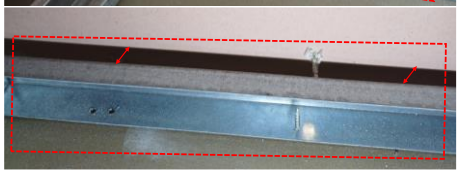

Inside the plenum — joint between the In-plane east wall and the east ceiling 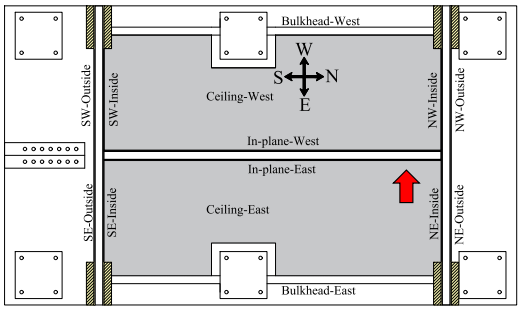	Separation between the wall track and ceiling plasterboard	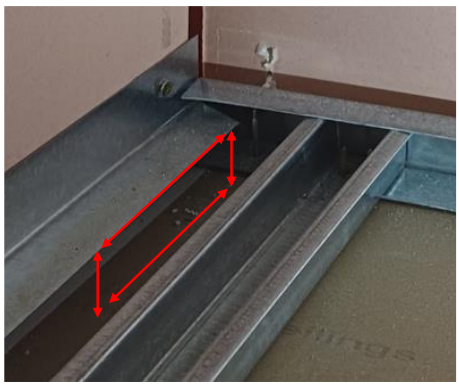
Middle of the East Ceiling 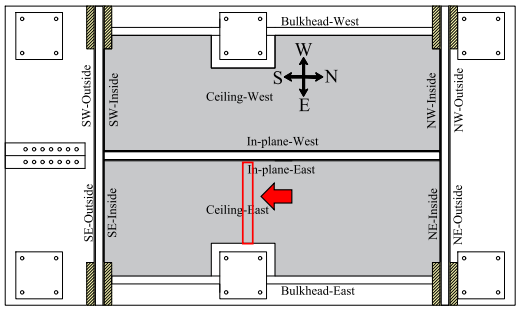	Cracks on the Plaster and Screw Impressions	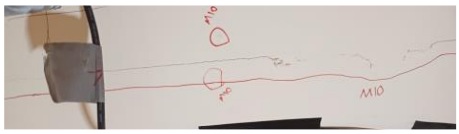
Top corner of the SE-Inside wall near its corner joint with the in-plane East wall 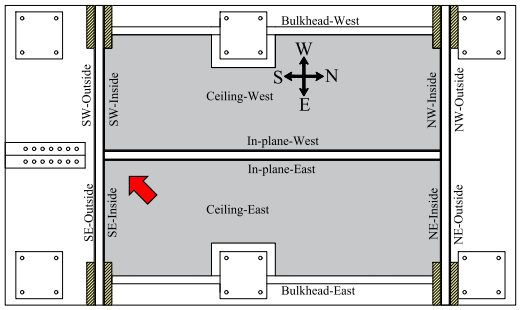	Major Crack in the plasterboard	
Inside the plenum — joint between the SE-inside wall and the east ceiling 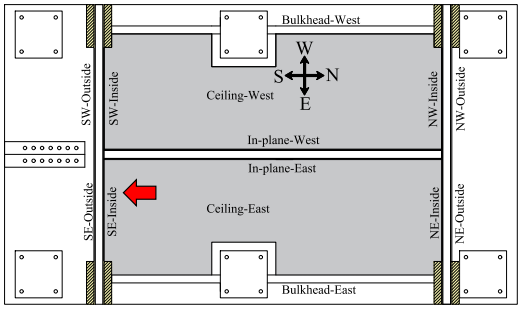	Screw pulling and minor deformation in the wall track	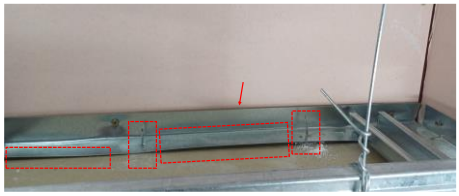
Corner joint interface between the NW-Inside wall and the west ceiling	Separation at the corner joint between the ceiling and wall	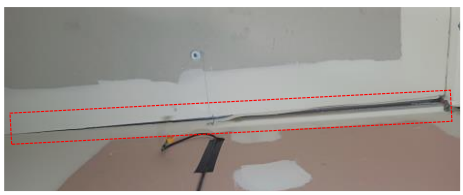

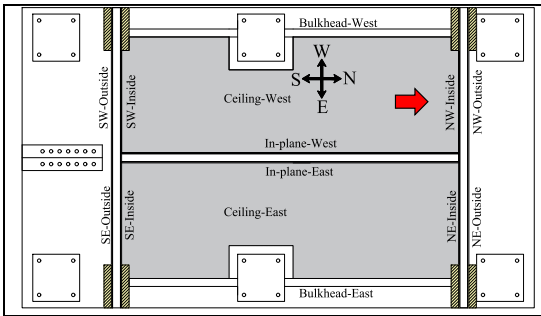		
Corner of the NW-inside wall near the joint with the in-plane west wall (from top to middle) 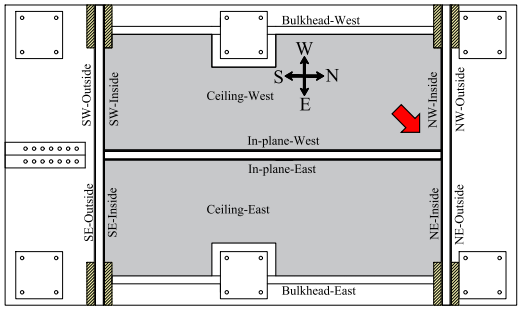	Major Crack in the plasterboard	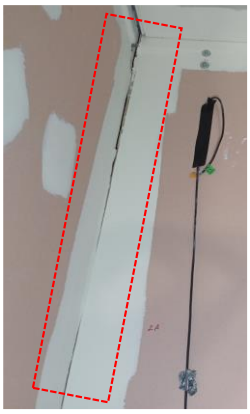
Corner of the SW-inside wall near the joint with the in-plane west wall (from top to middle) 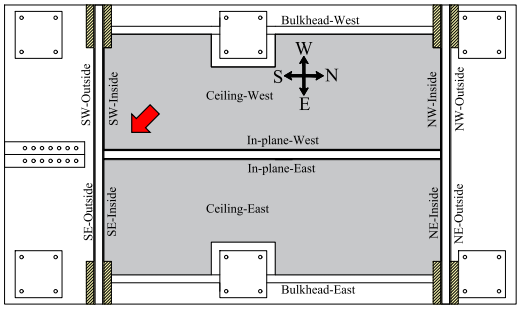	Major Crack in the plasterboard	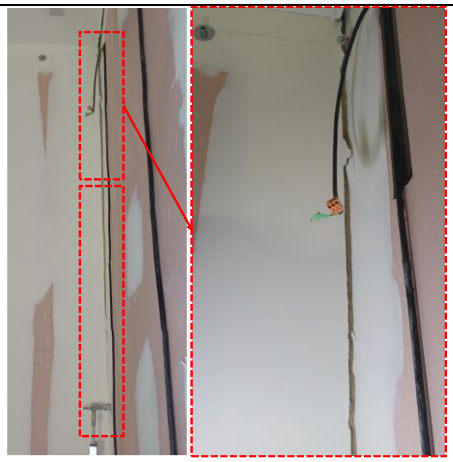
Inside the plenum — joint between the SW-inside wall and the west ceiling 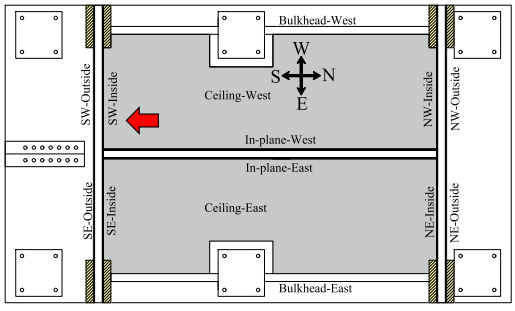	Screw pull-out, detachment and crumpling of the wall track, and localized crushing of the ceiling plasterboard	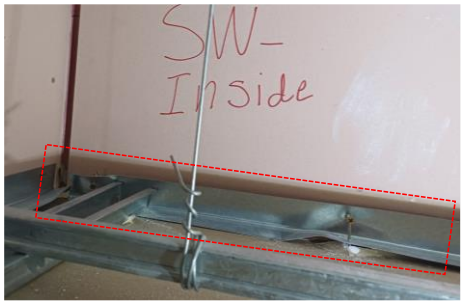

Inside the plenum — joint between the In-plane west wall and the west ceiling 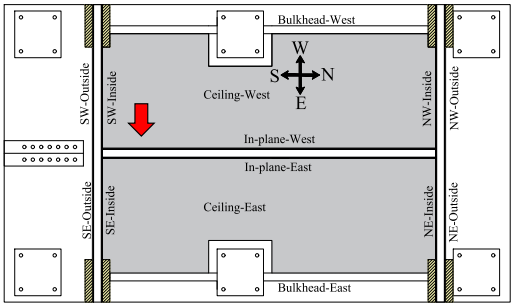	Separation between the wall track and ceiling plasterboard, some deformation in the wall track	
Middle of the southern wall (outside), from top to mid-height 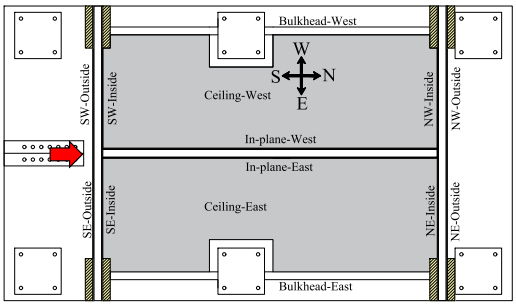	Crack in the plasterboard	
Top corner of the SE-Inside wall near the restraining timbers 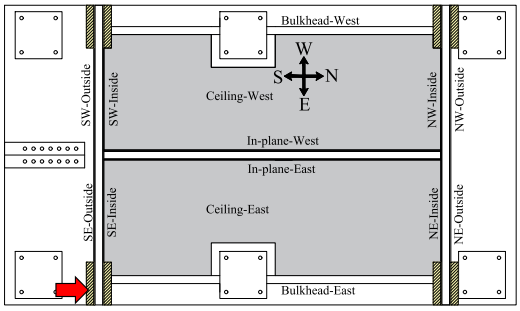	Crack in the plasterboard	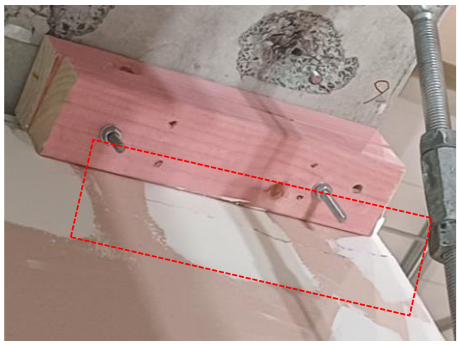
Pipe1-Back Side 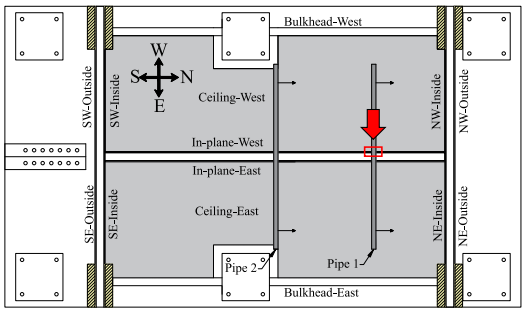	Visible Separation (Likely to Compromise Fire-Rating Performance)	

Table 3.13. Test #15, 2.25 % drift (PFA Top: 1.30 g)

Location	Observation	Photo
Middle of the northern wall (outside), from top to mid-height 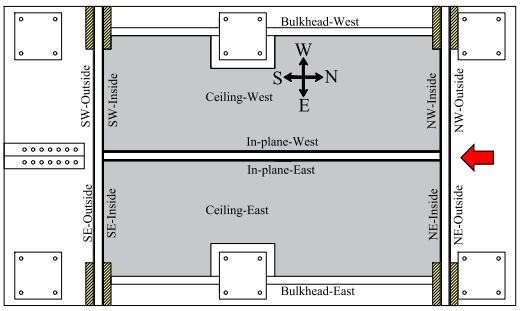	Crack in the plasterboard	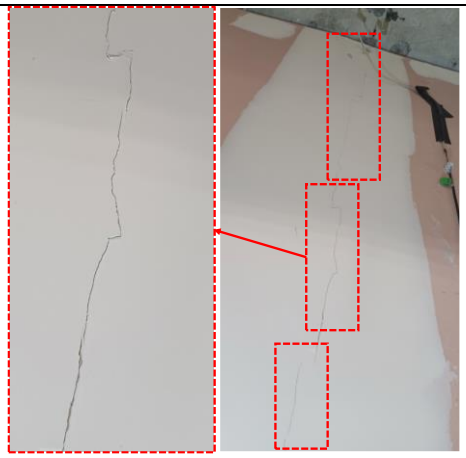
Corner joint interface between the NW-Inside wall and the west ceiling 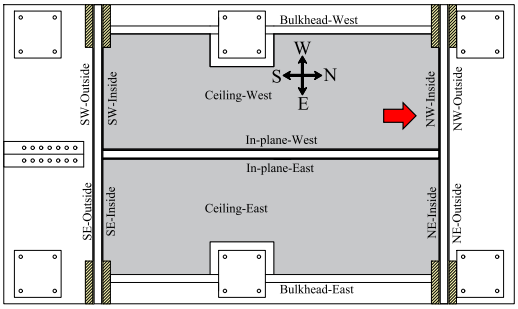	Separation at the corner joint between the ceiling and wall	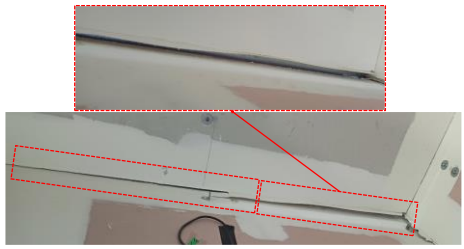
Corner of the NW-inside wall near the joint with the in-plane west wall (from top to middle) 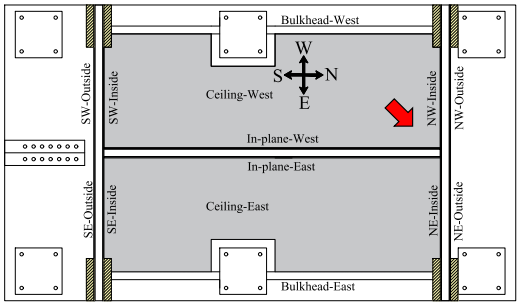	Major Crack in the plasterboard	
Top corner of the NW inside wall near its corner joint with the west bulkhead and the west ceiling 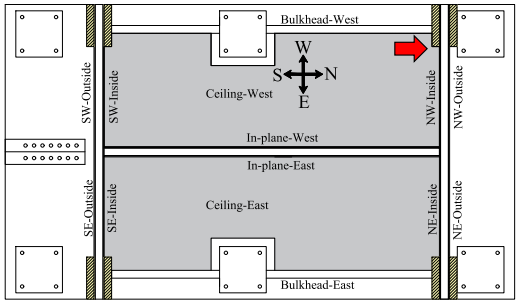	Crack in the plasterboard	

Corner of the SW-inside wall near the joint with the in-plane west wall (from top to middle) 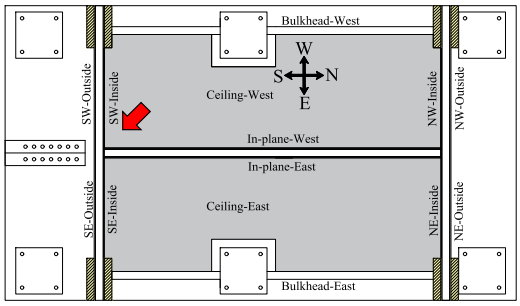	Major Crack in the plasterboard	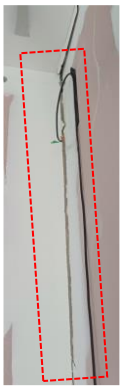
Corner joint interface between the SW-Inside wall and the west ceiling 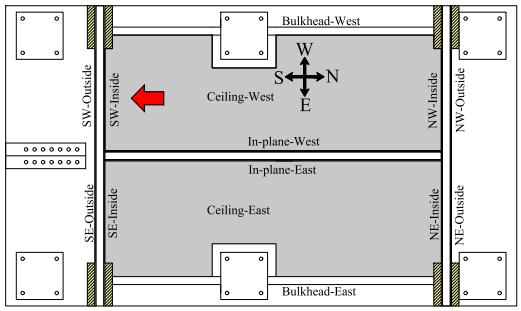	Separation at the corner joint between the ceiling and wall	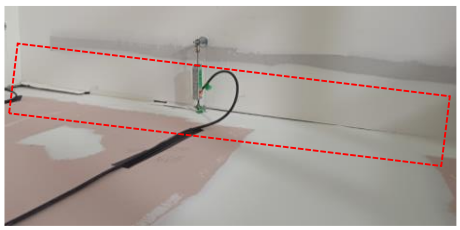
Corner joint interface between the In-plane west wall and the west ceiling 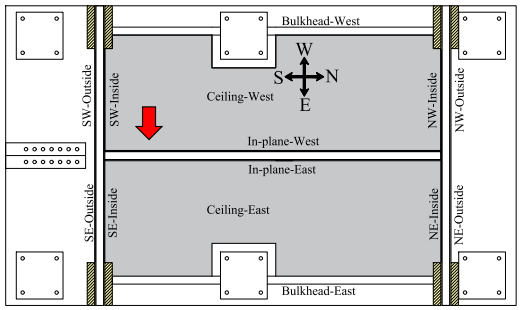	Split in the corner joint paper tape	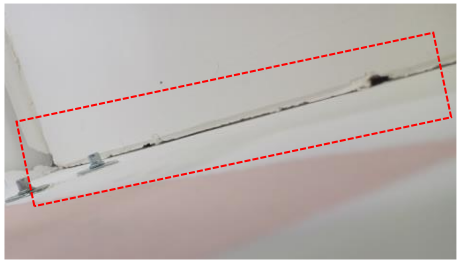
Inside the plenum — joint between the NW-inside wall and the west ceiling 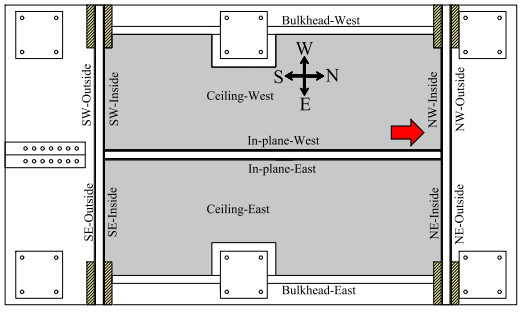	Crumpling at the end of the furring channel (due to inappropriate connection to the wall track)	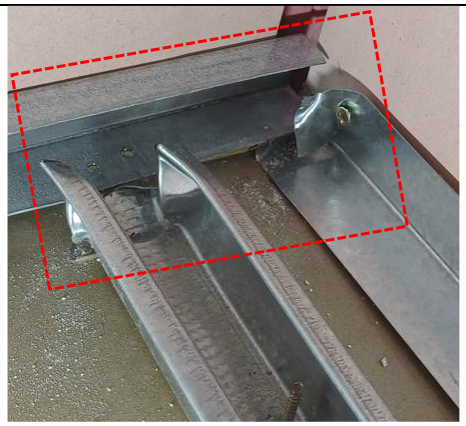

Inside the plenum — joint between the SW-inside wall and the west ceiling 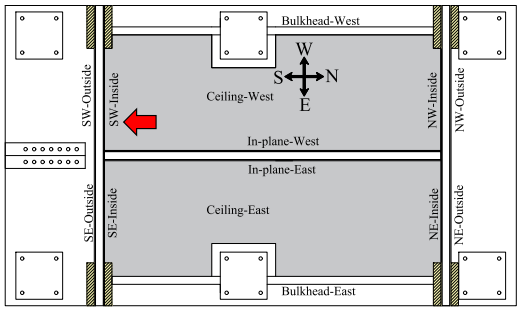	Screw pull-out, detachment and crumpling of the wall track, and localized crushing of the ceiling plasterboard	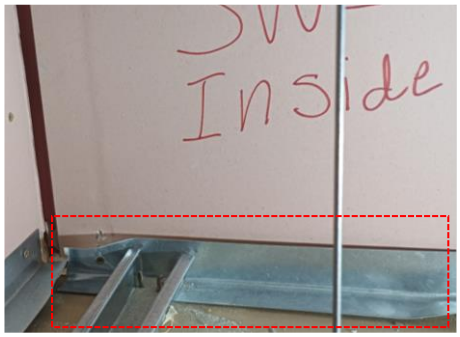
Inside the plenum — joint between the In-plane west wall and the west ceiling 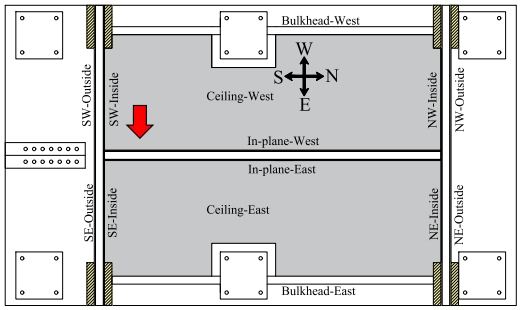	Separation between the wall track and ceiling plasterboard, some deformation in the wall track	 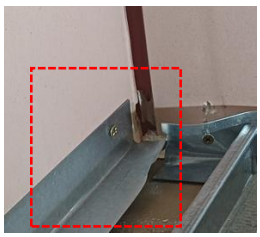
Middle of the southern wall (outside), from top to mid-height 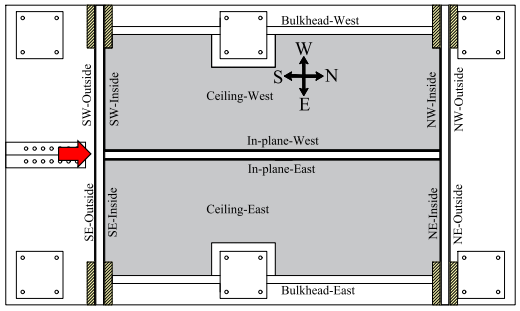	Crack in the plasterboard	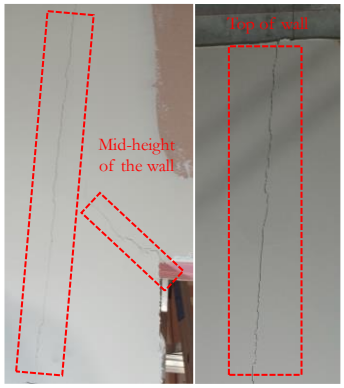
Top corner of the SE-Inside wall near its corner joint with the in-plane East wall 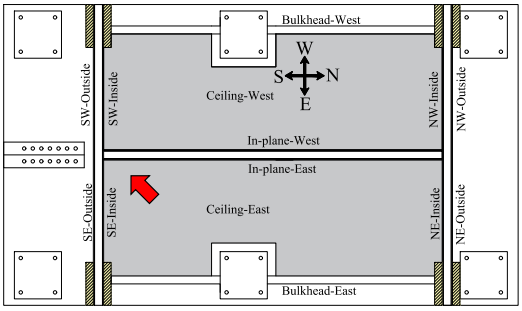	Crack in the plasterboard	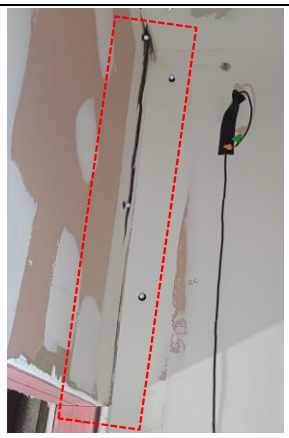

Corner joint interface between the SE-Inside wall and the east ceiling 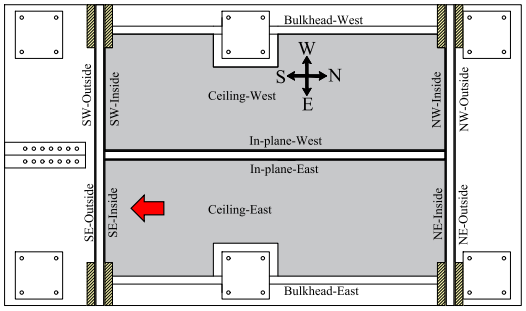	Separation at the corner joint between the ceiling and wall	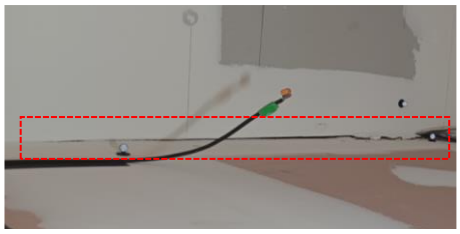
Pipe 1-Back Side 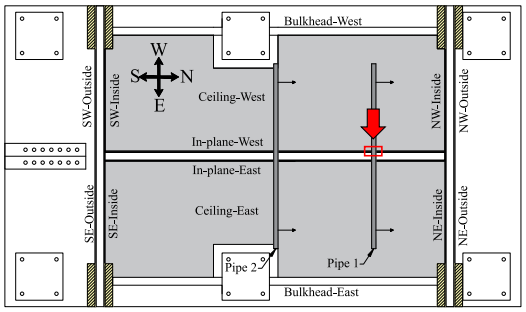	Visible Separation (Likely to Compromise Fire-Rating Performance)	

Table 3.14. *Test* #16, 2.75 % drift (PFA Top: 1.33 g)

Location	Observation	Photo
Top corner of the NE-inside wall near its corner joint with the in-plane East wall 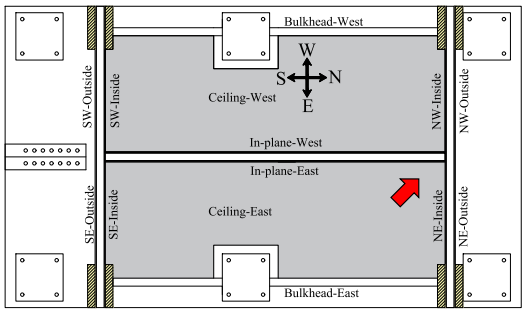	Major Crack in the plasterboard	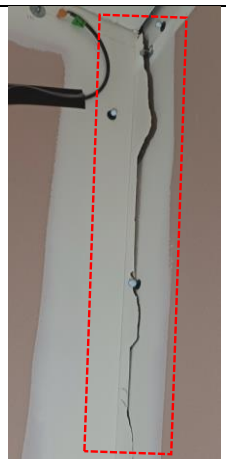
Corner joint interface between the NW-Inside wall and the west ceiling 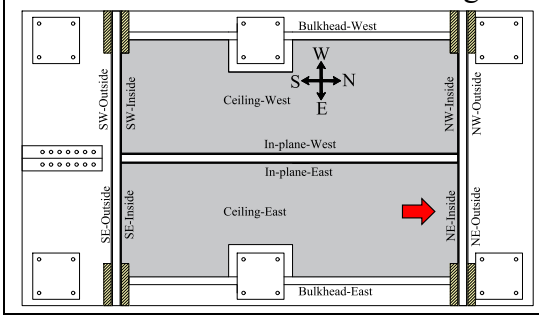	Separation at the corner joint between the ceiling and wall	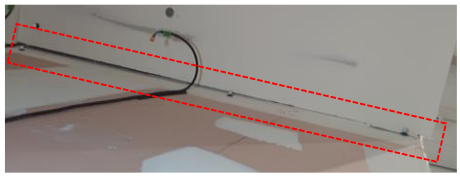

Corner joint interface between the In-plane east wall and the east ceiling 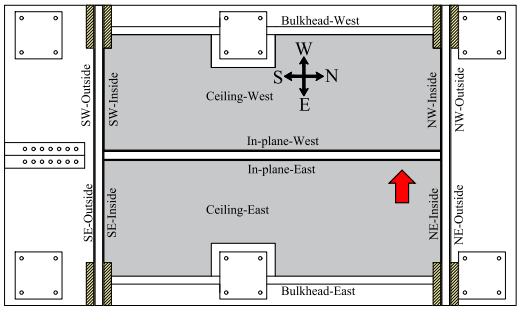	Separation at the corner joint between the ceiling and wall	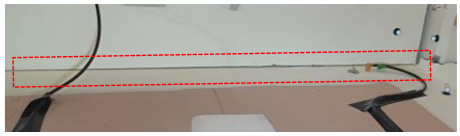
Middle of the East Ceiling 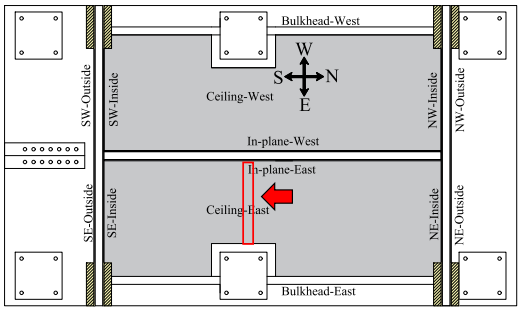	Cracks on the Plaster and Screw Impressions	
Top corner of the SE-Inside wall near its corner joint with the in-plane East wall 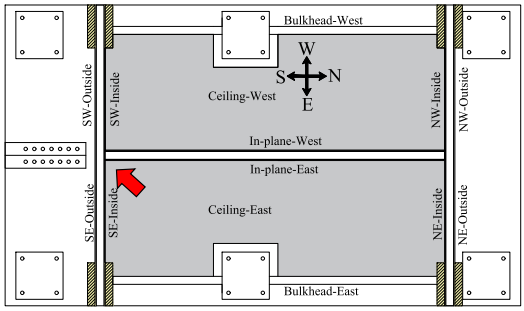	Major cracking and crushing in the plasterboard	
Corner joint interface between the SE-Inside wall and the east ceiling 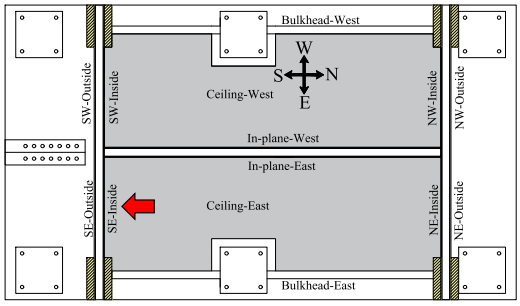	Separation at the corner joint between the ceiling and wall	

Middle of the southern wall (outside), from top to mid-height 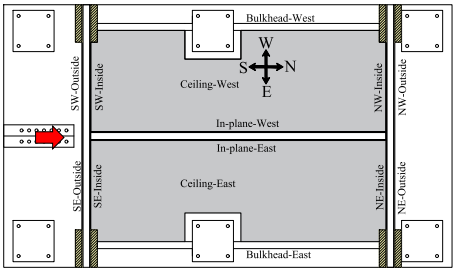	Crack in the plasterboard	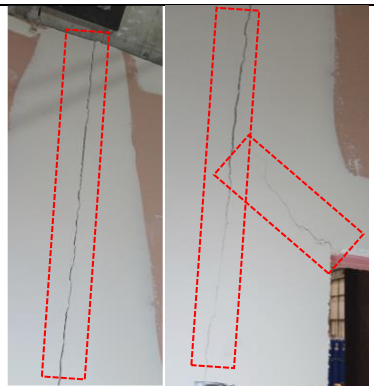
Corner joint interface between the NW-Inside wall and the west ceiling 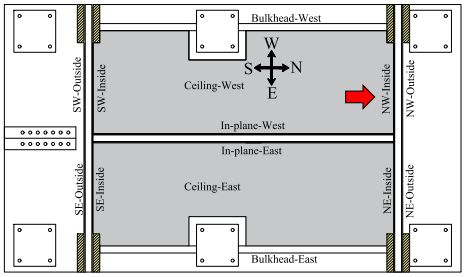	Separation at the corner joint between the ceiling and wall	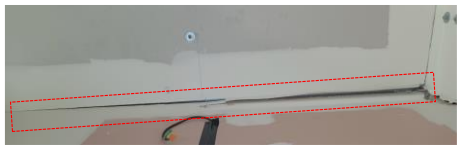
Corner of the NW-inside wall near the joint with the in-plane west wall (from top to middle) 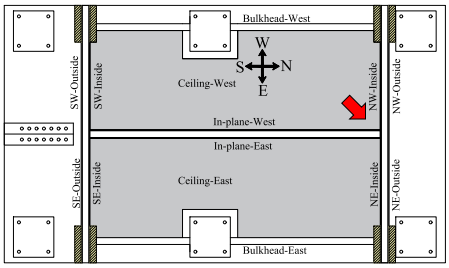	Major Crack in the plasterboard	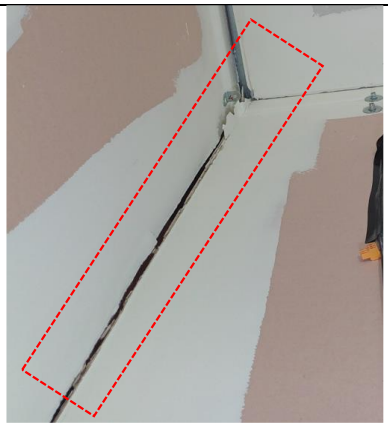
Corner joint interface between the In-plane west wall and the west ceiling 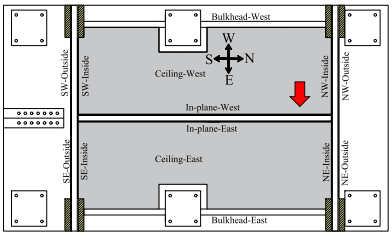	Split in the corner joint paper tape	
Corner joint interface between the SW-Inside wall and the west ceiling 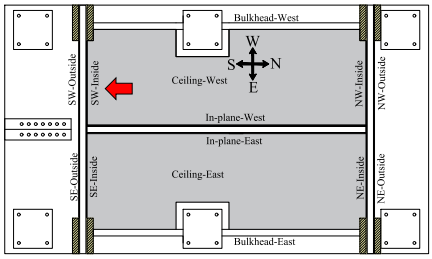	Separation at the corner joint between the ceiling and wall	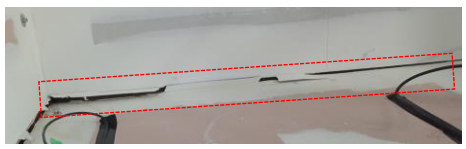

Corner of the SW-inside wall near the joint with the in-plane west wall (from top to middle) 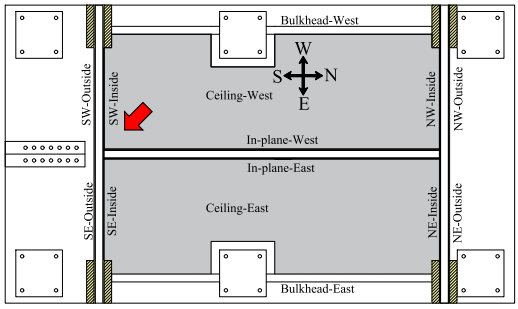	Major Crack in the plasterboard	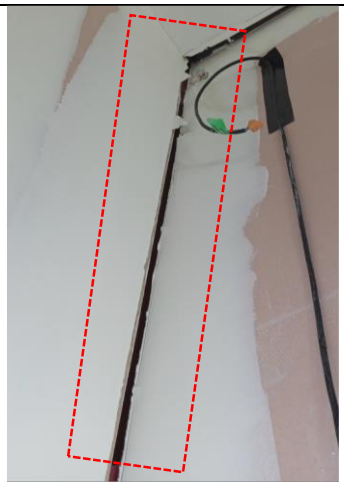
Top corner of the NW inside wall near its corner joint with the west bulkhead and the west ceiling 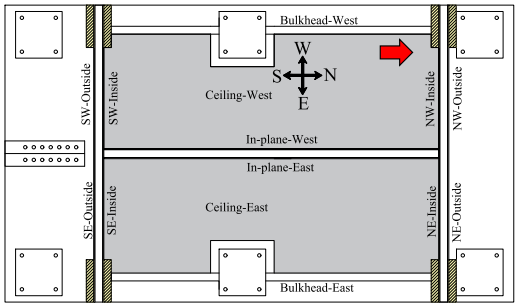	Crack in the plasterboard	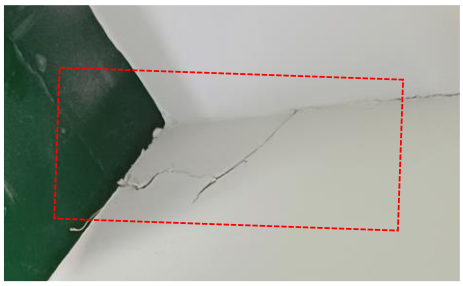
Inside the plenum — joint between the NW-inside wall and the west ceiling 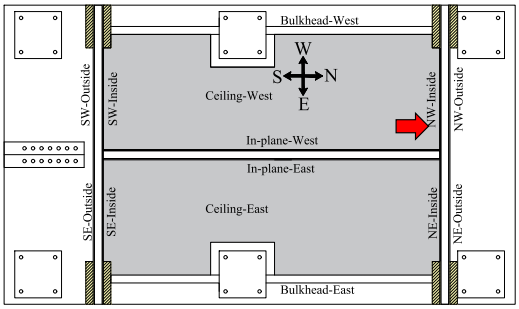	Crumpling at the end of the furring channel (due to inappropriate connection to the wall track)	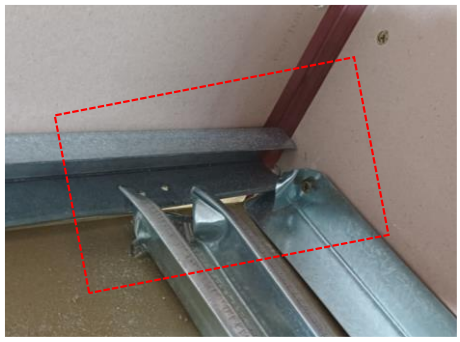
Inside the plenum — joint between the SW-inside wall and the west ceiling 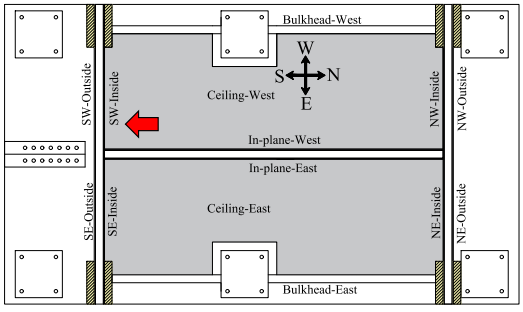	Screw pull-out, detachment and crumpling of the wall track, and localized crushing of the ceiling plasterboard	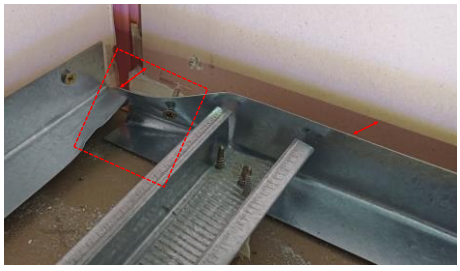

Middle of the northern wall (outside), from top to near the bottom 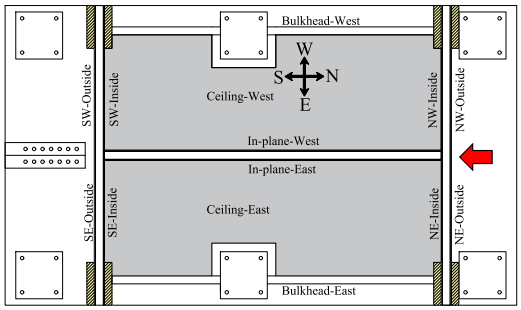	Crack in the plasterboard	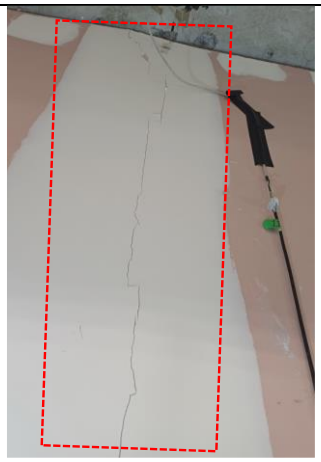
Pipe1-Back Side 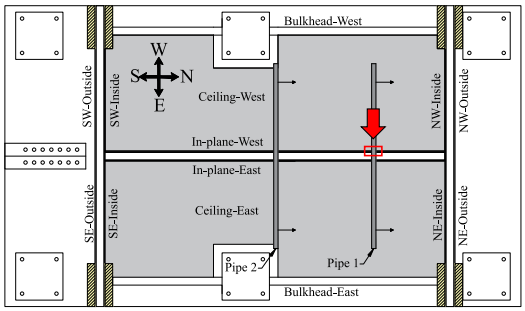	Major Separation (Likely to Compromise Fire-Rating Performance)	

Photos and videos of restrained wall specimens after final Test #16, 2.75 % inter-storey drift

Shaking videos during 2.75 % drift: West Elevation, Southeast Elevation, South Elevation

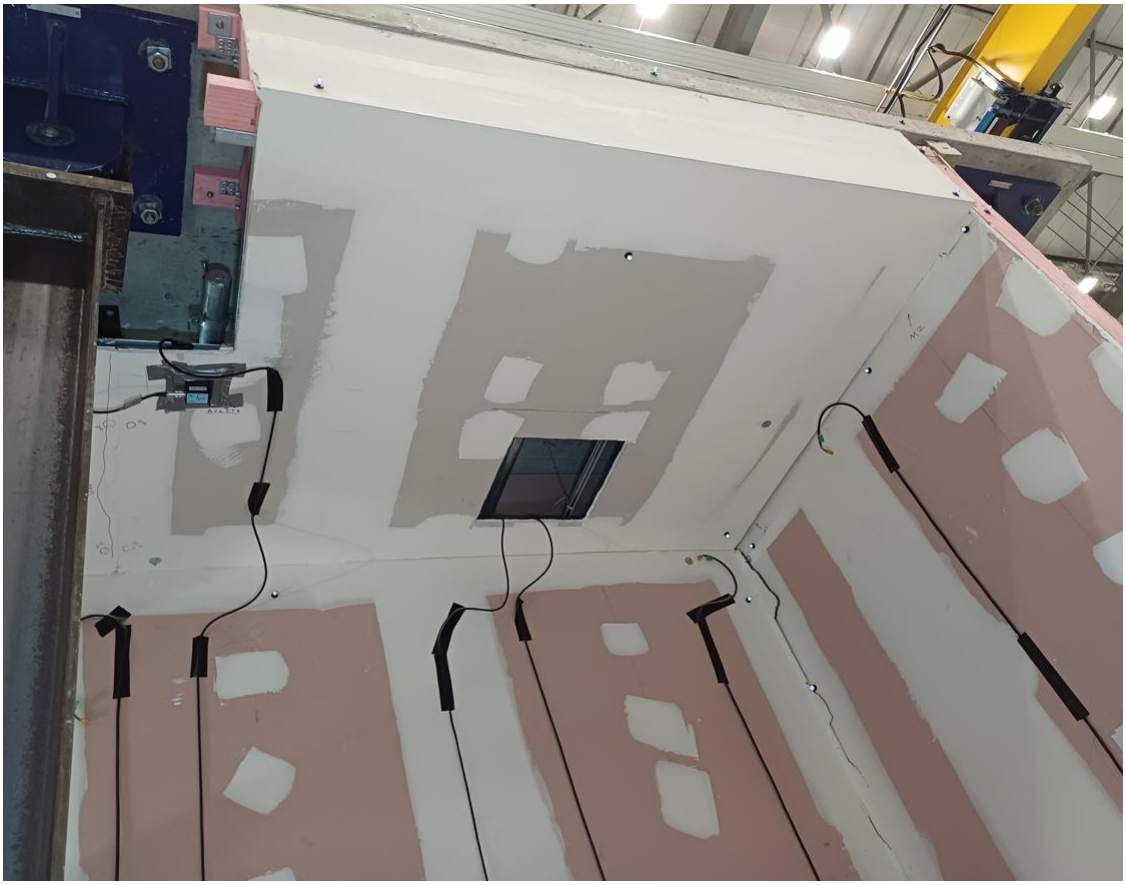

Figure 3.51. Northeast Elevation (looking at East Ceiling)

Figure 3.52. Southeast Elevation (looking at East Ceiling)

Figure 3.53. South elevation

Figure 3.54. West Elevation

PHASE III: SEISMIC PERFORMANCE OF "ROCKING" PARTITION WALL WITH "FULLY FLOATING" SUSPENDED CEILING

ABSTRACT

This chapter presents an experimental investigation into the seismic performance of three critical non-structural components: a damage-concentrated "rocking" timber-framed wall system, a fully floating plasterboard ceiling with perimeter isolation, and unbraced mechanical pipes. The investigation advances two concepts from prior research: extending the validated "rocking" wall design from steel to timber framing and evaluating the dynamic performance of a fully floating plasterboard ceiling for the first time. A series of dynamic tests subjected full-scale specimens to sequential ground motions on a shake table, with a complementary modified series examining configurations without sealant or isolation foam.

The primary aim of this full-scale test is to assess the combined behaviour of this proposed resilient assembly and to quantify the dynamic amplification effects within the system. The "rocking" wall system successfully concentrated damage within sacrificial sealant joints, protecting the wall, though the intended kinematic rocking was impeded by premature yielding of a steel angle connection. The fully floating ceiling demonstrated exceptional resilience, with the isolation foam proving critical for performance; its measured dynamic amplification was significantly higher than code assumptions for traditional ceilings. Unbraced pipes exhibited a consistent failure mode of sealant detachment at wall penetrations, compromising fire integrity.

A key outcome is the evaluation of current code provisions. The experimental median

component amplification (PCA/PFA) factors were compared to values in SNZ TS 1170.5 (2025) and ASCE/SEI 7-22 (2022). The New Zealand standard generally provided conservative estimates, contingent on the selected ductility factors. In contrast, the corresponding ASCE/SEI 7-22 (2022) provisions were unconservative, particularly for the novel ceiling system. These findings highlight a need for updated design guidelines that account for the dynamic behaviour particularly of novel fully floating ceilings. The study provides a foundational dataset for developing fragility functions and outlines essential future work.

DESIGN PHILOSOPHY OF "ROCKING" PARTITION WALLS

The drift capacity of "rocking" partition walls is achieved through a horizontal joint at the top of the wall, featuring a vertical gap (a) within a Dual-Slot Track (DST). The DST is formed by connecting two tracks to create slots for studs and plasterboards. Steel/aluminium angles at the DST ends prevent premature load transfer to the plasterboard from adjacent elements, instead directing forces to the end-studs to induce rocking during top-slab movement.

The system's behaviour depends on the joint material between plasterboards. With a rigid joint, the entire wall rocks as a unit, giving a drift capacity $\delta = (a\ /\ L) \times 100\%$,

where L is the total wall length.

If a flexible joint is used, adjacent walls, rock independently, with an increased drift capacity. Some joints, like the Sacrificial L-trim (SLT) used in (Bhatta, Dhakal, & Sullivan, 2023b), initially behave rigidly, allowing the full wall to rock undamaged up to a certain drift demand (for example: serviceability-level drift). After the joint fails under diagonal forces, behaviour shifts to independent rocking of walls adjacent to the joints,

limiting damage to joint tearing rather than panel crushing until the gap closes. This two-stage response allows damage to be controlled across limit states. Further details are provided in (Bhatta, Dhakal, & Sullivan, 2023a, 2023b; Bhatta & Dhakal, 2026).

EXPERIMENTAL PROGRAMME AND METHODOLOGY

Test Setup

The test setup for this phase remained consistent with that established in Phase I. For a comprehensive description of the test-setup configuration, please refer to the relevant section in the Phase I.

Specimen design, configurations and details

"Rocking" partition walls

A timber framed 'H' shaped "rocking" wall specimen were constructed between the concrete slabs of the test setup. The major details are as follows:

(1) The timber-framing and the plasterboards are allowed to rock inside the top and bottom Dual Slot Tracks (DSTs) with the vertical gap of 35 mm to 40 mm before the timber studs and plasterboards engage. The DSTs were custom fabricated. They consisted of an outer track measuring 122 mm x 60 mm with a 0.75 mm base metal thickness (BMT) and a nested inner track measuring 92 mm x 70 mm, also with a 0.75 mm BMT.

(2) The DSTs meeting at the in-plane and out-of-plane wall junctions have 15 mm gap between them.

(3) Anchors connecting the DSTs and the slabs are evenly spaced.

(4) The frames are lined with 13 mm GIB FYRELINE plasterboard following GIB EzyBrace® System specification GS2-N (GIB, 2016). However, the plasterboard is not fastened to the DSTs.

(5) 15 mm wide HILTI CP606 sealant is applied throughout the height at the joints between the plasterboards at junctions, in-plane and out-of-plane walls to allow relative shear displacements between adjacent walls,

Figure 4.1 and Figure 4.2 show the layout of the "rocking" partition walls constructed between two slabs, with their elevation provided in Figure 4.3. The wall oriented in the North-South direction, referred to here as the "in-plane" wall, is not mechanically connected to the northern and southern walls oriented in the East-West direction (referred as "out-of-plane" walls) at T-junctions. A 15 mm wide vertical joint gap is provided between the timber-framing (and plasterboard linings) of the in-plane and out-of-plane walls at the junction as shown in Figure 4.2. The schematic diagrams and photos of the top and bottom DSTs are shown in Figure 4.4. A 6 mm thick steel angle is placed near the junctions of the in-plane and out-of-plane walls to avoid the interaction between these walls and allow independent transfer of force to the in-plane wall to initiate the "rocking" mechanism as shown in Figure 4.5. The steel angles are omitted at the ends of the out-of-plane walls as the out-of-plane walls are not expected to undergo significant "rocking" and to clearly the movement of the timber-framing inside the plasterboard linings. The 15 mm wide vertical joint gap was sealed with HILTI CP606 sealant and white painted on the East side of the in-plane wall.

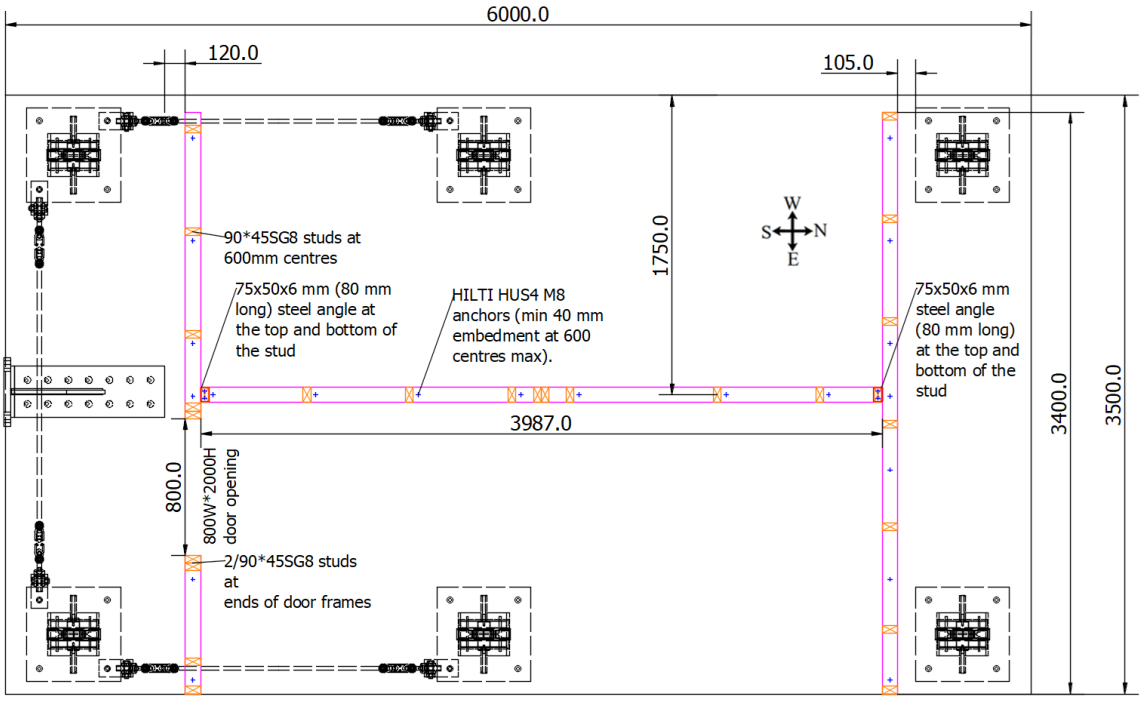

Figure 4.1. Timber framing plan (dimensions in mm)

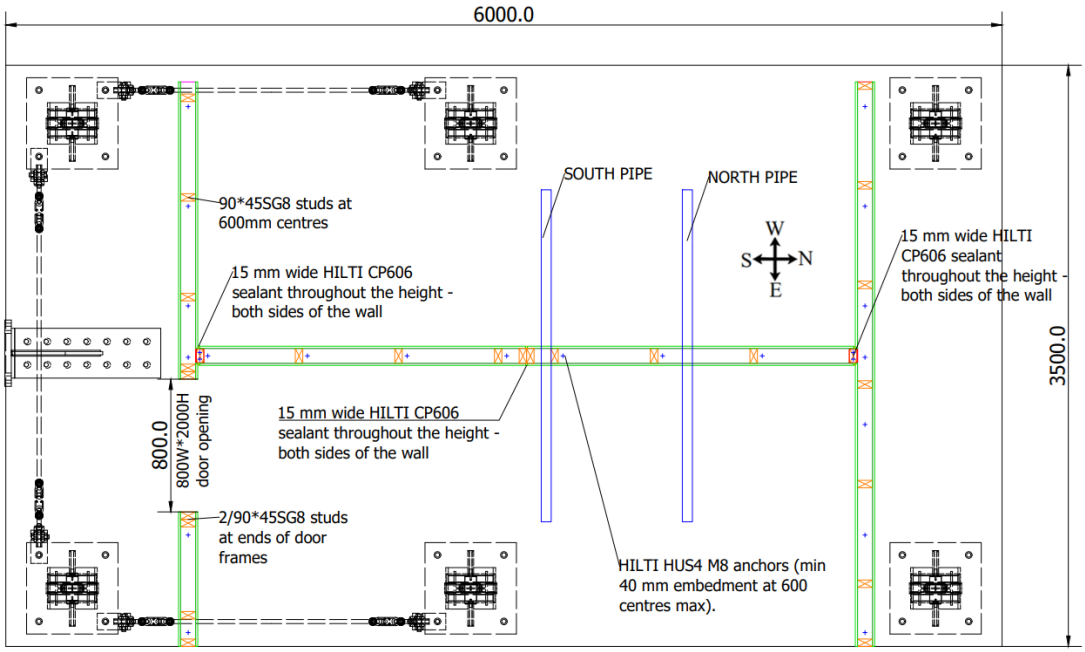

Figure 4.2. Plasterboard lining to timber framing attachment plan with 15 mm sealant joint locations shown (dimensions in mm)

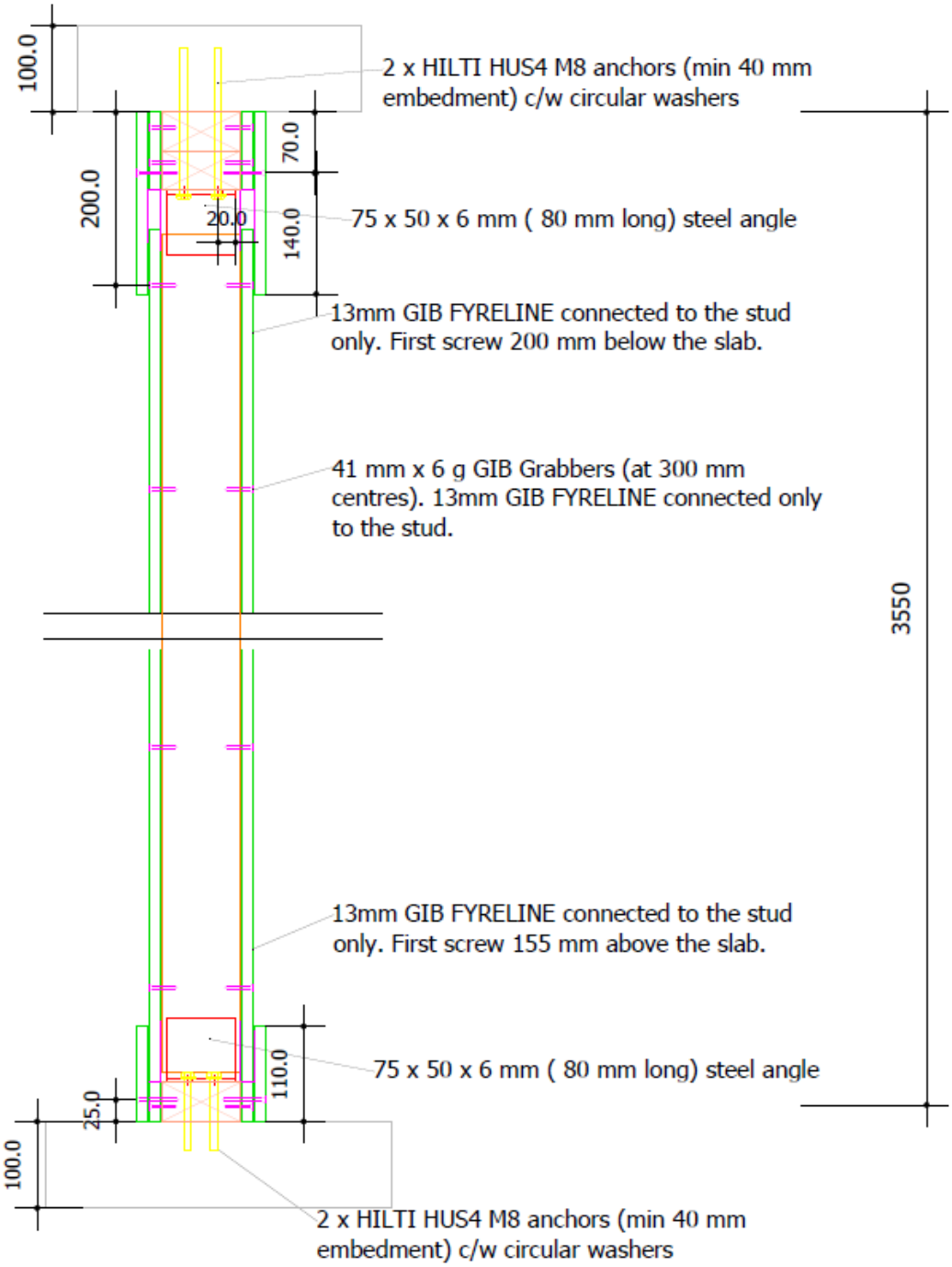

Figure 4.3. Wall section elevation for in-plane and north out-of-plane wall (dimensions in mm)

An 800 mm wide by 2000 mm high door opening was incorporated into the southern out-of-plane wall with similar details as that of Phase II. The elevation detail of the door lintel is shown in Figure 4.6.

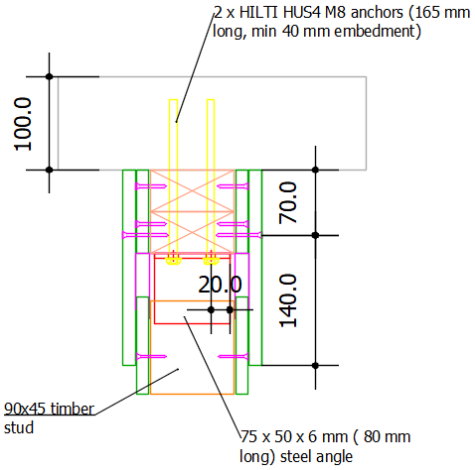

a) At top of North out-of-plane wall

b) Photo at top of North out-of-plane wall

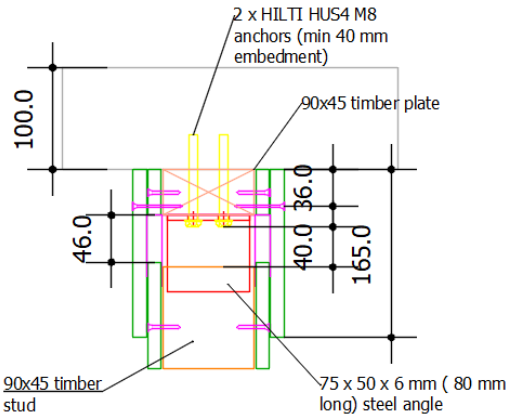

c) At top of South out-of-plane wall

d) Photo at top of South out-of-plane wall

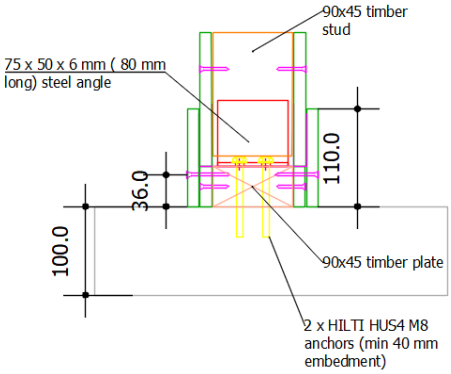

e) At bottom of walls

f) Photo at bottom of walls

Figure 4.4. Schematic diagrams and photos of the dual-slot tracks (DSTs) - steel angles are omitted for out-of-plane walls (dimensions in mm)

Figure 4.5. Steel angle at the wall T-junction

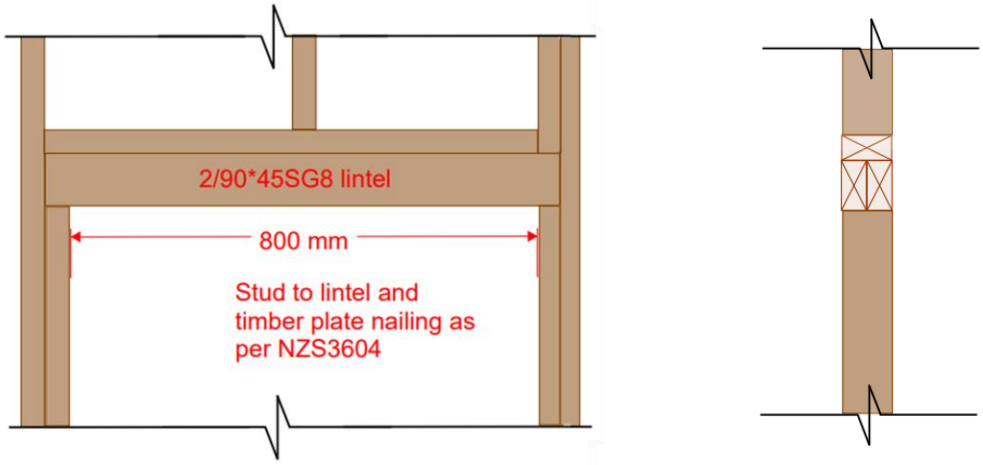

a) Front view b) side view

Figure 4.6. Door lintel elevation detail (similar to Phase II)

Suspended Ceilings

The fully floating plasterboard ceiling was installed within the space defined by the bulkheads and walls shown in Figure 4.7. Two bulkheads were installed on the east and west edges of the top slab to support and conceal the packing foam placed fully floating

ceiling. The elevation of the timber framed bulkheads is illustrated in Figure 4.8. Square inspection holes were placed at four locations to assess damage to the ceiling components.

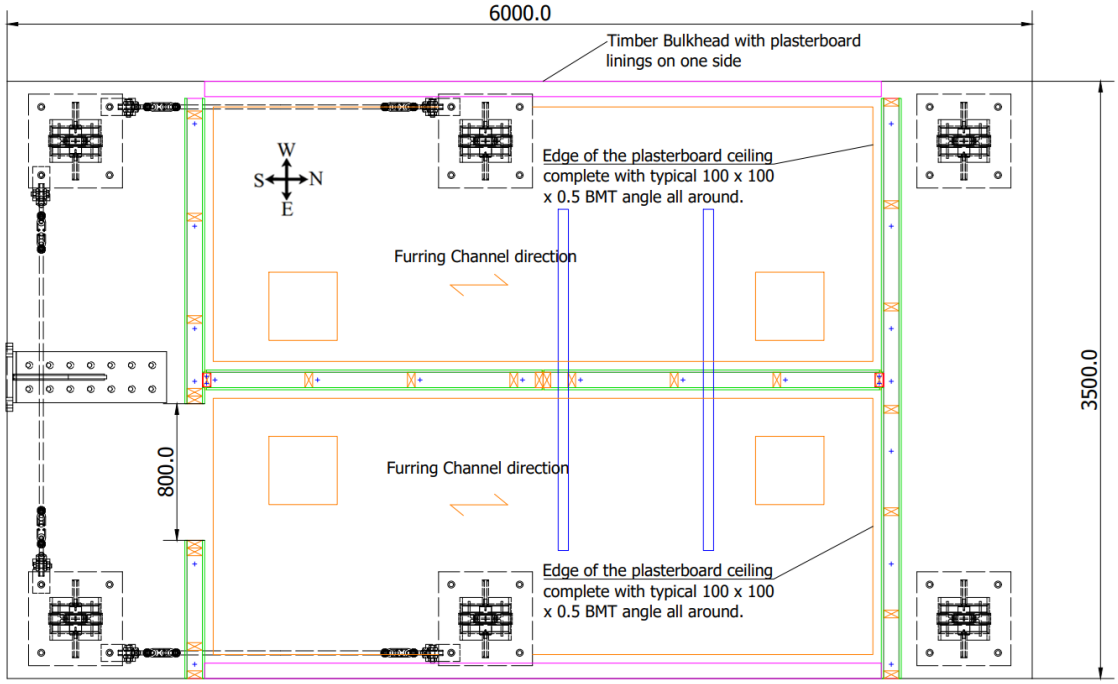

Figure 4.7.Area of ceiling installation with intended perimeter joint details (plan).

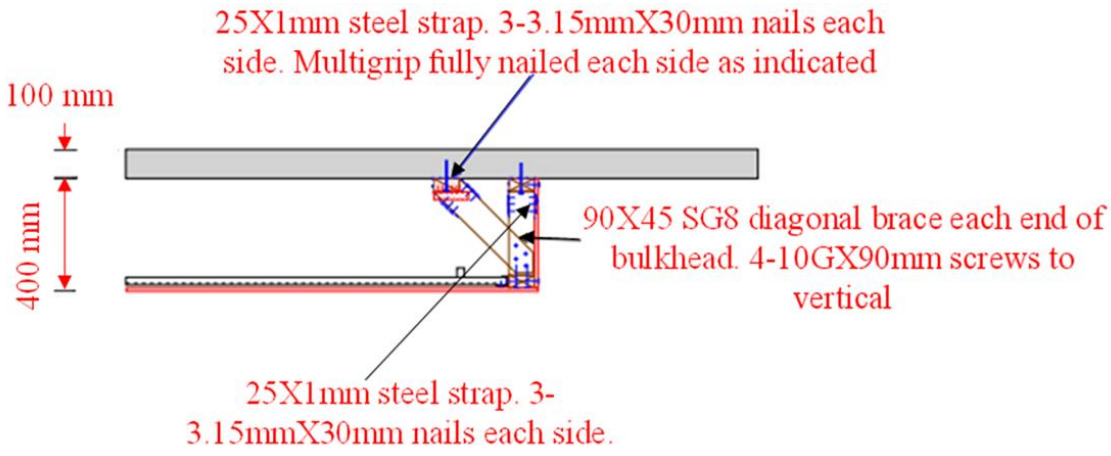

Figure 4.8. Side view of the timber-framed bulkhead (similar to Phase II but without plasterboard lining)

The side view of the edge details of the fully floating ceilings is shown in Figure 4.9. A 90 x 50 mm isolation foam (Packaging foam) was provided, attached to the wall angles using silicone-based glue) all around the ceiling edge between the wall and ceiling edges to absorb impacts during shaking as shown in Figure 4.10. The furring channel

and top-cross rail spacing remain the same as that for Phase II. The TCRs are spaced at 1200 mm centres with furring channels installed at 600 mm centres. however, the plasterboard lining used was 10 mm thick rather than 13 mm used in Phase II. The ceiling was lined with 10 mm GIB Standard plasterboard, which was fixed to the furring channels in compliance with GIB specifications. The plenum height of the ceiling remains the same as Phase II i.e., 400 mm.

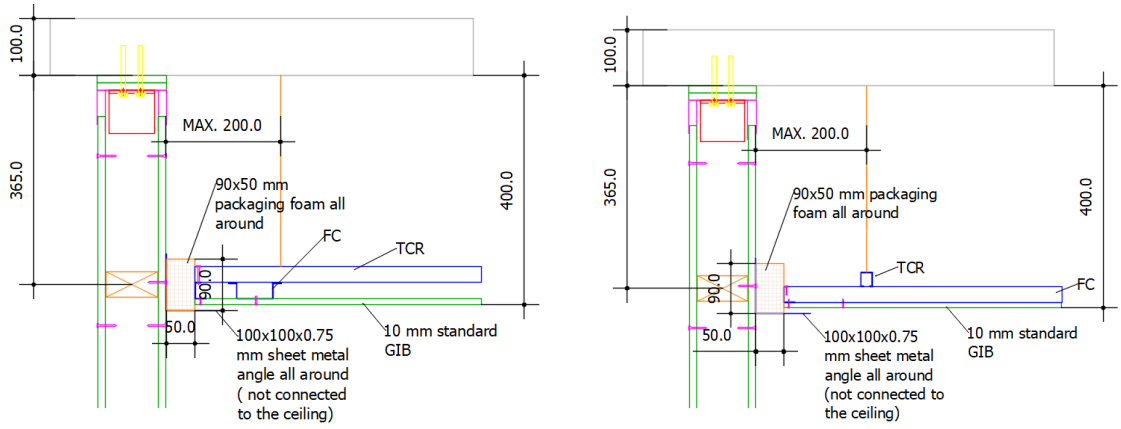

Figure 4.9.Edge details of the fully floating ceilings (side view)

Figure 4.10. Photo of edge of fully floating ceiling with isolation foam

Mechanical pipes

The details of the mechanical pipes remain the same as that of Phase II. To summarize, two 50 mm diameter mechanical pipes (South and North pipe), each approximately 2600 mm long, were installed within the ceiling plenum, passing through the in-plane wall as

shown in Figure 4.7. To increase their mass, additional steel sections were welded onto the pipe ends. An 80 mm clearance hole was created in the wall for each pipe. The pipes supported by M10 threaded rods (as shown in Figure 4.11 (a)) positioned 1 m from the in-plane wall, with their centreline located 240 mm below the top slab. The gap between the pipes and the wall openings was filled with HILTI CP606 sealant, as shown in Figure 4.11(b). Unlike Phase II, the sealant was smoothed flush, as would be typical in actual construction.

a) Pipe supported by M10 threaded hanger rod

b) Pipe penetrating through wall with fire-sealant applied

Figure 4.11.Mechanical pipe details

For the final two tests of the initial series (Tests #17 and #18), the sealant at both the in-plane and out-of-plane wall junctions was deliberately cut to assess its influence. Following the initial test series, further experiments were carried out with modifications to the walls and ceiling details (modified test series):

(1) The sealant in the vertical joints of the walls was cut to examine its effect on the walls' rocking behaviour.

(2) The isolation foam at the edges of the fully floating ceiling was removed to assess its influence on the ceiling's seismic performance and dynamic characteristics.

Photos of the constructed specimen

The photos of the constructed specimen are shown in Figure 4.12 through Figure 4.16.

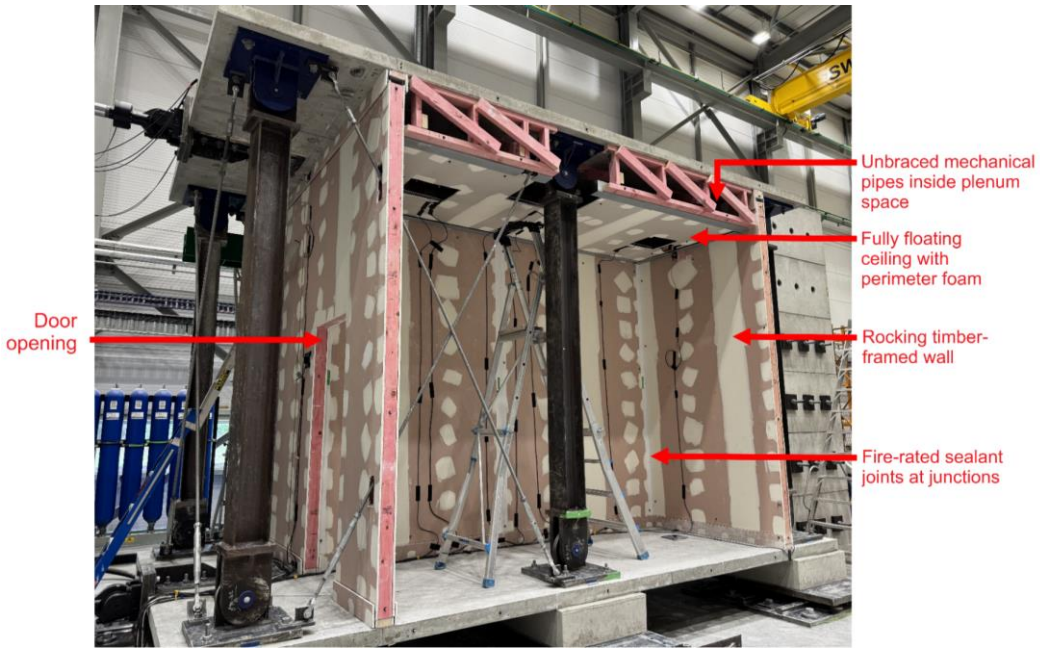

Figure 4.12. Photo of constructed specimen (Southeast elevation)

Figure 4.13. Photo of constructed specimen (East elevation)

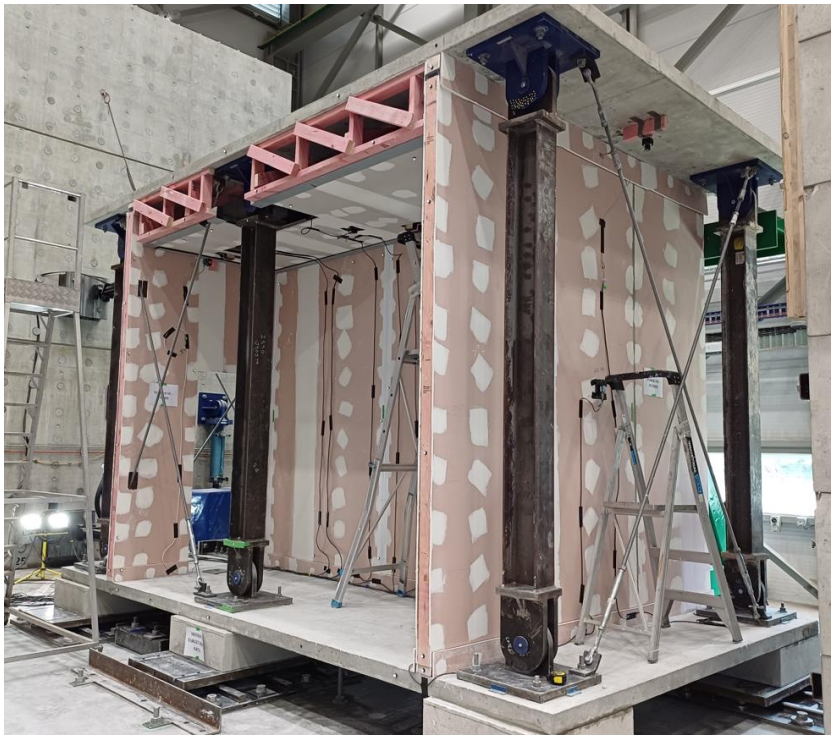

Figure 4.14. Photo of constructed specimen (Northeast elevation)

Figure 4.15. Photo of constructed specimen (South elevation)

Figure 4.16. Photo of constructed specimen inside the ceiling plenum

Loading protocols

For Phase III testing, the same displacement time histories from Phase I and Phase II were applied. To summarize, these "Motion" histories for the 2nd and 3rd floors were derived from a numerical model of a five-storey reinforced concrete structure subjected to the Imperial Valley earthquake record (El Centro, 1940, Array #9) at the peak ground velocities (PGVs) listed in Table 4.2. Refer to (Pledger, 2026) for details. The top and bottom slabs were subjected to the scaled motions presented in Table 4.2. These were generated by applying the scale factors from Table 4.1 to the original displacement histories, a process designed to achieve the target inter-storey drifts specified in Table 4.1.

The resulting spectral floor accelerations, velocities, and displacements for a selected PGV are presented in Figure 4.17, Figure 4.18, and Figure 4.19, respectively. Examples of the input scaled displacement time histories for Motions 5, 10, and 14 are shown in Figure 4.20. The Phase III specimens were tested up to Motion 16, which corresponds to a target inter-storey drift of 2.50% (Table 4.2).

Table 4.1. Input absolute floor motion demands from the 1.0% Design Level structure and corresponding scale factors to achieve the target drift (Pledger, 2026)

Motion	PGV[1] (cm/s)	PFA[2] Bottom slab (g)	PFV[3] Bottom slab (m/s)	PFD[4] Bottom slab (mm)	PFA Top slab (g)	PFV Top slab (m/s)	PFD Top slab (mm)	Target Inter-story drift (%)	Scale factor	Comments
0	10	0.11	0.11	27	0.15	0.15	34	0.03	0.1000	
1	10	0.11	0.11	27	0.15	0.15	34	0.10	0.3571	
2	10	0.11	0.11	27	0.15	0.15	34	0.20	0.7143	
3	10	0.11	0.11	27	0.15	0.15	34	0.30	1.0714	
4	20	0.23	0.22	53	0.31	0.3	67	0.40	0.6897	
5	20	0.23	0.22	53	0.31	0.3	67	0.50	0.8621	
6	20	0.23	0.22	53	0.31	0.3	67	0.60	1.0345	
7	30	0.34	0.33	68	0.39	0.45	88	0.70	0.8235	
8	30	0.34	0.33	68	0.39	0.45	88	0.80	0.9412	
9	30	0.34	0.33	68	0.39	0.45	88	0.90	1.0588	
10	40	0.42	0.42	88	0.5	0.56	113	1.00	0.8850	Motion run two times
11	50	0.51	0.49	114	0.63	0.63	130	1.25	0.9328	
12	70	0.73	0.62	158	0.88	0.76	163	1.50	0.9677	
13	90	0.94	0.8	193	1.13	0.86	196	1.75	0.9563	
14	110	1.19	0.96	233	1.37	0.97	247	2.00	0.8772	
15	110	1.19	0.96	233	1.37	0.97	247	2.25	0.8866	
15a	110	1.19	0.96	233	1.37	0.97	247	2.25	1.1029	Motion run two times
16	130	1.46	1.13	276	1.6	1.17	300	2.50	0.8961	

1Peak Ground Velocity, 2 Peak Floor Acceleration, 3 Peak Floor Velocity, 4 Peak Floor Displacement

Table 4.2. Actual input motions to the test setup (scaled using scale factors from Table 4.1)

Motion	PGV[1] (cm/s)	PFA[2] Bottom slab (g)	PFV[3] Bottom slab (m/s)	PFD[4] Bottom slab (mm)	PFA Top slab (g)	PFV Top slab (m/s)	PFD Top slab (mm)	Target Inter-story drift (%)	Comments
0	1.00	0.02	0.02	3.00	0.02	0.02	4.00	0.03	
1	3.58	0.04	0.04	10.00	0.06	0.06	13.00	0.10	
2	7.15	0.08	0.08	20.00	0.11	0.11	25.00	0.20	
3	10.72	0.12	0.12	29.00	0.17	0.17	37.00	0.30	
4	13.80	0.16	0.16	37.00	0.22	0.21	47.00	0.40	
5	17.25	0.20	0.19	46.00	0.27	0.26	58.00	0.50	
6	20.69	0.24	0.23	55.00	0.33	0.32	70.00	0.60	
7	24.71	0.28	0.28	56.00	0.33	0.38	73.00	0.70	
8	28.24	0.32	0.32	64.00	0.37	0.43	83.00	0.80	
9	31.77	0.36	0.35	72.00	0.42	0.48	94.00	0.90	
10	35.40	0.38	0.38	78.00	0.45	0.50	100.00	1.00	Motion run two times
11	46.65	0.48	0.46	107.00	0.59	0.59	122.00	1.25	
12	67.75	0.71	0.60	153.00	0.86	0.74	158.00	1.50	
13	86.07	0.90	0.77	185.00	1.09	0.83	188.00	1.75	
14	96.50	1.05	0.85	204.39	1.21	0.86	216.67	2.00	
15	97.53	1.06	0.86	206.59	1.22	0.87	219.00	2.25	
15a	121.33	1.32	1.06	256.99	1.52	1.07	272.43	2.25	Motion run two times
16	130.00	1.46	1.13	247.32	1.60	1.17	268.82	2.50	

[1] Peak Ground Velocity [2] Peak Floor Acceleration [3] Peak Floor Velocity [4] Peak Floor Displacement

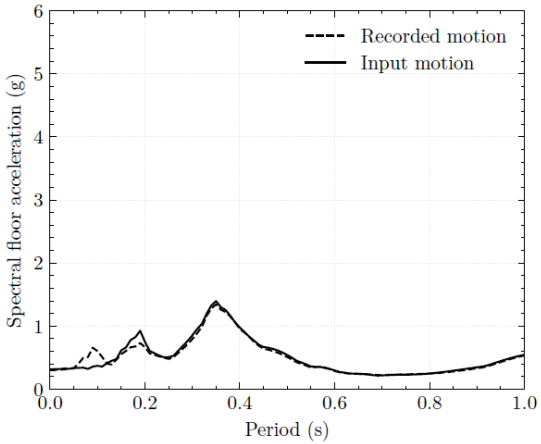

a) PGV = 20 cm/s

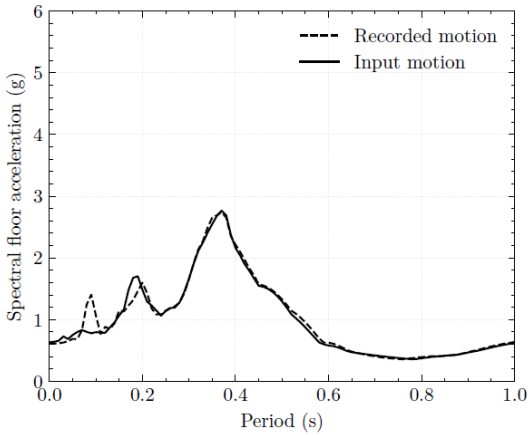

b) PGV = 50 cm/s

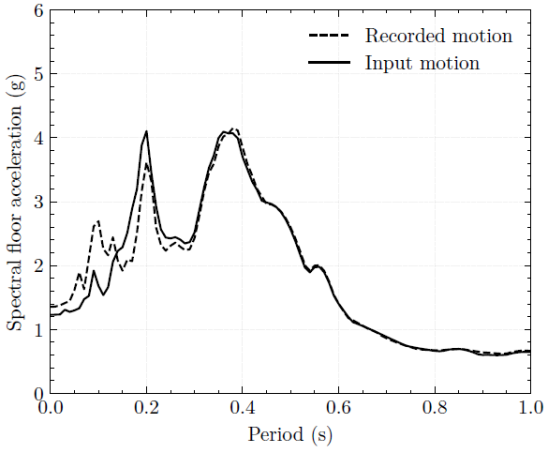

c) PGV = 100 cm/s

Figure 4.17. Spectral floor acceleration for 1.0 % design level structure at different peak ground velocities (PGVs) from Table 4.1 (Pledger, 2026)

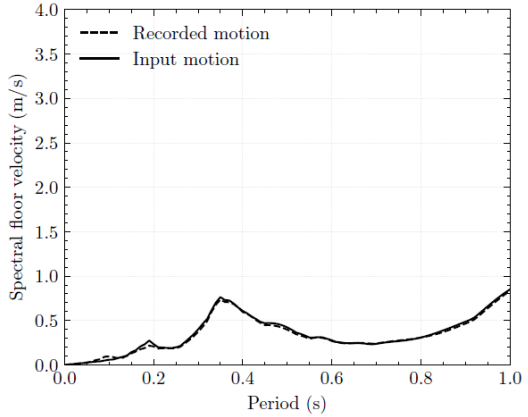

a) PGV = 20 cm/s

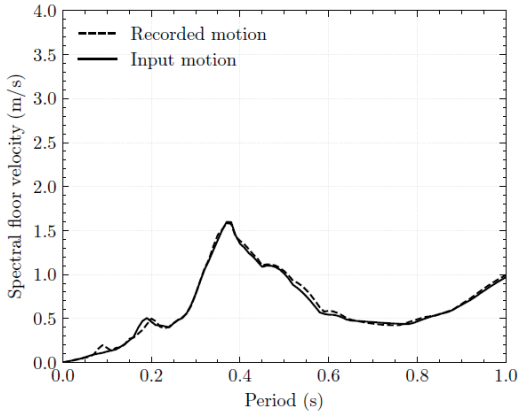

b) PGV = 50 cm/s

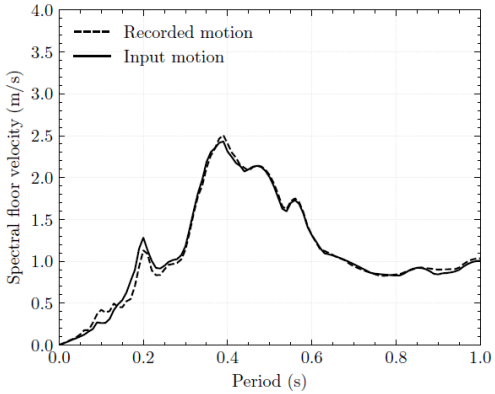

c) PGV = 100 cm/s

Figure 4.18. Spectral floor velocities for 1.0 % design level structure at different peak ground velocities (PGVs) from Table 4.1 (Pledger, 2026)

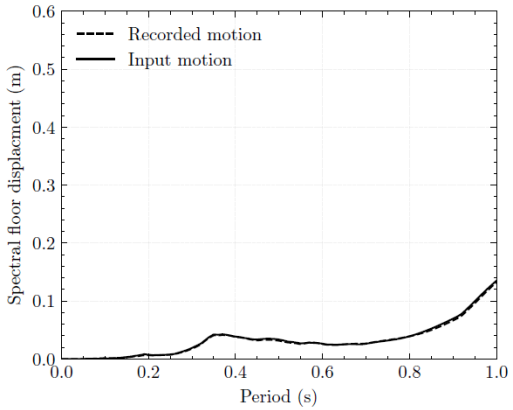

a) PGV = 20 cm/s

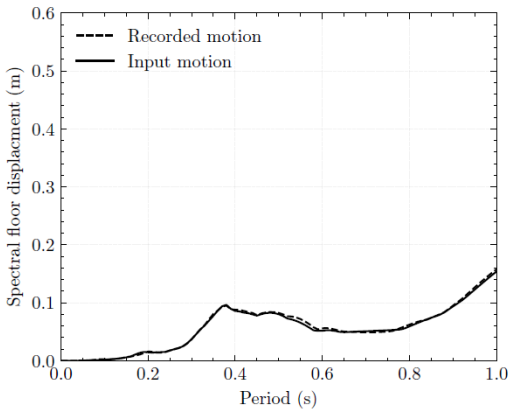

b) PGV = 50 cm/s

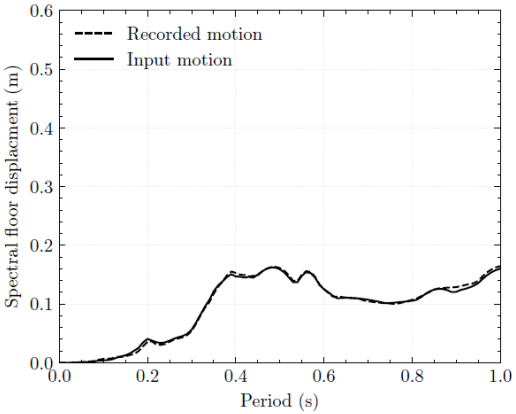

c) PGV = 100 cm/s

Figure 4.19. Spectral floor displacements for 1.0 % design level structure at different peak ground velocities (PGVs) from Table 4.1(Pledger, 2026)

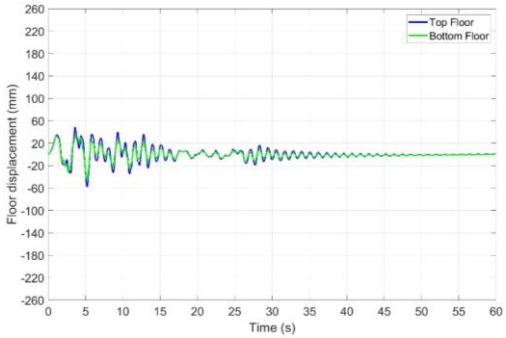

a) Motion 5

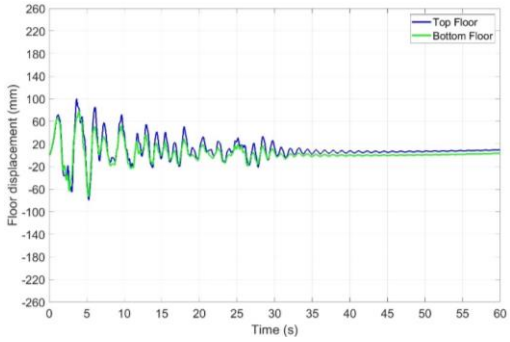

b) Motion 10

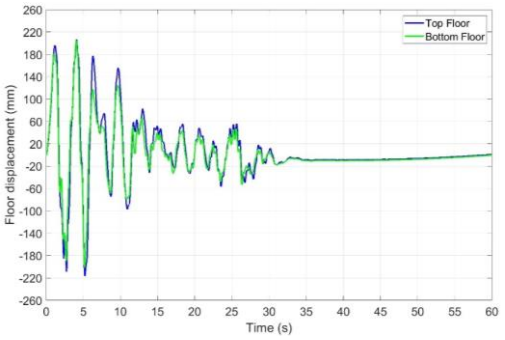

c) Motion 14

Figure 4.20. Floor displacement command time histories of top and bottom slabs during different scaled motions from Table 4.2

Instrumentation

Instrumentation of the structure

The test structure was instrumented with accelerometers placed on the top slab and beneath the bottom slab to record accelerations in the loading direction, i.e., the North–South (NS or X) axis. The accelerometer locations are illustrated in Figure 4.21 and Figure 4.22. The structure was further instrumented with Motion Capture (MoCap) target points (reflective markers) to measure deformations. Five MoCap cameras, positioned facing the east elevation of the test setup, recorded the response during the applied motions.

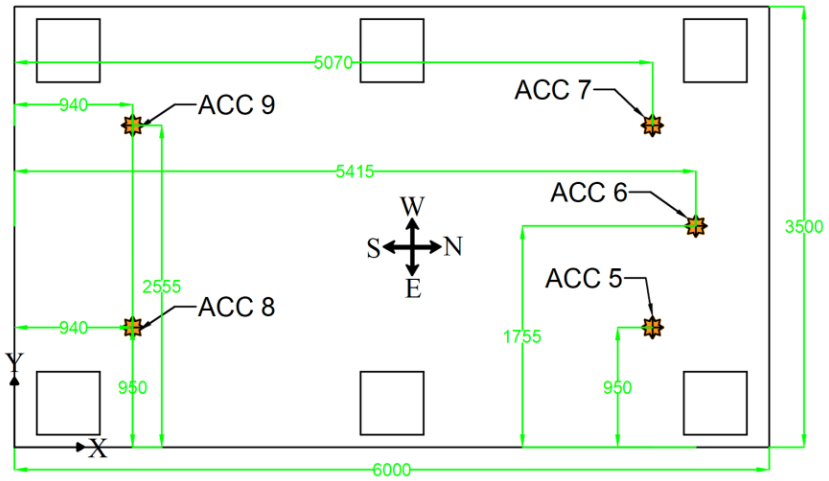

Figure 4.21. Location of accelerometers on top slab (dimensions in mm)

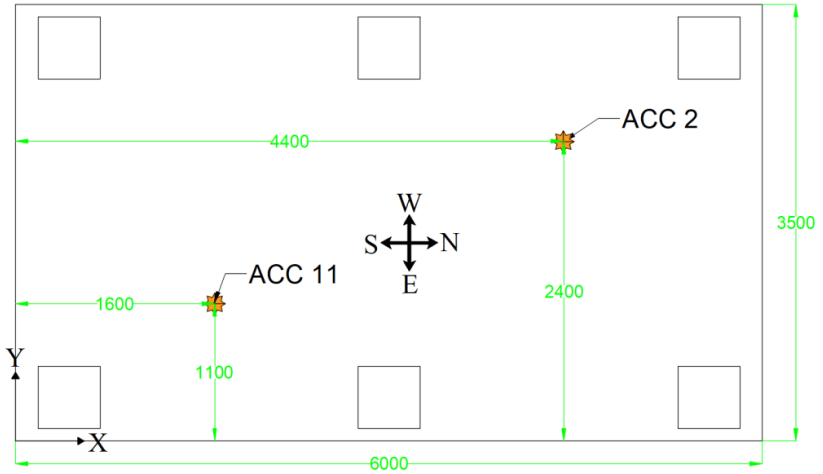

Figure 4.22. Location of accelerometers underneath the bottom slab (dimensions in mm)

Instrumentation of the specimens

The specimens were instrumented using displacement potentiometers, accelerometers and Motion Capture Camera reflectors at key locations as illustrated in Figure 4.23 through Figure 4.27. Go-Pro cameras were also installed in the ceiling plenum.

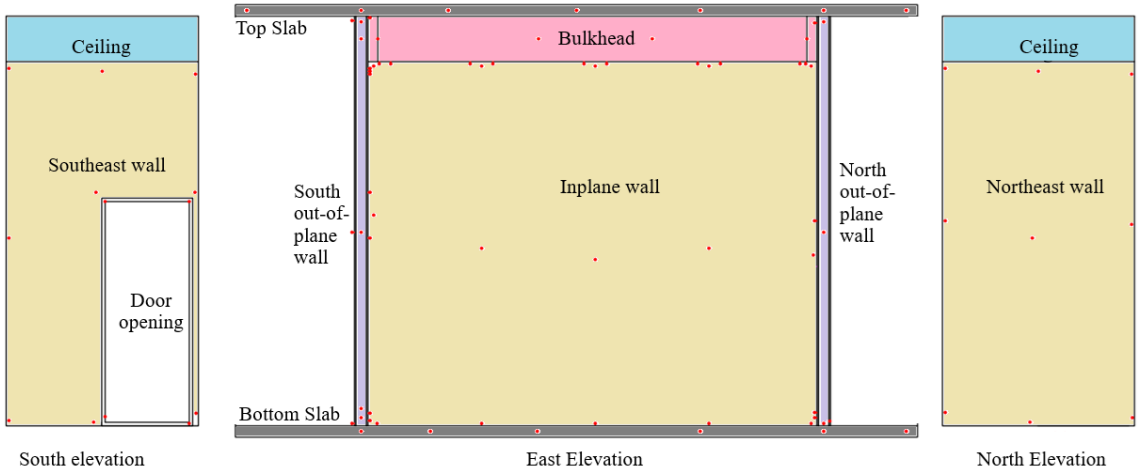

Figure 4.23. Approximate Motion Capture (MoCap) target (reflector) points to record the deformation of the test structure and wall and ceiling specimens

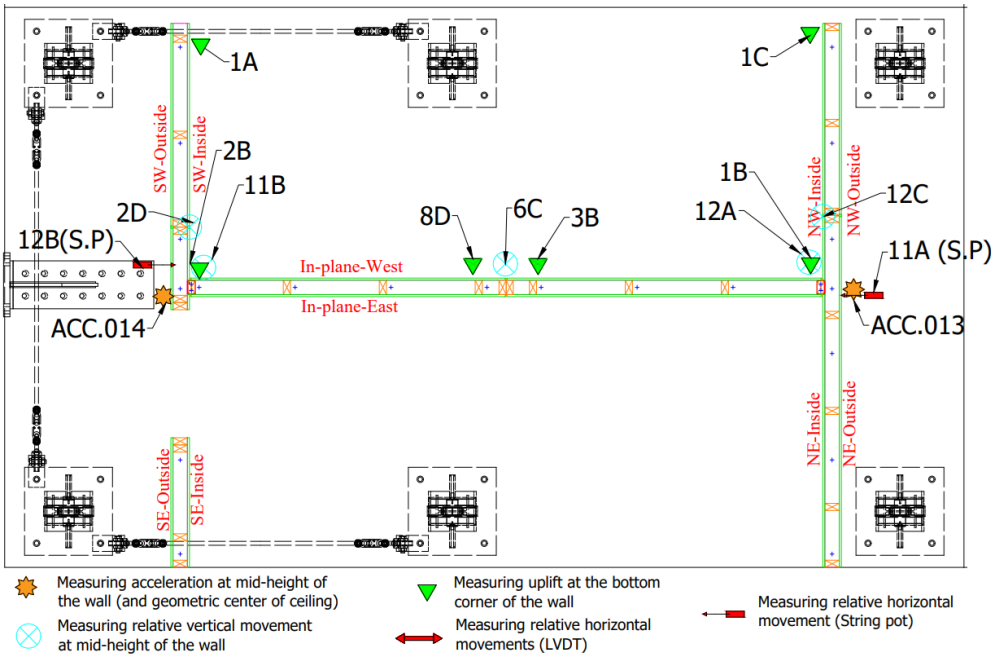

Figure 4.24. Instrumentation plan for walls (Part 1)

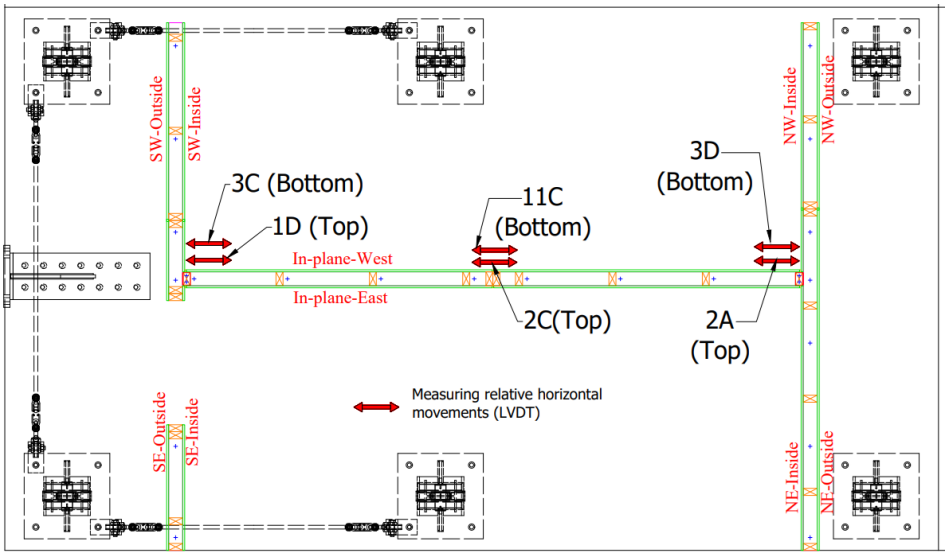

Figure 4.25. Instrumentation plan for walls (Part 2)

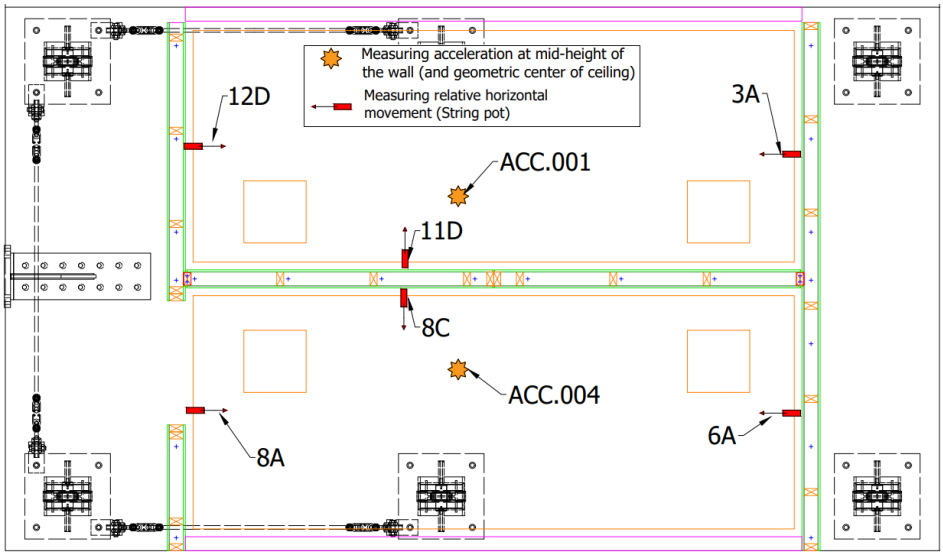

Figure 4.26. Instrumentation plan for fully floating ceilings

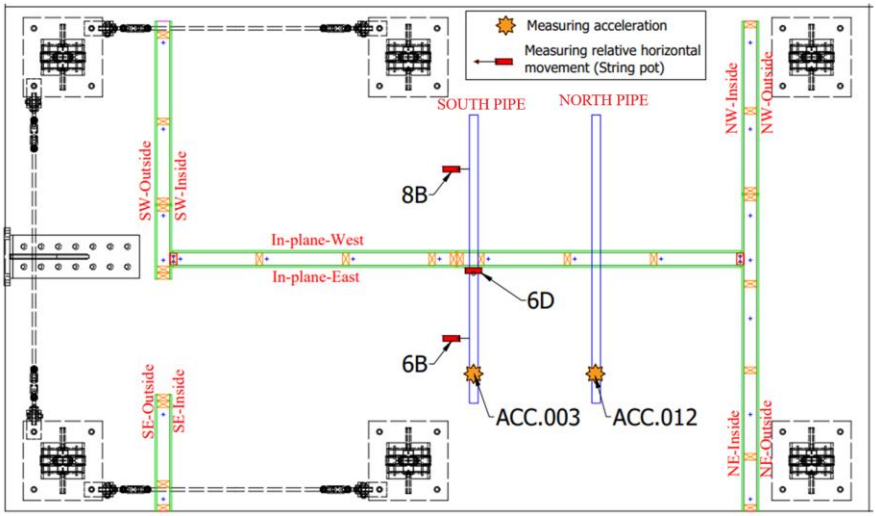

Figure 4.27. Instrumentation plan for pipes

Data processing

The recorded acceleration data were filtered to remove noise. A 4^{th} order low-pass Butterworth filter (Butterworth, 1930; Parks & Burrus, 1987; Sorrentino, 2007) with a cutoff frequency of 50 Hz was applied, using a sampling frequency of 180 Hz. The 50 Hz cutoff was selected to capture local high-frequency responses of the specimens. Furthermore, to address instantaneous impulse peaks in the acceleration readings, a 4^{th} order 1-dimensional median filter was employed for smoothing. This filter replaces each point with the median value within a sliding window of size 4, thereby removing impulse noise while preserving signal edges, with zero-padding applied at the ends. The displacement data were used without postprocessing.

While analysing the data from the experimental sensors, the acceleration responses recorded during Motion 0 are disregarded for both structural and component-level analyses due to their negligible magnitude. Similarly, Motion 0 data is excluded from all structural drift calculations. For component displacement analysis, the data from Motion 0 is included in the plots for completeness but is omitted from discussion, as the measured displacements are considered insignificant.

DAMAGE STATE CLASSIFICATION SCHEME

Four damage states: Superficial, Minor Repair, Moderate Repair and Critical have been defined to classify the damage observed in the test. These discrete damage states are separated based on the repair requirements and impact on the functionality of the non-structural elements.

Superficial

The Superficial damage state includes damage that is primarily aesthetic, meaning it may

not be immediately noticeable, and either does not require repair or only needs minor repair (not immediately). The damage does not impact the seismic performance and functionality of the non-structural element. Some examples include screw impressions, hairline cracks on plasterboard linings, wrinkles in sealants and paints, and bending of wall angle of ceilings.

Minor Repair

The Minor Repair damage state includes damage that does not immediately affect the seismic performance or functionality of the system but should be monitored and addressed during future repairs or routine maintenance. This damage state does not substantially affect the load-bearing capacity, alter the system's alignment, or compromise the non-structural element's ability to remain in place under normal conditions. In some cases, temporary measures can be adopted to limit the spread of damage to other components damage before the actual repairs occur. Some examples include cracks and crushing of plasterboard linings which compromise the fire-rating (or acoustics) and tear in sealants which remain open after earthquakes.

Moderate Repair

The Moderate Repair damage state includes damage that begins to affect its intended performance, but without creating an immediate safety hazard or causing complete loss of function. The system remains largely in place and attached to the structure, posing no immediate risk of falling or obstructing egress. However, the damage requires repair to restore full performance. For example, damage to few internal frame members while the wall remains standing and fully supported by the remaining framing, but the load path has been weakened and requires repair to restore full capacity.

Critical

The Critical damage state includes damage that impairs the seismic performance and/or functionality of the system, resulting in loss of function and demanding urgent repair. Some examples include severe damage to the plasterboard linings, complete separation of walls at junctions (fully reducing the fire-rating) and damage to frames of the walls and ceilings.

EXPERIMENTAL RESULTS

Response of the test structure

Inter-storey drifts

The measured peak inter-storey drifts applied to the test structure are shown in Figure 4.28 as derived from actuator data. Testing proceeded up to a peak drift of 2.65% (achieved in Test #19) for the initial test series configuration with "rocking" walls containing sealant at vertical joints and a fully floating ceiling with isolation foam. For the modified test series configuration with unsealed "rocking" walls and a ceiling without isolation foam, testing continued up to a peak drift of 2.68% (attained in Test #28). For reference, the floor displacement time histories from Tests 11 and 15 are provided in Figure 4.29.

Floor accelerations

The recorded peak floor accelerations, calculated as the average of the maximum in-direction readings from all floors-mounted accelerometers after postprocessing, are presented in Figure 4.30. The top floor consistently exhibited higher maximum horizontal acceleration than the bottom floor in the X direction (loading direction).

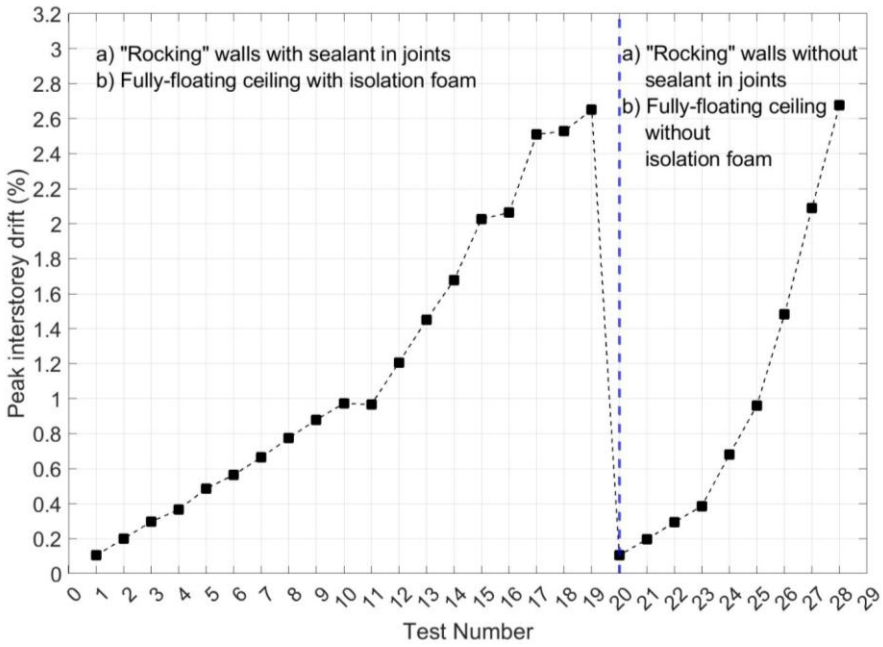

Figure 4.28 Recorded peak inter-storey drifts between floors

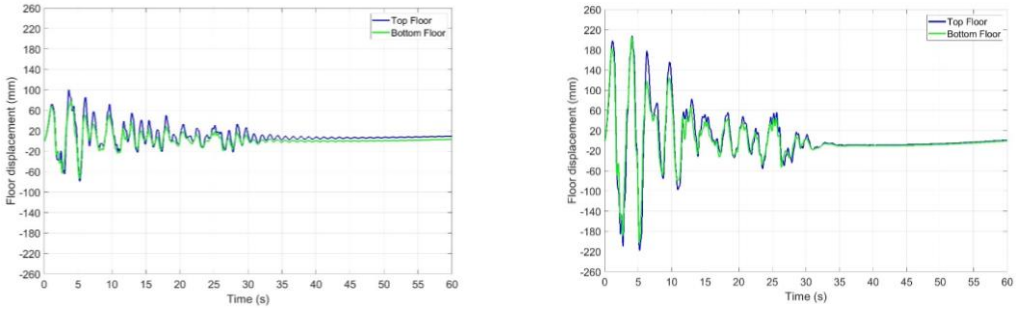

a) Test #11 (Target drift of 1.00 %) b) Test #15 (Target drift of 2.00 %)

Figure 4.29 Recorded lateral floor displacement in the loading direction (X)

During Tests #17 and #18, the peak horizontal accelerations reached 1.51 g on the top floor and 1.05 g on the bottom floor for the initial test series configuration with “rocking” walls containing sealant and a fully floating ceiling with isolation foam. While the peak horizontal accelerations reached 1.32 g on the top floor and 0.92 g on the bottom floor for the modified test series configuration with “rocking” walls not containing sealant at vertical joints and a fully floating ceiling without isolation foam. The acceleration time histories in the X-direction, recorded by the floor-mounted accelerometers and after postprocessing during Test #18, are shown Figure 4.31.

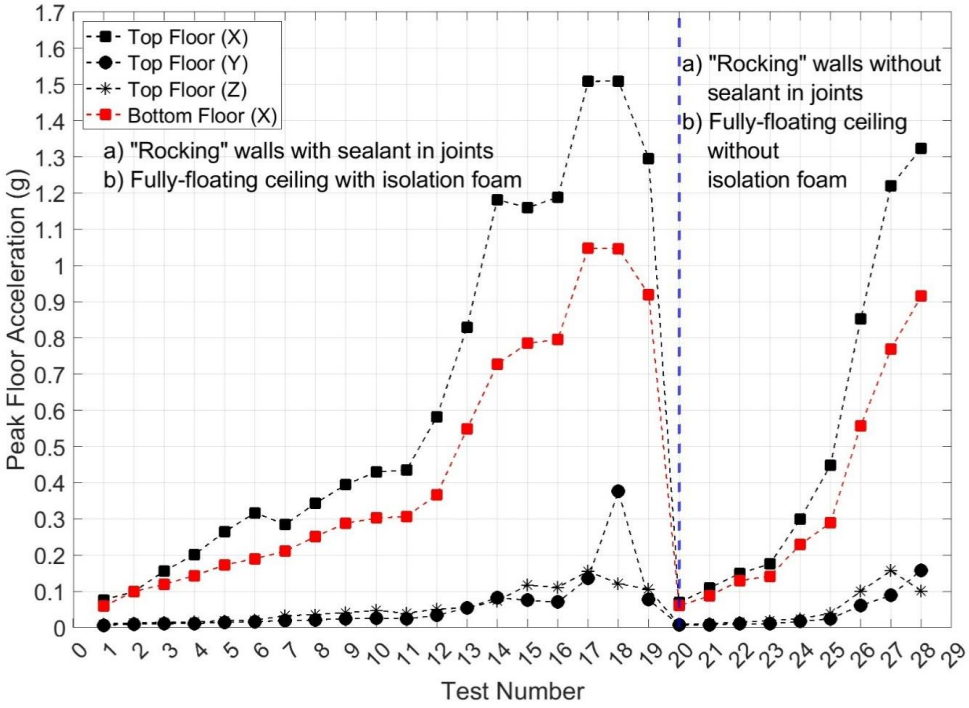

Figure 4.30 Recorded peak floor accelerations with direction shown inside brackets

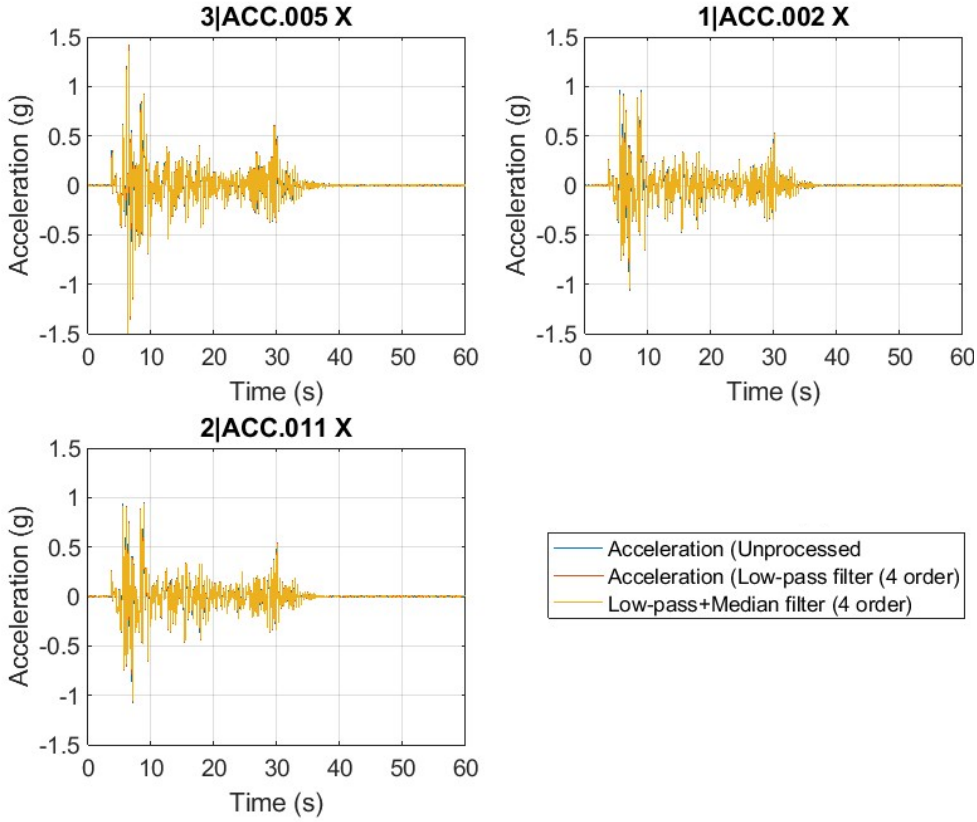

Figure 4.31 Recorded floor accelerations in X-direction (refer to Figure 4.21 and Figure 4.22 for locations of the accelerometers) during Test #18

Lateral forces

The measured peak lateral forces, recorded by the actuators connected to the floor slabs, are presented in Figure 4.32. It can be observed that the lateral force on the bottom floor is higher than that on the top floor, which is attributed to the greater portion of the specimen's mass being transferred downward. The maximum lateral forces recorded on the bottom and top floors were 145 kN and 122 kN, respectively, during Test #18. The variations in the recorded forces correspond to the changes in acceleration shown in Figure 4.31.

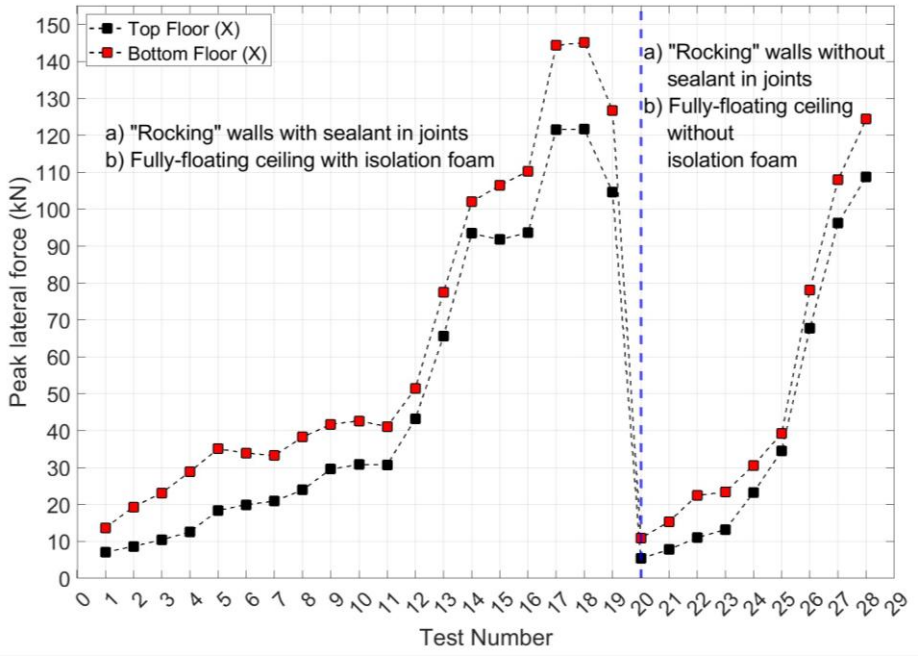

Figure 4.32 Recorded peak lateral forces on the floors

Component response

Damage observation to specimens and their damage state classification

The progression of damage throughout the experimental program is analysed and discussed using the inter-storey drift as the primary engineering demand parameter while peak floor accelerations are provided where relevant. Photographic documentation and

detailed descriptions of the damage observed in the specimens during testing, along with the corresponding inter-storey drift and peak floor acceleration levels at which each damage occurred, are provided in Table *4.5* through Table 4.13 in . Post-test photographs documenting the final condition of all specimens are also provided in **APPENDIX** C**.** Table 4.3 documents the observed damage and its damage state classification for the tested specimens.

"Rocking" timber-framed Walls

Damage to the rocking wall system initiated early and progressed with increasing drift and acceleration. The first signs of distress were cosmetic, appearing as wrinkles in the dried paint over the sealant at the in-plane wall's mid vertical joint during Test #1 (0.1% drift). By Test #5 (0.49% drift), these wrinkles had developed into distinct inclined lines across the sealant. At a drift of 0.56% a very minor tear in the sealant at the top of the southwest wall junction which initially closed after shaking but remained open following Test #10 (0.97% drift) likely compromising the fire-rating of the wall, requiring minor repair. At 1.21% drift a 4 mm localized separation between the sealant and plasterboard lining was observed at the wall junctions. Subsequent tests at higher intensities caused widespread minor tearing in the sealant joints. The most severe damage occurred during Test #17 (2.51% drift, 1.51 g PFA), which resulted in the visible bending of the steel angle at the North wall junction, leading to a bent plasterboard strip and the opening of the wall joint.

Beyond the damage described above, no other failure was observed in the walls. This indicates that damage was successfully concentrated within the sealant joints. Notably, the walls remained free of plasterboard cracking, corner crushing, and screw failures.

Table 4.3. Damage state of the tested specimen and corresponding inter-story drifts after which the damage was observed

Specimen	Damage State	Damage Type	Inter-story drift (%)	Peak Floor Accelerations (g)	Comment/Reference
"Rocking" Timber-framed partition wall	Superficial	Wrinkles in dried paint applied over sealant at wall junctions	0.10	Top: 0.08 g Bottom: 0.06 g	Table *4.5*
	Minor Repair	Very minor tear in the sealant but the tear gap remains open after shake (likely to reduce the fire rating)	0.97	Top: 0.43 g Bottom: 0.30 g	Table 4.8
	Moderate Repair	Bending of the steel angle at the junction is visible at the joint	2.51	Top: 1.51 g Bottom: 1.05 g	Table 4.13
Fully Floating Plasterboard Ceiling	Superficial	Bent in the wall angle at junction	2.03	Top: 1.16 g	Table *4.11*
		Top cross rail lodged inside the isolation foam	2.06	Top: 1.19 g	Table 4.12
Mechanical Pipes (without bracing)	Superficial	-	-	-	Difficult to notice if any
	Minor Repair	Detachment of sealant between pipe and wall at penetration (Likely compromised the Fire-Rating)	0.97	Top: 0.43 g	Table 4.8

Fully floating Plasterboard Ceilings

Damage to the fully floating ceiling was observed at high intensity levels. During Test #15 (1.16 g PFA, 2.03% drift), the wall angle near the Northwest junction was visibly bent leading to aesthetic concern. In the subsequent Test #16 (1.19 g, 2.06% drift), the

top cross rail of the ceiling near the Southwest junction became lodged into the isolation foam isolation material, indicating significant displacement and interaction with the boundary. The absence of any significant failure beyond the superficial damage described underscores the ceiling's superior seismic performance.

Mechanical Pipe

The mechanical pipe penetrations showed a consistent failure mode related to the sealant at the wall interface. The sealant detached from both the South and North pipe penetrations during Tests #10 (0.97% drift, 0.43 g PFA) and Test #12 (1.21% drift, 0.58 g), respectively. This detachment represents a loss of the fire rating around the pipe penetration.

Peak component accelerations and dynamic amplification factors

The recorded peak component accelerations (PCAs) for the tested wall, ceiling, and pipe specimens are briefly discussed in the following analysis. These PCA values are compared with the peak floor accelerations (PFA) at the corresponding attachment levels. From this comparison, the PCA/PFA ratios, or dynamic amplification factors, are derived from the experimental data and subsequently evaluated against the provisions of SNZ TS 1170.5 (2025) and ASCE/SEI 7-22 (2022).

It is important to note that while the accelerations were recorded on specific components, these elements interacted dynamically during testing. Consequently, the measured PCA values, although attributed to a particular specimen, were likely influenced by the behaviour of adjacent and connected elements. The authors contend that this interaction realistically represents conditions in an actual building, where various non-structural elements do not respond in isolation but as part of a coupled system (unless

absolutely detached – such as the case with fully floating ceiling in the absence of pounding between with the surrounding elements).

"Rocking" timber-framed wall specimen

The peak component accelerations (PCA) recorded in the out-of-plane (X) direction at the mid-height of the wall junctions (ACC.014, ACC.013) are plotted against the average of the peak floor accelerations of both floors (PFA) for the initial test series configuration with "rocking" walls containing sealant at vertical joints in Figure 4.33. Accelerometer locations are shown in Figure 4.21, Figure 4.22, and Figure 4.24.

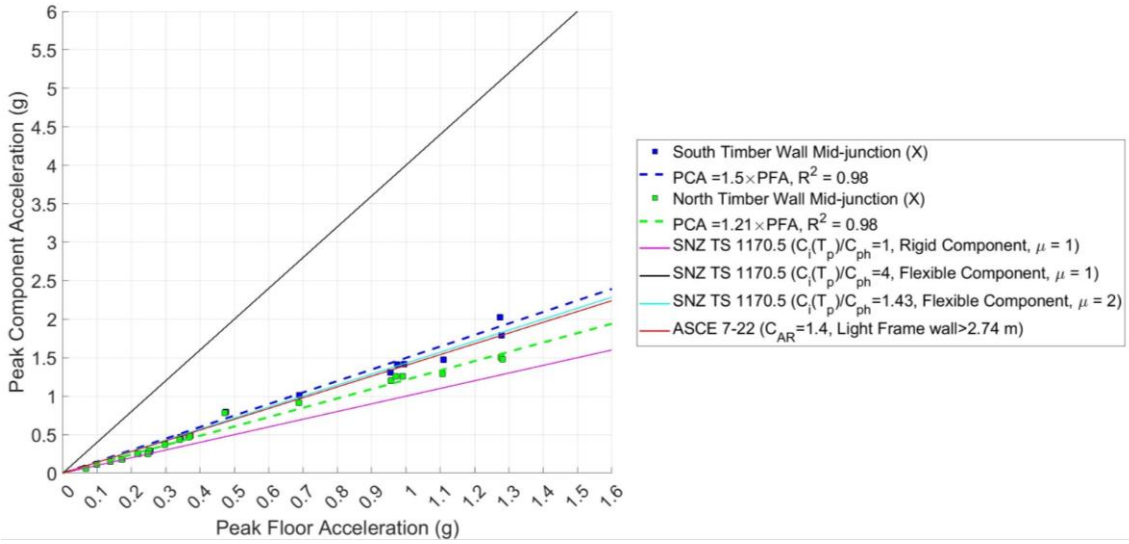

Figure 4.33 Peak accelerations of out-of-plane wall specimens in out-of-plane direction (X) as a function of peak floor acceleration (North and South walls shown separately) for initial test series

Figure 4.33 also presents PCA values calculated by multiplying the average PFA from both top and bottom floors by: (1) the ratio $C_i(T_p)/C_{ph}$ for different ductility levels (μ), per SNZ TS 1170.5 (2025), and (2) the Component Resonance Ductility Factor (C_{AR}) from ASCE/SEI 7-22 (2022). $C_i(T_p)$ is the component spectral-shape coefficient and (C_{ph}) is the component horizontal-response factor. Additionally, a linear fit through the

origin is plotted against the experimental data points. Provided that the walls are of similar details, the experimental data points of the South and North out-of-plane walls are combined into one and presented in Figure 4.34.

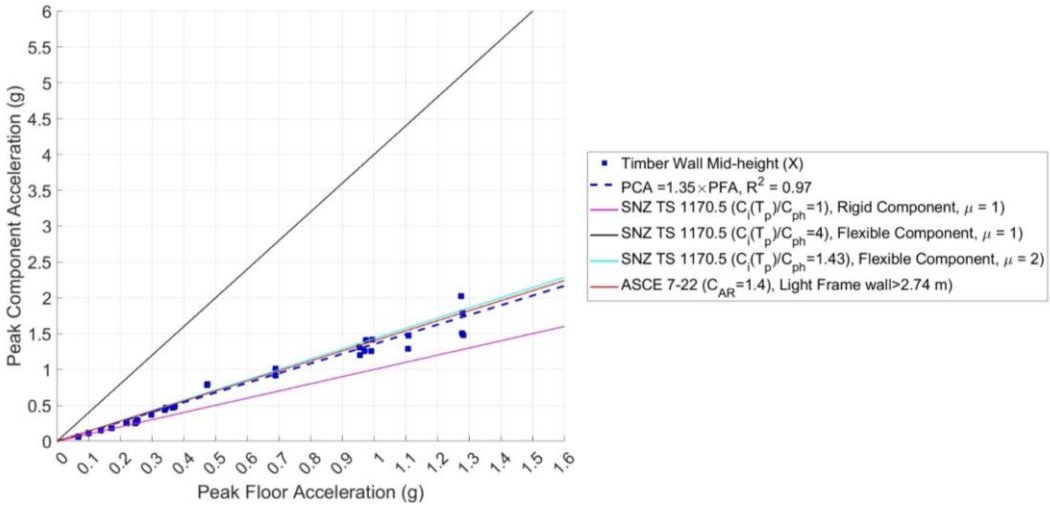

Figure 4.34 Peak accelerations of all out-of-plane wall specimens in out-of-plane direction (X) as a function of peak floor acceleration (North and South walls shown together) for initial test series

Figure 4.34 indicates that the PCA/PFA ratio (i.e., Dynamic Amplification Factors (DAF) inclusive of part ductility (μ)) for the timber-framed walls, as determined by the best-fit line through the origin, is approximately 1.35 with $R^2 = 0.97$. According to SNZ TS 1170.5 (2025), this experimental ratio corresponds to the design cases for a Flexible component with ductility ($2 < \mu < 2.5$). The standard's provision for a Flexible component with $\mu = 2$ provides a close estimate, exceeding the measured ratio by a factor of 1.06. A similarly close estimate is given by ASCE/SEI 7-22 (2022), with a factor of 1.04.

Figure 4.35 plots the PCA/PFA ratio for the walls, calculated by dividing the PCA by the PFA for each floor. The box plot in Figure 4.35 (c) shows a median PCA/PFA value of 1.26 for timber-framed walls which is conservatively estimated by the

recommended values by SNZ TS 1170.5 (2025) for Flexible component with $\mu = 2$ (1.43) and ASCE/SEI 7-22 (2022) (1.40).

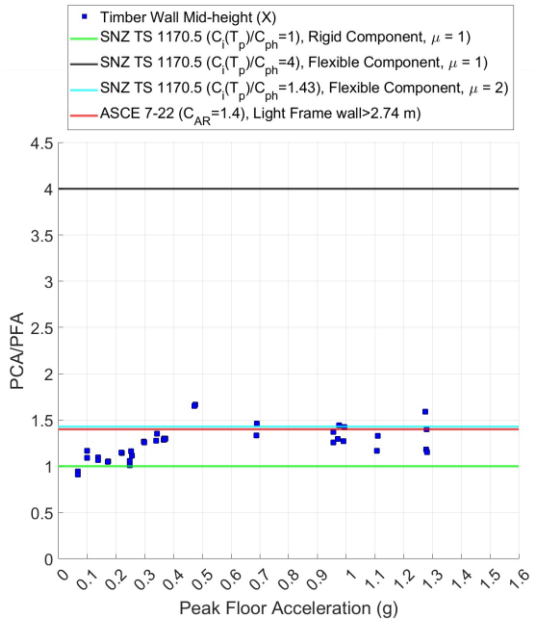

a) PCA/PFA as a function of PFA

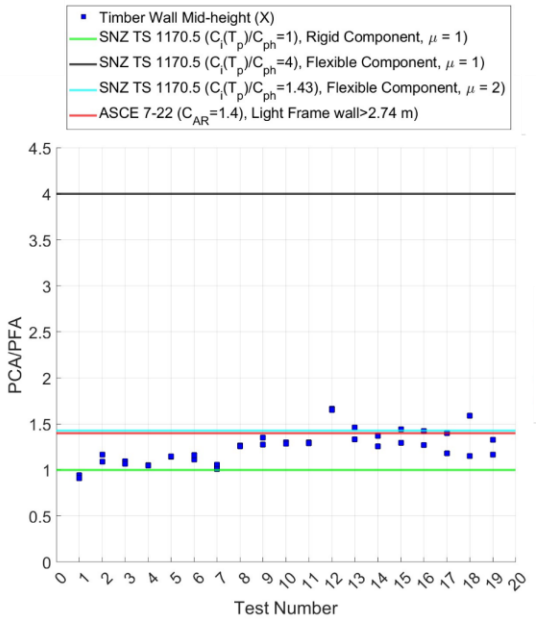

b) PCA/PFA as a function of Test number

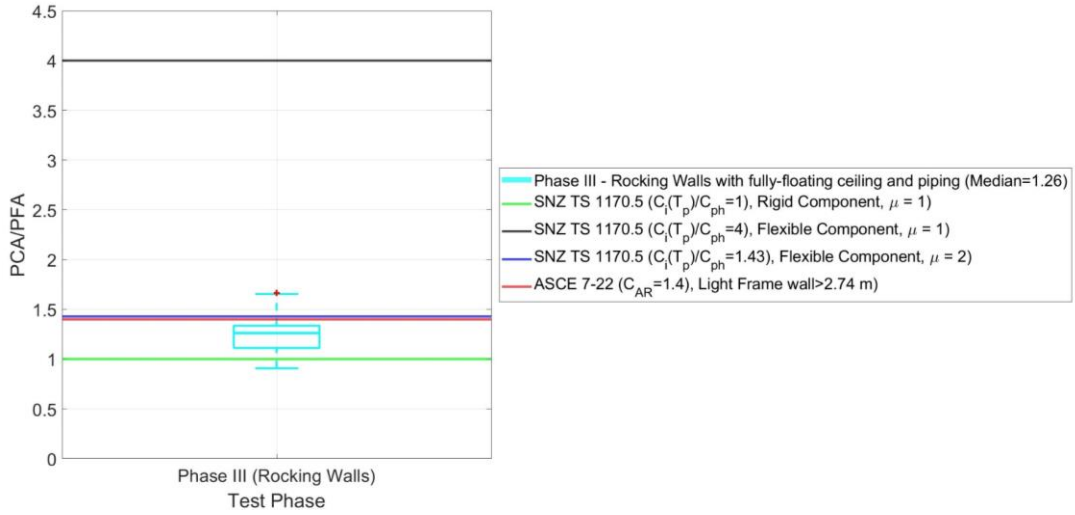

c) PCA/PFA box plot (Median = 1.26)

Figure 4.35 PCA/PFA in the out-of-plane direction (X) for "rocking" timber-framed walls for initial test series

Similar plots for the modified test series, for the configuration with unsealed "rocking" walls at vertical joints, are provided in Figure 4.36 and Figure 4.37. Figure 4.37

shows that the median PCA/PFA value for the unsealed “rocking” wall is 1.55, approximately 1.25 times greater than the value for the sealed configuration.

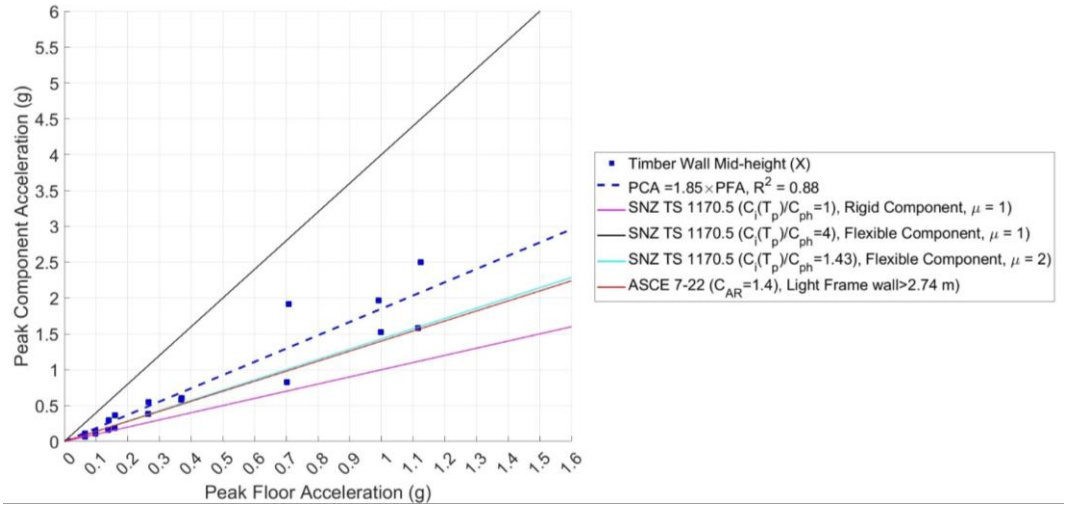

Figure 4.36 Peak accelerations of all out-of-plane wall specimens in out-of-plane direction (X) as a function of peak floor acceleration (North and South walls shown together) for modified test series

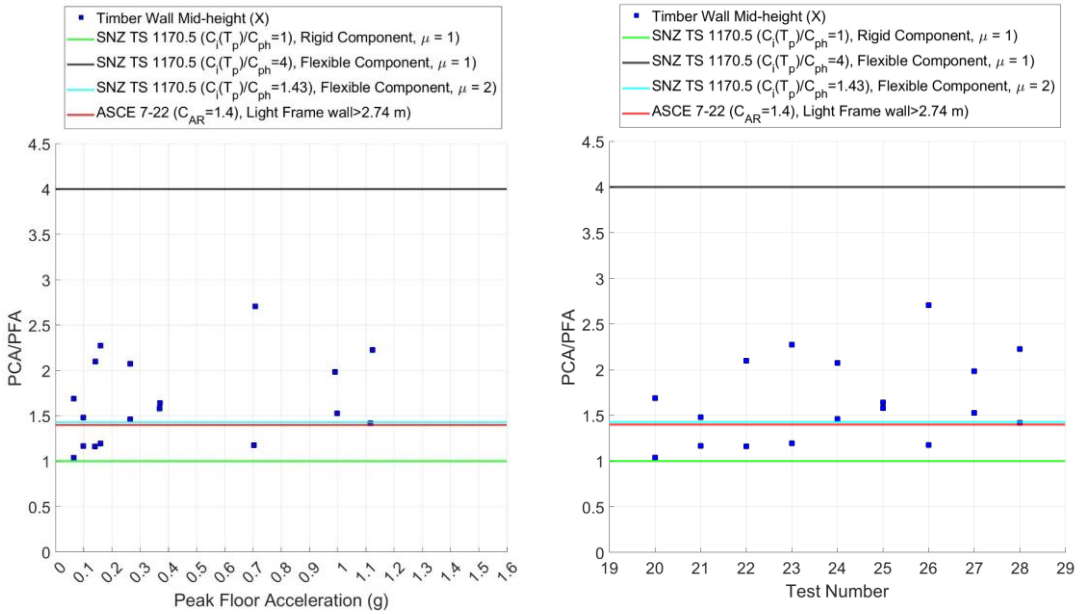

a) PCA/PFA as a function of PFA b) PCA/PFA as a function of Test number

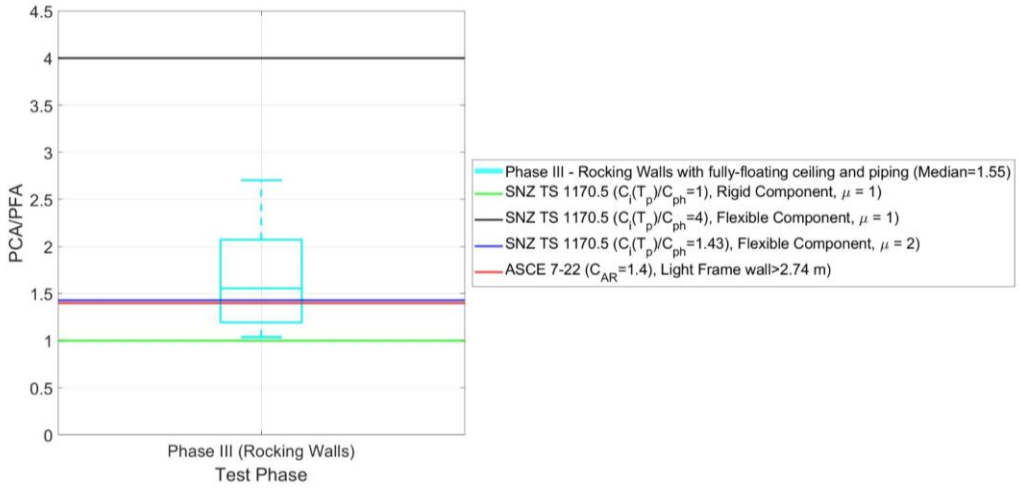

c) PCA/PFA box plot (Median = 1.55)

Figure 4.37 PCA/PFA in the out-of-plane direction (X) for "rocking" timber-framed walls for modified test series

Fully floating plasterboard ceiling

The peak component accelerations (PCA) recorded in the out-of-plane (X) direction located approximately at the geometric centre of the ceilings (attached to the plasterboard) (ACC.001, ACC.004) are plotted against the peak floor accelerations of top floors (PFA) for the initial test series configuration with fully floating ceiling with isolation foam all around the edges in Figure 4.38. Accelerometer locations are shown in Figure 4.21 and Figure 4.26.

Figure 4.38 also presents PCA values calculated by multiplying the PFA from the top floor by: (1) the ratio $C_i(T_p)/C_{ph}$ for different ductility levels (μ), per SNZ TS 1170.5 (2025), and (2) the Component Resonance Ductility Factor (C_{AR}) from ASCE/SEI 7-22 (2022). $C_i(T_p)$ is the component spectral-shape coefficient and (C_{ph}) is the component horizontal-response factor. Additionally, a linear fit through the origin is plotted against the experimental data points. The experimental data plots of PCA as a function of PFA

for both the East and West ceiling specimens were merged to derive a single, representative linear fit for PCA as a function of PFA as shown in Figure 4.39.

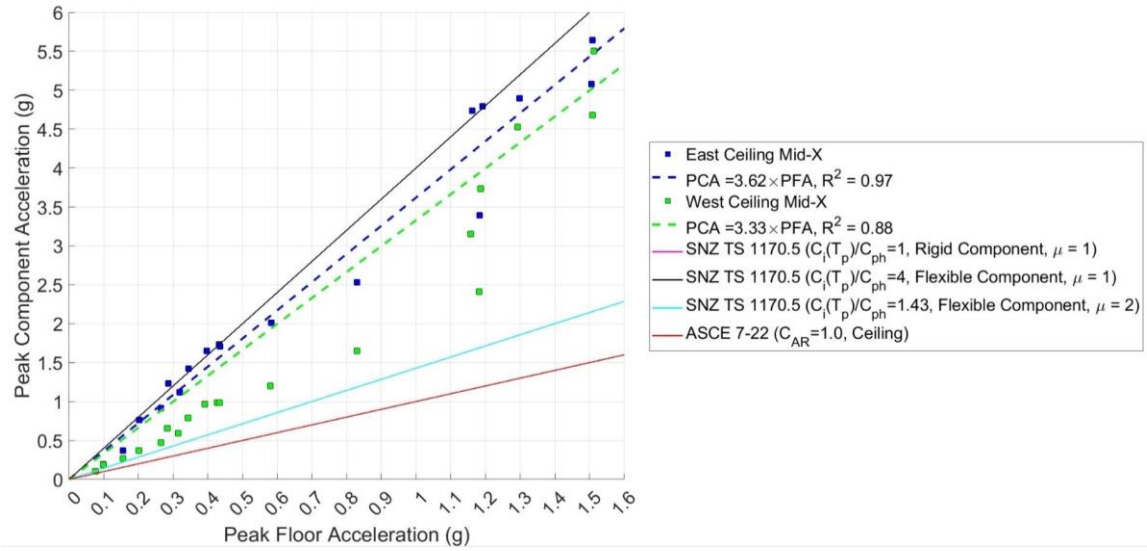

Figure 4.38 Peak accelerations of fully floating plasterboard ceiling specimens in loading direction (X) as a function of peak floor acceleration (West and East ceiling shown separately) for initial test series

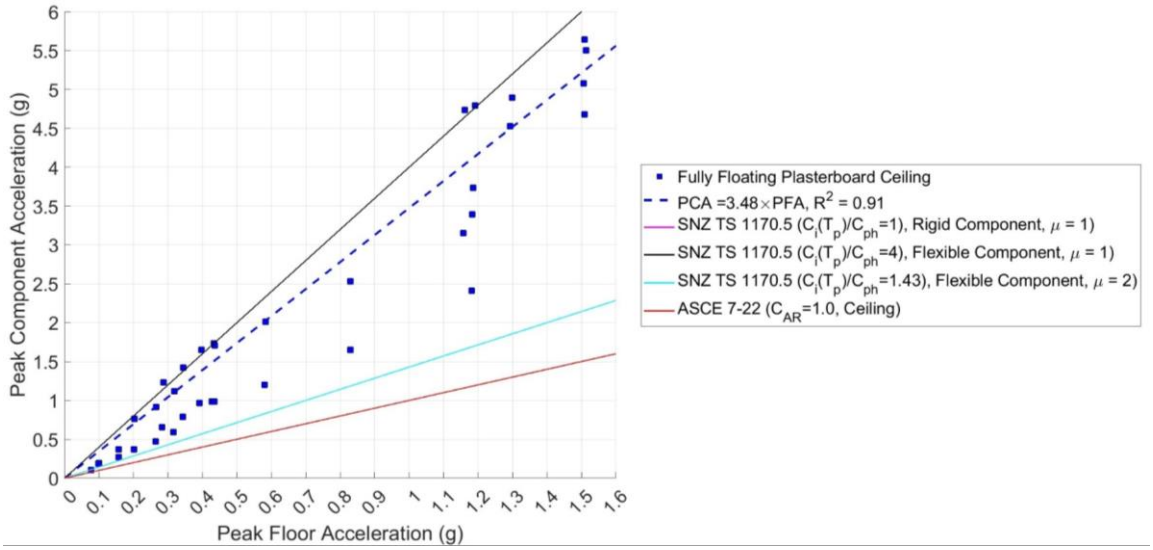

Figure 4.39 Peak accelerations of fully floating plasterboard ceiling specimens in loading direction (X) as a function of peak floor acceleration (West and East ceiling combined) for initial test series

Figure 4.39 indicates that the PCA/PFA ratio (i.e., Dynamic Amplification Factors (DAF) inclusive of part ductility (μ)) for the fully floating plasterboard ceiling

with isolation foam around all edges, as determined by the best-fit line through the origin, is approximately 3.48 with $R^2 = 0.91$. According to SNZ TS 1170.5 (2025), this experimental ratio corresponds closely to the design cases for a Flexible component with ductility ($\mu = 1.0$). The standard's provision for a Flexible component with $\mu = 1$ provides a conservative estimate, exceeding the measured ratio by a factor of 1.15. However, ASCE/SEI 7-22 (2022) recommends a factor of 1.00 for ceilings which is unconservative as compared to the experimental value of 3.48. These deviations from code provisions are expected, as fully floating ceilings represent a novel type of system. Unlike conventional ceilings, which are either attached to perimeter walls or back-braced to the floor above, fully floating ceilings are freely suspended.

Figure 4.40 plots the PCA/PFA ratio for the for fully floating plasterboard ceilings, calculated by dividing the PCA by the PFA of the top floor. The box plot in Figure 4.40 (c) shows a median PCA/PFA value of 2.96 for perimeter restrained concealed plasterboard ceilings with isolation foam. The SNZ TS 1170.5 (2025), provision for a Flexible component with μ=1 provides a conservative estimate, exceeding the measured ratio by a factor of 1.35. However, ASCE/SEI 7-22 (2022) recommends a factor of 1.0 for ceilings which is very unconservative as compared to the experimental median value of 2.96.

Corresponding plots for the modified test series for the fully floating plasterboard ceiling without isolation foam are shown in Figure 4.41 and Figure 4.42. Figure 4.42 (c) indicates that the median PCA/PFA value for this configuration is 3.19, which is approximately 1.08 times greater than the value for ceilings with isolation foam. Notably, the PCA/PFA values remain below 1.60 for Test #20 (PFA: 0.07 g) and Test #22 (PFA: 0.15 g), then rise to a range predominantly between 3.0 and 4.0. This increase likely

results from the ceiling pounding against the surrounding walls as the PFA exceeds 0.15 g.

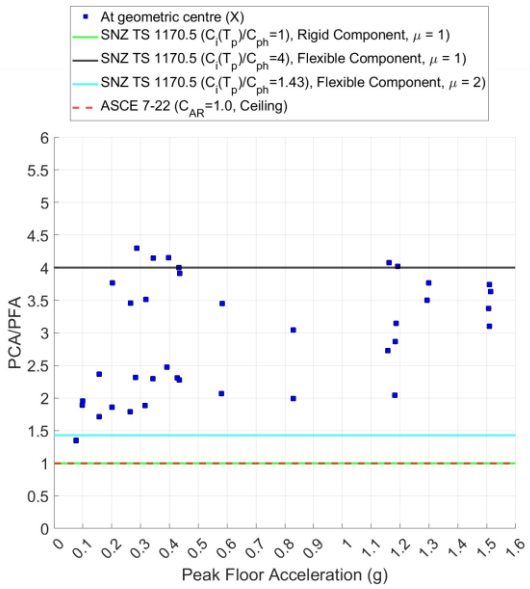

a) PCA/PFA as a function of PFA

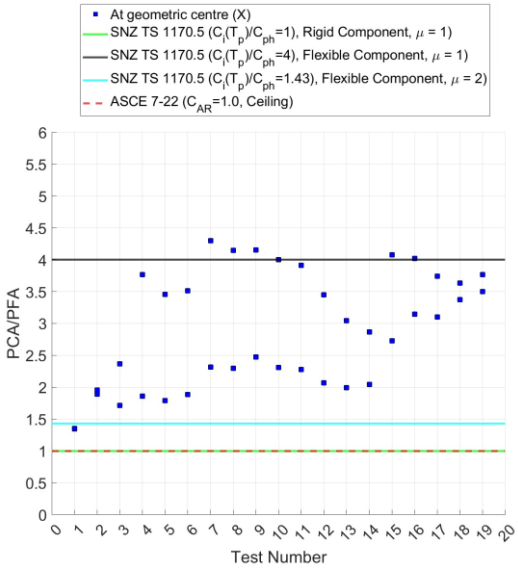

b) PCA/PFA as a function of Test number

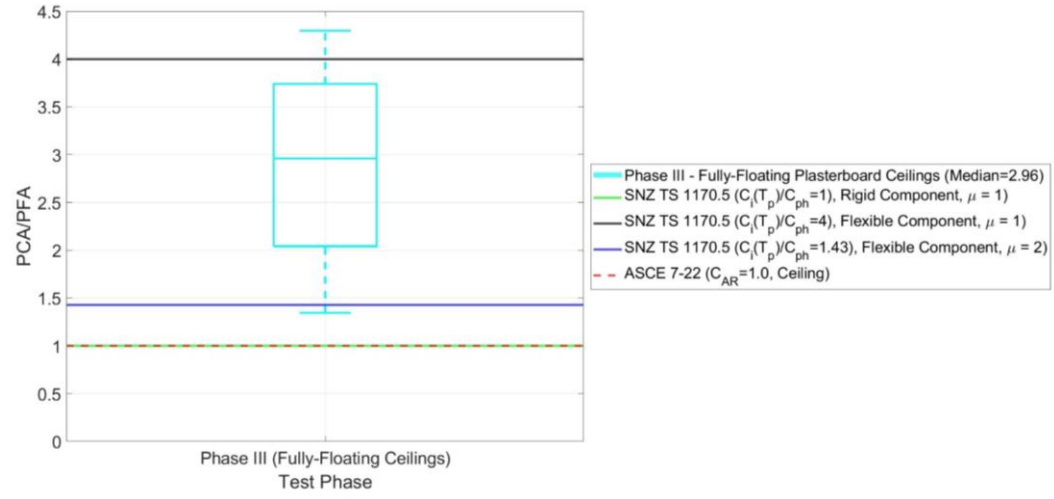

c) PCA/PFA box plot (Median = 2.96)

Figure 4.40 PCA/PFA in the loading direction (X) for fully floating plasterboard ceiling with isolation foam for initial test series

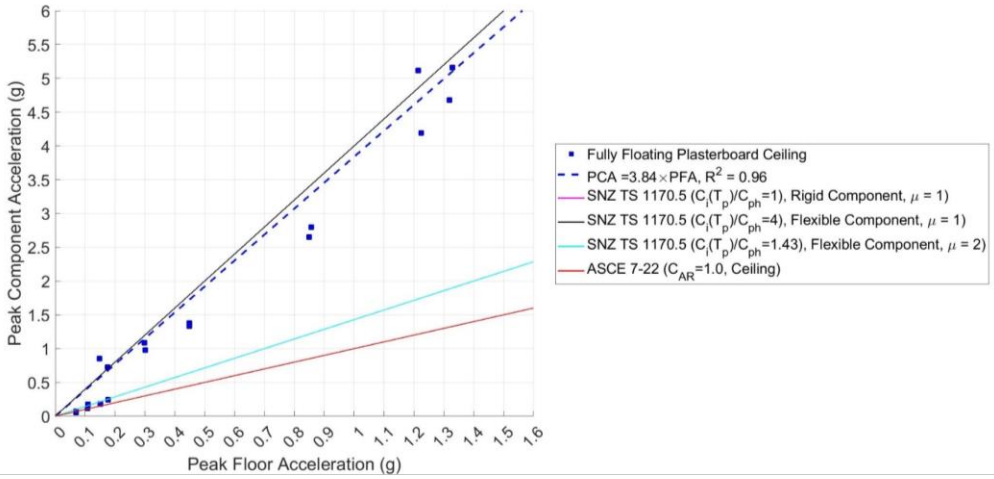

Figure 4.41 Peak accelerations of fully floating plasterboard ceiling specimens in loading direction (X) as a function of peak floor acceleration (West and East ceiling combined) for modified test series

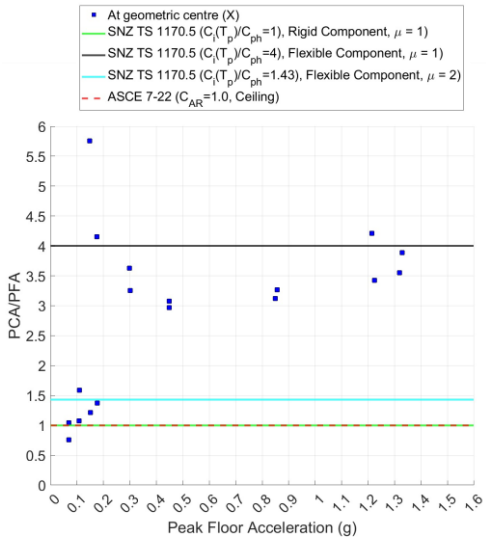

a) PCA/PFA as a function of PFA

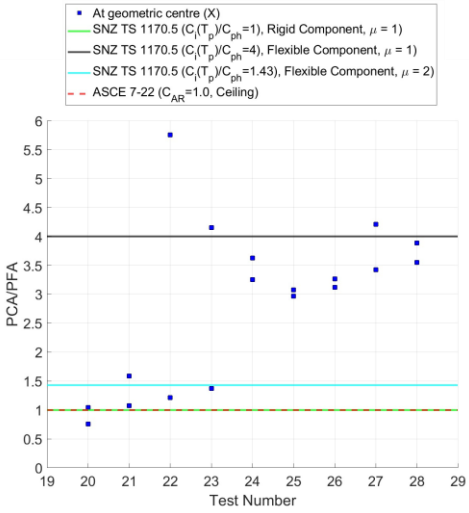

b) PCA/PFA as a function of Test number

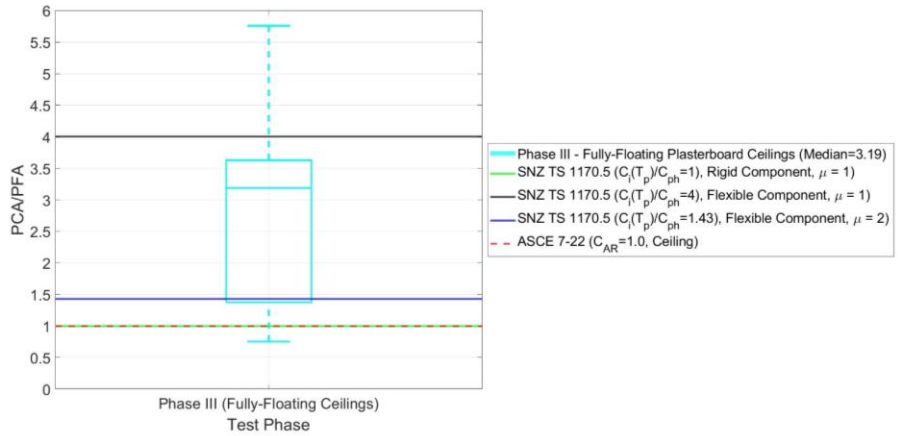

c) PCA/PFA box plot (Median = 3.19)

Figure 4.42 PCA/PFA in the loading direction (X) for fully floating plasterboard ceiling without isolation foam for modified test series

Mechanical Pipes

The peak component accelerations (PCA) recorded in the transverse direction of the pipe's orientation (X) direction located approximately at the hanger location (attached to the pipes) (ACC.003, ACC.012) are plotted against the peak floor acceleration of top floor (PFA) to which the ceiling is connected to for initial test series configuration up to Tests #18 in Figure 4.43. Accelerometer locations are shown in Figure 4.21 and Figure 4.27. It should be noted that the pipe hanger clamps were found to be loose, possibly from the start of testing after Test #10 (PFA: 0.43 g). This allowed the pipes to rotate within the clamps, disorienting the accelerometers during Test #10 (PFA: 0.43 g). The clamps were subsequently tightened, and the test was repeated at the same intensity as Test #11. The sudden increase in PCA beyond 0.43 g PFA in Figure 4.43 is attributed to this correction made to the pipes.

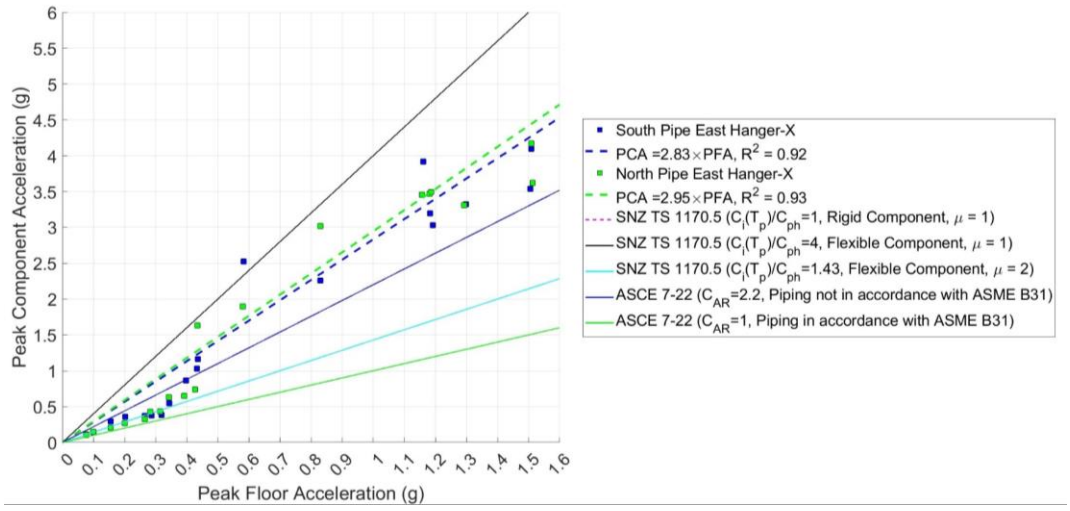

Figure 4.43 Peak accelerations of unbraced mechanical pipes specimens in the transverse direction of the pipe's orientation (X) as a function of peak floor acceleration (shown separately) for the initial test series

Figure 4.43 also presents PCA values calculated by multiplying the PFA from the top floor by: (1) the ratio $C_i(T_p)/C_{ph}$ for different ductility levels (μ), per SNZ TS 1170.5

(2025), and (2) the Component Resonance Ductility Factor (C_{AR}) from ASCE/SEI 7-22 (2022). $C_i(T_p)$ is the component spectral-shape coefficient and (C_{ph}) is the component horizontal-response factor. Additionally, a linear fit through the origin is plotted against the experimental data points.

The experimental data plots of PCA as a function of PFA for both the pipes were merged to derive a single, representative linear fit for PCA as a function of PFA as shown in Figure 4.44

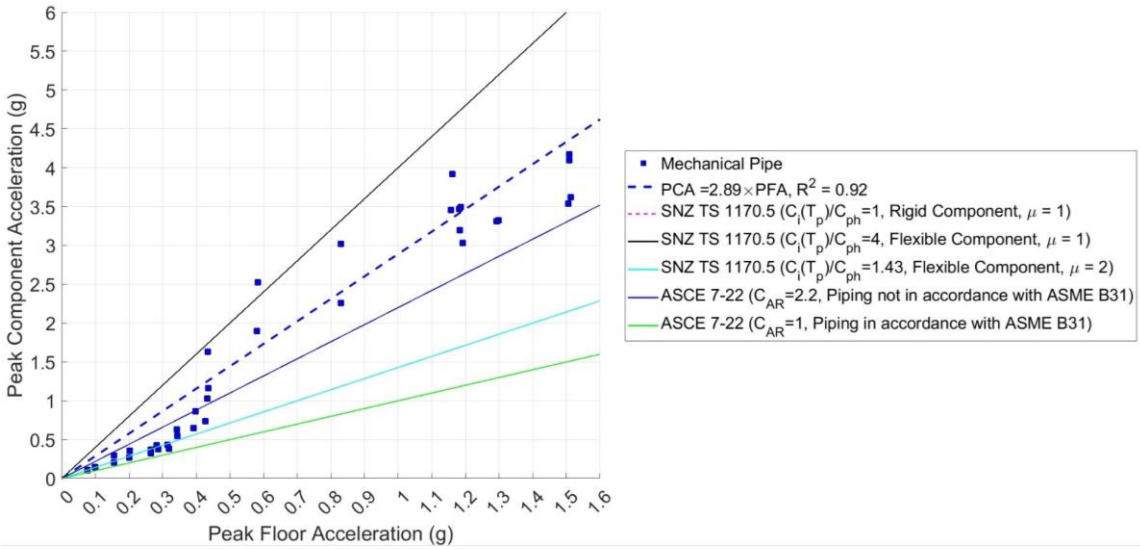

Figure 4.44 Peak accelerations of unbraced mechanical pipes specimens in the transverse direction of the pipe's orientation (X) as a function of peak floor acceleration (shown together) for the initial test series

Figure 4.44 indicates that the PCA/PFA ratio (i.e., Dynamic Amplification Factors (DAF) inclusive of part ductility (μ)) for the unbraced mechanical pipes, as determined by the best-fit line through the origin, is approximately 2.89 with $R^2 = 0.92$. According to SNZ TS 1170.5 (2025), this experimental ratio corresponds to the design cases for a Flexible component with ductility ($1 < \mu < 2$). The standard's provision for a Flexible component with $\mu = 1$ provides a conservative estimate, exceeding the

measured ratio by a factor of 1.38. However, ASCE/SEI 7-22 (2022) recommends a factor of 2.20 for pipes which is unconservative as compared to the experimental value of 2.89.

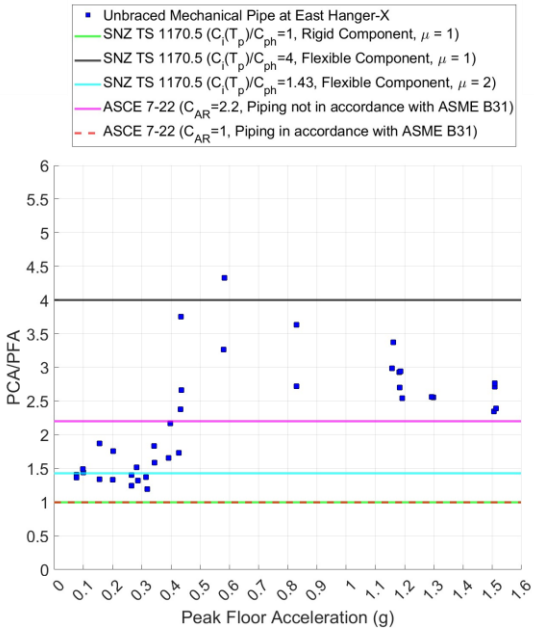

a) PCA/PFA as a function of PFA

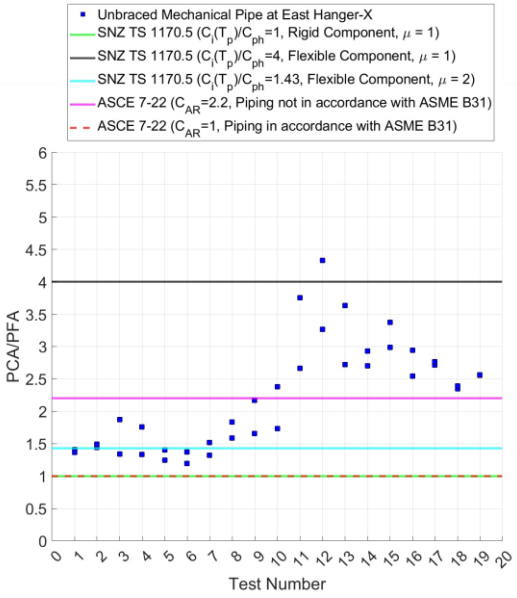

b) PCA/PFA as a function of Test number

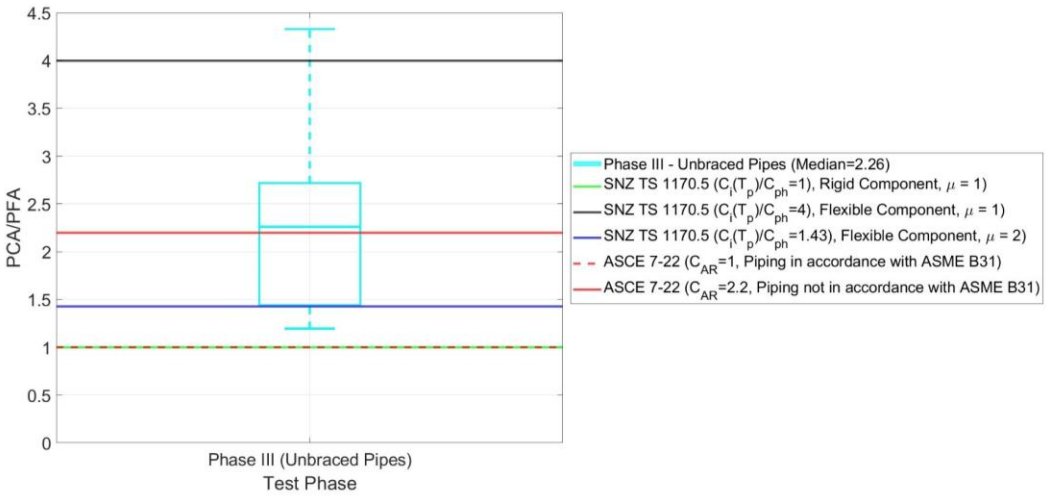

c) PCA/PFA box plot (Median = 2.26)

Figure 4.45 PCA/PFA for unbraced mechanical pipes specimens in the transverse direction of the pipe's orientation (X) for the initial test series

Figure 4.45 presents the PCA/PFA ratio for the unbraced mechanical pipes, calculated using the top-floor PFA. As shown in Figure 4.45 (a), the PCA/PFA for the

pipe remains below 2.0 up to a PFA of 0.39 g, corresponding to Test #9 in Figure 4.45 (b). Beyond this point, the values primarily range between 2.5 and 4.0, a shift that may correlate with increased interaction between the pipe and the wall at the penetration point.

The box plot in Figure 4.45 (c) shows a median PCA/PFA value of 2.26 for unbraced mechanical pipes. The SNZ TS 1170.5 (2025), provision for a Flexible component with μ=1.25 (not shown in Figure 4.45) provides a conservative estimate, exceeding the measured ratio by a factor of 1.26. However, ASCE/SEI 7-22 (2022) recommends a factor of 2.20 for mechanical pipes which is comparable to the experimental median value of 2.26.

Component acceleration analysis for the pipes in the modified test series was omitted due to issues with the attached accelerometers.

Displacement analysis

"Rocking" timber-framed walls

Figure 4.46 presents the vertical uplifts measured by displacement transducers at various locations on the "rocking" wall system. As shown in Figure 4.46 (a), while the wall did show "rocking" behaviour, the wall did not exhibit the expected in-plane rocking motion. The measured uplifts do not closely match the estimated rocking displacements, calculated as the drift ratio multiplied by half the in-plane wall length of 3987 mm (the segment adjacent to the middle vertical joint). This can be attributed to the premature bending or yielding of the 6 mm thick steel angle at the wall junctions, likely due to the higher force required to initiate wall rocking. The maximum uplift limit of 35 mm corresponds to the measured vertical gap available in the dual slot track. The same plot indicates that "rocking" motion in the in-plane walls reached a maximum of 18 mm at a

2.51% drift, while the ends of the South and North out-of-plane walls remained largely stationary. Figure 46 (b) shows negligible residual uplift displacements following each test.

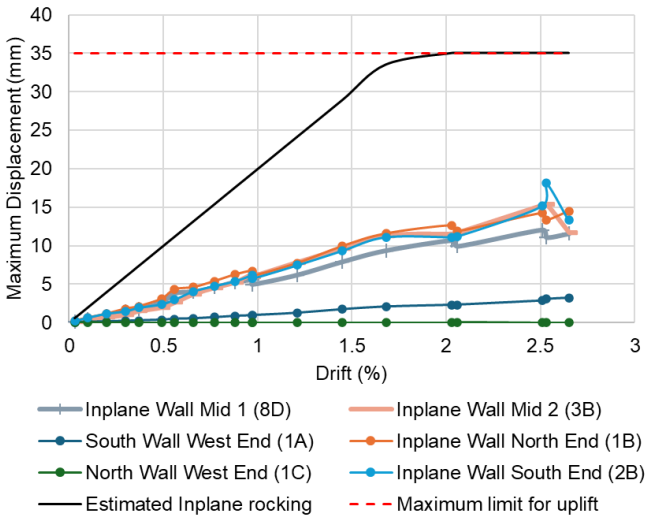

a) Maximum uplift displacements

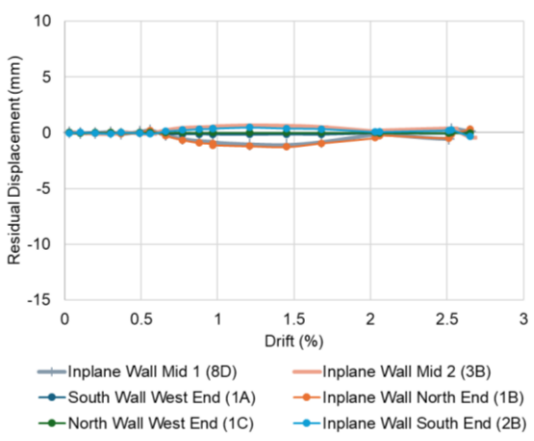

b) Residual displacements

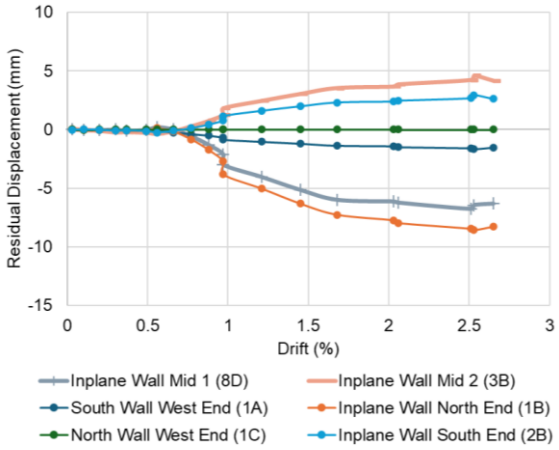

c) Cumulative residual displacements

Figure 4.46 Vertical displacement measurements for wall specimens with for initial test series – sealant in joints (approximate measurement locations shown and instrument numbers in brackets)

This behaviour is similarly reflected in the relative vertical displacement data at the wall junctions shown in Figure 4.47. Although the in-plane wall did not exhibit the expected rocking motion, it was observed to slide, alternately opening and closing the 15

mm vertical joint gaps. This movement is illustrated by the gap measurements at the vertical joints shown in Figure 4.48.

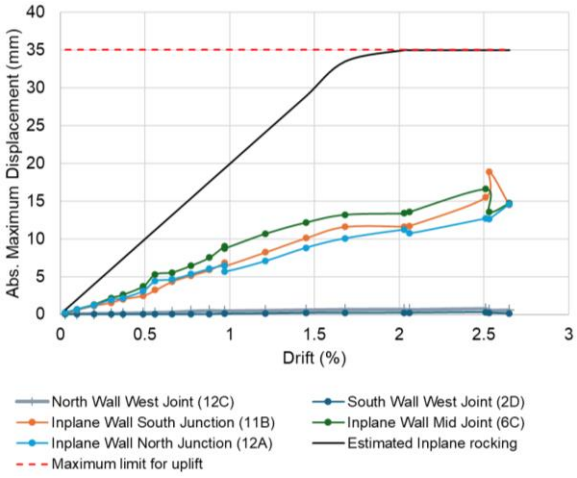

a) Absolute maximum displacements

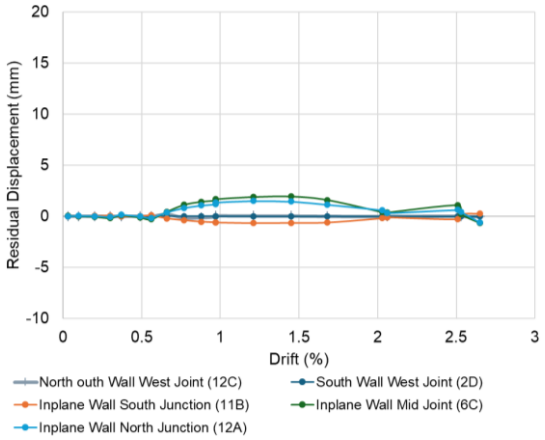

b) Residual displacements

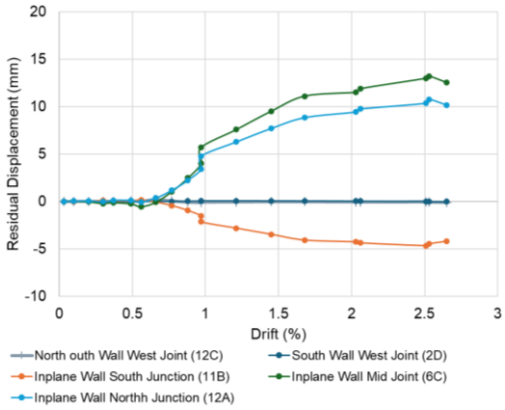

c) Cumulative residual displacements

Figure 4.47 Vertical relative displacement measurements for wall junctions for initial tests series– sealant in joints (approximate measurement locations shown and instrument numbers in brackets)

As shown in Figure 4.48 (a) and (b), the South junction between the in-plane and out-of-plane walls experienced both opening and closing of the joint. In contrast, the North junction exhibited predominantly gap opening. At the top of the walls, this opening and closing began early in the tests, while at the bottom it only became apparent after a

drift of 0.56%. The maximum joint widening from the initial position was approximately 25 mm, measured at the top of the North junction during the 2.51% drift test. The top portions of both the South and North junctions opened wider than the bottom portions. In contrast, the opening at the mid-junction of the in-plane wall was almost negligible. Figure 4.48 (c) shows negligible residual displacements after each test, while Figure 4.48 (d) shows a cumulative displacement of 10 mm at 2.51% drift. It should be noted that the 15 mm gap between the timber framing and the plasterboard linings is present only at the North and South wall junctions. At the mid-joint of the in-plane wall, this 15 mm gap exists only between the adjacent plasterboard linings.

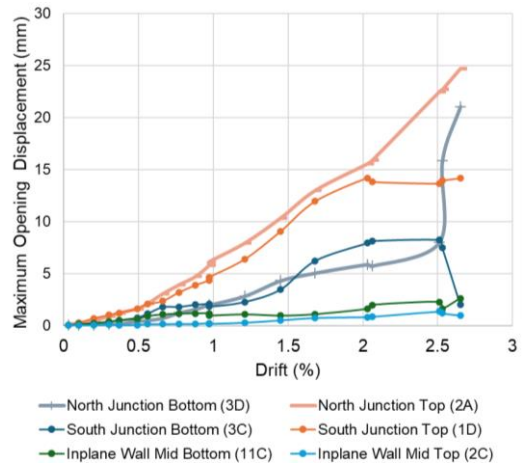

a) Maximum opening displacements

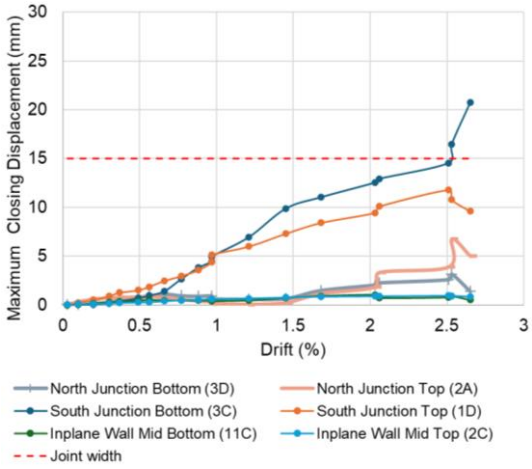

b) Maximum joint closing displacements

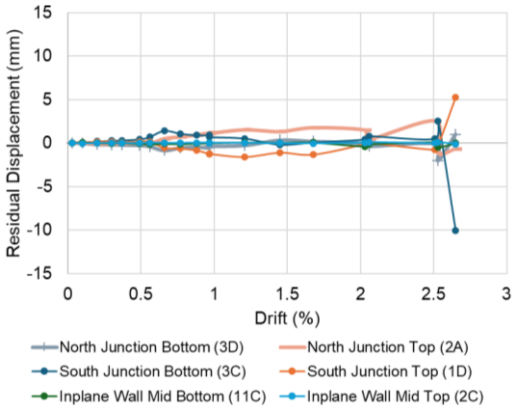

c) Residual displacement

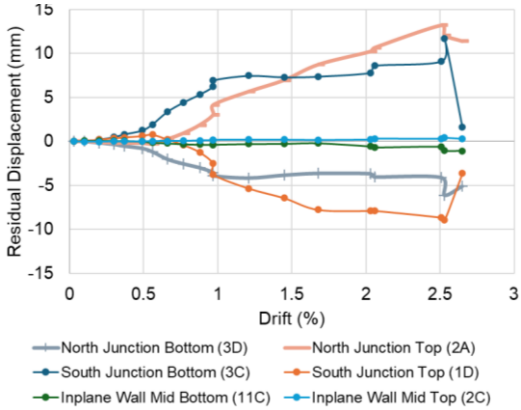

d) Cumulative residual displacement

Figure 4.48 Opening and closing measurements of wall junctions for initial test series– sealant in joints (approximate measurement locations shown and instrument numbers in brackets)

Figure 49 presents the out-of-plane lateral displacements measured at the mid-length of the plasterboard strips of the out-of-plane walls relative to the top slab. As shown in Figure 4.49 (a), the top of the North out-of-plane wall exhibits increasing maximum displacement from the start, attributable to the bending of the connecting steel angle. In contrast, the South out-of-plane wall shows displacement only after 0.97% drift, reaching a maximum of just 5 mm at 2.51% drift, compared to 20 mm for the North wall.

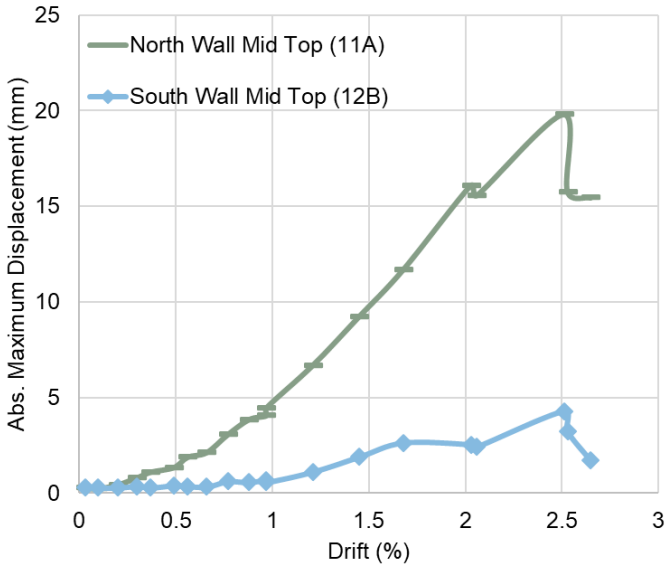

a) Absolute maximum displacements

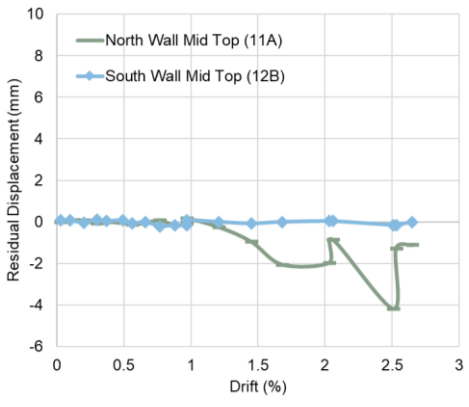

b) Residual displacements

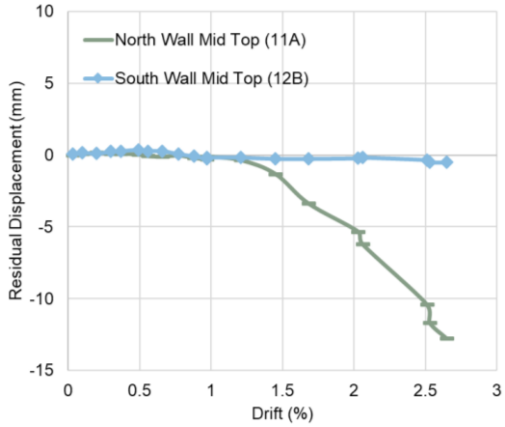

c) Cumulative residual displacements

Figure 4.49 Lateral displacement measurements of the plasterboard strip at the top of the out-of-plane walls for initial test series – sealant in joints (approximate measurement locations shown and instrument numbers in brackets)

Figure 4.49 (b) and (c) indicate that residual deformation at the top of the North wall begins at 1.21% drift. This corresponds to a relative inter-storey displacement of approximately 43 mm, which likely signifies the closure of the combined 30 mm of joint gaps at the North and South junctions. The onset of residual deformation suggests the transfer of significant forces from the in-plane to the out-of-plane wall through their interaction and implies that the steel angle has undergone plastic deformation.

Figure 4.50 through Figure 4.53 provide corresponding plots for the modified test series, which used unsealed in-plane wall joints. Broadly, these results demonstrate higher uplifts, greater joint opening and closing, and smaller top out-of-plane displacements of the out-of-plane walls compared to the initial series with sealed joints.

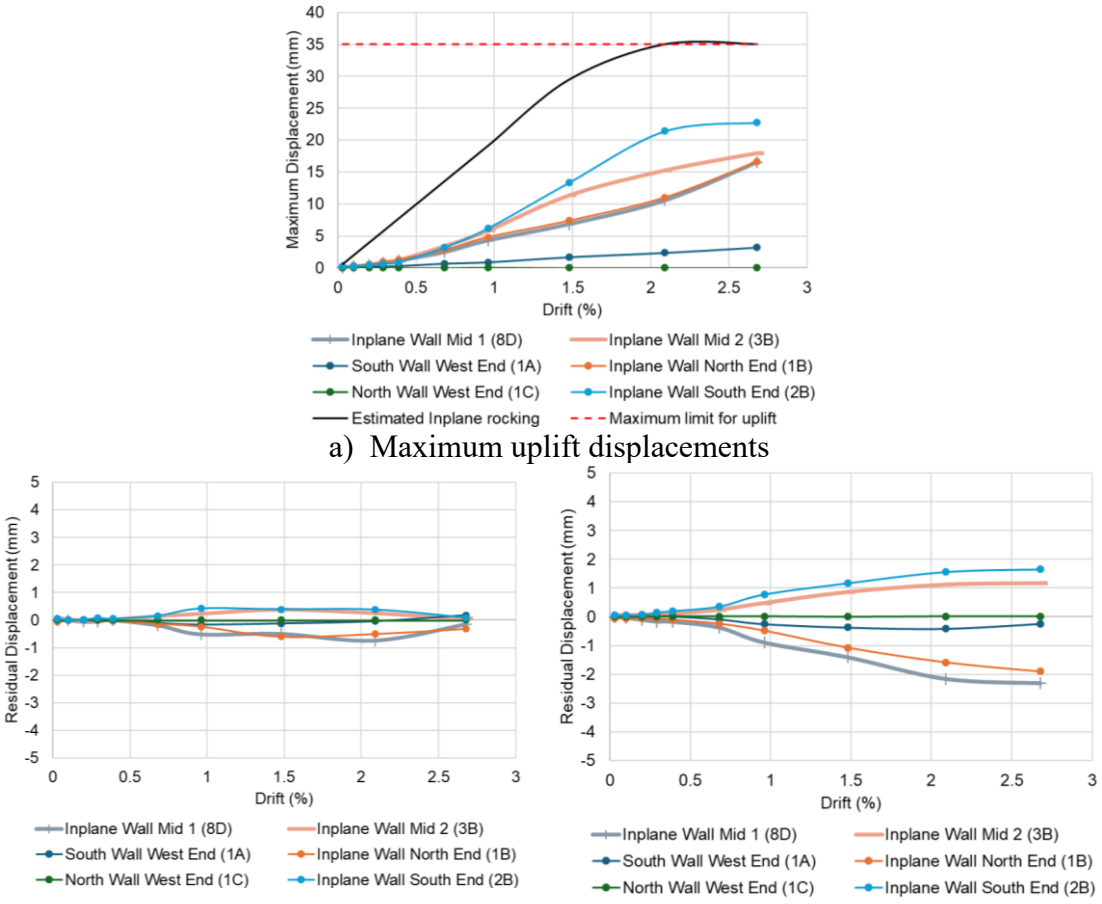

a) Maximum uplift displacements

b) Residual displacements

c) Cumulative residual displacements

Figure 4.50 Vertical displacement measurements for wall specimens for modified test series - no sealant at in-plane wall junctions (approximate measurement locations shown and instrument numbers in brackets)

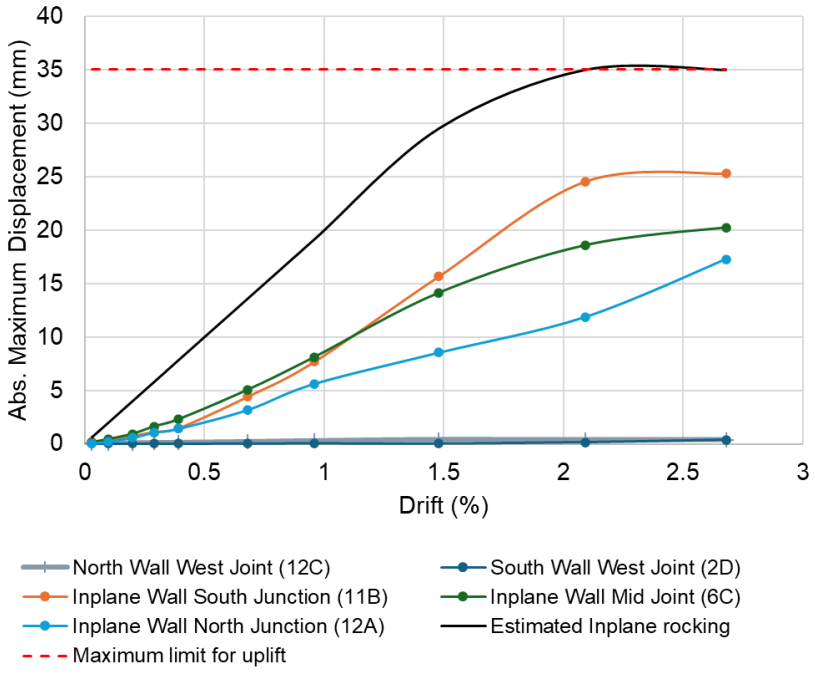

a) Absolute maximum displacements

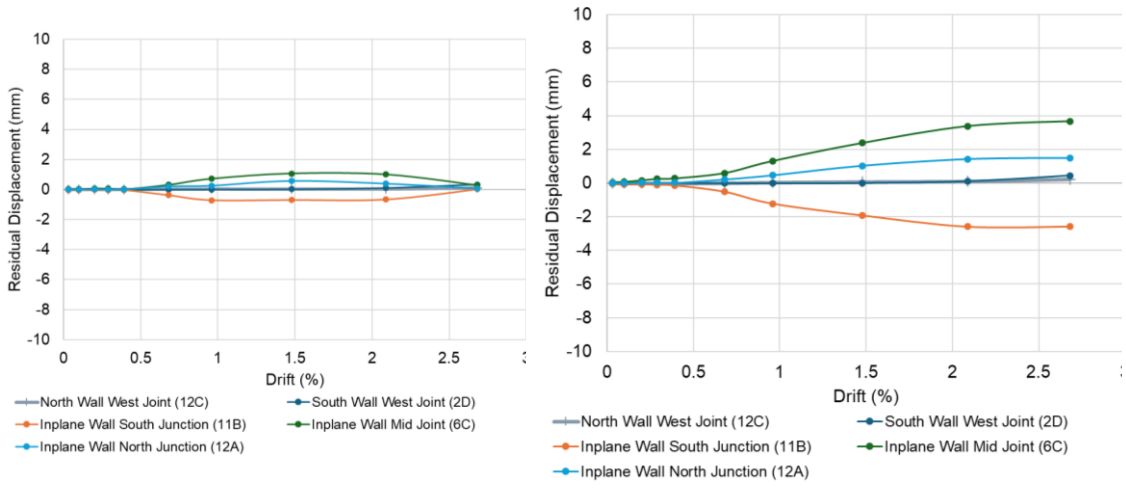

b) Residual displacements c) Cumulative residual displacements

Figure 4.51 Vertical relative displacement measurements for wall junctions for modified test series - no sealant at in-plane wall junctions (approximate measurement locations shown and instrument numbers in brackets)

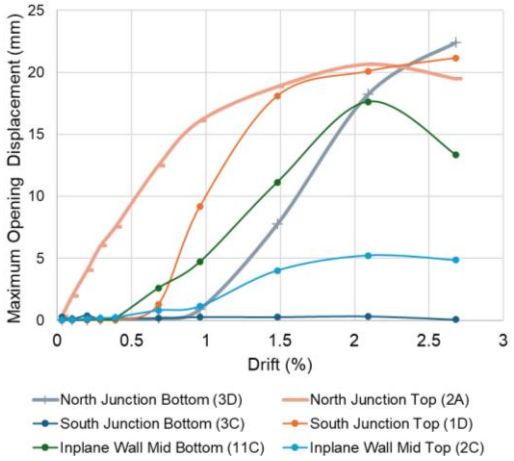

a) Maximum joint opening displacements

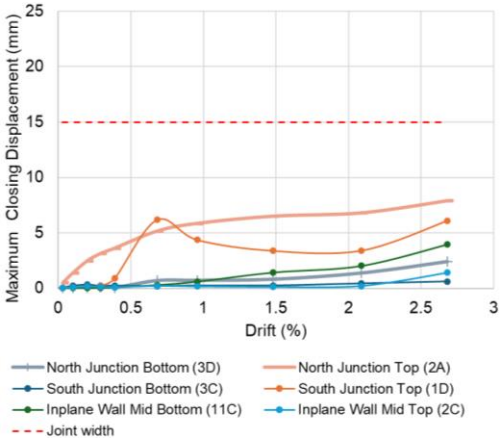

b) Maximum joint closing displacements

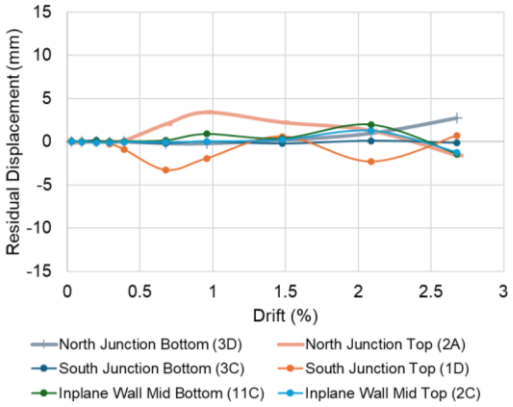

c) Residual displacement

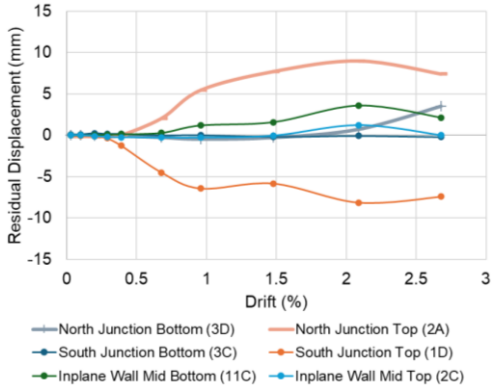

d) Cumulative residual displacement

Figure 4.52 Opening and closing measurements of wall junctions for modified test series - no sealant at in-plane wall junctions (approximate measurement locations shown and instrument numbers in brackets)

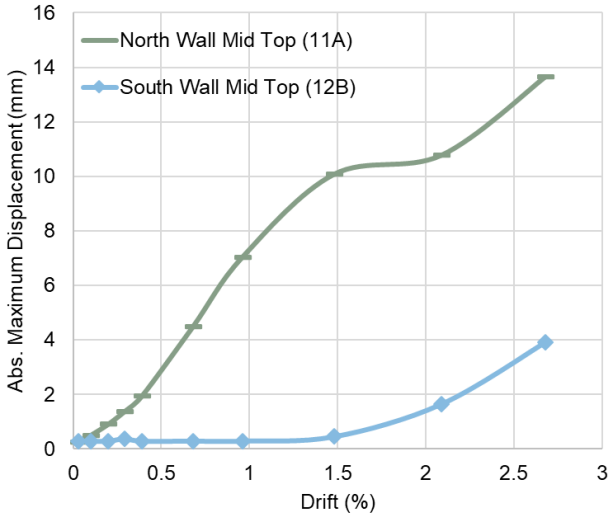

a) Absolute maximum displacements

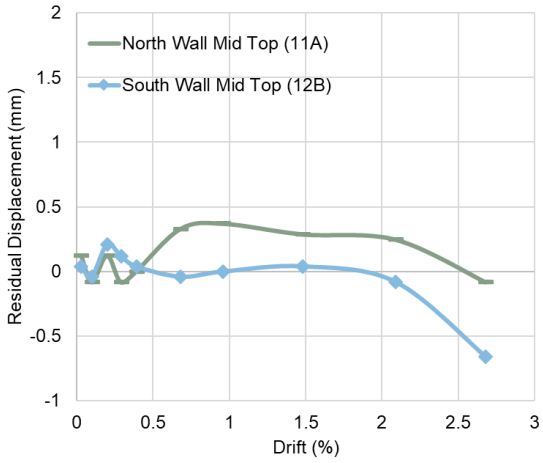

b) Residual displacements

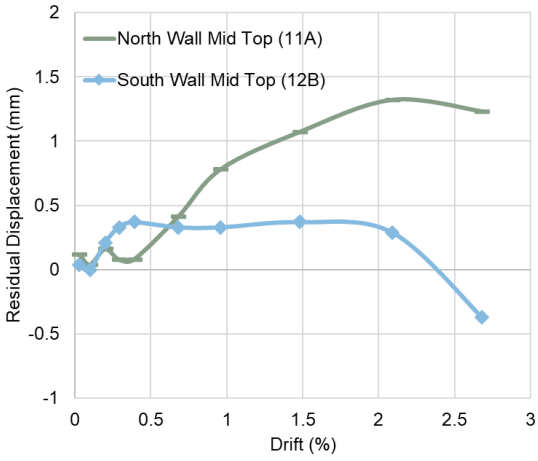

c) Cumulative residual displacements

Figure 4.53 Lateral displacement measurements for plasterboard strip at the top of the wall specimens for modified test series - no sealant at in-plane wall junctions (approximate measurement locations shown and instrument numbers in brackets)

Fully floating ceilings

As described previously, both the West and East fully floating ceilings share identical details: they are freely suspended by hanger wires, with an approximate 50 mm gap around all edges between the ceiling and the surrounding walls and bulkheads. This gap

is filled with 50 mm thick isolation (isolation) foam. Because the ceilings are freely hung and unattached to the boundary walls, they are expected to be more sensitive to floor accelerations. Figure 4.54 plots the relative opening and closing displacements between the ceilings and the surrounding walls, as measured by displacement transducers.

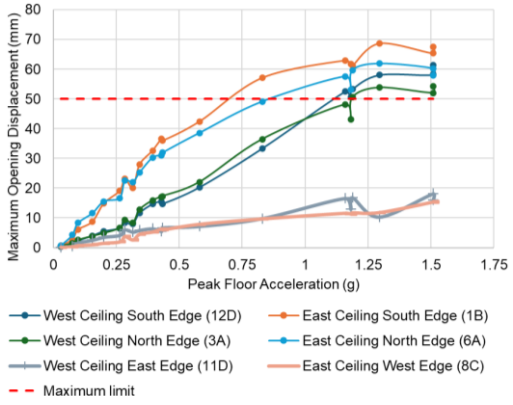

a) Maximum opening displacement

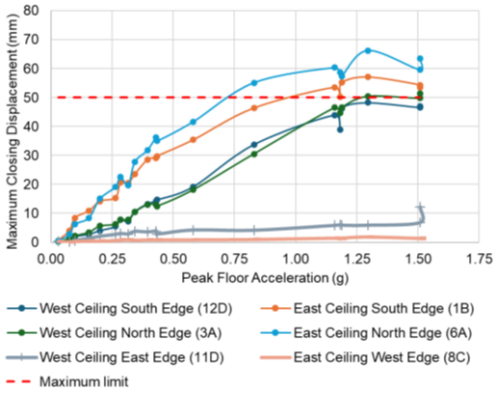

b) Maximum closing displacement

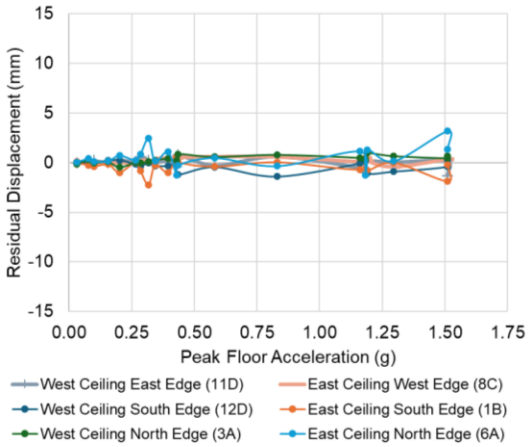

c) Residual displacement

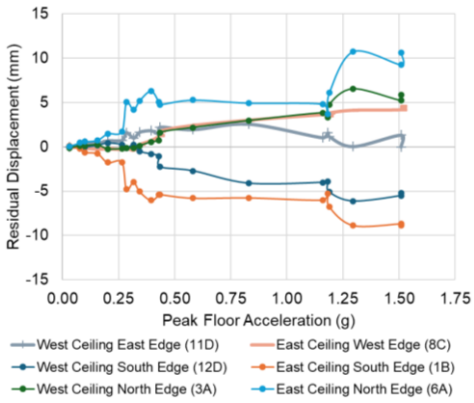

d) Cumulative residual displacement

Figure 4.54 Opening and closing of ceiling to wall gaps as a function of PFA for initial test series -ceilings with isolation foam placed between ceiling and wall gap (approximate measurement locations shown and instrument numbers in brackets)

Figure 4.54 (a) shows that the ceilings reach or exceed the 50 mm design gap at approximately 0.83 g. This exceedance may be attributed to construction tolerances or possible torsion in the ceiling assembly. As expected, the displacement measurements for

the West ceiling's East edge and the East ceiling's West edge are lower, as these transducers are oriented perpendicular to the primary loading direction. Figure 4.54 (b) indicates negligible residual displacements after each test, while Figure 4.54 (c) shows a cumulative displacement of about 5 mm up to 1.25 g, reaching 10 mm at 1.51 g. Corresponding plots as a function of inter-storey drift are provided in Figure 4.55.

Figure 4.55 (a) shows that the 50 mm gap was reached at approximately 1.45% drift.

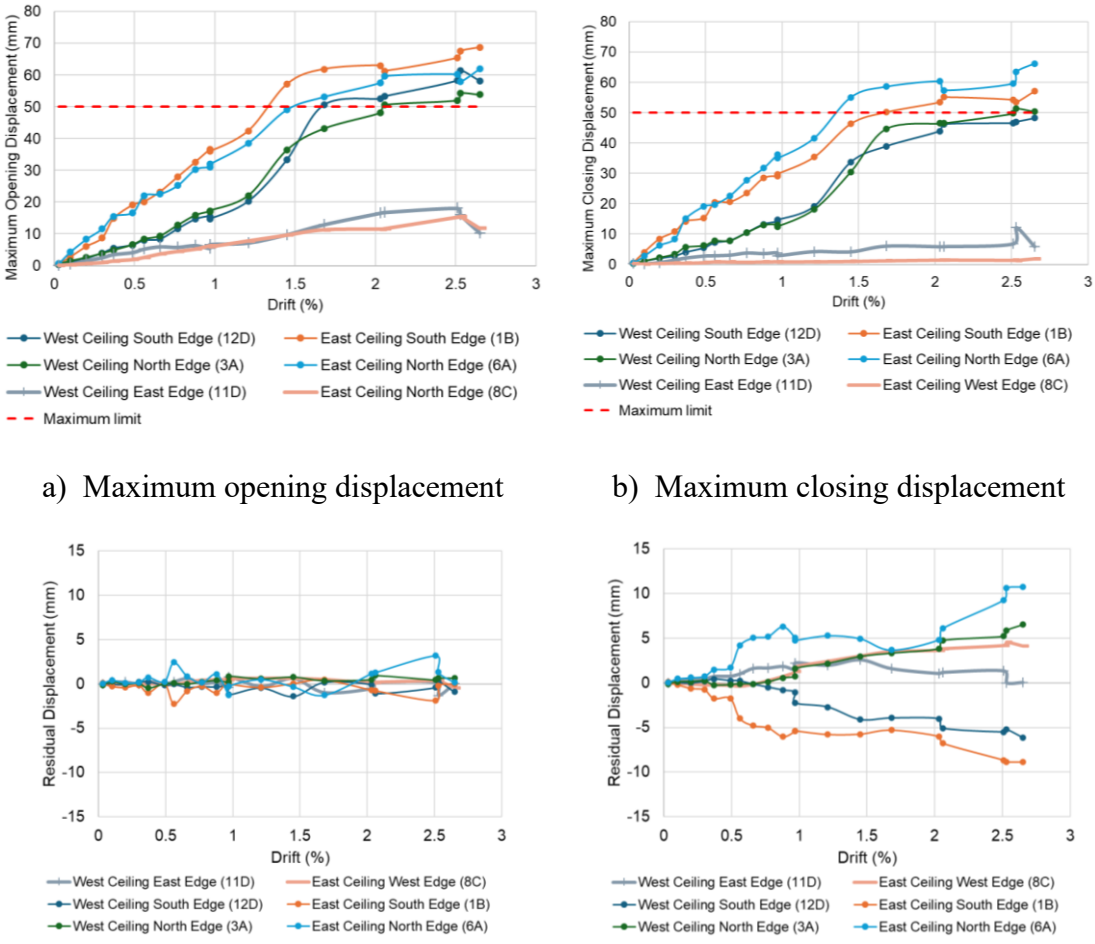

a) Maximum opening displacement

b) Maximum closing displacement

c) Residual displacements

d) Cumulative residual displacements

Figure 4.55 Opening and closing of ceiling to wall gaps as a function of drift for modified test series - ceilings with isolation foam placed between ceiling and wall gap (approximate measurement locations shown and instrument numbers in brackets)

Corresponding plots for the fully floating ceiling without isolation foam are provided in Figure 4.56 (as a function of PFA) and Figure 4.57,(as a function of inter-storey drift). These figures show that the 50 mm gap was reached and exceeded at only 0.18 g PFA and 0.39% drift. These thresholds are significantly lower than those for ceilings with isolation foam, which reached the gap at 0.83 g and 1.45% drift, highlighting the dampening effect of the isolation foam. The 0.39 % drift corresponds to a relative inter-storey displacement of approximately 14 mm, significantly less than the 50 mm gap. This suggests that the ceiling's movement is more sensitive to floor acceleration (PFA) than to inter-storey drift, as expected.

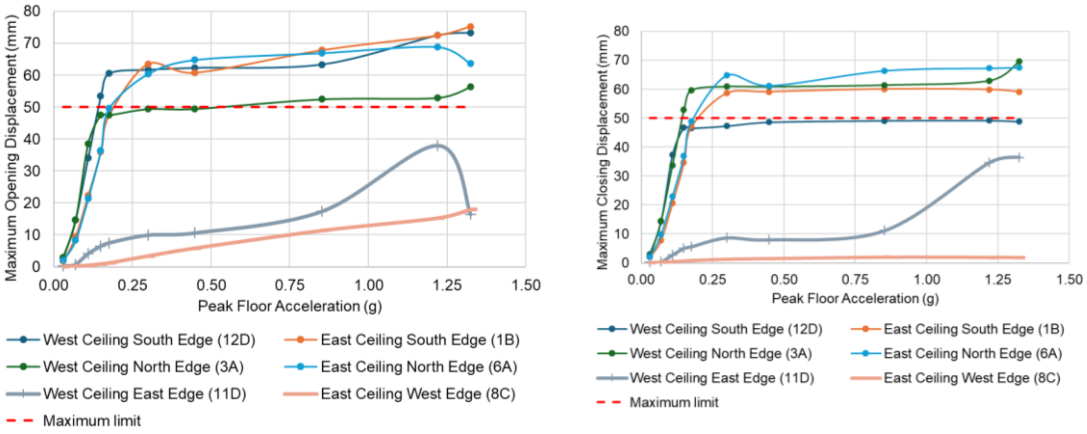

a) Maximum opening displacement

b) Maximum closing displacement

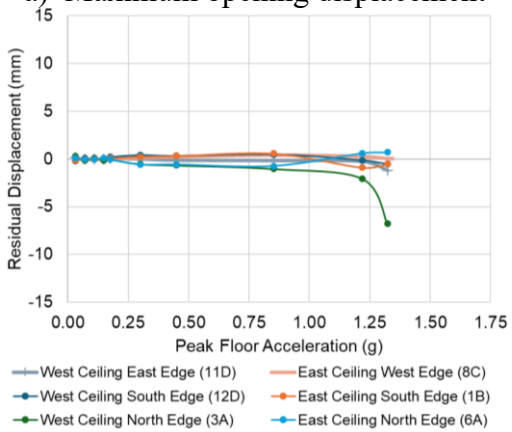

c) Residual displacement

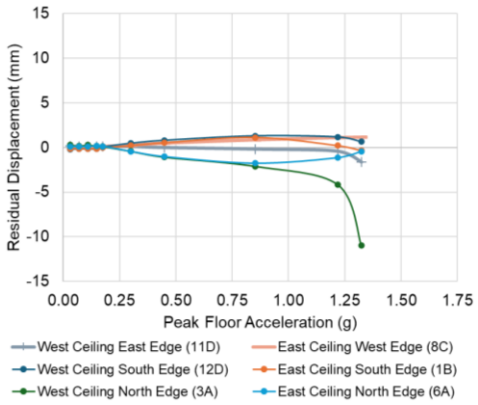

d) Cumulative residual displacement

Figure 4.56 Opening and closing of ceiling to wall gaps as a function of PFA for modified test series - ceilings without isolation foam placed between ceiling and wall gap (approximate measurement locations shown and instrument numbers in brackets)

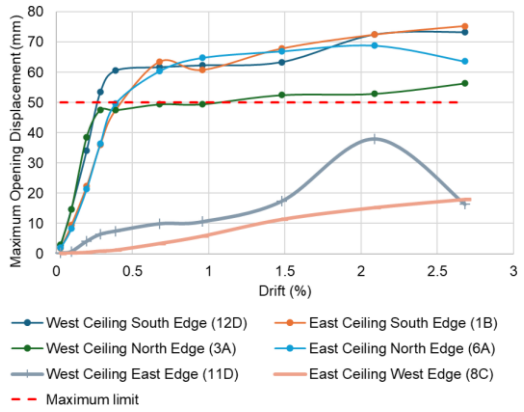

a) Maximum opening displacement

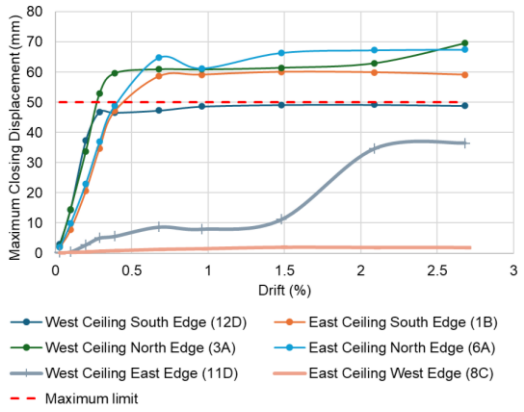

b) Maximum closing displacement

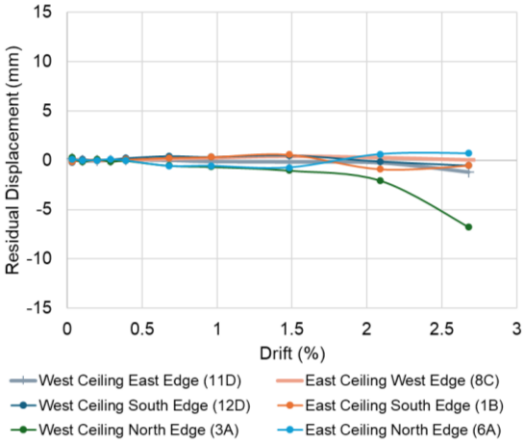

c) Residual displacement

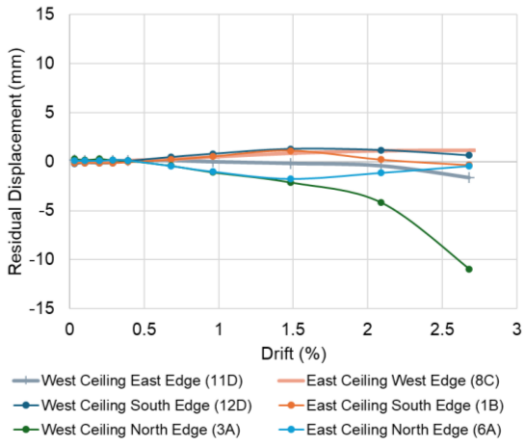

d) Cumulative residual displacements

Figure 4.57 Opening and closing of ceiling to wall gaps as a function of inter-storey drift for modified test series - ceilings without isolation foam placed between ceiling and wall gap (approximate measurement locations shown and instrument numbers in brackets)

Mechanical pipes

Figure 4.58 and Figure 4.59 plot the lateral displacement measurements for the unbraced mechanical pipe specimen as a function of drift and PFA, respectively, for the initial test series. These figures show that the relative displacement between the pipe and the top slab increases with drift demand, reaching a maximum of 33 mm at 2.51% drift (1.51 g

PFA). Residual displacement after each test was negligible. The video recordings show that the pipes interacted and moved together with the in-plane wall, a phenomenon that will be investigated in future analysis.

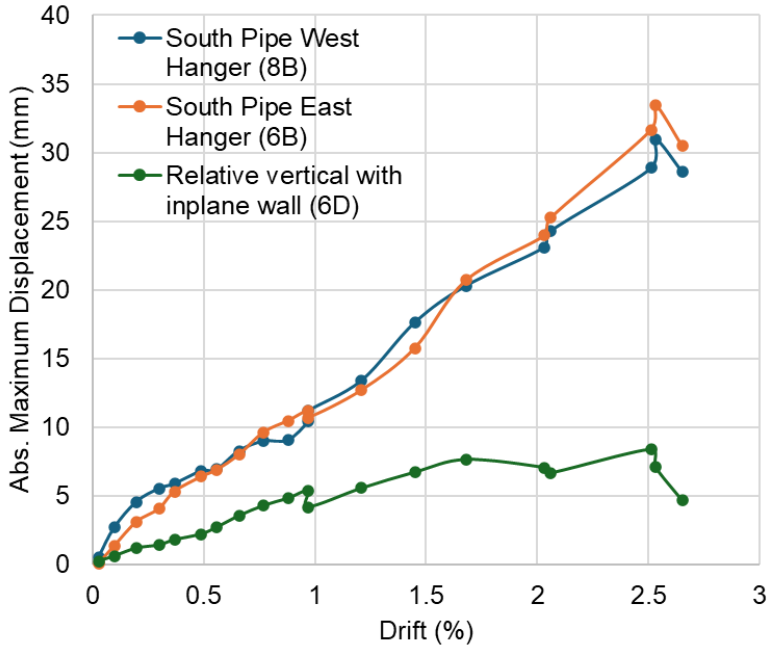

a) Absolute maximum displacements

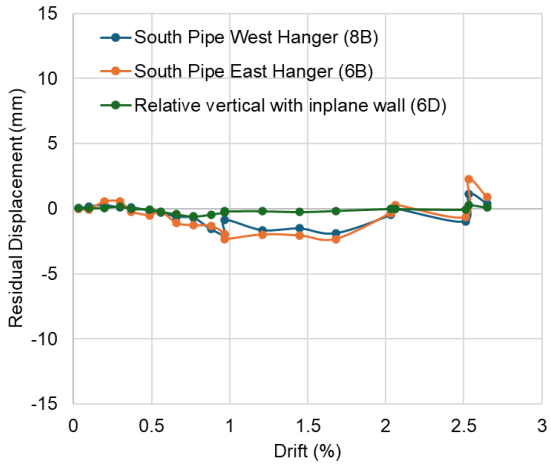

b) Residual displacements

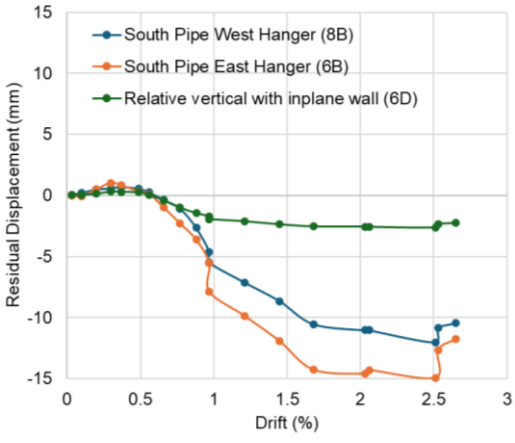

c) Cumulative residual displacements

Figure 4.58 Lateral displacement measurements for unbraced mechanical pipes as a function of inter-storey drift for initial test series (approximate measurement locations shown and instrument numbers in brackets)

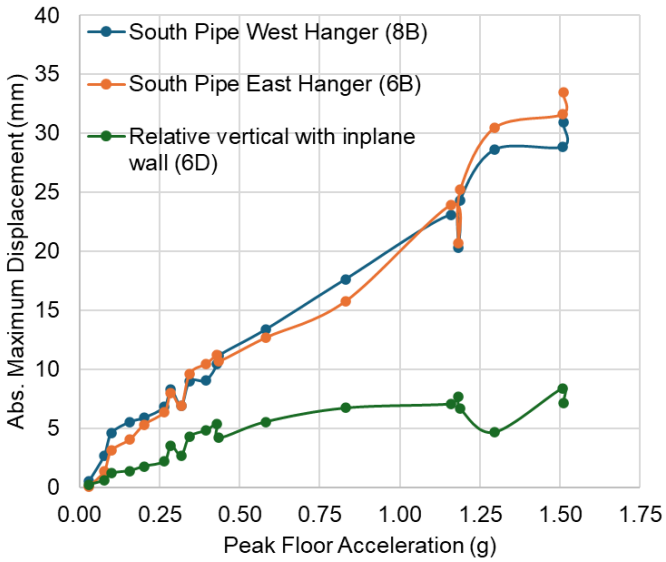

a) Absolute maximum displacements

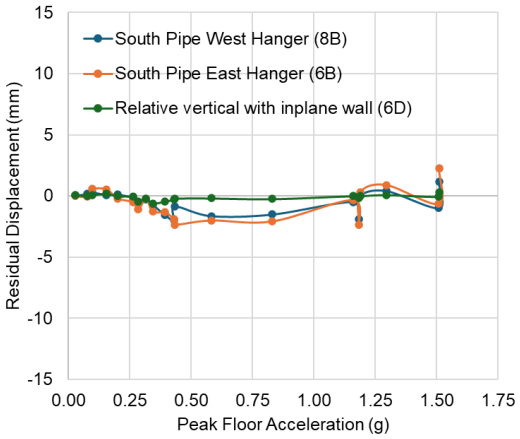

b) Residual displacements

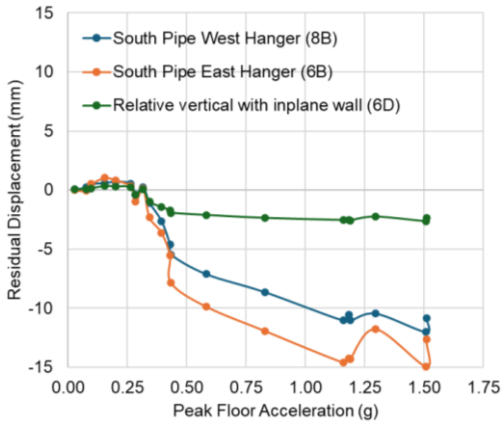

c) Cumulative residual displacements

Figure 4.59 Lateral displacement measurements for unbraced mechanical pipes as a function of PFA for initial test series (approximate measurement locations shown and instrument numbers in brackets)

Figure 4.60 and Figure 4.61 plot the lateral displacement measurements for the unbraced mechanical pipe specimen in the modified test series as a function of drift and PFA, respectively. The figures show that the relative displacement between the pipe and the top slab increases with drift demand, reaching a maximum of 35 mm at 2.68% drift

(1.32 g PFA). Residual displacement after each test was negligible. Overall, the pipes in this series exhibited higher displacements than those in the initial test series.

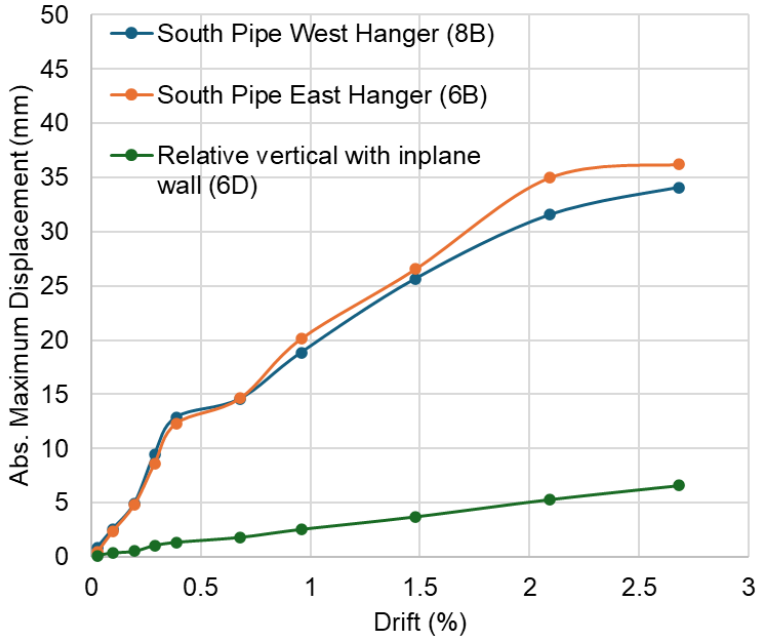

a) Absolute maximum displacements

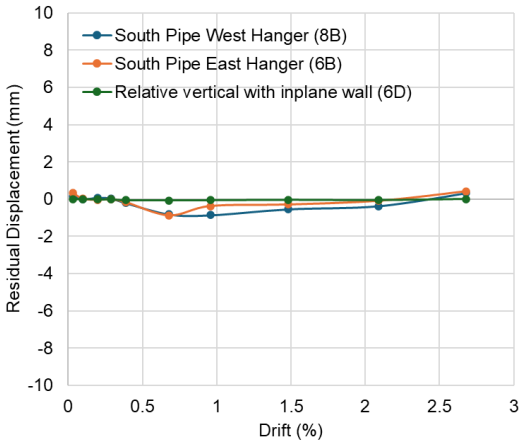

b) Residual displacements

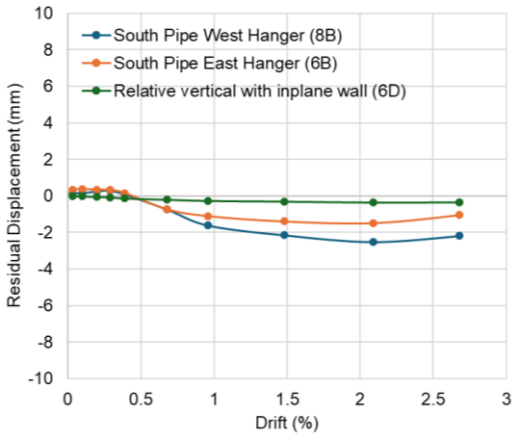

c) Cumulative residual displacements

Figure 4.60 Lateral displacement measurements for unbraced mechanical pipes as a function of inter-storey drift for modified test series (approximate measurement locations shown and instrument numbers in brackets)

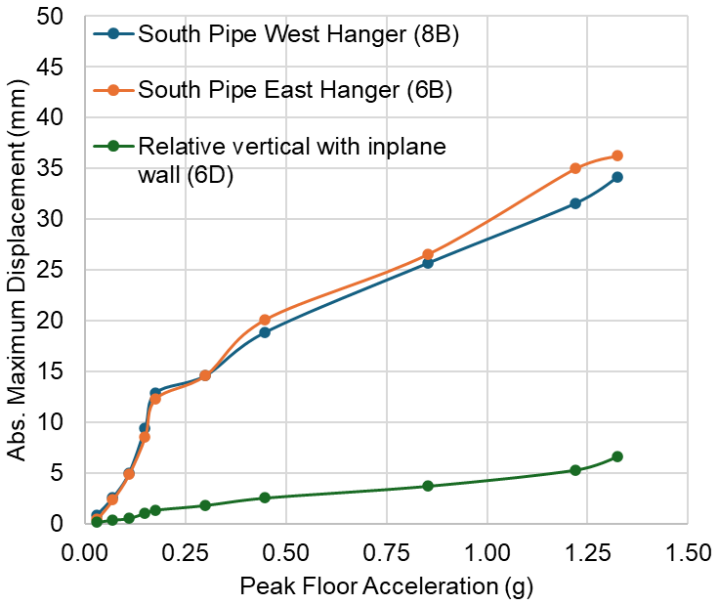

a) Absolute maximum displacements

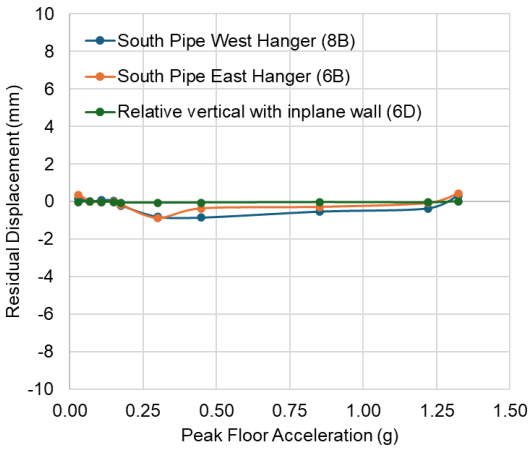

b) Residual displacements

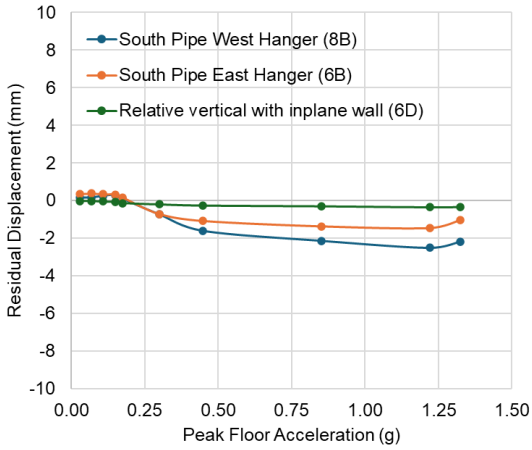

c) Cumulative residual displacements

Figure 4.61 Lateral displacement measurements for unbraced mechanical pipes as a function of PFA for modified test series (approximate measurement locations shown and instrument numbers in brackets)

DISCUSSION

The phase III experimental campaign successfully evaluated the seismic performance of three distinct non-structural systems under dynamic excitation. A key finding was the success of the damage concentration strategy in the “rocking” timber-framed walls. Damage progressed predictively within the sacrificial sealant joints, preserving the primary frame and plasterboard lining materials from failure. This confirms the viability of a controlled “rocking” mechanism with a designated fuse such as sealant. However, the intended kinematic in-plane rocking motion was not fully achieved due to the premature yielding of the 6 mm steel angle, a component requiring future design optimization to reliably initiate and control “rocking” of the walls.

For the fully floating plasterboard ceilings, the system demonstrated superior performance, sustaining only superficial damage at high intensities. The isolation foam played a critical role, providing significant damping and delaying interaction with boundary walls. The measured median PCA/PFA ratio of 2.96 for the foamed configuration was 1.35 times lower than the SNZ TS 1170.5 (2025) provision for Flexible components (μ=1), indicating the standard is conservative. In contrast, the ASCE/SEI 7-22 (2022) factor of 1.0 is unconservative. These results underscore that current code provisions, largely calibrated for conventionally perimeter restrained and braced ceilings, are not directly applicable to this novel, freely suspended system.

The mechanical pipes exhibited a failure mode defined by sealant detachment at penetrations, a critical loss of fire-stopping integrity. Code comparisons reveal a similar pattern: SNZ TS 1170.5 (2025) (μ=1.25) provides conservative estimates, while ASCE/SEI 7-22 (2022) values were comparable relative to experimental median value of 2.26.

The modified test series, featuring unsealed wall joints and ceilings without foam, provided valuable comparative data. As expected, the absence of sealant led to increased wall joint movements and higher PCA/PFA ratios, while the removal of isolation foam drastically increased the ceiling's displacements, confirming the foam's essential damping function.

COMPARISON BETWEEN PHASES I, II AND III

This following section reports fundamental comparison between the walls and ceiling s tested in each Phases in terms of damage progression and acceleration amplification.

Damage progression

A comparison table including the seismic performance and damage progression across the three phases is shown in Table 4.4. In Table 4.4., Phase I (walls only), the timber-framed wall exhibited brittle behaviour, with superficial hairline cracks appearing at a very low drift of 0.30% and critical failure, characterized by a broken top plate, occurring at just 0.99% drift. The steel-framed wall performed better, with critical damage (separation at junctions) not occurring until 2.56% drift, though it still showed minor repair-level cracks by 1.79%.

Phase II, which added a perimeter-restrained concealed ceiling, showed a complex interaction. While the timber wall's critical damage was delayed to 1.44% drift due to the ductile yielding of a steel strap, an improvement over Phase I's brittle timber failure, the overall system performance was compromised. The ceiling itself damaged early, with superficial cracks at 0.54% drift (0.27 g PFA), leading to partial detachment by 1.19% drift (0.54 g PFA) and critical failure (detachment of the wall track) concurrently with the wall at 1.44% drift (0.84 g PFA). This highlights a strong negative interaction where the rigid ceiling connection accelerated system-wide failure.

Table 4.4 Comparison of seismic performance and damage progression across the three Phases

Aspect	Phase I (Walls Only)	Phase II (Walls + Perimeter restrained Ceiling)	Phase III (Rocking Walls + Fully floating Ceiling)	Performance Comparison
Superficial Wall Damage	Timber: Very early (hairline cracks in plasterboard 0.30%). Steel: Later (minor tear in plaster paper joint 0.99%).	Timber: Pre-existing issues masked new hairline cracks	Timber: Very early superficial (0.10%), but this is a flexible sealant joint, not brittle plasterboard.	Phase III exhibited very early superficial damage in the flexible sealant joint rather than plasterboard.
Minor repair Wall Damage	Timber: 0.58% (crack in plasterboard reduced fire-rating) Steel: 1.79% (crack in plasterboard reduced fire-rating)	Timber: 1.19% (crack in plasterboard reduced fire-rating)	Timber: 0.97% (minor tear in sealant which remains open reduced fire-rating)	Phase II reached minor repair damage at higher drift with a crack in the plasterboard that reduced fire-rating, while Phase III achieved a comparable state earlier drift but with a minor tear in sealant that recued fire-rating.
Moderate Repair Wall Damage	Timber: 0.99% (top plate break and steel strap failure at junction).	Timber: 1.44% (connection steel strap failure at junctions)	Timber: 2.51% (visible bending of a steel angle at junctions).	Phase III sustained much higher drift before Moderate Repair damage state than Phase II. The Phase II timber-framed wall outperformed its Phase I counterpart, primarily because its failure mode involved the yielding of a steel strap, whereas Phase I failed through a brittle fracture of the timber plate.
Critical Repair Wall Damage	Steel: 2.56% (separation of walls at junctions).	Timber: 1.67% (separation of walls at junctions).	Not Observed	Phase III observed no critical damage, whereas Phase II experienced wall separation at junctions.
Ceiling Damage	Not Available (Walls only)	Superficial Damage started early (0.54%, 0.27 g), progressed to partial detachment of wall angle (1.19%, 0.54 g), and reached major failure at (1.44%, 0.84 g) with detachment of the wall angle along the wall.	Only superficial damage at very high drifts and floor accelerations (~2.0%, 1.16 g), with no damage requiring repair.	Phase III ceiling showed superior seismic performance, decoupling from wall movement than Phase II.
System Interaction	Not Available (Walls only)	The fixed ceiling-to-wall connection forced both systems to interact and damage at low drifts.	The fully floating ceiling and rocking wall detail minimized interaction, allowing each to perform independently.	Phase III's ceilings and walls showed decoupled behaviour.
Damage Progression Rate	Moderate (Timber) to Slow (Steel).	Rapid: Once initial damage occurred, the system quickly escalated to higher damage states.	Very Gradual. Superficial damage in a flexible material occurred early but did not escalate until very high demands.	Phase III has gradual damage progression as compared to Phase II.

In contrast, Phase III (rocking walls + fully floating ceiling) demonstrated a fundamentally superior approach. The wall was designed for ductile movement, showing very early superficial wrinkles in sealant at 0.10% drift, while critical damage (bending of a steel angle) was noticeable at the junction only after until 2.51% drift. Most notably, the fully floating ceiling showed exceptional resilience, sustaining only superficial damage at high drifts and accelerations (~2.0% drift, 1.16 g PFA) with no minor or critical damage observed. This design successfully decoupled the ceiling from wall movement, eliminating the damaging interaction seen in Phase II.

Overall, Phase III performed the better, offering the highest drift capacity, a gradual ductile damage progression, and a resilient ceiling system. Phase II, while showing improved wall ductility over Phase I, was undermined by its vulnerable and interactive ceiling, resulting in rapid system failure at comparatively low drifts and accelerations as compared to Phase III.

Dynamic amplification factors

Partition walls

Figure 4.62 plots the experimentally obtained Peak Component Acceleration to Peak Floor Acceleration (PCA/PFA) ratios for the tested wall specimens. It can be observed that the median PCA/PFA ratios for the "Rocking" walls (1.26) is close to that of the walls constructed with typical NZ construction details in Phase II (1.22). When Phase II (with perimeter-restrained plasterboard ceiling and piping) and Phase I (without ceiling and piping) walls which have similar typical NZ details is compared Phase II has slightly higher PCA/PFA which might be due to the interaction between the walls ceilings and pipes.

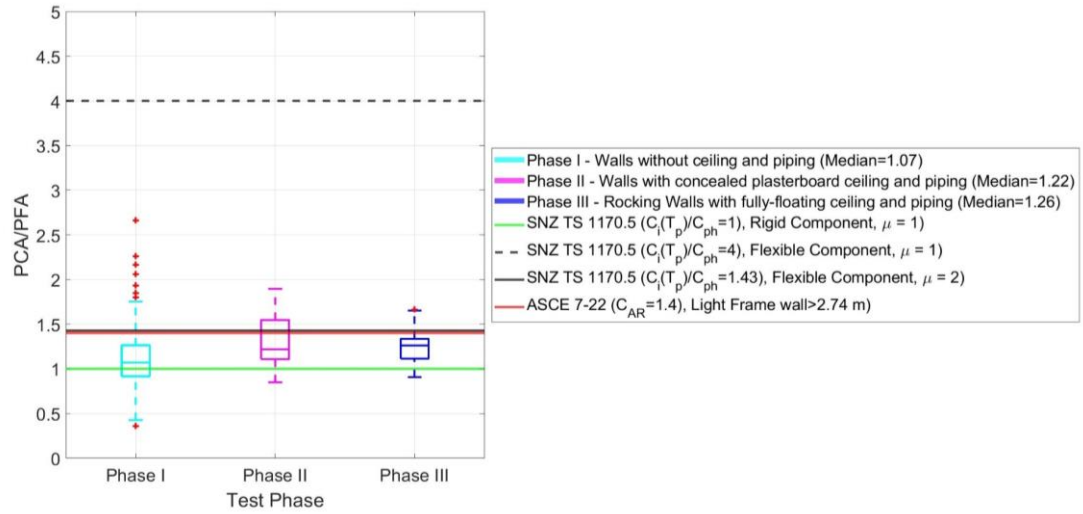

Figure 4.62 Median PCA/PFA ratios for the tested wall specimens

Suspended ceilings

Figure 4.63 plots the experimentally obtained PCA/PFA ratios for the tested ceiling specimens.

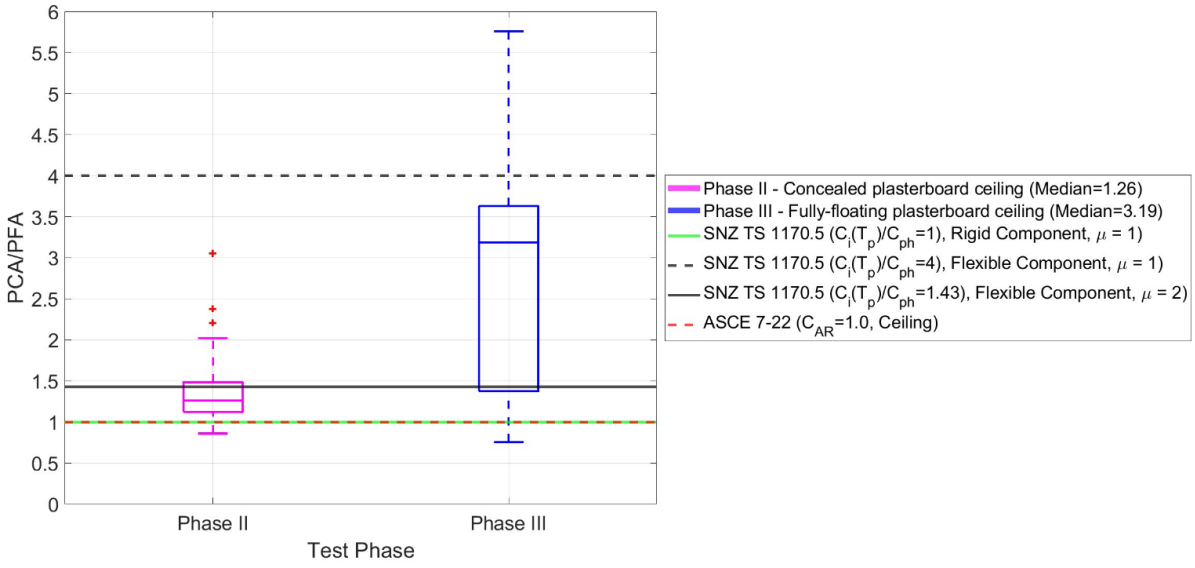

Figure 4.63 Median PCA/PFA ratios for the tested plasterboard ceiling specimens

The results show that the median PCA/PFA ratio for the fully floating ceiling with isolation foam (3.19) is significantly higher, approximately 2.5 times greater, than that of the typical perimeter-restrained ceiling from Phase II (1.26). This notable amplification

is likely attributable to pounding between the floating ceiling and the surrounding walls and bulkheads. The significantly PCA/PFA ratio of 3.19 highlights a critical design consideration. While the ceiling survives drift, its internal components (lights, ducts, sprinklers) must be securely anchored to withstand these amplified inertial forces, which are exacerbated by pounding at the isolation gaps.

CONCLUSIONS AND FUTURE STEPS

This study yielded the following primary conclusions:

(1) **Rocking Walls:** The damage concentration design philosophy was effective. The sealant joints performed as intended sacrificial elements, protecting the wall framing and linings. The kinematic rocking mechanism requires redesign, specifically of the steel angle connection, to perform as intended.

(2) **Fully Floating Ceilings:** The fully floating ceiling with perimeter isolation foam exhibited excellent seismic resilience. Its dynamic amplification is significantly higher than that assumed for traditional ceilings in current US codes, highlighting a need for code updates to address this innovative system. The isolation foam is a critical component for performance.

(3) **Mechanical Pipes:** The unbraced pipe behaviour was mostly governed by connection details in the walls the pipe is penetrating through. Existing code factors for component amplification showed mixed accuracy, with SNZ TS 1170.5 (2025) generally conservative and ASCE/SEI 7-22 (2022) mostly comparable.

(4) **Code Implications:** The experimental data consistently indicates that New Zealand provisions (SNZ TS 1170.5 (2025)) tend to be conservative for these non-structural components based on the selection of the ductility factors for the

component. In contrast, relevant ASCE/SEI 7-22 (2022) factors were unconservative for the fully floating ceilings a potential gap in the US standards for predicting the dynamic response this ceiling system.

The findings from this test series point to several critical paths for future research and development:

(1) **Future tests:**

- Redesign and test an improved connection detail (e.g., a thicker or differently configured steel angle) for the rocking wall system to ensure the intended kinematic rocking motion is achieved without premature yielding.

- Evaluate the post-earthquake fire performance of partition walls that have already sustained seismic damage. It may include experimental fire testing of seismically damaged wall assemblies which would quantify the extent to which earthquake-induced damage compromises their fire-rating performance. The findings could provide the empirical basis needed to confirm or refine current code-prescribed drift limits.

(2) **Parametric and Fragility Studies:** This test series advances the state of knowledge on seismic performance, enabling the development of fragility functions and guiding future parametric studies on key variables such as foam density, sealant properties, component mass, and dimensions.

(3) **System Interaction Analysis:** Conduct in-depth studies utilizing motion capture data and video recordings, combined with analytical modelling, to characterize

the interaction mechanisms and force transfer between pipes and walls, and between ceilings and boundary elements.

(4) **Code Development and Validation:** Use the comprehensive dataset to propose and validate new code provisions or design guidelines specifically for fully floating ceiling systems and to refine existing factors for unbraced pipes and rocking wall systems.

(5) **Fire Performance:** Investigate and develop robust, tested solutions for maintaining fire rating integrity at pipe penetrations and wall joints.

(6) **Dynamic Characterization:** Investigate the dynamic characteristics (natural frequencies and damping ratios of the tested non-structural elements.

REFERENCES

ASCE/SEI 7-22,. (2022). Minimum design loads and associated criteria for buildings and other structures. Reston, VA: American Society of Civil Engineers (ASCE). doi: https:/doi.org/10.1061/9780784415788

Bhatta, J., & Dhakal, R. P. (2026). Seismic response assessment of “rocking” interior partition walls with dual-slot tracks under different construction details. Journal of Earthquake Engineering, , 1–25.

Bhatta, J., Dhakal, R. P., & Sullivan, T. J. (2023a). Seismic evaluation of rocking internal partition walls with dual-slot track under quasi-static cyclic drifts. Journal of Earthquake Engineering, 27(14), 4161–4181.

Bhatta, J., Dhakal, R. P., & Sullivan, T. J. (2023b). Seismic performance of ‘rocking’dual-slot track internal partition walls with concealed joints under lateral cyclic drift demands. Journal of Earthquake Engineering, 27(8), 2198–2223.

Butterworth, S. (1930). On the theory of filter amplifiers. Wireless Engineer, 7(6), 536–541.

GIB. (2016). GIB-EzyBrace-system-sheet-GS2-N GIB. Retrieved from https://www.gib.co.nz/assets/Uploads/GIB-EzyBrace-System-sheet-GS2-N.pdf

Parks, T. W., & Burrus, C. S. (1987). Digital filter design Wiley-Interscience.

Pledger, L. (2026). The effects of reducing design drift limits for structures. (PhD, University of Canterbury).

SNZ TS 1170.5, &. (2025). Structural design actions – part 5: Earthquake actions – New Zealand. Wellington, New Zealand:

Sorrentino, R. (2007). Electronic filter simulation & design McGraw-Hill Professional.

APPENDIX C

OBSERVED DAMAGE DURING TESTS

Table 4.5. Test #1, 0.10 % drift (PFA Top: 0.08 g)

Location	Observation	Photo
Bottom part of the vertical joint 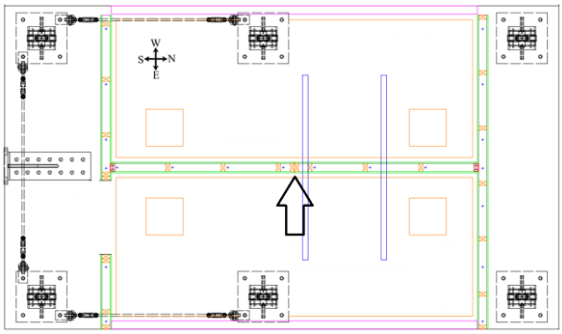	Wrinkles in dried paint applied over sealant	

Table 4.6. Test #5, 0.49 % drift (PFA Top: 0.26 g)

Location	Observation	Photo
Throughout the height of the vertical joint 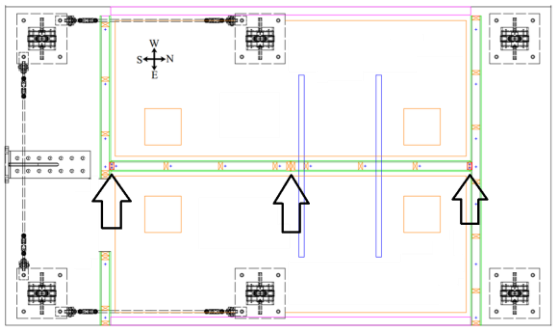	Wrinkles and inclined ties in dried paint and sealant	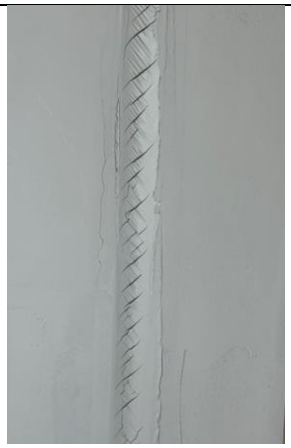

Table 4.7. Test #6, 0.56 % drift (PFA Top: 0.32 g)

Location	Observation	Photo
Top of southwest wall junction above ceiling plenum 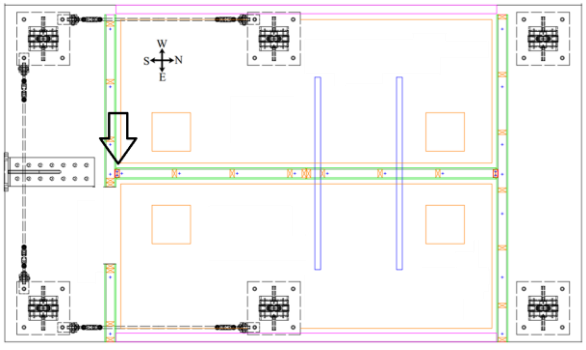	Very minor tear in the sealant but the tear gap closes after shake	

Table 4.8. Test #10, 0.97 % drift (PFA Top: 0.43 g)

Location	Observation	Photo
Top of southwest wall junction above ceiling plenum 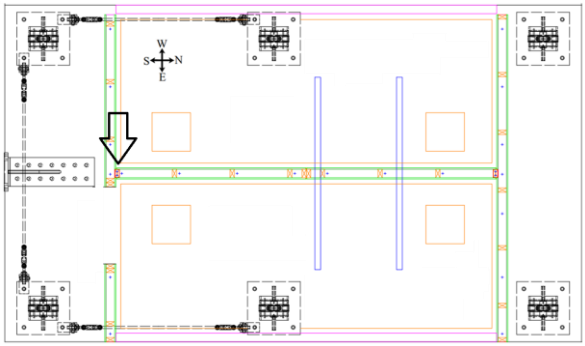	Very minor tear in the sealant but the tear gap remains open after shake	
At South Pipe and in-plane wall penetration 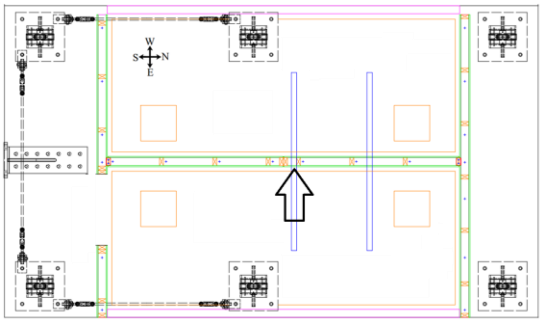	Detachment of sealant between pipe and wall at penetration	

Table 4.9. Test #12, 1.21 % drift (PFA Top: 0.58 g)

Location	Observation	Photo
Near top and bottom of Southeast wall junction 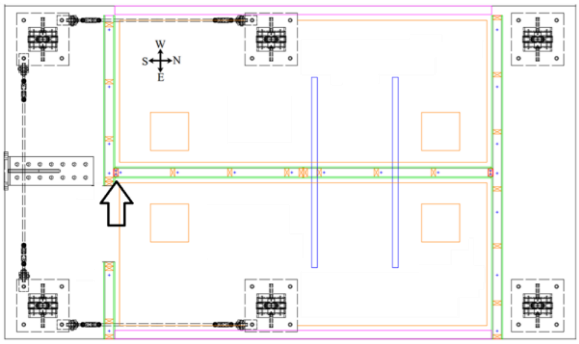	4 mm wide localized separation between the sealant and plasterboard	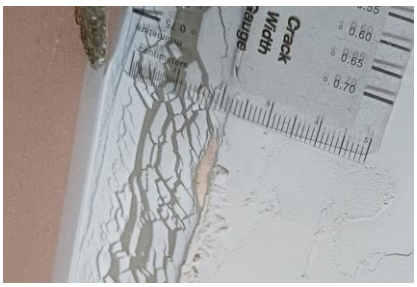

At North Pipe and in-plane wall penetration 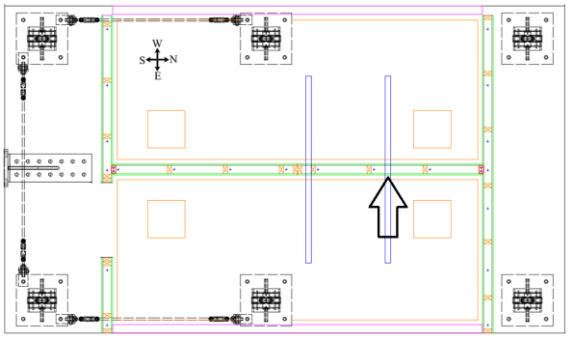	Detachment of sealant between pipe and wall at penetration	

Table 4.10. *Test* #13, 1.45 % drift (PFA Top: 0.83 g)

Location	**Observation**	**Photo**
Throughout the height of the in-plane wall joint 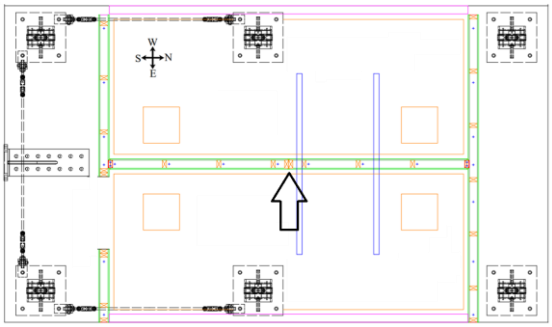	Abundant minor inclined tears in the sealant joint (not see through). This side has a DPC layer behind the sealant in the framing	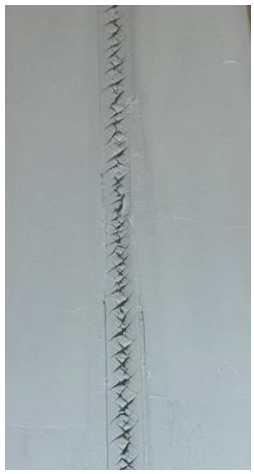
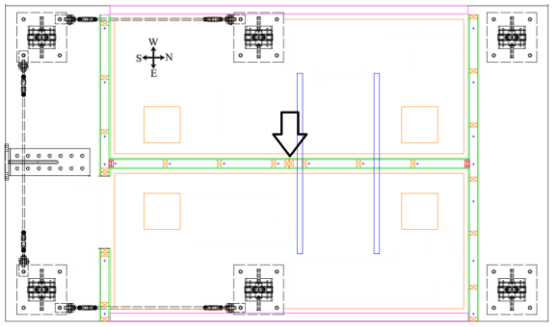	No inclined ties/tears in the joint on the other side. This side does not have a DPC layer behind the sealant in the framing	

Table 4.11. Test #15, 2.03 % drift (PFA Top: 1.16 g)

Location	Observation	Photo
Near top of Northwest wall junction 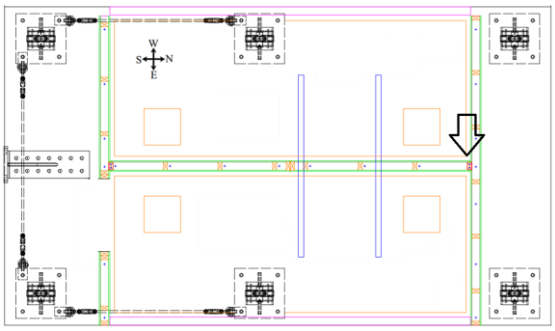	Bent in the wall angle	

Table 4.12. Test #16, 2.06 % drift (PFA Top: 1.19 g)

Location	Observation	Photo
Near Southwest wall junction 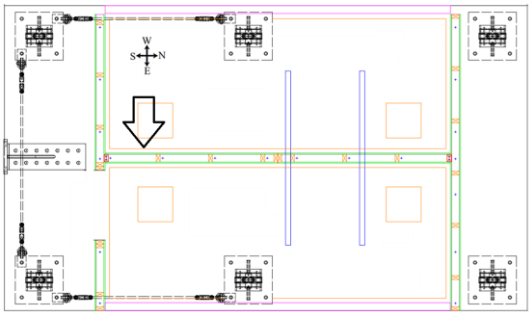	Top cross rail lodged inside the isolation foam	

Table 4.13. Test #17, 2.51 % drift (PFA Top: 1.51 g)

Location	Observation	Photo
Near the top of the Northeast wall junction 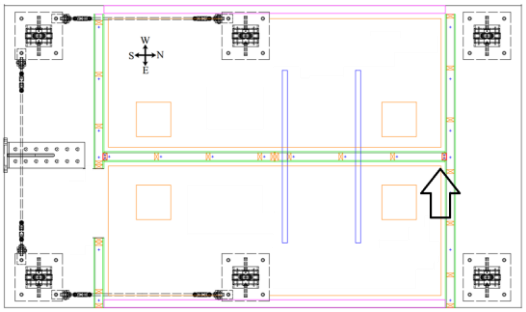	Opening of the wall joint	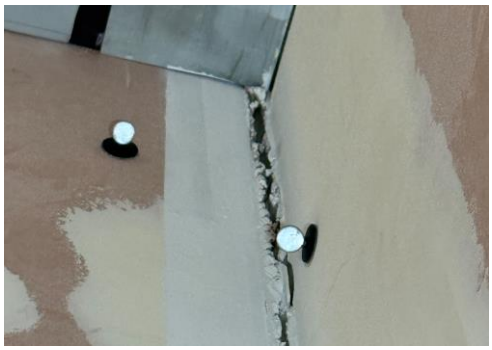

Opposite side of the North wall junction at the top of the North out-of-plane wall 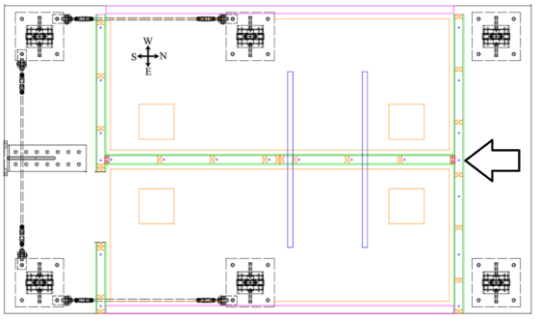	Bent in the top plasterboard strip	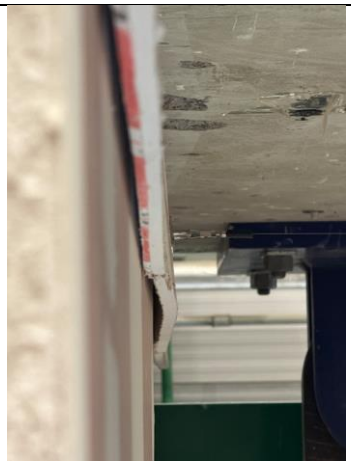
At the top of the North wall junction 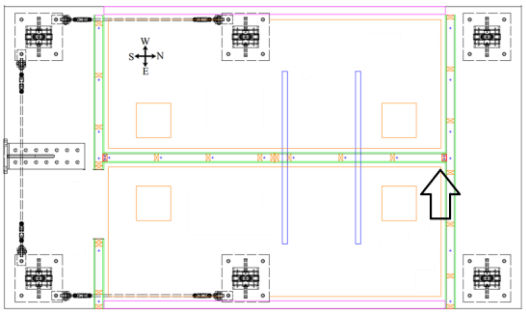	Bending of the steel angle at the junction is visible at the joint	

Videos of specimens during Test #17, 2.51 % inter-storey drift (Top PFA: 1.51 g and Bottom PFA:1.05 g)

Shaking videos during Test #17: Southeast Elevation, Southeast Junction, South Elevation, Northeast Elevation, East Elevation

Photos of specimens after the final Test #28 (Top PFA: 1.32 g and Bottom PFA:0.92 g).

Please note sealant at wall junctions were deliberately cut to test their influence in the rocking motion of the walls during the modified test series.

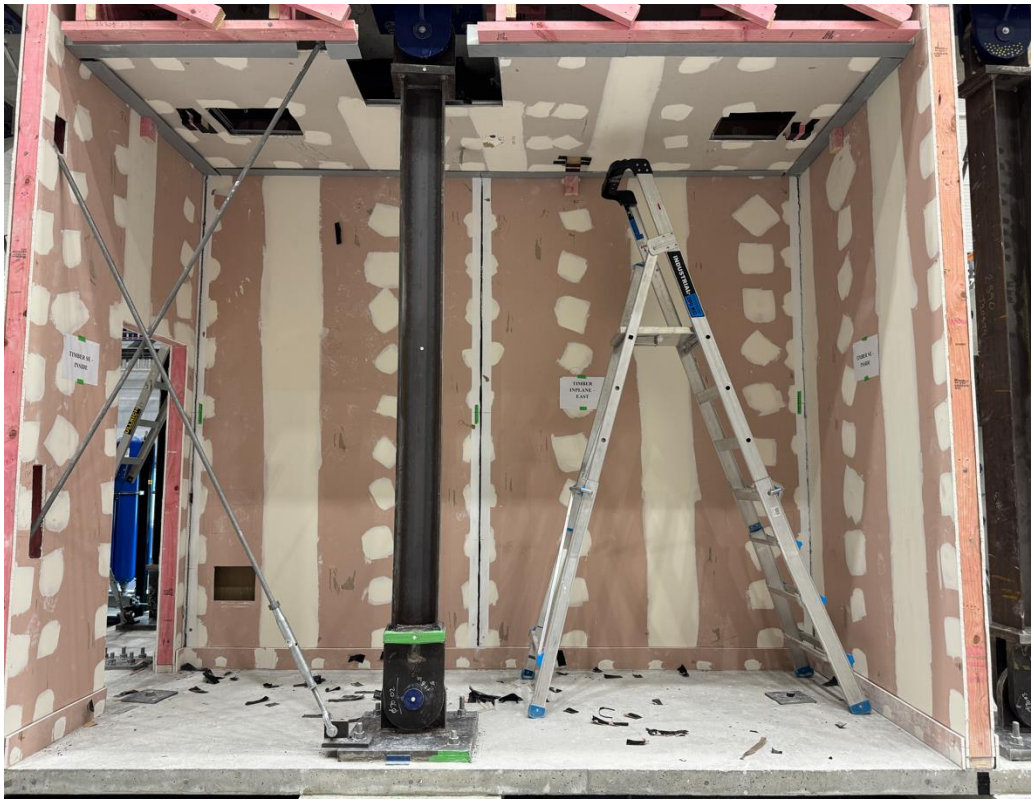

Figure 4.64. East Elevation

Figure 4.65. West Elevation

Figure 4.66. North Elevation

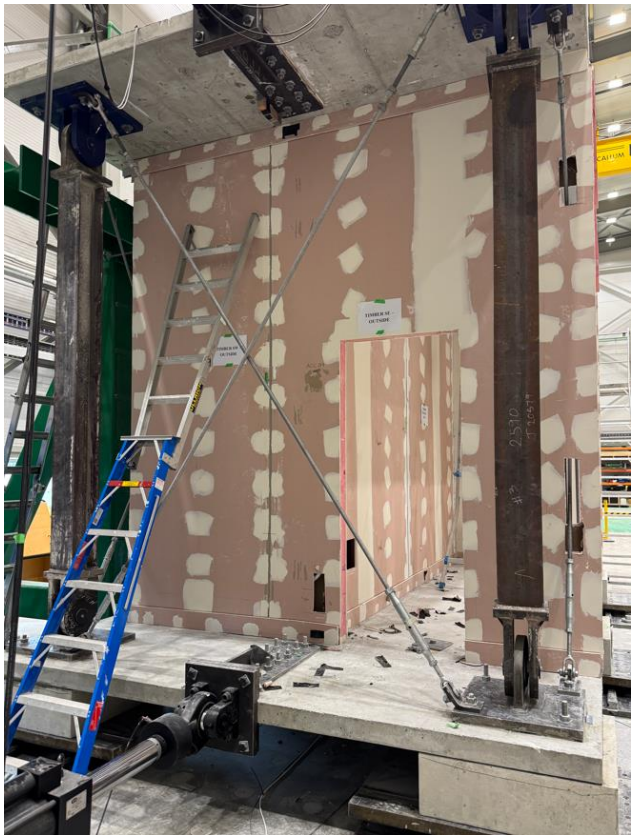

Figure 4.67. South elevation

Figure 4.68. Photo of bent top steel angle at North wall junction taken during demolition

Figure 4.69. Photo of bottom steel angle at South wall junction taken during demolition